Chromatin architecture and transcriptional regulation at the Epidermal Differentiation Complex (EDC) locus

The role of epigenetic factors in modulating chromatin structure and tissue-specific gene expression at the murine EDC locus during epidermal differentiation

Joanne Lauren Yarker

Thesis submitted for the degree of Doctor of Philosophy

School of Life Sciences

University of Bradford

2014

Abstract

The epidermal differentiation complex (EDC) encodes co-ordinately regulated genes critically involved in epidermal differentiation, however knowledge of the molecular mechanisms involved in co-ordinating EDC gene expression is limited.

Recent findings indicate p63 dependent changes in the nuclear localisation and higher-order chromatin folding the EDC coincide with the onset of epidermal stratification during embryonic development. Here it is demonstrated that a direct transcription target of p63, the chromatin-remodelling enzyme Brg1, modulates the specific nuclear positioning of the EDC and transcription of differentiation-specific gene encoded at the EDC.

In addition, the results of high-resolution 5C-based analyses of the spatial chromatin interactome at a 5.3Mb region spanning the murine EDC in epidermal keratinocytes, and the silenced EDC in thymocytes, are presented. Chromatin interactions at the EDC region in keratinocytes include long-range interactions between multiple proximal and distal candidate gene regulatory regions. Many candidate regulatory elements involved in looping chromatin interactions at the EDC region are enriched for both active (H3K4me1, H3K27ac) and repressive (H3K27me3) chromatin marks and are bound by Sin3a and RBP2 co-repressor complexes.

The chromatin interactome at the EDC in epidermal progenitor cells is enriched for bound chromatin architectural proteins Satb1, Satb2, and the cohesin subunit Rad21. Further, a substantial degree of co-localisation is observed between these chromatin architectural proteins, transcription factors and co-factors.

Findings presented here suggest that a functional chromatin interactome, mediated by Satb proteins and cohesin, acts in conjunction with transcriptional repressor complexes to facilitate co-ordinated gene expression at the EDC in epidermal progenitor cells upon differentiation. These results provide a foundation for further study of the mechanisms controlling EDC gene expression in health and disease.

Acknowledgments

I would like to thank to my supervisors Prof Vladimir Botchkarev and Dr Michael Fessing (University of Bradford, UK) for their guidance and support.

I would like to pay special thanks to Dr Krzystof Poterlowicz (University of Bradford, UK) for his collaboration in applying computational methods to perform high-throughput data analyses essential to the completion of this thesis. I would also like to pay special thanks to Dr Andrei Mardaryev (University of Bradford, UK) for his collaboration in generating a proportion of the ChIP-Seq data used in analyses presented in this thesis.

I would also like to thank Dr Michal Gdula (University of Bradford, UK) Dr Vladimir Benes (EMBL, Heidelberg, Germany), Dr Natasha Naumova, Dr Gaurav Jain and Dr Job Dekker (Job Dekker lab, University of Massachusetts, Medical School, Worcester MA, USA) for their guidance.

Contents

List of abbreviations ..... **viii**
List of figures ..... **xi**
List of tables ..... **xv**
1 Introduction **1**

1.1 The spatial hierarchy of genomic organisation 3

1.1.1 Architecture of the chromatin fibre 3
1.1.2 Chromosome territories and inter-chromatin lacunae 5
1.1.3 The genome is compartmentalised according to function by the spatial organisation of genes and chromatin within the nucleus 7
1.1.4 Topological chromatin domains 11
1.1.5 Chromatin looping and long-range gene regulation 13

1.2 The epidermis: its structure, development and the maintenance of epidermal barrier function 17

1.1.6 Epidermal ontogenesis and homeostasis 18
1.1.7 The role of epigenetic mechanisms and spatial nuclear organisation in the regulation of epidermal proliferation and differentiation 24

1.1.7.1 The role of DNA methylation in regulating epidermal proliferation and differentiation 25
1.1.7.2 Post translational histone modifications and the maintenance of epidermal progenitor state and function by histone methyltransferases 26
1.1.7.3 Histone acetyl and de-acetyl transferase complexes regulate progenitor cell renewal and keratinocyte differentiation 28
1.1.7.4 The role of Polycomb repressor complex proteins in mediating epidermal cell survival, proliferation and differentiation 29

1.1.7.5 Chromatin remodellers and remodelling in progenitor and differentiating cell populations within the epidermis 31
1.1.7.6 Remodelling of the architecture of keratinocyte nuclei occurs during epidermal differentiation 32

1.1.8 The Epidermal Differentiation Complex 35

2 Aims 38
3 Materials and Methodology 39

3.1 Experimental animals and tissue collection 39
3.2 Isolation of primary mouse keratinocytes 39
3.3 Isolation and purification of BAC clone DNA 39
3.4 Chromosome conformation capture carbon copy (5C) technology 40

3.4.1 Keratinocyte isolation and fixation 41
3.4.2 Thymocyte isolation and fixation 41
3.4.3 Chromosome conformation capture (3C) 42

3.4.3.1 Cell lysis 42
3.4.3.2 Chromatin Digestion 42
3.4.3.3 Ligation of digested chromatin and subsequent reversal of cross-linking 43
3.4.3.4 Extraction and purification of 3C template and control DNA 43

3.4.4 3C quality control 46
3.4.5 Generation of chromosome conformation capture carbon copy (5C) and 5C control libraries 47

3.4.5.1 Design and preparation of 5C primers for 5C 48

3.5 5C quality control and 5C optimisation 50

3.5.1 Optimisation of 5C conditions using 5C titration 51
3.5.2 5C Quality Control 52

3.5.2.1 5C quality control 2: sequencing of 95 5C products using the Sanger method 52
3.5.2.2 Recombinant plasmid isolation and purification 54
3.5.2.3 Screening of purified plasmid DNA from individual 5C clones 55
3.5.2.4 Sample preparation for Sanger sequencing 57
3.5.2.5 Analysis of sequencing output 57

3.6 5C sample preparation for paired-end deep-sequencing 60

3.6.1 Custom oligonucleotide design and preparation 61
3.6.2 PE sample preparation 62

3.7 Analysis of deep-sequenced 5C libraries 65
3.8 Microarray gene expression profiling 66
3.9 Microaray gene expression profiling of laser capture micro-dissected epidermis 66
3.10 RT-PCR Microarray validation 67
3.11 Haematoxylin and Alkaline Phosphatase staining 68
3.12 Immunofluorescence staining 68
3.13 Terminal deoxynucleotidyl transferase dUTP nick end labeling 69
3.14 Fluorescence Activated Cell Sorting 70
3.15 Directional whole transcriptome sequencing 70
3.16 Chromatin immunoprecipitation followed by sequencing (ChIP-Seq) analysis using cross-linked chromatin 72
3.17 Native chromatin immunoprecipitation followed by sequencing (NChIP-Seq) analysis 77
3.18 3D Fluorescent *In Situ* Hybridization 78

3.18.1 Preparation of mouse metaphase spreads 79
3.18.2 Preparation of histological sections for the preservation of 3D nuclear architecture 79
3.18.3 Preparation of cells for the preservation of 3D nuclear architecture 80
3.18.4 Generation of modified dUTPs for the generation of labelled DNA probes 81
3.18.5 Generation of labelled DNA probes for 3D FISH 81

3.18.6 Labelling and amplification of chromosome painting probe 83
3.18.7 2D Fluorescent *In Situ* Hybridization 84
3.18.8 3D Fluorescent *In Situ* Hybridization 85

3.19 Immuno-FISH 87
3.20 3D FISH image acquisition and analysis 87
3.21 BACs, oligo sequences, and antigens 90

3.21.1 Primer/NGS adapter sequences 90
3.21.2 Antigen and antigen dilutions used in immunostaining reactions 91

4 Results 92

4.1 The chromatin remodeler BRG1 modulates nuclear positioning of the EDC and programmes of EDC gene expression during epidermal ontogenesis 92

4.1.1 The expression of differentiation specific genes encoded at the EDC locus is altered in the epidermis of E16.5 K14BRG1$^{\Delta/\Delta}$ mice 93
4.1.2 BRG1 deficiency during epidermal ontogenesis results in a significant reduction in epidermal thickness at E16.5 95
4.1.3 BRG1 binds multiple sites at the EDC in epidermal keratinocytes 96
4.1.4 The nuclear position of the EDC locus within basal keratinocyte nuclei is altered in the absence of BRG1 98
4.1.5 The association of the EDC with nuclear speckles is reduced in the absence of BRG1 102

4.2 Higher-order chromatin folding and transcriptional regulation at the EDC locus 104

4.2.1 The 3D higher-order structure of chromatin at the EDC region 104
4.2.2 Identification of a network of potentially regulatory long-range interactions involving putative enhancer elements and gene core promoters at the EDC 113
4.2.3 Regions bound by Special AT-rich binding proteins and cohesin are preferentially involved in looping interactions 122
4.2.4 Special AT-rich binding proteins and cohesin co-localise with multiple additional transcriptional regulators at sites of looping chromatin interaction 128

5 Discussion 136

5.1 BRG1 regulates the transcriptional activity and spatial nuclear position of the EDC locus in basal epidermal keratinocytes 136

5.2 Higher-order chromatin folding and potential mechanisms of long-range gene regulation at the EDC 142

6 Conclusions 149

7 Future directions 151

8 Appendix 153

List of abbreviations

3C – chromosome conformation capture

3C – carbon copy/5C - chromosome conformation capture carbon copy

3D-SIM – 3D structured illumination microscopy

4C – circular chromosome conformation capture

6C - Combined 3C-ChIP-cloning

AP1 – activator protein 1 transcription factors

AP2 – activator protein 2 transcription factors

BAC – bacterial artificial chromosome

BRG1 – brahma-related gene 1 protein

CBX4 – chromeobox 4 E3-SUMO ligase protein

CE – cornified envelope

CHD – chromodomain helicase DNA-binding proteins

CHD4 – chromodomain helicase DNA-binding protein 4 protein

ChIA-PET – Chromatin Interaction Analysis by Paired-End Tag Sequencing

ChIP – chromatin immunoprecipitation

CT – chromosome territory

DI – directionality index

ECM – extra cellular matrix

EDC – epidermal differentiation complex locus

EKLF – Erythroid Krüppel- like factor transcription factor

EM – electron microscopy

EZH1 – Enhancer Of Zeste Homolog 1 protein

EZH2 – Enhancer Of Zeste Homolog 2 protein

FC – fold change

FISH – fluorescence in situ hybridisation

GADD45 – growth arrest and DNA damage inducible 45 proteins

GATA-1 – GATA-binding protein 1 transcription factor

GRHL3 – Grainyhead-head like 3 transcription factor

HAT – histone acetyltransferase

HDAC – histone de-acetylase complex

HMT – histone methyltransferase

IF – interaction frequency

IFE – interfollicular epidermis

ISWI – imitation switch protein

KLF4 – Krüppel-like factor 4 transcription factor

LAD – lamina associated domain

LB – Luria-Bertani broth

LCR – locus control region

LDB1 – LIM domain binding-protein 1

LMA – ligation mediated amplification

MAD – median absolute deviation

MAR – matrix attachment region

MLL2 - myeloid/lymphoid or mixed-lineage leukemia 2 protein

MXI1 – Max interacting protein 1 transcription factor

NAD – nucleolar associated domains

NGS – next-generation sequencing

NL – nuclear lamina

NPC – Nuclear pore complex

NT – nick translation

OVO1 – OVO-like zinc finger 1 transcription factor

PcG – polycomb group complex

PE – paired end

PKC – protein kinase C

PML – promyelocytic leukaemia nuclear body

PNK – polynucleotide kinase

PRC – polycomb repressive complex

PRE – polycomb responsive element

RCF – relative centrifugal force

RNAPII – RNA polymerase II

SATB1 – special AT-rich sequence-binding protein 1

SATB2 – special AT-rich sequence-binding protein 2

SC-35 – splicing factor SC-35 protein

SIN3A – SIN3 transcription regulator family member A

SP1 – specificity protein 1 transcription factor

SUMO – small ubiquitin-like modifier protein

TAD – topologically associating domains

SWI/SNF – switch/sucrose nonfermentable complex

WDR5 – WD40-repeat protein

List of figures

1. Introduction

Figure 1. Architecture of the nucleus……..……...……...…...**7**

Figure 2. Spatial organization of the genome in a mammalian (mouse) nucleus……..…**15**

Figure 3. Stratification of the murine interfollicular epidermal barrier during epidermal ontogenesis…….……**20**

Figure 4. Hierarchical organisation of the interfollicular epidermis…….……**24**

Figure 5 Changes in nuclear shape, volume, and nuclear architecture occur as keratinocytes stratify and terminally differentiate…….….**34**

3. Method

Figure 6 Example electrophoretic gel image showing 3C IF library and controls……....**45**

Figure 7 3C quality control: Representative 3C template titration gel image and plot…**46-47**

Figure 8 Example electrophoretic gel image showing 5C IF libraries and controls…….**48**

Figure 9 Example electrophoretic gel image showing phosphorylated and ligated 5C primers……**50**

Figure 10 5C optimisation: titration plot and corresponding electrophoregram……...**52**

Figure 11 5C quality control**:** example electrophoretic gel image showing purified 5C product……**53**

Figure 12 5C quality control: example electrophoretic gel image showing amplified plasmid DNA purified from 5C clones……..**56**

Figure 13 Example electrophoretic gel image showing EcoRI restriction products generated after overnight digestion of recombinant plasmid DNA purified from 5C clones.……**57**

Figure 14 Plot representing the results of Sanger DNA sequencing of 5C product clones……...**58-59**

Figure 15 Size distribution looping interactions in a population of 95 5C product clones……**59-60**

Figure 16 Custom design of barcoded PE NGS adapters……**61-62**

Figure 17 Example electrophoretic gel image showing concentrated and purified 5C product ready for conversion into NGS libraries……...**63**
Figure 18 Example electrophoretic gel image showing barcoded PE adapter ligated 5C product……**64**
Figure 19 Example electrophoretic gel image showing amplified, adapter ligated 5C product after size selection……**65**
Figure 20 Representative electrophoretic gel and electropherogram showing the fragment size distribution of total RNA sample, corresponding rRNA depleted RNA, and RNS-Seq libraries……..**71-72**
Figure 21 Electrophoretic gel image showing fragment size distribution of chromatin following sheering using sonication and of ChIP-Seq libraies……..**76**
Figure 22 Representative plot showing the relative fold enrichment at positive (GAPDH promoter) and negative (intergenic) control regions obtained following ChIP-qPCR analysis of ChIP samples……**78**
Figure 23 Electrophoretic gel image showing BAC DNA before and after NT……...**82**

4. Results

Figure 24 Administering tamoxifen to E10.5 K14BRG1$^{\Delta/\Delta}$ mice results in a reduction in epidermal thickness at E16.5……**94-95**
Figure 25 BRG1 deficiency during epidermal ontogenesis impacts upon the expression of differentiation specific genes within the epidermis……**96**
Figure 26 Analysis of BRG1 ChIP-Seq signal density at the Epidermal Differentiation Complex (EDC) in mouse epidermal keratinocytes and the distribution of ChIP-Seq peaks called at candidate gene regulatory elements……**97**
Figure 27 BRG1 is involved in regulating the nuclear localisation of the EDC locus.....**101-102**
Figure 28 Epidermal knockdown of BRG1 results in the reduced spatial association of the EDC with SC35 positive speckles……..……**103**
Figure 29 Transcript expression levels at a 5.3Mb region (89.9-95.2Mbp, Mmu9) spanning the murine epidermal differentiation complex (EDC) locus in keratinocytes and in thymocytes……**106-107**

Figure 30 Position of topological chromatin domains at the EDC region in keratinocytes and in thymocytes……..**111-113**
Figure 31 RNA-Seq assembly and histone modification ChIP-Seq peaks called for a 5.3Mbp region spanning the mouse EDC……**116**
Figure 32 Distribution and level of histone mark enrichment at looping chromatin interactions at a 5.3Mb region spanning the EDC in keratinocytes……..**118-120**
Figure 33 Distribution of 5C interactions called for a candidate enhancer element located at the EDC and distribution of ChIP-Seq peaks called for epigenomic and chromatin binding factors that occupy interaction sites……**122**
Figure 34 Level of enrichment for looping chromatin interactions involving chromatin regions occupied by epigenomic factors, chromatin remodelling and architectural proteins in keratinocytes……**126-128**
Figure 35 Level of enrichment for looping chromatin interactions involving chromatin regions occupied by epigenomic factors, chromatin remodellers, architectural proteins and the transcription co-factors RBP2 and SIN3A……...**130-131**
Figure 36 Level of enrichment for looping chromatin interactions involving chromatin regions occupied by chromatin remodellers, architectural proteins and transcription factors……**133-135**

5. Discussion

Figure 37 Structure and evolutionary conservation of the human and mouse EDC regions……..**141**

8. Appendix

Figure A1 Levels of apoptosis and proliferation in E16.5 K14BRG1$^{\Delta/\Delta}$ and wild type control epidermis……...……...**156**
Figure A2 Replicate 5C 2D IF heatmaps and schematic representation of the alternating 5C primer deign scheme used to generate 5C libraries……**157**
Figure A3 Side-by-side representation of 4C and 5C *Lor* locus interaction profiles…..**158**
Figure A4 Histograms of the position of, and separation distance between, labelled DNA probes corresponding to *Lor* and *Rps27* loci in E16.5 K14BRG1$^{\Delta/\Delta}$ and control (wild type) basal epidermal keratinocyte nuclei and average nuclear radii……...……**159-160**

Figure A5 Histograms of the position of approximately equidistant EDC loci (A, B, and C) in freshly isolated normal collagen adherent neonate keratinocytes (KC), basal epidermal keratinocytes, and thymocytes freshly isolated from wild type 8 week old mice (TC) and average nuclear radii……...……...**160-162**
Figure A6 Total count of SC35 positive nuclear speckles detected at the mid-section of E16.5 K14BRG1$^{\Delta/\Delta}$ and wild type control basal epidermal keratinocyte nuclei……..**162**

List of tables

3. Method

Table 1. 3C titration primers…….…….**90**

Table 2 RT-PCR primers…….…..**90**

Table 3 ChIP-qPCR control region primers…….…….**90**

Table 4 Custom designed PE NGS adapters and illumina NGS PCR primers……..…**91**

Table 5 Antibodies and antibody dilutions used for immunostaining……...……**91**

8. Appendix

Table A1 Labelled DNA probe BACs…….**153**

Table A2 Buffers and cell culture reagents……..**153-154**

Table A3 Buffers and solutions used for ChIP.……..**154**

Table A4 ChIP and FACS antibodies and antibody dilutions……..**154-155**

Table A5 5C primers…….**.....**…..….**.....Compact Disc**

Table A6 Microarray profiling of the relative epidermal expression of genes encoded at the EDC locus in E16.5 K14CreER/BRG1$^{fl/fl}$ and control (wild type) mice..**Compact Disc**

Table A7 Microarray profiling of the relative expression of genes encoded at mouse Chr3:89.9-95.2 in freshly isolated normal collagen adherent neonate keratinocytes (KC), and thymocytes freshly isolated from wild type 8 week old mice (TC)**.....Compact Disc**

Table A8 Statistical comparison the position of approximately equidistant EDC loci (A, B, and C) in freshly isolated normal collagen adherent neonate keratinocytes (KC), normal neonate basal epidermal keratinocytes, and thymocytes freshly isolated from wild type 8 week old mice (TC)…….**...**……..**Compact Disc**

Tables A9 and A10 Levels of histone mark and chromatin binding factor enrichment at interrogated chromatin regions involved in looping interactions at mouse Chr3: 89.9-95.2Mb…….**...**……..……..**Compact Disc**

1 Introduction

Metazoan development requires the concerted specification of divergent lineages among a genetically homogenous cell population and the tightly controlled, coordinate genesis of cellular functional and structural diversity. During post-natal life, the maintenance of a fine equilibrium between proliferation and differentiation among adult stem cell populations preserves the integrity of many tissues. Proper spatial and temporal regulation of transcription is critical for the genesis of functional and cellular diversity during development and cellular differentiation. Changes in patterns of transcriptional activity are often pathogenic and a full understanding of the mechanisms that act to regulate gene expression is critical for the identification and targeting of factors that contribute to the onset of disease.

In the post-genomic era, it has become clear that the regulatory potential of genomes is much greater than previously appreciated. Within the genome, genes are non-randomly arranged relative to other genes and to a large number of genomic elements potentially involved in the regulation of gene expression. Recent technological advances have enabled researchers to study not only the linear structure of the genome but also genome-wide patterns of spatial chromatin organisation within the nucleus. Chromatin state dynamics, higher-order chromatin folding, and the spatial partitioning of the genome into distinct functional domains within the nucleus have been shown to play fundamental part in regulating gene expression, with important implications for our understanding of the evolutionary origin and function of gene clusters.

Key components of the mammalian epidermal layer of the skin are encoded within three gene clusters, the keratin intermediate filament type I and II gene clusters and the epidermal differentiation complex (EDC). A highly evolutionarily conserved ‘supercluster’, the EDC comprises genes belonging to at least three different families as well as a number of genes unrelated to epidermal development. Genes within these separate families exhibit shared patterns of spatial and temporal gene expression and functional interdependence, however little is known as to the function of gene clustering within the EDC or of the mechanisms acting to control the coordinate expression of EDC genes.

This thesis explores the role higher-order chromatin folding at the EDC plays in regulating transcription at the EDC and looks at what factors are involved in controlling spatial chromatin organisation and gene expression at the EDC. Results presented here suggest multiple chromatin remodelling proteins, including SWI/SNF-BRG1 chromatin remodelling protein complex and matrix attachment-region Special AT-rich binding proteins, have diverse functions in regulating functional local linear and higher-order chromatin structural states at the EDC.

1.1 The spatial hierarchy of genomic organisation

Control of the function and maintenance of the genome can be said to occur at three different broadly defined levels: the linear structure of DNA and chromatin; the spatial and temporal organisation of nuclear processes, including DNA replication and repair, the control of transcription, and the post-translational control of gene expression; and the spatial organisation of the chromatin fibre. The compilation of a complete picture as to how manifold regulatory mechanisms operating at these different levels act to direct genome function, and the elucidation of how they combine to form a complex architecture of genome regulation, is one of the current fundamental questions in biology.

Recent years have seen a rapid advance in our understanding of nuclear structure and organisation, owing to the generation and application of novel sub-nuclear imaging techniques. A paradigm shift in the perception of nuclear organisation has occurred. Once viewed as random in comparison to the organisation of factors and processes within the cell cytoplasm, organisation within the interphase nucleus is now known to be highly complex, compartmentalised, and fundamental to the cell's orchestration of gene expression, genome replication and repair.

A hierarchy of spatial structures, formed by the packaging and folding of chromatin within the nucleus, have been identified, some relatively stable, others transient. At one level, the chromatin fibre has been found to fold into dynamic kilo-base scale loops that bring gene regulatory elements involved in the regulation of transcription into propinquity. Larger mega- multi-mega base scale domains comprising multiple chromosomal interactions spatially and functionally partition the genome. On a larger scale still, the folding of chromosomes and the spatial localisation of nuclear bodies creates nuclear compartments that partition the genome within the nucleus (figure 2).

1.1.1 Architecture of the chromatin fibre

About two metres of DNA are packaged into chromatin– a compact complex of DNA and protein – within the eukaryotic nucleus, which is typically around 5-6μm in diameter. At

the most basic level of organisation, the DNA molecule is organised into nucleosomes connected by short stretches of linker DNA. Each nucleosome is ~10nm in diameter and consists of 1.7 turns of DNA (147bp of DNA) wound around an octameric histone core. ~75% of each histone core consists of two copies of four core histones: H2A, H2B, H3, and H4. N- and C-terminal histone tails extrude from nucleosomes and are involved in multiple functional intermolecular interactions (Kornberg, 1977; McGhee and Felsenfeld, 1980).

In vitro in solutions of physiological ionic strength, a further level of organisation identified is the 30nm fibre, which compacts DNA 30-40 fold more as nucleosomes interdigitate (Dorigo et al., 2004; Grigoryev et al., 2009; Widom and Klug, 1985; Williams et al., 1986; Woodcock et al., 1984; Woodcock and Ghosh, 2010; Wu et al., 2007). However, whether the 30nm-fibre is a feature of chromatin organisation within the confines of a typical eukaryotic nucleus *in vivo* is a long-standing and controversial question (Court et al., 2011; Markaki et al., 2010; Pederson, 2012; Scheffer et al., 2011; Umbarger et al., 2011; Woodcock and Ghosh, 2010). DNA bound architectural proteins such as cohesin (Peters et al., 2008) and CTCF (Phillips and Corces, 2009), binding by long non-coding RNA (Ng et al., 2007) and components of the transcriptional machinery (Lodish, 2012) as well attachment of the chromatin fibre to nuclear scaffold proteins (Chattopadhyay and Pavithra, 2007; Heng et al., 2004) are all factors that influence the further, higher level, packaging of chromatin *in vivo*.

Statistical modelling based upon chromatin interaction frequency data acquired using the chromosome conformation capture (3C) derivative technique Hi-C suggests that chromatin within the nucleus is folded into dense fractal globules. This structure forms spontaneously within the constraints imposed by the degree to which the chromatin fibre is compacted within the limiting space of the nucleus. Importantly, while being a highly dense, organised structure, the fractal globule model permits rapid unfolding and translocation of any one region of chromatin, thereby enabling interaction with components of the transcriptional machinery and regulatory interactions between proximal and distally located regulatory elements and functional sub-nuclear compartments involved in the regulation of gene expression (Lieberman-Aiden et al., 2009; Mirny, 2011).

1.1.2 Chromosome territories and inter-chromatin lacunae

Within the nucleus, DNA is organised into separate chromosome territories (CT) occupying demarcated areas within the nucleus. The arrangement of CT within nuclei has been mapped extensively using multi-colour fluorescence *in situ* hybridisation (FISH) to label or 'paint' individual chromosome territories (Bolzer et al., 2005; Cremer and Cremer, 2010; Lichter et al., 1988; Pinkel et al., 1988) and the architecture of CT and the nuclear environment between CT studied in detail using microscopy based super-resolution imaging techniques, (Baddeley et al., 2010; Cseresnyes et al., 2009; Markaki et al., 2010; Schermelleh et al., 2008) (figure 1 and figure 2). Data generated by the application of the 3C-derivate technique, Hi-C, (figure 2) to the study of 3D genome organisation show *cis* interactions predominate within the nucleus and corroborate evidence from the study of CT using fluorescence microscopy based approaches (Lieberman-Aiden et al., 2009; Zhang et al., 2012).

The arrangement of CT in mouse and human nuclei is non-random and their organisation within the nucleus has been shown to depend upon size, replication timing, GC content, and gene-density (Croft et al., 1999; Tanabe et al., 2002). Small and gene-dense chromosomes preferentially interact with one another and cluster together towards the nuclear centre while larger, less gene-dense, chromosomes tend to co-localise towards the nuclear periphery(Boyle et al., 2001; Lieberman-Aiden et al., 2009; Sengupta et al., 2008; Tanabe et al., 2002; Zhang et al., 2012). The spatial organisation of intermediate sized chromosomes is less well defined (Zhang et al., 2012) however, and, although largely static due to the large size of chromosomes, translocation of CT has been shown to coincide with changes in cell state (Bridger et al., 2000; Croft et al., 1999; Meaburn et al., 2007; Meaburn et al., 2008; Mehta et al., 2010), leading to cell-cell variations in the position of CT.

Dynamic intermingling of territories is connected with the establishment of interactions between loci located on different chromosomes and with active transcription (Branco and Pombo, 2006; Lieberman-Aiden et al., 2009; Zhang et al., 2012). Transcription foci (see page 13) characterised by a high concentration of serine 2-phosporylated RNAPII (elongating RNAPII) have been shown to co-habit regions of CT intermingling (Branco

and Pombo, 2006; Kumaran et al., 2008). Interchromatin lacunas or ‘channels’ separate CT and narrower lacunas also intersperse CT between chromatin domains – defined regions of condensed chromatin within CT that form structures ~100kb - ~1Mb in size characterised by a gene dense outer-layer enriched in ribonucleoprotein complexes called perichromatin fibrils. Channels issue from nuclear pore complexes and emanate throughout the nucleus. Macromolecular nuclear bodies, including speckles, Cajal bodies, paraspeckles, and promyelocytic (PML) bodies, occupy interchromatin channels 400nm or more wide. Between chromatin domains and lacunas are regions of decondensed chromatin rich in histone marks typical of active chromatin, nascent DNA and RNA transcripts and RNAPII called perichromatin regions (Cremer and Cremer, 2010; Markaki et al., 2010) (figure 1 and figure 2).

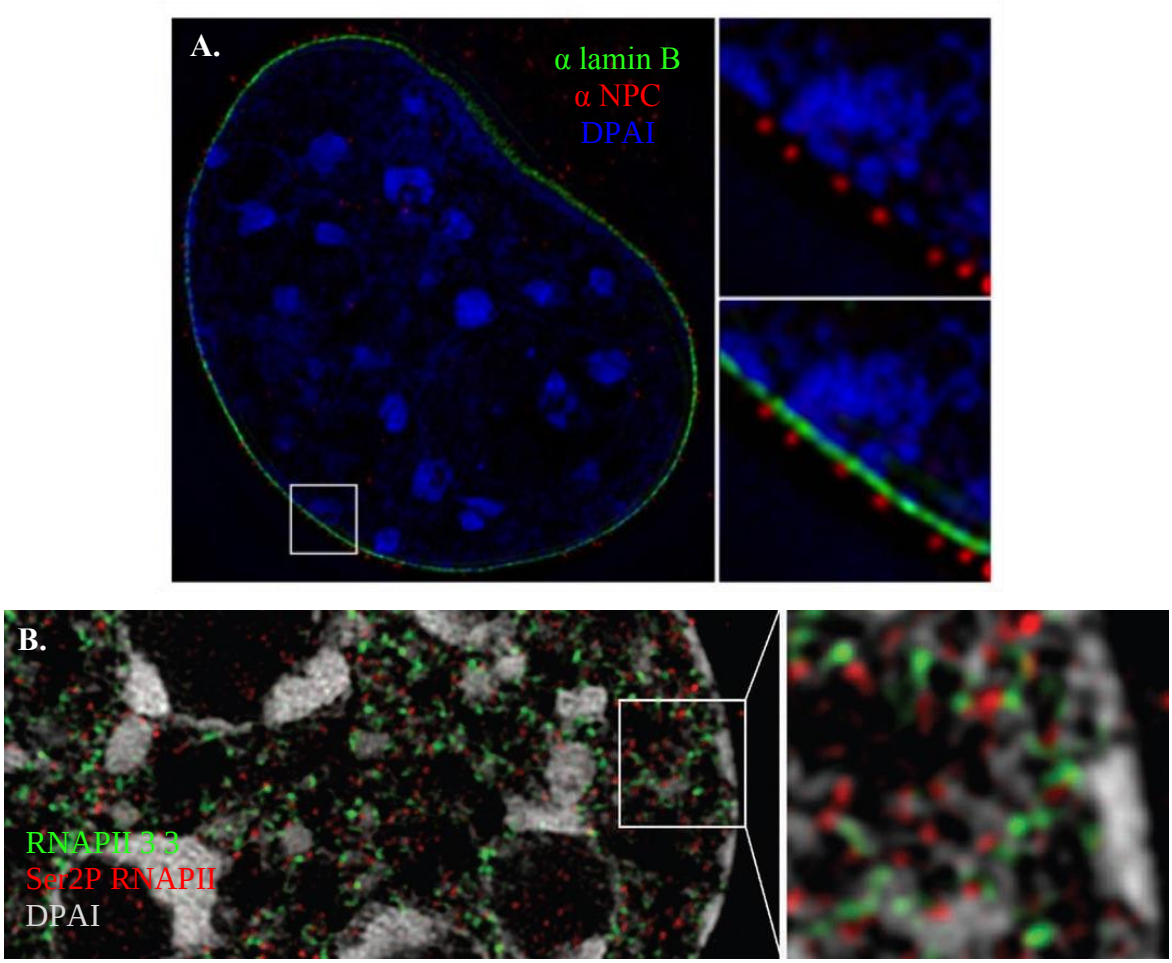

Figure 1 Architecture of the nucleus (**A**) three-dimensional structured illumination microscopy (3D-SIM) image showing the nucleus and (inset) the nuclear periphery, nuclear pore complexes (NPC) (red), nuclear lamina (green), and chromatin surface (blue). Reproduced from Schermelleh *et al*, 2008 (Schermelleh et al., 2008) with the permission of the American Association for the Advancement of Science. Super resolution imaging shows that lacunae between condensed chromatin domains emanate from NPC. (**B**) Super-resolution imaging of special nuclear organisation using 3D-SIM (Markaki et al., 2010) showing de-condensed regions of chromatin adjacent condensed domains, intermingling between domains, and the distribution of enrichment for RNAPII signals (red and green). Adapted from Baker *et al* (Baker, 2011) with the permission of Macmillan Publishers Ltd.

1.1.3 The genome is compartmentalised according to function by the spatial organisation of genes and chromatin within the nucleus

Within CT, and throughout the interphase nucleus, the positioning of genes at shared sub-nuclear compartments and genome-wide networks of chromosomal interactions functionally partition the genome. With the exception of a handful of genes, most genes are only transiently expressed and patterns of nuclear gene positioning and global patterns of chromosomal interactions reflect fluctuating levels of transcriptional activity (de Wit and de Laat, 2012; Dekker et al., 2013; Egecioglu and Brickner, 2011). Changes in transcriptional activity are associated with changes in chromatin mobility (Chuang et al., 2006) and with higher-order chromatin remodelling and the dynamic association of genes with visible sub-nuclear structures (Chambeyron and Bickmore, 2004; Chambeyron et al., 2005; Harmon and Sedat, 2005; Morey et al., 2007; Volpi et al., 2000; Williams et al., 2002).

High-resolution analysis of genome-wide patterns of association between loci in human and in mouse cells using the 3C-based technique Hi-C indicates regions of 'open' and regions of 'closed' chromatin are separated by folding of the chromatin fibre within chromosomes into separate cell-specific multi-mega base scale sub-chromosomal compartments. Called A and B compartments (see figure 2), these regions, which are ~5Mb in size, compartmentalise CT according to markers transcriptional status such as enrichment for regions of DNA hypersensitivity, gene density, GC content, replication timing and covalent histone modifications. While A compartments correlate with markers of active transcription, B compartments appear to comprise a primarily a repressive transcriptional environment (Dixon et al., 2012; Lieberman-Aiden et al., 2009; Zhang et al., 2012). The organisation of these compartments has been shown to depend upon a combination of sequence and chromatin state characteristics upon and comprises the sustained establishment of chromosomal interactions upon the basis of shared features (Dekker et al., 2013; Imakaev et al., 2012).

Transcription foci – or factories – have been observed to act as hubs around which chromatin is organised, with multiple genes co-localised at, and in dynamic association with, shared factories (Osborne et al., 2004; Osborne et al., 2007; Schoenfelder et al., 2010a). The term transcription factory was coined in the early 1990s to describe relatively immobile and stable foci of active extra-nucleolar transcription, 40-85nm in diameter (Chakalova et al., 2005; Chakalova and Fraser, 2010; Cook, 2010; Ghamari et al., 2013;

Iborra et al., 1996; Misteli, 2007; Papantonis and Cook, 2011; Razin et al., 2011; Sutherland and Bickmore, 2009). In erythroid nuclei in particular, in which there are relatively few transcription factories (100-300 foci) (Osborne et al., 2004), transcription factors have been shown to play an important part in facilitating the clustering of co-regulated genes. In erythroid cells, EKLF is required for the co-association of EKLF target genes at transcription factories in erythroid cells (Schoenfelder et al., 2010b).

Frequent enrichment for SC-35 splicing speckles within the vicinity of transcription factories suggests transcription factories may advantageously located within sub-nuclear compartments enriched for splicing factors and active RNA splicing. Speckles are highly active dynamic nuclear bodies enriched in pre-mRNA splicing factors implicated in facilitating the transcription of highly active genes (Hall et al., 2006). They have also themselves been suggested to be associated with the clustering and physical association of genes within regions active chromatin, although speckles are not extant in all cell types (Brown et al., 2008b; Brown et al., 2006; Shopland et al., 2003; Szczerbal and Bridger, 2010; Takizawa et al., 2008a).

Loci transcribed by RNAPII are also found to co-localise at the nuclear periphery and within proximity with nucleoli. The eukaryotic nucleus is separated from the cell by the nuclear envelope – a lipid bilayer impenetrable save for nuclear pore complexes (NPCs), which act as gateways and selectively controlling traffic across the nuclear envelope (NE) (Dingwall and Laskey, 1992). The nuclear lamina (NL) lines the interior membrane of the NE and components of the nuclear lamina associate with hundreds of 0.1-10Mb regions of chromatin called lamina-associated domains (LADs), which are characterised by a low gene density and transcriptional repression (Goldman et al., 2002; Guelen et al., 2008).

Changes in genome-nuclear lamina interactions are associated with tissue-specific changes in gene activity (Harmon and Sedat, 2005; Kind and van Steensel, 2010; Peric-Hupkes et al., 2010). Genes up-regulated during development have been shown to locate away from the nuclear periphery and towards the nuclear interior when active (Hewitt et al., 2004; Kosak et al., 2002; Lee et al., 2006a; Ragoczy et al., 2006; Williams et al., 2006; Yao et al., 2011; Zink et al., 2004) and the activation of gene expression is linked with the disassociation of LADs from the NL whereas gene silencing is associated with

the formation of new LADs (Peric-Hupkes et al., 2010). Artificial tethering of loci to the nuclear lamina has been shown to result in the silencing of genes targeted to the nuclear periphery and also adjacent genes (Reddy et al., 2008). The internalisation of genes not physically connected with the NL upon transcriptional activation has also been observed (Chambeyron and Bickmore, 2004; Chambeyron et al., 2005; Takizawa et al., 2008a). Movement towards the nuclear interior has been linked to the association of genes at functional nuclear sub-compartments associated with transcription and the processing of transcripts, including shared transcription factories (Xu and Cook, 2008) nuclear speckles (Brown et al., 2008b), PML, and Cajal bodies (Meister et al., 2010) (see figure 2). The latter are conglomerations of multiple different proteins that are implicated in modulating a variety of key processes, including gene expression and senescence (Lallemand-Breitenbach and de The, 2010; Machyna et al., 2013).

It should be noted however that there is considerable variation in the relationship between the radial position and activity among individual genes (Deniaud and Bickmore, 2009; Ferrai et al., 2010; Kosak et al., 2002; Takizawa et al., 2008b). Individual genes exhibit a differential response to artificial tethering to the nuclear lamina (Egecioglu and Brickner, 2011; Takizawa et al., 2008b) and, as the distribution of complexes involved in the regulation of chromatin folding and transcriptional regulation is not confined to the nuclear interior (Ferrai et al., 2010), an internal nuclear position is not *per se* required for transcription. Active genes and chromatin marks characteristic of transcriptionally active regions of chromatin have been observed at the nuclear periphery (Egecioglu and Brickner, 2011; Takizawa et al., 2008b) and NPC are enriched for euchromatin and active genes (Brown et al., 2008a; Capelson et al., 2010)**.** The nuclear periphery must therefore be considered to be involved in the spatial organization of both active and inactive regions of the genome.

When silenced, loci transcribed by RNAPII have also been shown to localise within nucleolus-associated domains (NADs) comprising loci transcribed by RNAPI, RNAPIII, and satellite DNA – arrays of tandem repeats – that are of a size similar to that of LADs (Nemeth et al., 2010). Partial overlap exists between the patterns of chromatin association with LADs and with NADs and both types of domain are re-formed following cell division (Nemeth et al., 2010; van Koningsbruggen et al., 2010). In *Drosophila*, inactive

loci have also been shown to co-associate at shared polycomb bodies - foci identified using 4C (Bantignies et al., 2011; Choi et al., 2011) and 6C (Tiwari et al., 2008a) that are enriched for polycomb proteins and repressive histone mark H3K27me3. PcG dependent networks of long-range interactions in *cis* and in *trans* have been identified in mammalian cells as well as in *Drosophila* (Bantignies et al., 2011; Choi et al., 2011; Hodgson and Brock, 2011; Pirrotta and Li, 2012; Simon and Kingston, 2009; Tiwari et al., 2008a; Tiwari et al., 2008b), although empirical evidence supporting a functional role for PcG mediated long-range chromatin interactions remains limited, particularly as regards their import in mammalian cells.

1.1.4 Topological chromatin domains

While multi-mega base scale sub-chromosomal compartments have so far only been identified in human and in mouse cells, the application of Hi-C and 5C techniques to the study of genome architecture has identified that folding of the chromatin fibre forms domains of a smaller size that partition the genome according to function in a manner that is conserved across species (Dixon et al., 2012; Nora et al., 2012; Sexton et al., 2012). The size of these domains, which are referred to as topologically associating domains (TAD) (see figure 2), ranges from tens to thousands of kilo bases in mice and humans, although the median size range is a few hundred-kilo bases. The organisation of the genome in to TADs in multiple human and mouse cell types appears to be conserved and while the organisation of A and B compartments reflects cell-cell variation in patters of transcriptional activity this does not appear to be the case with TAD. Moreover, while adjacent A and B domains are characterised by contracting states of transcriptional activity, this is not necessarily the case with TAD. On a similar scale, clustering of long-range interactions between enhancers and promoters, and between different gene promoters, has been shown to form three-dimensional chromatin domains (Bau et al., 2011; Li et al., 2012a; Shen et al., 2012) that appear to be involved in facilitating active transcription and in coordinating the transcriptional regulation of multiple genes, and perhaps also of enhancers encoding long-non coding RNAs.

Loci located within individual TADs preferentially interact, whereas interaction between loci located within separate domains is infrequent. As such individual TAD appear as largely discrete structures demarcated by a 'boundary' region (Dixon et al., 2012). These 'boundaries' between TADs appear to be conserved between different cell types across mammalian species and, in mammalian cells, correlate with regions of enrichment for histone modifications associated with heterochromatin (H3K27me3 and H3K9me2) and for insulator binding sites and bound architectural protein CTCF (Dixon et al., 2012; Nora et al., 2012). CTCF binding sites are highly prevalent throughout the genome (Phillips and Corces, 2009) and most CTCF bound sites are located within TADs, however CTCF is posited to act both as an insulator and a mediator of long-range chromatin interactions in conjunction with additional proteins, and in particular cohesin (Merkenschlager and Odom, 2013). TAD boundaries in *Drosophila melanogaster* cells are enriched for insulator protein binding, but also for DNase hypersensitivity (Sexton et al., 2012). In Drosophila, TAD boundaries are enriched for binding by mitotic spindle protein Chromator, which acts as an insulator protein and is enriched for at CTCF binding sites. CTCF binding sites in Drosophila are also enriched for additional Drosophila specific insulator proteins (Sexton et al., 2012; Van Bortle et al., 2012).

In mammalian embryonic stem cell and neural progenitor cell populations, conserved chromatin interactions spanning tens to hundreds of kilo-base pairs within TAD that are enriched for bound CTCF and cohesin comprise constant sub-domains within TAD (Phillips-Cremins et al., 2013). In the absence of CTCF and the cohesin sub-unit Smc1, the collapse of selected conserved interactions has been shown, suggesting binding by CTCF and cohesin may act to establish and/or stabilise conserved sub-domains within TAD. Data also suggest TAD contain a hierarchy of cell-type specific sub-domains enriched for promoter-enhancer interactions characterised by enrichment for bound tissue specific transcription factors. In embryonic stem cells, the topology of these sub-domains reflects cell-type specific differences in gene expression and has also been shown to correlate, to a certain degree, with enrichment for varying combinations CTCF, cohesin and mediator protein sub-unit and transcription factor binding at regions throughout the genome. In addition, it has been shown that the knockdown of the cohesin Smc1 or mediator Med12 subunits results in aberrant patterns of lineage-specific gene expression in embryonic stem cells (Phillips-Cremins et al., 2013).

1.1.5 Chromatin looping and long-range gene regulation

Looping of the chromatin fibre within the nucleus brings regulatory genomic elements, including gene promoters, enhancer elements, and insulator motifs, which may be located large distances apart within the linear genome sequence, into spatial proximity (Fraser and Bickmore, 2007). This juxtaposition of distal and proximal gene regulatory elements plays a key role in the regulation of transcription. Long-range chromosomal interactions between gene regulatory elements involved in promoting transcription have been identified for numerous loci in multiple models (Apostolou and Thanos, 2008; Fullwood et al., 2009; Hu et al., 2008; Liu and Garrard, 2005; Lomvardas et al., 2006; Noordermeer et al., 2011; Osborne et al., 2004; Osborne et al., 2007; Schoenfelder et al., 2010a; Simonis et al., 2006; Spilianakis and Flavell, 2004; Spilianakis et al., 2005) and a growing area of interest is the identification of pathogenic chromatin conformation signatures and the identification of disease associated regulatory element variants and changes in the genomic distribution of epigenetic marks that are associated with long-range transcriptional regulation (Crutchley et al., 2010; Gondor, 2013; Petrov et al., 2006).

Much of what is understood regarding long-range gene regulation and chromatin looping derives from study of the mouse globin genes in erythroid cells. The appropinquity of co-ordinately regulated genes with the β-globin LCR, which acts as a long-range enhancer of transcription, involves binding by transcription factors, including EKLF, GATA-1, and the LDB1 complex, to regulatory elements (Drissen et al., 2004; Jing et al., 2008; Schoenfelder et al., 2010b; Vakoc et al., 2005). In addition, CTCF is required for association of the LCR with active globin genes in *cis* (Noordermeer et al., 2011; Osborne et al., 2004; Palstra et al., 2008). Evidence presented by Noordermeer *et al* suggests the β-globin LCR acts as a long-distance enhancer of transcription in *cis* and also in *trans*, preferentially associating with globin genes regulated by shared transcription factors EKLF and GATA1 within a restricted nuclear sub-volume (Noordermeer et al., 2011). Interestingly, targeting LDB1 to the β-globin promoter has been shown to result in the up-regulation of β-globin expression that is dependent upon interaction with the β-globin LCR but not GATA-1 (Deng et al., 2012).

AT-rich binding protein SATB1 is implicated in the control of tissue-specific and cell-specific gene expression patterns via the establishment of specific (state dependent) loop structures that mediate interactions among *cis*-acting DNA regulatory motifs, the mediation of regional patterns of histone modification, and the recruitment of transcription factors, and chromatin modifiers, including the ATP-dependent chromatin-assembly factor (ACF), imitation switch (ISWI) chromatin remodelling proteins, and HDACs. Loss of SATB1 activity results profound changes in the spatial organisation of the chromatin fibre into distinct loop structures and widespread changes in gene expression (Cai et al., 2003; Cai et al., 2006; Galande et al., 2007; Han et al., 2008; Kumar et al., 2007; Yasui et al., 2002). The non-random distribution of SATB1 and PML proteins at matrix attachment regions (MARs) throughout the MHCI locus suggests a SATB1 acts as both a regulator of chromatin conformation and as structural component involved in tethering the chromatin fibre to PML bodies at matrix attachment regions (MARs) (Kumar et al., 2007).

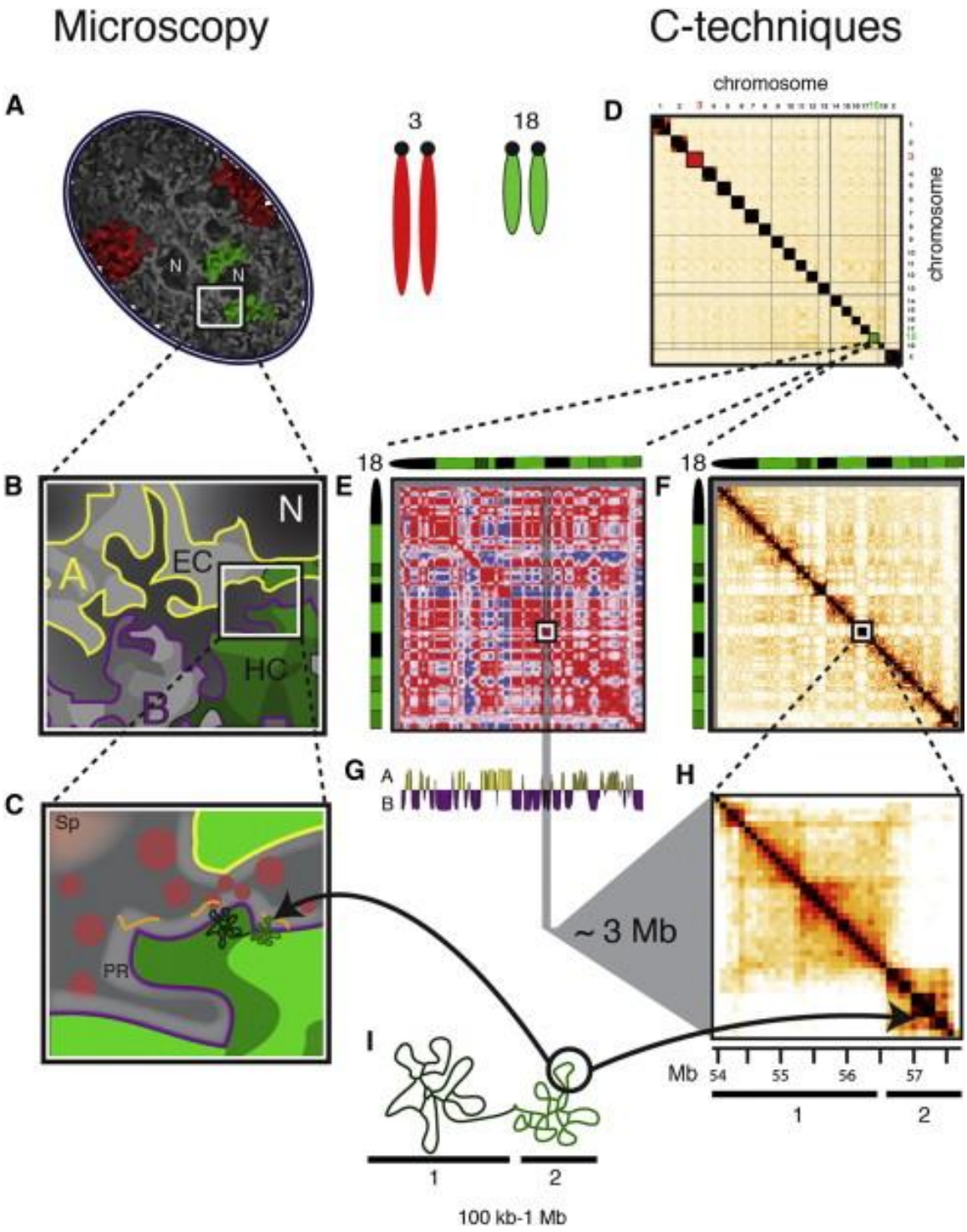

Figure 2 Spatial organization of the genome in a mammalian (mouse) nucleus (A) In eukaryotic nuclei, the nuclear space is divided into non-randomly arranged chromosome territories. Chromosome 3 and the territory corresponding to chromosome 3 are shown in red. In green, chromosome 18 and its corresponding territory are also shown. Also visible are regions of condensed and relatively de-condensed regions of DAPI stained DNA (grey) within and between CT and nucleoli (N). **(B)** A schematic showing a region of the

nucleus shown in A at higher resolution. A continuum of preferential chromosomal interactions forms A (yellow) and B (purple) compartments that partition chromosomes into regions of largely active (euchromatin, EC) or inactive chromatin (heterochromatin, HC), respectively. **(C)** A detailed hypothetical representation of chromatin domains visualized using Hi-C and the surrounding nuclear landscape. The schematic shows the spatial organization of factors within the nucleus into foci or nuclear bodies (pink circles), including splicing speckles (SP). Clusters of chromatin interactions associated with the co-localisation of multiple loci at foci within the perichromatin region (PR) are shown in green in (C) and also in (I). RNA is shown in orange. **(D)** Hi-C chromatin interaction matrix showing interactions between and within all chromosomes in the mouse genome. **(E)** Chromosome 18 Hi-C interaction matrix transformed using Pearson correlation to compare regional interaction profiles. Two domains, red and blue, characterised by distinct interaction profiles are visible **(F)** Chromosome 18 Hi-C interaction matrix of equivalent resolution to (E). **(G)** Further analysis of (E) reveals chromosomal interactions are partitioned into two distinct compartments, called A and B compartments. **(H)** Higher resolution interaction matrix showing a 3Mb region of (F) and the organisation of the chromatin fibre into two mega-base scale domains called TAD within this region. **(I)** Schematic representation of TADs 1 and 2 visible in (H). This figure is based upon data previously published by Zhang et al, 2012 (Zhang et al., 2012) and was reproduced from Gibcus and Dekker, 2013 (Gibcus and Dekker, 2013) with the permission of Elsevier B. V.

1.2 The epidermis: its structure, development and the maintenance of epidermal barrier function

Adult skin is a complex protective and sensory bicompartmental organ. The outermost compartment, the epidermis, is a self-renewing stratified squamous epithelial sheet that comprises a range of integument types, including interfollicular epidermis (IFE), glabrous palmar and plantar skin, and regions of hair, feathers and scales. Separated from the dermal compartment of the skin by a basement membrane of ECM proteins and growth factors, the IFE functions as an essential permeability barrier preventing transcutaneous loss of water and electrolytes and the penetration of radiation in a terrestrial environment. A multiplicity of cell types reside within the IFE; the predominate cell type, keratinocytes, are responsible for epidermal cohesion, barrier function and renewal predominate; also present are bone marrow derived cells involved in immune surveillance and neural crest derived cells involved in pigmentation, among others (Fuchs and Raghavan, 2002; Nestle et al., 2009).

Disruption of the balance between proliferation and differentiation within the epidermis can result in epidermal or pellage abnormalities and is associated with a number of human skin diseases, including hyperproliferative disorders such as psoriasis, and basal- and squamous-cell carcinomas. The use of genetic mouse models and *in vitro* keratinocyte and epidermal explant culture models has proven instrumental in identifying and studying the function of individual cytoarchitectural proteins, cell signalling molecules and transcription factors in the epidermis. However, the scope of reductionist approaches in studying the mechanisms necessary to balance proliferation and differentiation during epidermal morphogenesis and homeostasis is limited. A growing body of evidence that indicates interconnected gene regulatory networks operate to specify cell type, state and function is being generated in the wake of technological advances enabling the efficient analysis of the different structural and functional elements of large genomic regions and entire genomes. Systematic approaches to the study of transcriptional regulation in the epidermis implicate an array of epigenetic mechanisms in the regulation of gene expression within the epidermis and link alterations in nuclear shape, nuclear architecture and the spatial organisation of chromatin within keratinocyte nuclei with changes in the transcriptional sate of epidermal keratinocytes.

1.1.6 Epidermal ontogenesis and homeostasis

Barrier function of the IFE is established *in utero* (between E8.5 and E18.5 in mice) with the completion of epidermal stratification and is maintained through life-long self-renewal. Following gastrulation, cells of the surface ectoderm commit to an epidermal cell fate in response to an initial inductive signal and, between E8.5 and E12.5, a monolayer of mitotically active multipotent epidermal cells expressing cytokeratins K5 and K14 is formed (Hardman et al., 1998). Between E12.5-E14.5 stratification of the developing IFE is initiated as these K5/K14 positive basal keratinocytes give rise to a proliferative intermediate layer characterised by apical-basal cell polarity (Koster and Roop, 2007; Smart, 1970).

Although the exact nature of this inductive signal is not yet known, commitment of the surface ectoderm to epidermal differentiation coincides with an increase in levels of Wnt signalling, which in turn leads to the elevated expression of bone morphogenic proteins (BMPs) (Fuchs, 2007; Stern, 2005), and with the induction of p63 expression. A homologue of p53, p63 is implicated in orchestrating the transcriptional up-regulation of epidermal genes and markers of epidermal differentiation required for epidermal specification and deposition of the epidermal basement membrane (Koster et al., 2006; Koster et al., 2004; Koster and Roop, 2007; Medawar et al., 2008; Shalom-Feuerstein et al., 2011). Extensive regions of p63 deficient epithelium remain as a monolayer expressing ectodermal cytokeratins K8 and K18 and $p63^{-/-}$ mice (figure 3) die perinatally due to dehydration resulting from lack of an epidermal barrier (Koster et al., 2004; Mills et al., 1999; Shalom-Feuerstein et al., 2011; Yang et al., 1999). Of note, p63 has been shown to regulate, and in some cases be regulated by, key signalling pathways required for ectodermal appendage organogenesis and epidermal development, including the Wnt/β-catenein and BMP pathways pathways (Bergholz and Xiao, 2012; Laurikkala et al., 2006).

At ~E15.5, the spinous layer of the epidermis is formed (Koster and Roop, 2007; Lechler and Fuchs, 2005; Smart, 1970). Spinous keratinocytes remain transcriptionally active and produce a durable cytoskeletal matrix. Basal K5/K14 expression is succeeded by the copious expression of K1 and K10, forming a resilient filaments network interconnected

with robust desmosomal intercellular junctions. At ~E16.5, as keratinocytes enter the next stage of maturation, the granular layer, K1/K10 expression is reduced, lipid lamellar and keratohylin granules are produced, and a tough proteinaceous layer, the cornified envelope (CE), is formed beneath the plasma membrane (Marshall et al., 2001).

The culmination of the epidermal stratification process is the formation of the corneal layer (Hardman et al., 1998), which occurs between E16.5 and E18.5. At this final stage of terminal differentiation, keratinocytes become metabolically inactive. In response to an influx of calcium, the cell plasma membrane is replaced as transglutaminases cross-link CE proteins with durable γ-glutamyl-ε-lysine bonds. Nuclei and organelles are degraded and keratinocytes become flattened forming squames filled with a dense network of keratins as filaggrin released from keratohylin granules promotes the aggregation of keratins. A matrix composed of secreted intercellular lipid becomes covalently bound to cross-linked CE proteins, forming a lipid encasement around corneocytes that protects against water loss, potentially harmful soluble environmental factors, and confers flexibility to the epidermal barrier (Bickenbach et al., 1995; Hardman et al., 1998; Marshall et al., 2001; Segre, 2003).

A.

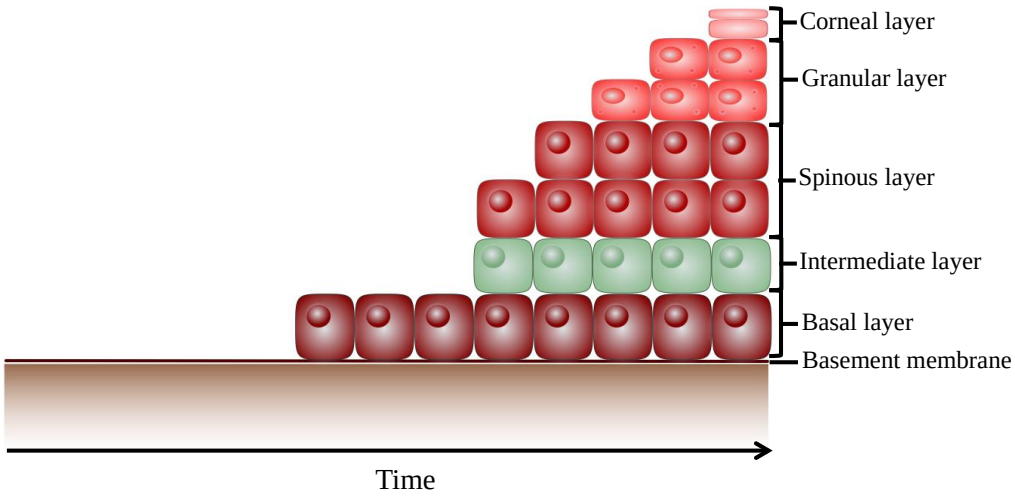

B.

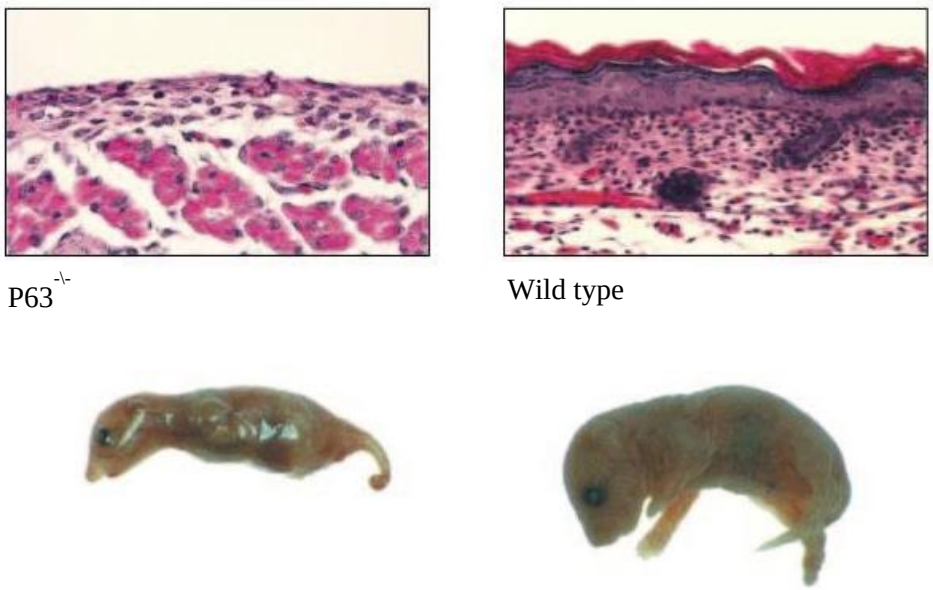

Figure 3. Stratification of the murine interfollicular epidermal barrier during epidermal ontogenesis occurs systematically between E8.5 and E18.5 and requires the expression of p63. (A) The epidermis is a stratified epithelial sheet. Between E8.5 and E12.5 cells of the surface ectoderm undergo commitment to epidermal differentiation. Multipotent committed epidermal cells subsequently give rise systematically to the spinous, granular, and corneal supra-basal epidermal layers between E15.5 and E18.5. An intermediate layer forms transiently at ~E14.5 and is replaced by development of the spinous layer at ~E15.5. Last to form is the outermost, cornified layer, which waterproofs the skin. (**B-C)** Epidermal development is arrested at an early stage in

P63 null mice. Failure to form a stratified epidermis prior to birth results in perinatal death due to desiccation. Figure adapted from Koster and Roop (Koster and Roop, 2007).

Within the adult IFE, a heterogeneous population of progenitor cells resides contiguous with the basement membrane. Quiescent adult epidermal stem cells strongly attach to the basement membrane and appear to be activated predominantly only following injury to the epidermis. During epidermal homeostasis, a basal population of more actively cycling committed progenitor cells with reduced plasticity gives rise to differentiated progeny and is renewed through a stochastic but population balanced pattern of cell fate specification among daughter cells (Blanpain and Simons, 2013; Mascre et al., 2012; Schluter et al., 2011). Squames continually slough from the corneal layer of the IFE during adult life (Milstone, 2004) and in undamaged skin the corneal layer is continually replenished as committed progenitor cells periodically withdraw from the cell cycle, undergo asymmetric cell division, and give rise to differentiating basal keratinocytes. Differentiating basal keratinocytes subsequently execute a program of terminal differentiation that closely recapitulates the process of keratinocyte differentiation during epidermal morphogenesis and distinct transcriptional stages mark the transition of differentiating suprabasal keratinocytes as they give rise to the spinous, granular, and eventually corneal layers of the epidermis (figure 4). The basal population of committed progenitor cells within the epidermis appears to be maintained by a population-based balance of stochastic cell fate decisions (Blanpain and Simons, 2013; Mascre et al., 2012; Schluter et al., 2011).

A combination of intrinsic cues and micro-environmental stimuli is understood to facilitate this process of homeostatic epidermal renewal (epidermopoiesis). Several cytoarchitectural proteins, components of the mitotic apparatus (Simpson et al., 2011), cell signalling molecules, and transcription factors (Dai and Segre, 2004; Fuchs and Raghavan, 2002) that play an important role in regulating the maintenance of a basal progenitor cell population in the epidermis and in regulating cell cycle arrest and commitment to differentiation have been identified. Key regulators of epidermal stem and progenitor cell activity and epidermopoiesis already identified include Notch and its ligands, and the transcription factors p63 and c-Myc (see below).

In the postnatal epidermis Notch and its ligands are differentially expressed and together regulate epidermopoiesis (Blanpain et al., 2006; Nickoloff et al., 2002; Rangarajan et al., 2001). Delta-like 1 signalling is implicated in keratinocyte stem cell cluster cohesion and the initiation of differentiation in contiguous committed progenitor cells (Lowell et al., 2000; Rangarajan et al., 2001). Notch/Jagged 1 signalling, on the other hand, has an apparent role in in later stages of keratinocyte maturation, including cornification, which appear to be regulated by NF-κB and PPAR dependent Notch/Jagged 1 signalling (Nickoloff et al., 2002).

Notch signalling within the epidermis is modulated by cross-talk with p63, which in turn is regulated by Notch signalling (Nguyen et al., 2006). The expression of p63 in basal keratinocytes is required for epidermal stratification and has essential pleiotropic functions in facilitating cell survival, proliferation, cell cycle arrest and the initiation of differentiation in the epidermis. The ontology of gene and protein regulated by p63 in basal keratinocytes is diverse and includes several of the cell-cycle regulatory machinery (Beretta et al., 2005; McDade et al., 2011; Pellegrini et al., 2001; Testoni and Mantovani, 2006) as well as genes and proteins associated with cell adhesion, cell signalling, and chromatin remodelling (see section 1.1.7) (Ferone et al., 2013; Ihrie et al., 2006; Ihrie et al., 2005; Kouwenhoven et al., 2010; Nguyen et al., 2006; Okuyama et al., 2007; Westfall et al., 2003; Wu et al., 2012).

In suprabasal layers, the depletion of p63 isoform ΔNp63 (the predominate p63 isoform in the epidermis) is required for keratinocyte maturation (King et al., 2003; Nguyen et al., 2006; Parsa et al., 1999). Dlx3 mediated proteosomal degradation (Di Costanzo et al., 2009; Moretti and Costanzo, 2009; Rossi et al., 2006), C/EBP DNA binding (Lopez et al., 2009), and Notch signalling (Nguyen et al., 2006) drive the suprabasal depletion of ΔNp63, thereby enabling the expression of suprabasal differentiation specific genes supressed by ΔNp63 in basal keratinocytes. Supra basal p63 expression is also restricted by the p63-specific microRNA (miR203) (Yi et al., 2008). In the absence of p63 in maturing keratinocytes, factors required for terminal differentiation, including ZNF750 (Sen et al., 2012) Klf genes (Li et al., 2012b; Segre et al., 1999) IKKα (Candi et al., 2006; Hu et al., 1999; Hu et al., 2001; Li et al., 1999) and Dlx3 (Morasso et al., 1996), are up-regulated.

A downstream target of p63 (Sen et al., 2012), the proto-oncogene c-Myc plays a key role in balancing of proliferation and differentiation in the epidermis. Activation of c-Myc induces epidermal stem cells to exit the stem cell niche, initiating the proliferation and differentiation of stem cell progeny (Arnold and Watt, 2001; Frye et al., 2003; Frye and Watt, 2006). In co-operation with the co-repressor SIN3A, c-Myc directly regulates the expression of genes encoded within the EDC that are required for terminal differentiation and acts to simultaneously recruit and displace discrete clusters of transcriptional regulators present at EDC regulatory regions, including KLF4 and OVOL1 (recruited) and C/EBPα, MXI1, and SIN3A (displaced). SIN3A and c-Myc also cooperatively regulate the expression of genes located outside of the EDC that involved in the control of cell growth and proliferation. The K14-Cre mediated epidermal deletion of SIN3A alone results in the aberrant post-translational processing of c-Myc and increased epidermal proliferation (Nascimento et al., 2011).

Additional factors required for normal epidermal proliferation and keratinocyte differentiation include basally expressed factors such as the transcriptional co-activator Yes-activated protein (YAP), which binds members of the transcription enhancer activator domain (TEAD) family of transcription factors (Schlegelmilch et al., 2011; Zhang et al., 2011), and basonuclin, which appears to stimulate rRNA synthesis (Tseng et al., 1999); suprabasally expressed factors required for terminal keratinocyte differentiation such as Blimp1 (Chiang et al., 2013; Magnusdottir et al., 2007; Sellheyer and Krahl, 2010), members of the Oct class of POU domain transcription factors (Andersen et al., 1997; Faus et al., 1994), basic helix-loop-helix protein ARNT (Geng et al., 2006) and GRHL3 (Auden et al., 2006; Mistry et al., 2012; Ting et al., 2005a; Ting et al., 2005b; Yu et al., 2006); and members of the AP1, AP2 and Sp1 transcription factor families, which are expressed both basally and in suprabasal layers (Byrne et al., 1994; Casatorres et al., 1994; DiSepio et al., 1995; Efimova et al., 1998; Jang et al., 2000; Jang et al., 1996; LaPres and Hudson, 1996; Leask et al., 1991; Sinha et al., 2000; Sinha and Fuchs, 2001).

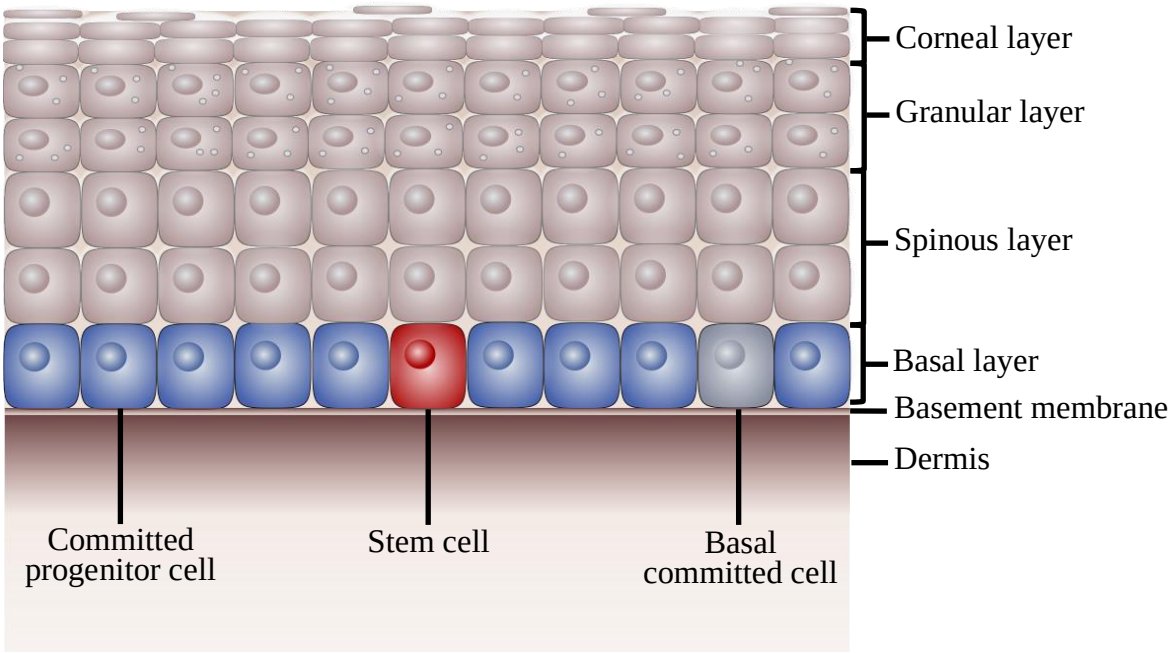

Figure 4 Hierarchical organisation of the interfollicular epidermis. Adult stem cells, committed progenitors cells with reduced plasticity, and differentiated keratinocytes are found within the basal epidermal layer while suprabasal layers of the epidermis comprise solely of terminally differentiating keratinocytes. Following differentiation, keratinocytes disconnect from the basement membrane, stratify, and transit through distinct transcriptional stages as they migrate progressively towards the surface of the epidermis and give rise successively to layers of the suprabasal epidermal compartment. Finally, differentiated keratinocytes are shed from the outer surface of the corneal layer. In undamaged skin, adult epidermal stem cells remain largely quiescent, becoming active following injury to the epidermis. More actively cycling committed progenitor cells of the interfollicular epidermis act to maintain the integrity of the epidermis by giving rise to terminally differentiating daughter cells.

1.1.7 The role of epigenetic mechanisms and spatial nuclear organisation in the regulation of epidermal proliferation and differentiation

Dynamic changes in chromatin folding and chromatin state play an important role in regulating the survival, proliferation and differentiation of progenitor cells and their progeny. An array of epigenetic regulators that regulate these processes within the

epidermis has been identified, including regulators of histone methylation (Driskell et al., 2012; Ezhkova et al., 2011; Ezhkova et al., 2009; Luis et al., 2011; Mejetta et al., 2011; Sen et al., 2008) and acetylation (LeBoeuf et al., 2010; Nascimento et al., 2011), regulators of DNA methylation (Sen et al., 2010), and factors involved in chromatin remodelling (Bao et al., 2013; Fessing et al., 2011; Indra et al., 2005; Kashiwagi et al., 2007; Mulder et al., 2012). Evidence from the large-scale RNA interference based analysis of the function of epigenetic regulators in epidermal progenitor cells suggests heterogeneous groups of factors, which are involved in diverse epigenetic mechanisms of transcriptional regulation, operate to regulate the expression of genes involved in either promoting progenitor cell renewal or differentiation, including a number of genes known to be regulated by p63 (Mulder et al., 2012).

P63 binds a genome-wide array of targets in keratinocytes (Kouwenhoven et al., 2010). In addition, a significant number of chromatin factors, including histone methyltransferases EZH1 and EZH2, several Polycomb complex components, and chromatin remodellers, including CHD4, BRG1, and SATB1, exhibit altered expression patterns within the epidermis of $P63^{-/-}$ mice. (Fessing et al., 2011). Findings suggest that key epigenetic and genetic regulatory pathways within the epidermis interconnect, however knowledge of the epigenetic mechanisms controlling and coordinating cell fate specification and differentiation during the morphogenesis and homeostasis of the skin, and not least the IFE, remains highly limited (Botchkarev et al., 2012; Cangkrama et al., 2013).

1.1.7.1 The role of DNA methylation in regulating epidermal proliferation and differentiation

DNA methylation occurs post-replication and in vertebrates primarily results in the modification of CpG dinucleotides. CpG methylation is predominantly maintained by maintenance DNA methyltransferase termed DNA (cytosine-5)-methyltransferase 1 (DNMT1), which is recruited to the replication fork during cell division. The SRA (Set and RING-finger-associated domain) domain protein UHRF1 acts to recruit DNMT1 to replicated DNA and works in concert with DNMT1 to regulate the maintenance of DNA methylation as well as to facilitate cross-talk between methylated H3K9 and DNA methylation (Liu et al., 2013; Sharif and Koseki, 2011; Smith and Meissner, 2013).

Demethylation of many epidermal differentiation-specific gene promoters occurs during keratinocyte differentiation. Within epidermal progenitor cells, a significant number of epidermal differentiation gene promoters, including several EDC gene promoters, are methylated. DNMT1 and UHRF1 are expressed basal keratinocytes where they act in concert to repress differentiation genes and to maintain the proliferative capacity of basal keratinocytes, at least in part via regulating expression of the INK4b-ARF-INK4a locus, which encodes members of the INK4 family of cyclin-dependent kinase inhibitors, p15 (INK4b) and p16 (INK4a). GADD45 proteins in turn appear to act in opposition to DNMT1-UHRF1 to promote active DNA demethylation as required for keratinocyte differentiation (Sen et al., 2010).

The promoters of differentiation specific genes activated by C/EBPα are, on the contrary, methylated. CpG methylation of the CRE sequence (TGACGTCA) is crucial in determining C/EBPα mediated activation. DNMT1 or 5-azacytidine induced CRE demethylation in keratinocytes cultured *in vitro* perturbs C/EBPα binding and the activation of C/EBPα mediated differentiation gene activation (Rishi et al., 2010). Global changes in CpG methylation and methylation-dependent changes in gene expression have also been shown to characterise Psoriatic skin (Roberson et al., 2012). The expression of EDC differentiation specific genes is also, differentially, affected by 5-azacytidine treatment of keratinocytes cultured *in vitro* (Elder and Zhao, 2002) in a manner consistent with the suggestion DNA methylation acts to promote both gene repression and gene activation within the epidermis.

1.1.7.2 Post translational histone modifications and the maintenance of epidermal progenitor state and function by histone methyltransferases

Specific covalent post-translational modifications of histone tail residues influence chromatin architecture and transcriptional state. Modifications identified include methylation, phosphorylation, and acetylation, amongst a plethora of others. Enzymes functioning to deposit or remove histone marks have been demonstrated to act in a site-specific manner and are often components of multiprotein complexes involved in the regulation of gene expression or other facets of genome function. The ‘‘histone code’’

hypothesis proposes combinations of post-translational histone modifications comprise, in addition to regulatory DNA elements, an additional source of information involved in the regulation of transcription and other facets of genome regulation (Allis et al., 2007; Fischle et al., 2003).

The regulation of histone modification dynamics is a key part of transcriptional regulation and the preservation or transmutation of global patterns of histone modification has been linked to senescence, pathogenesis, and heredity. The hyper-acetylation of histones characterises regions of active chromatin whereas repressive modifications typical of condensed, inactive regions of chromatin include tri-methylation of histone H3 lysine 9 (H3K9me3) and lysine 27 (H3K27me3) residues. Histone modifications have also been linked to the long-range regulation of transcriptional repression or activation by insulator motifs and cis-acting enhancer elements with promoter regions through chromatin looping, although it is not yet known whether histone modification is a consequence of looping or a causal factor driving the formation of chromatin loops involved in long-range gene regulation (Fischle et al., 2003; Greer and Shi, 2012; Wang et al., 2004).

High levels of repressive histone marks H3K9me3 and H4K20me3 and low levels of H4 acetylation and of H4K20 monomethylation mark quiescent epidermal stem cells. Activation stimulated by c-Myc results in the genome-wide re-patterning of histone methylation mediated, at least in part, the H4K20 specific methyltransferase SET domain-containing protein 8 (Set8) (Driskell et al., 2012; Frank et al., 2001; Frye et al., 2007; Wanzel et al., 2003). Set8 is targeted by c-Myc and operates to control programmes of proliferation and differentiation initiated by c-Myc. Set8 is essential for the survival of epidermal stem cells where it acts to inhibit apoptosis by promoting the expression of ΔNP63 and the repression of p53 (Driskell et al., 2012). Components of the vertebrate trithorax-group (TrxG) MLL/SET complex, histone methyltransferases MLL2 and WDR5 (Schuettengruber et al., 2011) regulate progenitor cell expression of GRHL3 differentiation specific target genes, including Polycomb-repressed genes and genes silenced independent of PcG repression in basal keratinocytes (Hopkin et al., 2012).

1.1.7.3 Histone acetyl and de-acetyl transferase complexes regulate progenitor cell renewal and keratinocyte differentiation

Global re-patterning of histone acetylation also accompanies the c-Myc induced differentiation of epidermal stem cells and may involve both the c-Myc dependent addition and removal of acetyl moieties from H4 lysine tails (Frank et al., 2001; Frye et al., 2007; Wanzel et al., 2003). Both the *in vitro* treatment of cultured keratinocytes with either of the HDAC inhibitors trichostatin A (TSA) or sodium butyrate (Elder and Zhao, 2002; Saunders et al., 1999) and the treatment of skin explant cultures with TSA (Markova et al., 2007) causes cell-cycle arrest and induces the selective up-regulation of differentiation specific genes (Elder and Zhao, 2002; Markova et al., 2007; Saunders et al., 1999). However, perturbation of HDAC activity leads to a reduction, rather than an increase, in the expression level of a number of EDC differentiation-specific genes. Notably, perturbation of HDAC activity leads to a reduction in the expression profilaggrin (Markova et al., 2007), aberrations in which are linked to the genesis of several epidermal barrier and atopic disorders (Sandilands et al., 2009). Study of the downstream effects of the knockdown of basic helix-loop-helix protein ARNT in keratinocytes cultured *in vitro* suggests HDACs may act to mediate regulation of the AREG/EGFR pathway by ARNT and the expression of terminal differentiation specific genes modulated by ARNT (Robertson et al., 2012).

The activity of HDAC1 and HDAC2 has been shown to be necessary in maintaining the survival and proliferative capacity of basal keratinocytes. K14-Cre driven deletion of both HDAC1 and HDAC2 during embryonic development precludes epidermal stratification and results in the ectopic expression of negatively regulated ΔNp63 targets involved in regulating cell cycle progression, including p21, 14-3-3σ, and p16(INK4a) (LeBoeuf et al., 2010). HDAC1 and HDAC2 bind and actively acetylate promoters belonging to this subset of ΔNp63 targets, suggesting the activity of HDAC1 and HDAC2 is required to repress the expression of cell cycle inhibitor genes negatively regulated by ΔNp63 (LeBoeuf et al., 2010). While the absence of either HDAC1 or HDAC2 does not appear to impact upon epidermal development, although HDAC1 null mice exhibit hypertrophic scaring in response to wounding, the complete deletion of HDAC1 and ablation of only one HDAC2 allele results in epidermal hyperproliferation, alopecia, and increased

tumorigenesis. HDAC1 null mice expressing only one HDAC allele also exhibit corneal layer abnormalities resulting from aberrant EDC gene expression reminiscent of a lack of SIN3A activity (Winter et al., 2013).

A complex of the MORF complex, ING5 binds trimethylated H3K4 histone and forms a complex with the bromodomain-PHD finger protein BRPF1, which promotes the acetylation of histone H3 (Ullah et al., 2008). In keratinocytes, ING5 has been shown comprise part of a group of epigenetic factors implicated in promoting epidermal progenitor cell self-renewal. In addition, p63 has been shown localise at ING5 target genes, including genes encoding integrins involved in the cohesion and attachment of actively cycling basal keratinocytes with the basement membrane, although physical interaction between p63 and ING5 has not been demonstrated (Mulder et al., 2012).

1.1.7.4 The role of Polycomb repressor complex proteins in mediating epidermal cell survival, proliferation and differentiation

Multi-protein polycomb group (PcG) complexes control a wide array of developmental pathways and are indispensable for the development of multicellular organisms. In mammals two polycomb repressive complexes, PRC1 and PRC2, are recruited to chromatin by transcription factors and non-coding RNAs, where they act to promote transcriptional silencing through the modification of histone tail residues and higher-order structure of chromatin (Bantignies and Cavalli, 2011; Morey and Helin, 2010). In the skin, PcG proteins are expressed throughout the epidermal compartment and show differential patterns of expression during development, under pathological conditions, or following insult to the skin. In basal and suprabasal layers they appear to play an important role in regulating keratinocyte survival, proliferation, differentiation and apoptosis (Eckert et al., 2011; Mulder et al., 2012).

EZH2, the catalytic polycomb repressor complex 2 (PRC2) subunit responsible for methylating H3K27 (Margueron and Reinberg, 2011), is predominantly expressed in rapidly cycling embryonic progenitor cells where it acts to maintain the proliferative capacity of progenitors and to supresses the premature expression of multiple differentiation specific genes during embryonic development, notably by blocking the

recruitment of AP1 factors to EDC genes (Ezhkova et al., 2009). Specifically affecting keratinocytes of the neonatal basal epidermal compartment, conditional deletion of PRC2 associated protein Jarid2 leads to reduced levels of PRC2 occupancy and of H3K27 trimethylation at differentiation specific gene promoters, and the ectopic expression of differentiation specific genes, many of which are also targets of EZH2 mediated gene silencing (Ezhkova et al., 2009; Mejetta et al., 2011).

Conversely, the H3K27 demethylase JMJD3 acts to reverse H3K27me3 mediated gene repression, promoting the expression of EDC differentiation specific genes (Sen et al., 2008). *In vitro,* the mammalian *Grainyhead* homologue GRHL2 acts to inhibit the recruitment of JMJD3 to EDC gene promoters thereby preventing premature keratinocyte differentiation (Chen et al., 2012). In addition, GRHL3 appears to act to promote the up-regulation of EDC gene expression and *in vitro* keratinocyte differentiation via the recruitment of the mammalian trithorax group H3K4 methyltransferases MLL2 and WDR5 to the EDC (Hopkin et al., 2012). It is interesting to note, however, that a role for H3K27 trimethylation in meditating the expression of differentiation genes *in vivo* in adult epidermis has not been identified, although H3K27 trimethylation does appear to act to some degree to control proliferative capacity of basal keratinocytes by regulating activity of the INK4b-ARF-INK4a locus (Ezhkova et al., 2011; Ezhkova et al., 2009).

A component of the polycomb repressive 1 (PRC1) complex (Schwartz and Pirrotta, 2013), CBX4 acts in concert with, as well as independently of, PcG proteins to maintain epidermal stem cell quiescence and longevity (Luis et al., 2011). PRC-dependent CBX4 activity acts to prevent the senescence of epidermal stem cells, in part through the suppression of INK4A/p16 (Luis et al., 2011) Independent of PRC proteins, CBX4 acts as a SUMO-protein E3 ligase (Schwartz and Pirrotta, 2013) to prevent the proliferation and differentiation of epidermal stem cells (Luis et al., 2011). BMI1, another component of PRC1 (Schwartz and Pirrotta, 2013), also supresses expression of p16(INK4A) and is present at reduced levels in the epidermis of ichthyotic and prematurely aged skin (Cordisco et al., 2010). The ectopic expression of BMI1 is also associated with aberrant expression of selected cyclin D kinases and altered keratinocyte proliferation and survival (Cordisco et al., 2010; Lee et al., 2008).

1.1.7.5 Chromatin remodellers and remodelling in progenitor and differentiating cell populations within the epidermis

Collectively, the ATP-dependent chromatin remodelling complexes utilise ATP hydrolysis to actively transform the structure of chromatin through the modification of composition of histones and re-arrangement of the association of nucleosomes and DNA. ATP-dependent chromatin remodelling complexes contain an ATPase subunit belonging to the SNF2 family of helicase-related proteins and are categorised as belonging either to SWI/SNF, ISWI, or CHD groups according to the identity of this subunit (Narlikar et al., 2013). Epidermal ontogenesis is dependent upon the activity of CHD4, a subunit belonging to the CHD ATP-dependent remodelling complex group, which appears to play an important role in determining the capacity of basal keratinocytes to self-renew and fuel differentiation during embryonic development (Kashiwagi et al., 2007).

The mammalian SWI/SNF ATP-dependent chromatin-remodelling complex contains either ATP catalytic subunits BRG1 (SMARCA4) or BRM (SMARCA2) and comprises an additional 11 subunits (Martens and Winston, 2003). Deletion of BRG1 during epidermal stratification severely impairs development of the corneal envelope and epidermal barrier function. Whilst BRM deletion alone does not appear to impair epidermal differentiation, the deletion of both BRG1 and BRM results in increased suprabasal abnormalities, suggesting partial BRG1-BRM redundancy (Indra et al., 2005).

BRG1/BRM knockdown also leads to an increase in levels of Klf4 (Bao et al., 2013) Actin-like 6a (ACTL6a) appears to act in concert with SWI/SNF ATP-dependent chromatin-remodelling complex to regulate cell state in the epidermal basal layer. Mainly expressed within the basal layer, ACTL6a is required to maintain proliferation and to repress premature differentiation, in part via SWI/SNF induced expression of KLF4 (Bao et al., 2013). Another member of the SWI/SNF family of ATP-dependent chromatin remodelling proteins, SMARCA5 has been shown to form a complex with the ING5 and BPTF HAT complex, EZH2, and UHRF1, which regulates the expression of a broad array of genes required for the maintenance of epidermal progenitor self-renewal (Mulder et al., 2012).

Special AT-Rich Sequence Binding Protein 1 (SATB1) binds DNA, in particular the nuclear matrix attachment regions of DNA, and recruits a broad spectrum of chromatin modifiers and transcription factors to establish tissue-specific patterns of gene expression (Alvarez, 2000; Cai et al., 2003; Cai et al., 2006; Han et al., 2008; Kumar et al., 2007; Yasui et al., 2002). A direct regulatory target of p63, SATB1 directly binds multiple sites at the EDC, keratin type I and II loci, and the keratin-associated protein locus. SATB1 deficiency results in changes in the spatial organisation of the chromatin fibre at the EDC locus, down regulation of a number of EDC genes, reduced epidermal thickness and aberrant terminal differentiation. Analysis of the distribution of SATB1 binding events at the EDC locus suggests SATB1 acts to regulate transcription at the EDC through regulation of chromatin folding at the EDC locus rather than by targeting the core promoter regions of EDC genes (Fessing et al., 2011).

In basal keratinocytes of the developing murine epidermis, developmentally regulated changes in the spatial position of the lineage-specific EDC locus coincide with the beginnings of a gradual increase in the expression level of differentiation-specific genes encoded at the EDC during epidermal stratification. While the inactive murine EDC locus is preferentially situated towards the nuclear periphery, p63-depedent translocation of the active EDC locus towards the nuclear interior during epidermal stratification results in heightened spatial association between the EDC locus and splicing speckles. Notably, while the nuclear position of the EDC locus is changed during stratification, that of loci flanking the EDC that encode ‘housekeeping’ genes is not (Mardaryev et al., 2014).

1.1.7.6 Remodelling of the architecture of keratinocyte nuclei occurs during epidermal differentiation

Cell shape, nuclear shape, and nuclear architecture are altered during keratinocyte differentiation. Changes in nuclear size, shape, and the structure of nucleoli occur within the outermost layer of the granular compartment preceding the termination of RNA synthesis and programmed nuclear degradation (Karasek et al., 1972). Alterations in nuclear morphology and ultrastructure also occur during the transit of maturing keratinocytes from basal to granular layers and are associated with aberrant keratinocyte

maturation (Gdula et al., 2013; Tsuji and Cox, 1977). Analysis of three-dimensional nuclear organisation in murine plantar keratinocytes *in vivo* has revealed changing patterns in the physical association of chromosome territory 3, nucleoli, and pericentromeric heterochromatin clusters accompany the differentiation of keratinocytes as they detach from the basement membrane, stratify, and move towards the epidermal surface. In addition to a reduction in the expression of markers of active transcription as keratinocytes transit from spinous to granular layers (figure 5 A-C), a reduction in nuclear volume and numbers of nucleoli is also seen (figure 5 D). Conversely, an increase in pericentromeric heterochromatin clusters, which comprise transcriptionally inactive repetitive regions of chromatin, is observed. In addition, the nuclear arrangement of nucleoli in differentiating keratinocytes shifts from predominantly peripheral to mostly internal as cells exit the basal layer and stratify and an increase in spatial proximity between nucleoli, heterochromatin clusters, and CT3 is seen as keratinocytes progress towards the corneal layer, transcriptional silencing, and programmed nuclear degradation (figure 5 E) (Gdula et al., 2013). Together, these findings suggest widespread changes in the transcriptional landscape of the keratinocyte nucleus occur as keratinocytes differentiate.

Of note, changes in keratinocyte cell shape effect changes in keratinocyte gene expression that are mediated by transcription factor SRF, actins, and HDAC activity (Connelly et al., 2010; Connelly et al., 2011; Luxenburg et al., 2011; Simpson et al., 2011). Changes in cell shape induced via the manipulation of the size and shape of micro-patterned substratum areas have been shown to induce changes in proliferation and in the expression of differentiation specific genes in keratinocytes *in vitro* (Connelly et al., 2010; Connelly et al., 2011; Watt et al., 1988). Correspondingly, a separate study has shown that varying substratum micro-pattern results in cytoskeletal actin dependent, coordinated, changes in endothelial cell and nuclear size and shape that effect changes in cell proliferation and organisation of the chromatin fibre (Versaevel et al., 2012). Adhesion to the basement membrane is important in regulating stem cell state within the epidermis (Connelly et al., 2010; Simpson et al., 2011; Zhu et al., 1999) and changes in epidermal stem cell adhesion to the basement membrane result in changes in in keratinocyte cell shape, altered polarity of the mitotic spindle, and ultimately altered cell proliferation and differentiation (Adams and Watt, 1989; Connelly et al., 2010;

Luxenburg et al., 2011). It has been shown that the linker of nucleoskeleton and cytoskeleton (LINC), SUN, and nesprin proteins at the nuclear envelope act to connect chromatin adjacent the nuclear periphery, nuclear lamins, and the cytoskeleton (Crisp et al., 2006; Mellad et al., 2011; Starr and Fridolfsson, 2010) and cytoskeletal interactions at the nuclear envelope mediated by these proteins may mean the cell cytoskeleton is able to transduce forces that induce changes in nuclear shape.

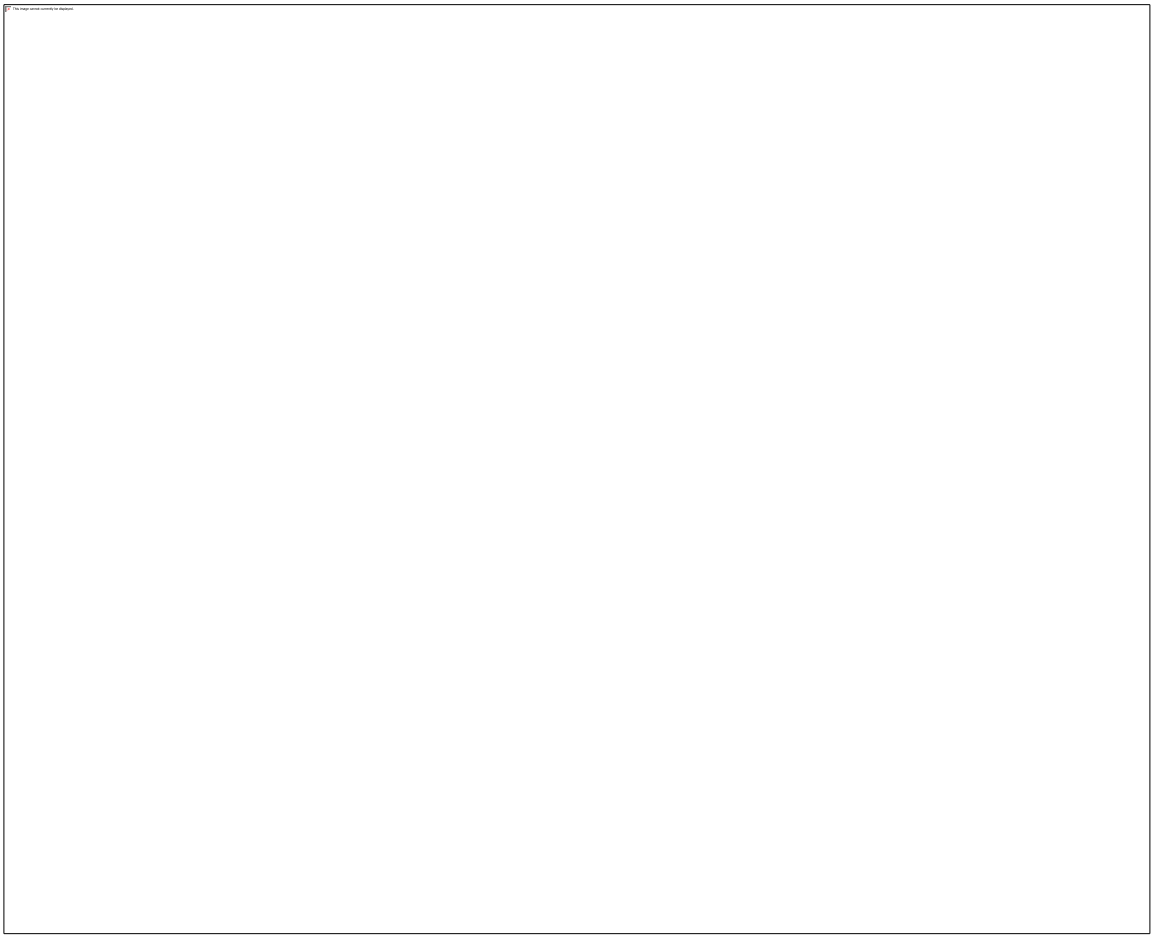

Figure 5 Changes in nuclear shape, volume, and nuclear architecture occur as keratinocytes stratify and terminally differentiate. (**A-C)** The enrichment for markers of active transcription in basal and spinous keratinocytes is reduced as keratinocytes transit from spinous to granular layers and reflects the changing transcriptional state of terminally differentiating keratinocytes (**D)** A three-dimensional reconstruction of nuclear morphology within murine plantar epidermis generated using image stacks acquired by confocal laser scanning microscopy of three-dimensionally preserved histological sections. The volume of keratinocyte nuclei is reduced and nuclei acquire a more

flattened, elliptical shape, as keratinocytes detach from the basement membrane, stratify, and differentiate. Proliferative (Ki67 positive) basal keratinocyte nuclei are shown in red (**E)** Changes in the position and spatial association of nucleoli, pericentromeric heterochromatin domains, and the position of chromosome territory three occur during the progressive transition of keratinocytes from basal to granular layers and are suggestive of global changes in the transcriptional landscape of the keratinocyte nucleus during differentiation. Figure adapted from Gdula *et al* 2013 (Gdula et al., 2013) with the permission of the Macmillan Publishers Ltd.

1.1.8 The Epidermal Differentiation Complex

The EDC encodes over 30 genes of several families involved in epidermal differentiation that can be grouped into three families (*S100A*, CE precursor and 'fused-type' families) upon the basis of shared gene and protein structures (Kypriotou et al., 2012). The *S100A* genes encode calcium-binding regulatory proteins critically involved in the activation of signalling cascades during epidermal differentiation (Denning et al., 2000; Lee and Yuspa, 1991; Marenholz et al., 2004). CE precursor proteins expressed during terminal keratinocyte differentiation are encoded by the late cornified envelope (*LCE*) and *SPRR* gene clusters as well as by *IVL*, *LOR*, and *NICE* (newly identified cDNA from the EDC) (Marenholz et al., 2001; Marshall et al., 2001). Members of the 'fused-type' gene family encode proteins that posses structural features typical of both CE precursor and S100 calcium-binding proteins (Contzler et al., 2005; Huber et al., 2005). Separate clusters of related genes comprise the *LCE* (Marshall et al., 2001) and *FLG-like* gene families of structural proteins, 10 members of the *SPRR* subfamilies 1-3, and also *S100A1-13* members of the *S100* gene family. Additional CE precursor proteins and 'fused-type' intermediate filament-associated proteins profilaggrin and trichohyalin, among others, are also encoded at the EDC (Mischke et al., 1996; South et al., 1999), as are a number of genes that appear to have no direct involvement in epidermal differentiation.

Sub-clusters within gene families comprise differentially expressed genes with distinct functions during keratinocyte differentiation. It is hypothesised these sub-clusters confer flexibility in the response of the epidermal barrier to environmental stimuli and as such

likely have arisen through evolutionary gene duplication and subsequent diversification (Jackson et al., 2005; Marshall et al., 2001).

The EDC region is largely evolutionarily conserved among phylogenetic classes of mammalian species, including marsupial as well as eutherian species. Concerted expression, conserved synteny, linear co-localisation of genes encoding both structural and calcium binding proteins suggest a role for co-regulation of genes within the EDC locus. Mapping of DNase I hypersensitive sites and conserved non-coding sequences (CNSs) has identified putative *cis*-regulatory elements within the *SPRR* gene cluster that potentially coordinate the up-regulation of *SPRR* genes during differentiation, although adjacent genes can be independently regulated (Martin et al., 2004). Potentially, *cis*-regulation of gene expression may act to coordinate pan-EDC transcriptional activity, as is the case for genes of the beta-globin locus, among other gene complexes, although in the case of the EDC this has yet to be established.

Genes belonging to different gene families within the EDC have an identified direct function in or are implicated in the pathogenesis of a number of skin disorders characterised by barrier dysfunction, including psoriasis, ichthyosis vulgaris, atopic dermatitis, eczema, and Vohwinkels keratoderma. The etiology of polygenic inflammatory skin disorders is not yet fully understood. It is thought that a complex interplay and environment, immune response and epidermal barrier are involved in the pathogenesis of these disorders. In the case of each, genetic linkage to the EDC has been established (Bowcock and Cookson, 2004; Cork et al., 2009; Kelsell and Byrne, 2011; Maestrini et al., 1996; Marenholz et al., 2011; Morar et al., 2006; Palmer et al., 2006; Smith et al., 2006). (Bowcock and Cookson, 2004; Hoffjan and Stemmler, 2007; Marenholz et al., 2011).

de Guzman Strong *et al* (2010) report that the 30kb region within the psoriasis linked LCE3C_LCE3B-del mutation includes deletion of a CNS that demonstrates in vivo enhancer activity and identify loss of enhancer function as potential functional variant in psoriasis (de Guzman Strong et al., 2010). Another CNS at the EDC has been shown to exhibit specific patterns of enhancer activity during epidermal development *in vivo* and to act as a long-range enhancer of transcription at multiple EDC gene targets under

proliferating and differentiating conditions *in vitro* (Oh et al., 2014). It is also possible hitherto unidentified non-coding regions within the EDC will be identified as *cis*-regulatory regions that play a part in the pathogenesis of one or more epidermal barrier disorders. Chromatin remodelling and disease variants affecting long-range transcriptional regulation in *cis* motifs have been identified as risk factors in relation to several diseases that affect other organs and systems (Bodega et al., 2009; Chavanas et al., 2008; Horike et al., 2005; Pirozhkova et al., 2008; Verlaan et al., 2009).

2 Aims

In basal keratinocytes during epidermal ontogenesis, P63 dependent centripetal nuclear re-positioning and increased spatial association of the EDC with SC-35 positive nuclear speckles are associated with the transcriptional up-regulation of EDC gene expression during epidermal stratification. P63 has been shown to directly regulate the transcription of BRG1, an ATPase catalytic unit of the SWI/SNF chromatin-remodelling complex implicated in regulating nuclear repositioning of MHC class II loci upon transcriptional activation.

P63 has also been shown to regulate the expression of SATB1, a genome organiser shown to tether chromatin at MARs that acts to mediate the formation of chromatin loops and recruitment of chromatin remodelling enzymes involved in regulating chromatin state and gene transcription. In basal keratinocytes, SATB1 ablation has been shown to impact upon patterns of developmental EDC gene expression and chromatin compaction at the EDC locus.

This study aims to:

- To investigate the role of BRG1 in regulating the nuclear positioning of, and gene transcription at, the EDC locus during epidermal morphogenesis.
- Map higher-order chromatin folding at the EDC locus and interaction of candidate regulatory elements involved in long-range gene regulation at high-resolution using 3C-carbon copy (5C) technology.
- Further investigate the mechanisms by which SATB1 acts to regulate higher-order chromatin folding at the EDC region
- Reveal potential regulators of higher-order chromatin folding at the EDC in keratinocytes by employing an integrative approach to analyse 5C data and data mapping the distribution of histone modifications, binding of chromatin remodellers, transcription factors and co-factors at the locus.

3 Materials and Methodology

3.1 Experimental animals and tissue collection

Animal studies were performed using C57Bl/6 mice following protocols in accordance with the UK Home Office Animals (Scientific Procedures) Act 1986. K14BRG1$^{\Delta/\Delta}$ mice were obtained by breeding K14CreER^{T2} mice with BRG1$^{L2/L2}$ mice and administering tamoxifen to pregnant females via intraperitoneal injection, as described previously (Indra et al., 2005). K14BRG1$^{\Delta/\Delta}$ E16.5 3D and cryopreserved mouse embryos were kindly supplied by Vladimir Emelyanov and Andrei Sharov (Boston University School of Medicine, Boston, MA, USA).

3.2 Isolation of primary mouse keratinocytes

Euthanized neonatal mice were washed twice with 70% ethanol. Fore and lower hind limbs, and the tail and genital region were removed and discarded. Skins were removed by making an incision made along the dorsal midline, as described previously (Lichti et al., 2008) and incubated overnight at 4°C with 0.25% trypsin in Hanks Balanced Salt solution. After overnight digestion, skins were placed epidermal side down on the culture surface of a fresh p10 plate and the dermis easily removed using sterilised forceps. Epidermal tissue was added to pre-chilled, supplemented, primary keratinocyte culture medium (appendix table A2) and epidermal tissue triturated to obtain a single cell suspension. This cell suspension was filtered through a 70μm silicon strainer and viable cells counted viable using a haemocytometer and trypan blue solution (Sigma).

3.3 Isolation and purification of BAC clone DNA

BAC clone LB agar stab cultures were previously purchased by Dr M. Fessing (University of Bradford) from the BACPAC resource centre (BPRC) of the Children's Hospital Oakland Research Institute (CHORI) (Osoegawa et al., 2000). BAC from two libraries, the RPCI-23: Female (C57BL/6J) Mouse BAC Library (pBACe3.6) and the RPCI-24: Mouse (C57BL/6J Male) (*Mus musculus*) BAC Library (vector pTARBACC1) were purchased and glycerol stocks prepared and stored at -80°C.

BACs (appendix table A1) were selectively grown on agar plates containing 12.5µg/mL chloramphenicol over night at 37°C. Selective starter cultures were then prepared for each BAC by inoculating 2.5mL TB (terrific broth) microbial growth medium (Sigma) containing 12.5µg/mL chloramphenicol with a single colony selected from a freshly streaked plate using a sterile pipette tip. Inoculated starter cultures were grown for ~8 hours at 37°C, with shaking at 200rpm. 2.5mL of starter culture were then used to inoculate 500mL TB broth and bacteria cells grown with shaking, 200-250rpm, at 37ºC for 12-16 hours.

Bacterial cells were subsequently harvested by centrifugation at ~1000 RCF. The weight of pelleted bacterial cells was checked in order to confirm that an appropriate yield was obtained (approximately 1.5g/500mL) following growth and pelleted bacterial cells quick frozen on dry ice and stored at -80ºC. Growth conditions were selected to produce a yield of around 3-4 x 109 cells mL-1, a yield optimal for the method used to isolate and purify BAC.

BACs were isolated and purified using the Qiagen Large-Construct Kit. High yield was favoured over purity of BAC versus genomic DNA content and as such the Qiagen '*protocol for high yields of Large-construct DNA without removal of genomic DNA*' was used to isolate BACs (Qiagen® Large-Construct Kit Handbook). Isolated and precipitated BAC DNA was re-suspended in 70µL TE buffer, pH 8.0. The concentration and purity of BAC DNA was estimated using UV spectrophotometry.

3.4 Chromosome conformation capture carbon copy (5C) technology

A derivative of chromosome conformation capture (3C) technique, 3C-carbon copy (5C) is used to generate a 'matrix' of intra-chromosomal interaction frequencies throughout a given genomic region. 5C is able to capture and represent in vivo patterns of chromosomal interactions between hundreds of thousands of specific loci without necessitating treatments that may cause disruption to spatial chromosome organisation (Dekker et al., 2002; Simonis et al., 2007). 5C libraries were generated in duplicate from primary mouse keratinocyte and thymocytes cell populations.

3.4.1 Keratinocyte isolation and fixation

Freshly isolated keratinocytes were seeded in supplemented primary keratinocyte culture medium (appendix table A2) at high density onto collagen solution (appendix table A2) coated culture dishes at a density of 1 skin per p100 dish. Keratinocytes were left to adhere overnight at 32ºC, 8% $C0_2$, 90% relative humidity.

Adherent keratinocytes were washed once with PBS (appendix table A2) and once with low calcium media. 10mL low calcium media was then added per plate and cells fixed for 10 minutes at room temperature in 1% EM grade methanol-free paraformaldehyde (Electron Microscopy Sciences), with gentle mixing every 2 minutes. To each plate, glycine was added to a final concentration of 125mM and plates placed on ice for 5 minutes to stop cross-linking. Medium was substituted for a reduced volume of ice cold PBS and a rubber policeman was used to dislodge cells. Once collated, cells were counted using a haemocytometer and cells then pelleted by centrifugation at 500 RCF for 10minutes at 4ºC. Aliquots of $6x10^7$ pelleted cells were quick frozen and stored at -80ºC.

3.4.2 Thymocyte isolation and fixation

Dissected thyme were transferred to pre-chilled T cell medium (appendix table A2) on ice and frosted microscope slides used to rend and crush each thymus, releasing cells. T cells media containing cells in suspension and tissue debris was filtered through a 70µm cell strainer. Thymocytes were pelleted by centrifugation at 400 RCF for 5 minutes at 4ºC.

The supernatant was removed and pelleted thymoctes re-suspended in 15mL Red Blood Cell lysing buffer (Sigma) for 3 minutes. 30mL of T cell medium (appendix table A2) was then added, cells, medium, and lysis buffer (Dostie and Dekker, 2007) gently mixed, and cells then pelleted. Pelleted thymocytes were then re-suspended in 30mL T cell medium (5mL per thymus) and passed through a 70µm cell strainer and EM grade methanol-free paraformaldehyde (Electron Microscopy Sciences) added to a final concentration of 1%. Cells were fixed in formaldehyde for 10 minutes at RT, after which glycine was added to a final concentration of 125mM and incubated for a further 10 minutes on ice. Cells were counted, and aliquots of $6x10^7$ pelleted cells quick frozen and stored at -80°C.

3.4.3 Chromosome conformation capture (3C)

The following protocol was used to generate both keratinocyte and thymocyte 3C libraries. All materials and reagents used were molecular biology grade and were stored as single use aliquots.

3.4.3.1 Cell lysis

To a frozen pellet of $6x10^7$ cells, 1.2mL of ice cold lysis buffer (Dostie and Dekker, 2007) and 120µL of protease inhibitor cocktail (Sigma) were simultaneously added. Cells were incubated on ice for 30 minutes and then cells further lysed, manually, on ice, using a dounce homogenizer. Cells were then pelleted by centrifugation at 2000 RCF for 5 minutes at room temperature. Cells were washed twice by re-suspending in 500µL cold 1X restriction buffer (NEBuffer 2, New England Biolabs) and pelleting before being re-suspended in 630µL 1X restriction buffer (NEBuffer 2, New England Biolabs).

3.4.3.2 Chromatin Digestion

50µL of nuclei suspension were distributed into 12 microcentrifuge tubes and 312µL of 1X buffer (NEBuffer 2, NEB) were added to each tube. Nuclei were incubated at 65ºC for 10 minutes with 0.1% SDS (w/v) to remove proteins not cross-linked to DNA. After

precisely 10 minutes incubation at 65ºC, tubes were removed from 65ºC heat and placed on ice. Triton X-100 was added to a final concentration of 1% in order to quench SDS and avoid removal of DNA cross-linked protein complexes. Solutions were again mixed by gentle inversion. To solubilised chromatin contained within 11 of the 12 tubes, 800U of *Hin*dIII (NEB) were added to a final concentration of 1.77U/µl and solubilised chromatin digested over night at 37ºC with continual rotation. In order to control for cell DNA degradation, restriction enzyme was not added to one of the 12 tubes. Digested DNA was incubated at 65ºC for 30 minutes in 1.6% SDS (w/v).

3.4.3.3 Ligation of digested chromatin and subsequent reversal of cross-linking

Digested chromatin was ligated at low DNA concentration in a reaction containing 0.9% triton X-100, 0.9X T4 ligation buffer (van Berkum and Dekker, 2009), 100µg/mL BSA, 1.0mM ATP, and 0.0024U/µL T4 DNA ligase (Invitrogen) for 2 hours at between 15°C and 16ºC. No ligase was added to one of the tubes containing digested DNA. Neither was ligase added to the tube containing un-digested DNA. Together these two samples control for digestion efficiency and cell DNA integrity, respectively. After 2 hours, 50µL of 10mg/mL proteinase K were added to each tube and tubes then incubated at 65ºC for 4 hours. A further 50µL of proteinase K was added to each tube after 4 hours and tubes incubated at 65ºC overnight.

3.4.3.4 Extraction and purification of 3C template and control DNA

Tubes containing 3C template were removed from incubation at 65ºC and their contents divided evenly amongst 4 clean 50mL falcon tubes. Controls were transferred respectively into 50mL falcon tubes. A 1X volume of phenol/Tris-HCl, pH 8.0, was added to each tube, tubes vortexed for 1-2 minutes and tubes centrifuged at 3,000 RCF for 10 minutes at room temperature. Aqueous phases were removed to fresh 50 mL conical tubes. A 1.5X volume of 1:1 phenol, pH 8.0: chloroform was added, tubes vortexed for 1-2 minutes and tubes centrifuged at 3, 220 RCF for 10 minutes, room temperature.

Following phenol: chloroform extraction, control DNA (aqueous phase) was transferred, respectively, to labelled 30mL polycarbonate high-speed centrifuge tubes. 3C template DNA (aqueous phase) was combined in one 500mL polycarbonate high-speed centrifuge tube. The volume of samples was increased by ~25% with 1X TE buffer, pH 8.0 and a 0.1X volume of 3M sodium acetate, pH 5.2, and a 2.5X volume of ice-cold absolute ethanol was added to each tube and tubes incubated at -80ºC for >1 hour.

30mL tubes containing controls were centrifuged at 10, 000 RCF for 30 minutes at 4ºC using a Beckman JA-25.50 rotor. The resultant supernatant was removed and DNA pellets briefly air-dried. The 500mL tube containing 3C template DNA was centrifuged at 8, 000 RCF for 1 hour at 4ºC using a Beckman JLA 10.500 rotor (maximum rotor speed: 10, 000 RCF; maximum speed when used with polycarbonate 500mL centrifuge tubes: 8, 000 RCF). Supernatant was removed and the resultant pellet briefly air-dried. Pelleted control DNA was re-suspended respectively in 400µL of 1X TE buffer, pH 8.0 and stored at 4ºC in 1.5mL tubes.

Pelleted 3C template DNA was re-suspended in 4mL of 1X TE buffer, pH 8.0 and transferred to a fresh 15mL falcon tube for further purification. Two rounds of phenol chloroform extraction using a 1.5X volume of 1:1 phenol, pH 8.0: chloroform were performed. To remove excess phenol, a 1.5X volume of chloroform was added to aqueous phases isolated after the second round of phenol: chloroform extraction, tubes vortexed for 30 seconds, and then centrifuged at 3,000 RCF for 5 minutes. The aqueous phase containing 3C template was split between ten 1.5mL microcentrifuge tubes and DNA precipitated using ethanol and a 0.1X volume of 3M, pH 5.2, NaAc buffer solution (Sigma). DNA was pelleted by centrifuging at 18,000 RCF for 1 hour. Pelleted DNA was washed in 70% ethanol and re-suspended in 50µL of 1X TE buffer, pH 8.0.

Samples were combined, DNase-free RNase A added to a final concentration of 0.1µg/µL, and samples incubated at 37ºC for 1 hour. Samples were then further purified using Amicon® Ultra Centrifugal Filter for DNA Purification and Concentration (Millipore®, 30K device) to remove RNase and remaining salt. Using Millipore columns, samples were washed twice with 1X TE buffer. Following sample recovery from Millipore columns, initial sample volume was then restored with 1X TE buffer, pH 8.0.

Dilutions of 3C template and of each control were run alongside a molecular weight standard of known concentration on a 0.8% agarose/0.5X TBE gel containing 0.5µg/mL ethidium bromide and 3C template concentration ascertained (figure 6). 3C template and control undigested genomic DNA is visible as a single band positioned just above the top (10,000bp) band of the DNA ladder. A smear a little above and below a single major band representing 3C template is evident. This is expected. A smear manifesting only above the major band is indicative of an overly long ligation period. A smear manifesting only below the major band is indicative of not enough ligation. Control undigested DNA forms a band similar in appearance to that of the 3C template; the presence of more smearing (not visible in fig 6) is indicative of DNA degradation. Control digested but un-ligated DNA runs as a smear of different digest fragments. The presence of definite bands, particularly of a high molecular weight band, would indicate incomplete enzymatic digestion. Aliquots of library were stored at -80ºC.

A. **B.**

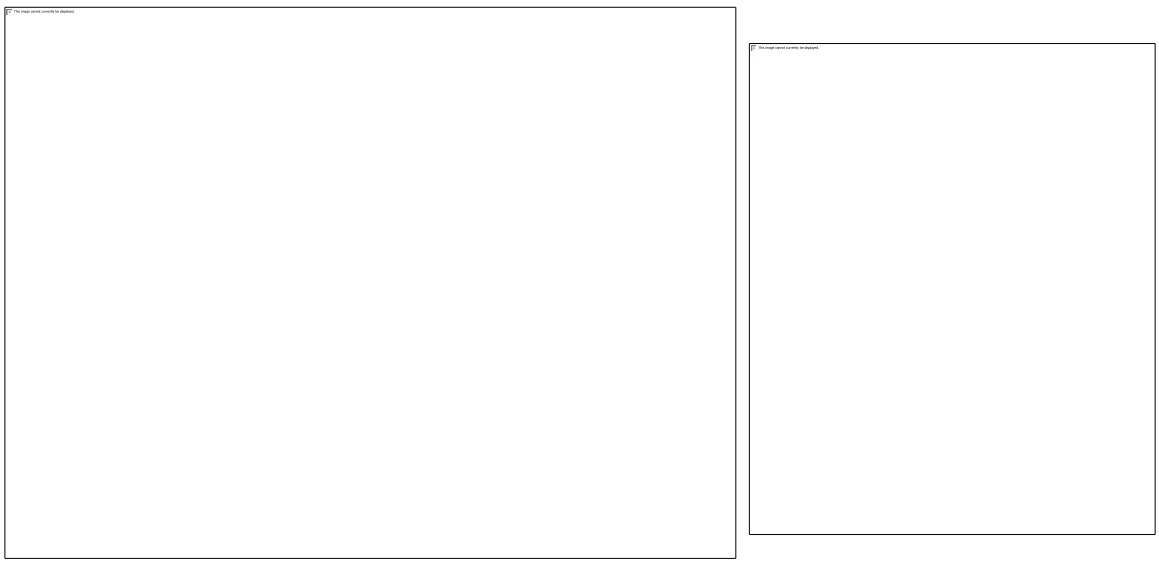

Figure 6 Representative gel images showing multiple dilutions of a 3C 'library' of chromatin interactions produced using murine primary keratinocytes. Gel (A) left to right, lanes 1 & 2: 0.2µL, 0.4µL of control for DNA integrity; 3-5: 1, 2, and 4µL high DNA mass molecular weight marker (top band 10, 000bp, bottom band 1000bp); 6-8: 0.1µL, 0.2µL, 0.4µL of Keratinocyte 3C template (repeated), 12 & 13: 0.2µL, 0.4µL of digest efficiency control. B left to right, lanes 1 & 2: 1µL, 2µL of control for DNA integrity; 3 & 4: 1µL, 2µL of digest efficiency control; 5: blank; 6 & 7: 0.2µL, 0.4µL of Keratinocyte 3C template; 8: 2µL high DNA mass molecular weight marker.

3.4.4 3C quality control

3C template titration was performed using 3C primers (table 1) detecting head-head 3C ligation product comprising predicted restriction fragments 1164bp apart. Primers were designed using the my5C 3C primer design algorithm (Lajoie et al., 2009). Primers are unidirectional and designed to detect loci 50-150bp upstream from the 3' end of predicted restriction sites (Dostie and Dekker, 2007).

Starting with a 1:4 dilution of 200ng μL^{-1} control 3C template, 10 two-fold serial dilutions of 3C template were prepared in duplicate and amplified as described previously (Dostie and Dekker, 2007; van Berkum and Dekker, 2009) using 3C titration primers (table 1). PCR product corresponding to each respective dilution of 3C template was resolved on a 1.5% agarose/0.5X TBE gel containing 0.5µg/mL ethidium bromide alongside a 1Kb DNA ladder (figure 7A, ladder not shown). PCR product yield was quantified using the TotalLab Quant™ gel densitometry software and intensity values plotted against the corresponding input 3C template amount used in each PCR (figure 7B). 3C titration plots (figure 7B) produced showed an acceptable linear increase in product yield throughout each dilution series that reaches a plateau which corresponds to the highest concentrations of 3C template used in each dilution series. (Dostie and Dekker, 2007; van Berkum and Dekker, 2009).

A.

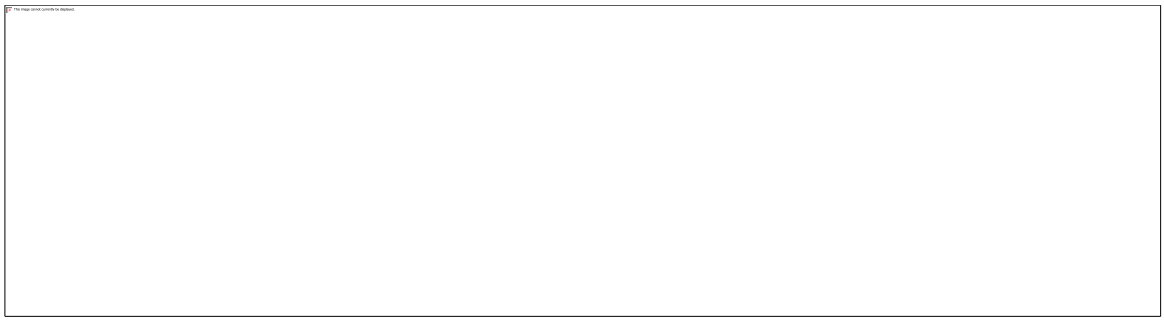

B.

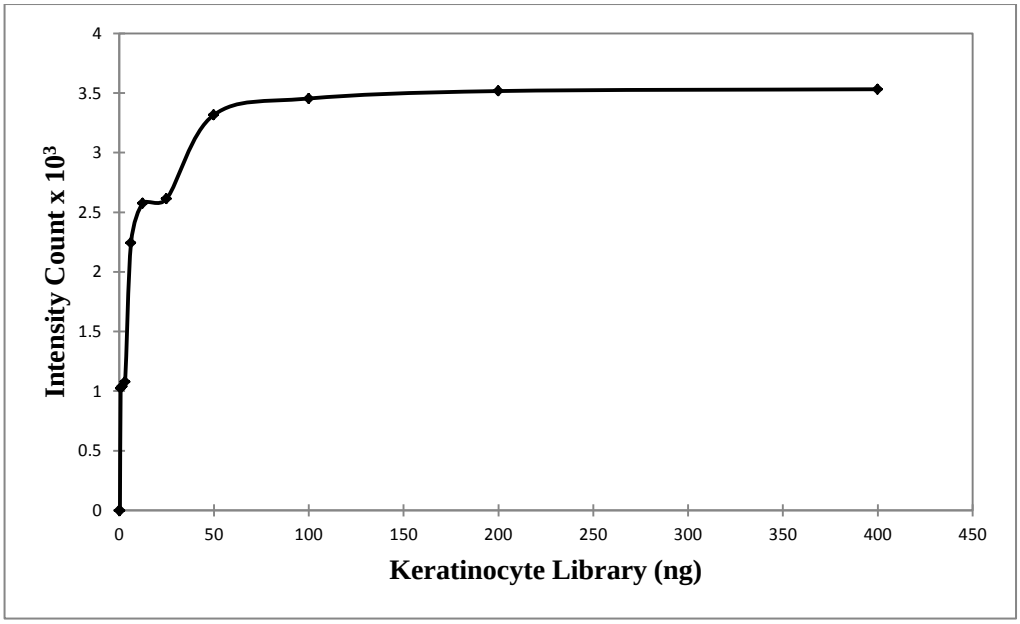

Figure 7 Representative 3C template titration gel image and plot. (**A**) Keratinocyte 3C library titration PCR reactions resolved on a 1.5% agarose/0.5X TBE gel. A two-fold serial dilution of 3C template was amplified by PCR with 3C titration primers (table 1) primers. (**B**) Representative 3C keratinocyte titration plot. Starting amount of 3C template (keratinocyte library) is shown on the *x*-axis. The *y*-axis indicates product yield intensity values obtained by gel densitometry.

3.4.5 Generation of chromosome conformation capture carbon copy (5C) and 5C control libraries

5C libraries were generated from 3C template DNA as per van Berkum and Dekker, 2009 (van Berkum and Dekker, 2009). The libraries generated detect a possible 130, 670 interactions occurring between loci within a 5.3Mb region on mouse 3q (89900000-95200000bp, assembly mmu9) spanning the murine EDC. Controls implemented during the generation of 5C libraries establish that 5C preparations are 3C template dependent and not the result of the ligation or amplification of non-3C material or cross-contamination with other 5C product. Gel lanes 1 and 2 of figure 8 show ~200ng of replicate 5C libraries (101bp) run alongside controls (figure 8. lanes 4-7) on a 2% agarose/0.5X TBE gel containing 0.5μg/mL ethidium bromide.

Figure 8 5C products (lanes 2 & 3) and experimental controls (lanes 4-7) run on a 2% agarose/0.5X TBE gel. Control lanes: Lane 4: no 5C template control; lane 5: no ligation control; lane 6: no 5C primer control; lane 7: no 5C product. The absence of product in controls lanes is demonstrative of the template specificity of 5C preparations and the absence of cross-contamination between 5C libraries.

3.4.5.1 Design and preparation of 5C primers for 5C

5C primers (appendix table A5) were designed as previously described (Phillips-Cremins et al., 2013) using the my5C primer design algorithm (Lajoie et al., 2009) with the help of Brian Lajoie, Job Dekker lab, University of Massachusetts Medical School, Worcester, MA, USA, and were synthesised by Sigma-Aldrich Corp. 5C primers were designed to detect head-head ligation of *Hin*dIII restriction fragments. The 3' end of each forward 5C primer carries half of the 5' end of the *Hin*dII restriction site, whilst the 5' end of each reverse primer incorporates the 3' end of the *Hin*dIII restriction site. Forward and reverse 5C primers anneal to opposite strands of the regular DNA molecule but anneal to the same strand of head-head ligation products, which represent chromatin interactions, comprising in part a 3C matrix. Each primer, forward or reverse, contains a unique sequence complementary to the 3' region flanking each *Hin*dIII restriction site throughout the ~5Mb region studied.

Sanger sequencing of cloned 5C library generated from a thymocyte 3C template was used to screen the interaction frequency of individual 5C primers. 5C primers shown to

interact more frequently in proportion to other 5C primers in the thymocyte 5C library screened were removed. Primers detected that, for instance, could competitively bind to the same target, and primers containing identical sequences, were removed, thereby reducing the risk of problematic inter-primer ligation. After screening, alternate primers contained within the 5C primer pool represent 1, 702 fragments, which interrogate will interrogate 130, 670 interactions across 5, 300, 000 Mb covering the murine EDC region (chr3: 89900000-95200000, assembly Mm9).

A 5' phosphate group was added to reverse 5C primers. A 100µM stock pool comprising all selected reverse 5C primers was diluted by adding a 1X volume of 1X TE, pH 8.0. As per van Berkum and Dekker, 2009 (van Berkum and Dekker, 2009), the following reaction was set up: 70µL 50µM reverse primer pool, 10µL 10mM ATP, 10µL PNK buffer (NEB), 10µL 10U/mL PNK (NEB). Reverse primers were incubated with PNK and ATP for 30 minutes at 37ºC, after which PNK was inactivated by incubating at 65ºC for 10 minutes. To generate a working stock of 5C primer pool, an aliquot of a 100µM stock pool of all forward 5C primers selected was diluted down to 35µM with 1X TE, pH 8.0. Forward primer pool and reverse primer pool were then mixed in equimolar ratio by combining 35µM forward primer pool and phosphorylated reverse primer pool in a 1:0.98 ratio. 5C primer pool generated was stored in single use aliquots at -80ºC.

To assess the efficiency of 5C reverse primer phosphorylation efficiency, phosphorylated reverse primers and forward primers were randomly ligated using the following mix of reaction components: 15µL 5C primer pool, 4µL 10X T4 RNA ligase buffer (NEB), 40% PEG 8000, 1µL T4 ssRNA ligase (NEB). Primers were ligated at 37ºC for 30 minutes. Ligase was inactivated by incubating at 65ºC for 10 minutes. The following amplification reaction was set up: 2.5µL 10X PCR buffer (van Berkum and Dekker, 2009), 0.8µL 50mM MgSO4, 0.2µL 25mM dNTP mix, 0.5µL 80µM T3 primer (TATTAACCCTCACTAAAGGGA), 0.5µL 80µM T7 primer (TAATACGACTCACTATAGCC), 0.2µL 5 U/mL *Taq* DNA polymerase (NEB), 14.3µL water. Ligated primer was amplified using the following reaction conditions: 1 cycle 5 minutes at 95ºC, 34 cycles 30 seconds at 95ºC, followed by 30 seconds at 60ºC, followed by 30 seconds at 72ºC, 1 cycle 30 seconds at 95ºC, followed by 30 seconds at 60ºC, followed by 8 minutes at 72ºC. Ligation product was amplified in duplicate using 4 ratios

of primer to template amount in moles: 10, 10^3, 10^5, and 10^7. Amplification product was run on a 2% agarose/0.5X TBE gel containing 0.5µg/mL ethidium bromide alongside a 1kb DNA ladder (figure 9).

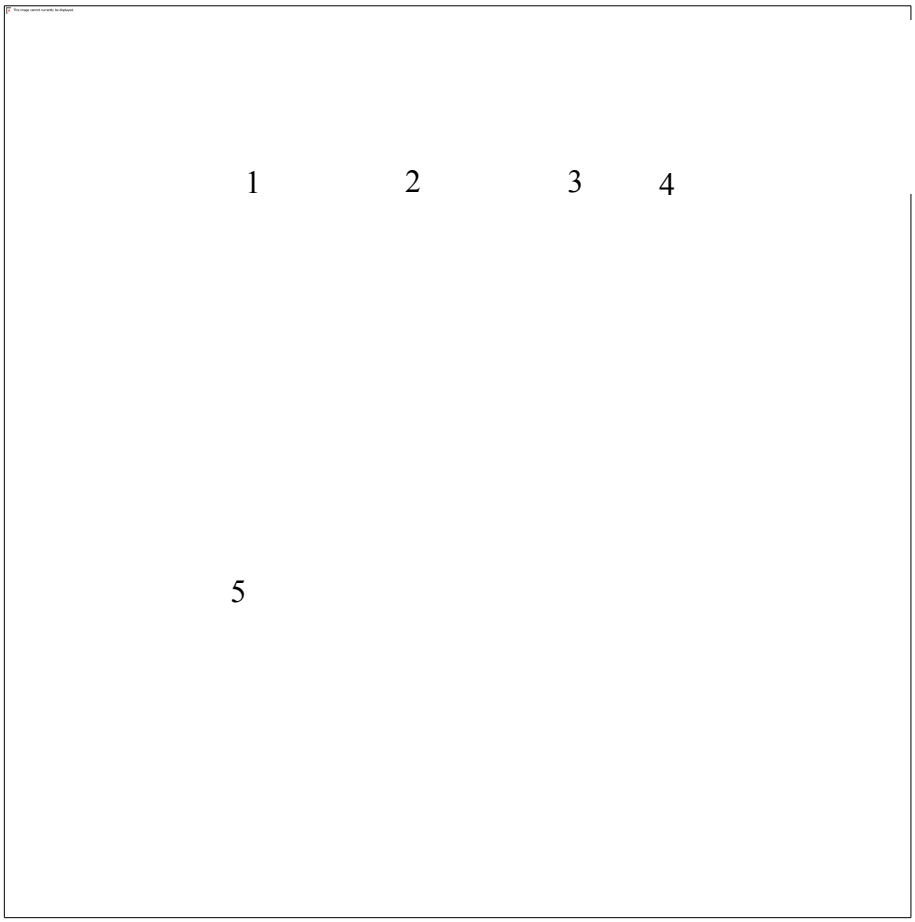

Figure 9 Randomly ligated 5C primers amplified and resolved on a 2% agarose/0.5X TBE gel alongside a 1Kb DNA ladder. Duplicate ligation reactions were amplified in two PCR reactions. Ratio of primer: template amount: 10 (bracket 2), 10^3 (bracket 1), 10^5 (bracket 3), and 10^7 (brackets 4 & 5) moles.

3.5 5C quality control and 5C optimisation

5C preparations have not before been generated using primary mouse keratinocytes and thymocytes. 5C conditions must be optimised by running a series of titration reactions with 5C preparations (figure 10) prior to the deep-sequencing of 5C preparations in order to maximise fidelity with which 5C preparations represent *in vivo* chromosomal interaction frequencies. Based upon the results of 5C titration (figure 10), as detailed

below, conditions of 200 kilo genome copies (KGC), 25 PCR cycles, and a primer pool concentration of 0.4fmol per 5C primer (appendix table A5) were selected for the generation of 5C product for deep sequencing. These conditions increase output 5C complexity whilst minimising the potential detrimental impact of PCR component depletion during the ligation mediated amplification of 5C primer bound 3C ligation product.

3.5.1 Optimisation of 5C conditions using 5C titration

In order to optimise 5C, several 5C 'titrations' were performed; a series of 5C primer pool dilutions (0.05fmol per primer, 0.25fmol per primer, 0.5fmol per primer, and 0.75fmol per primer) were used in separate 5C reactions to generate a 5C library under conditions varying in PCR cycle number and genome copy number. Each primer dilution was used to generate 5C template under the following conditions: 100, 000 genome copies, 27 PCR cycles; 200, 000 genome copies, 25 PCR cycles with the aim of selecting the optimal genome copy number, PCR cycle number and primer concentration to use. For each primer dilution under each set of conditions, 5C product was run on a 2% agarose/0.5X TBE gel containing 0.5µ/mL ethidium bromide (figure 10) and densitometry used to plot band intensity of 5C product yield against 5C primer pool concentration (fmol of individual 5C primer/reaction) used (figure 10).

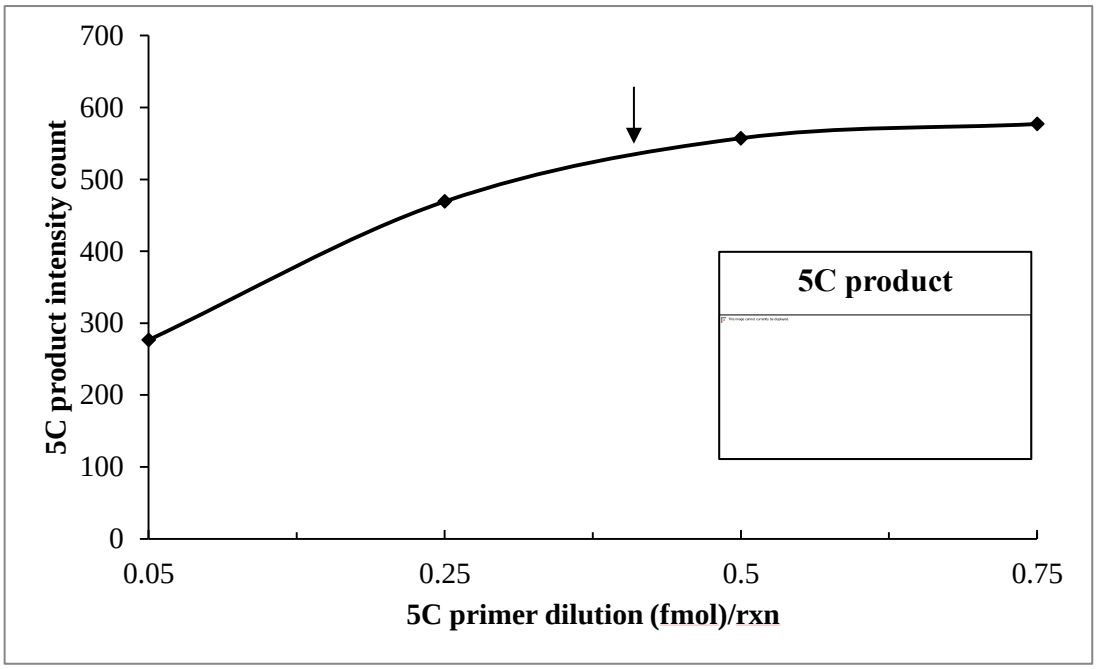

Figure 10 Final titration plot: 5C product produced under selected conditions of 200KGC, 25 PCR cycles using 0.05, 0.25, 0.5, and 0.75fmol/5C primer. The *x*-axis shows the amount of each individual 5C primer used per 5C reaction and the *y*-axis the measure of product yield intensity. Box: Corresponding titration gel showing 5C product produced by running a 5C preparation using ~200, 000 GC per 5C reaction and 25 PCR cycles at four different 5C primer pool concentrations resolved on a 2% agarose/0.5X TBE gel. Lanes left-right: 0.1, 0.5, 1, and 1.5 fmol per each 5C primer in reaction.

3.5.2 5C Quality Control

Cloning and sequencing of a 5C library is required as a check for spurious 5C primer activity. As 5C detection of interaction frequencies between genomic loci is PCR dependent, it is essential to check a 5C control library for the presence of an overabundance any particular primer pair product and to remove any such problematic primers from the 5C primer pool.

3.5.2.1 5C quality control 2: sequencing of 95 5C products using the Sanger method

5C product was generated using conditions of 0.4fmol/5C primer, 25 PCR cycles and 200KGC (as determined by optimisation). 8µL of 5C product were loaded onto two lanes

of a 1.2% agarose/1X TAE gel containing 0.5µg/mL ethidium bromide and run alongside a 1kb DNA ladder at 60 volts for a minimal period of time at ~ 6°C. Using minimal exposure to UV, the bands containing 5C product were excised and transferred to a clean microcentrifuge tube of known weight. Tube and gel were then weighed and the number of grams of gel present recorded. The Machery-Nagal NucleoSpin Gel and PCR Clean-up kit was used to extract 5C product. Wash steps were performed. In order to maximise elution yield, elution was performed twice using kit supplied EDTA-free (Tris·Cl) elution buffer pre-warmed to 70ºC. Sample and elution buffer were incubated for 5 minutes at room temperature prior to centrifugation.

5µL of extracted 5C product were run alongside a gradient of molecular weight ladder of known concentration on a 1.2% agarose/1X TAE gel (figure 11). Product concentration (1ng/µL) was ascertained using densitometry to compare product/sample band intensity to with that of molecular weight standard band intensities.

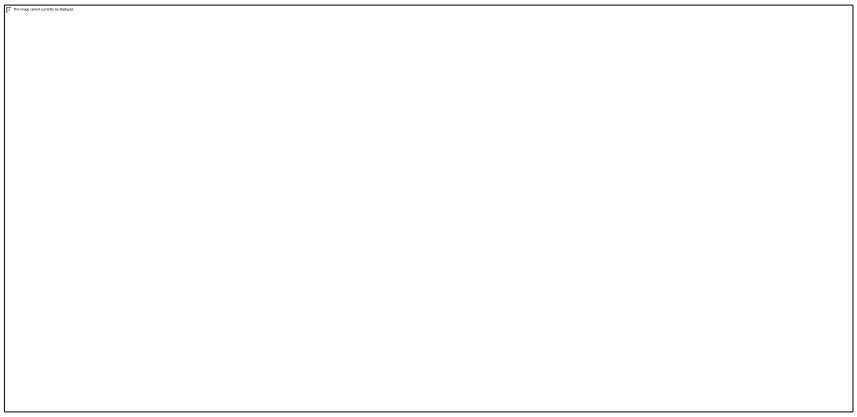

Figure 11 Gel-eluted 5C product (lanes 2 & 3) resolved on a 1.2% agarose/1X TAE gel alongside a low mass DNA ladder gradient of known concentration (lanes 1, 4, 5, & 6).

The Novagen pSTBlue-1 Perfectly Blunt Cloning Kit was used to clone 0.05pmol of 5C product. End conversion using kit reagents and protocol was performed prior to cloning. Supplied competent cells were transformed as per the kit protocol and cells containing cloned plasmid selected for upon the basis of kanamycin resistance. An outgrowth period of 30 minutes was included prior to plating cells; SOC microbial growth medium was added to tubes containing transformation mixture and tubes incubated with shaking at 200rpm for a period of 30 minutes at 37ºC. Transformation mixture containing transformed cells and SOC medium was then streaked onto 1X kanamycin selective LB

agar plates (0.05mg/mL kanamycin/mL). 50µL of mixture was streaked per plate using a sterilised spreader and spread mixture allowed to absorb into the agar (to obtain an even distribution for growth of single colonies). Inverted plates were incubated at 37ºC overnight and subsequently stored at 4ºC.

Colonies were screened for the presence of recombinant plasmid prior to growth for plasmid isolation using colony PCR. Colonies 1mm in diameter were selected using a sterile pipette tip (yellow/p100). In total 18 colonies were selected and screened. Selected colonies were deposited into 1.5mL microcentrifuge tubes containing 50µL of molecular biology water. Before transferring to water, a pipette tip once loaded with a colony was then touched to a fresh 1X kanamycin LB agar master plate, which was incubated overnight at 37ºC and subsequently stored at 4ºC. Using this master plate, colonies were individually numbered and propagated for future use.

Tubes containing colonies were placed in boiling water for 5 minutes in order to lyse cells. After incubation, tubes were centrifuged at 12, 000 RCF for 1 minute. The following PCR reaction was prepared: 1µL of 10mM dNTP mix, 1µL of 5pmol/µL pSTBlue-1 vector SP6 promoter primer (primer sequence: GAT TTA GGT GAC ACT ATA G), 1µL of 5pmol/µL pSTBlue-1 vector R-20 mer primer (LacZ start codon, primer sequence: CAG CTA TGA CCA TGA TTA CG), 5µL of standard *Taq* DNA polymerase buffer (NEB), 10µL of supernatant, 1.75µL of water, 0.25µL of 5U/µL *Taq* DNA polymerase. Product was amplified using the following PCR cycling regime: 35 cycles, 1 minute at 94ºC followed by 1 minute at 55ºC followed by 2 minutes at 72ºC; final extension, 5 minutes at 72ºC. 8µL of loading buffer (appendix table A2) were added to each reaction and 10µL of each run on a 1.2% agarose/1X TAE gel containing 0.5µg/mL ethidium bromide alongside a DNA ladder. The majority (83%) of colonies were found to contain recombinant plasmid.

3.5.2.2 Recombinant plasmid isolation and purification

2.5mL LB broth/1X kanamycin mini-preps were inoculated with master plate colonies known to comprise recombinant plasmid. In addition a random selection of un-screened primary colonies 1mm in diameter was used to start 2.5mL LB broth/1X kanamycin mini-

prep cultures. In order to isolate and purify a minimum of 96 5C clones for sequencing, 120 colonies were selected for plasmid isolation in total to allow for a transformation efficiency of ~80%. Inoculated mini-preps were incubated at 37ºC for ~8 hours overnight with shaking at 200-250rpm. Cells were pelleted at 3, 000 RCF, the supernatant removed, and cell pellets quick frozen and stored at -80ºC. Plasmid DNA was extracted from frozen cell pellets and purified using the Qiagen QIAprep Spin Miniprep Kit.

3.5.2.3 Screening of purified plasmid DNA from individual 5C clones

Purified plasmid DNA of 120 plasmids was screened using pSTBlue-1 vector SP6 promoter (primer sequence: GAT TTA GGT GAC ACT ATA G) and pSTBlue-1 vector R-20mer (LacZ start codon, primer sequence: CAG CTA TGA CCA TGA TTA CG) primers. Plasmids were screened using the following reaction set-up: 0.5µL 10mM dNTP mix, 0.5µL 5pmol/µL 5' primer, 0.5µL 5pmol/µL 3' primer, 2.5µL standard *Taq* DNA polymerase buffer (NEB), 0.125µL 5U/µL *Taq* DNA polymerase, 19.875µL molecular biology water, 1µL of a 1:1000 dilution of plasmid DNA. The following amplification parameters were used: 31 cycles, 1 minute at 94ºC followed by 1 minute at 55ºC followed by 2 minutes at 72ºC; 1 cycle, 1 minute at 94ºC followed by 1 minute at 55ºC followed by 5 minutes at 72ºC. Product was run on a 1.5% agarose/0.5X TBE gel containing 0.5µg/mL ethidium bromide alongside a 1kb DNA ladder (figure 12).

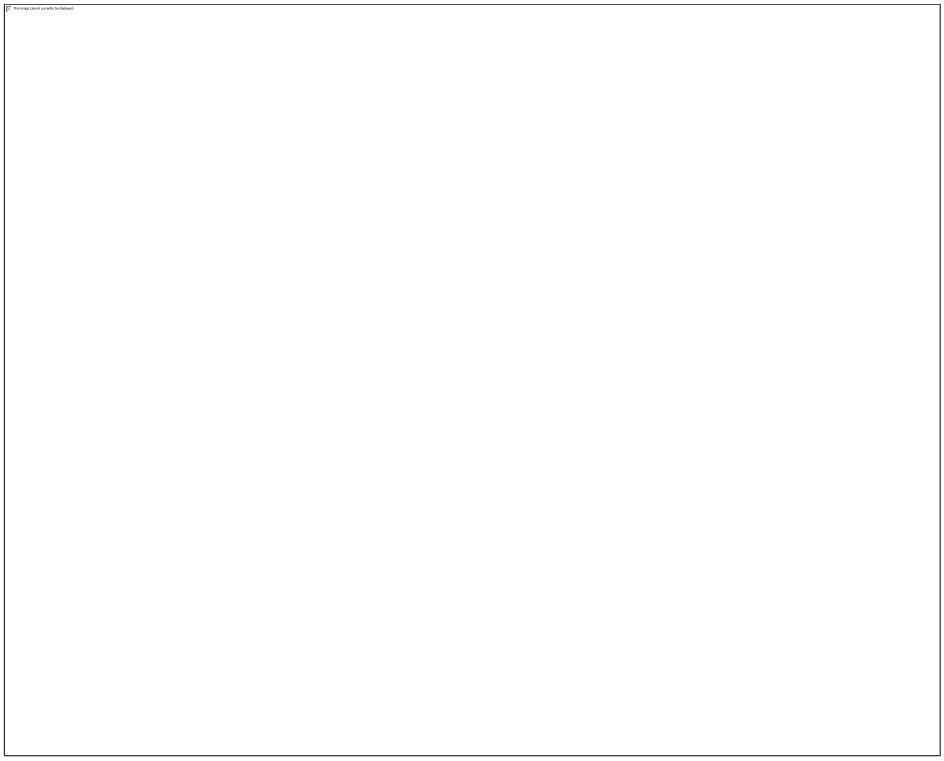

Figure 12 Representative gel image showing amplified plasmid DNA purified from 5C clones resolved on 1.5%/0.5X TBE gel. In total plasmid DNA from 120 colonies were likewise analysed.

5 plasmids, including a putative multimer, were digested with *Eco*RI. Plasmid DNA was digested for 1 hour at 37ºC in a 10µL reaction containing the following: 4µL purified plasmid DNA, 1.5µL 10X buffer (NEB), 0.5µL 20U/µL *Eco*RI, 4µL water. Restriction product was run on a 1.5% agarose/0.5X TBE gel containing 0.5µg/mL ethidium bromide (figure 13). Results confirm those acquired by PCR.

Figure 13 *Eco*RI restriction products generated after overnight digestion of recombinant plasmid DNA resolved on a 1.5% agarose/0.5X TBE gel (lanes 2-6) alongside a 1Kb ladder (lane 1).

3.5.2.4 Sample preparation for Sanger sequencing

Isolated recombinant plasmid DNA from 96 colonies was sent for Sanger sequencing, 96-well format, by DNA Sequencing and Services ™, Dundee, UK. Recombinant plasmid DNA concentration was estimated using UV spectrophotometry. As specified by the sequencing facility used, each plasmid was diluted to 300ng/15µL in molecular quality water, 15µL of each dilution added per well of a 96-well plate and 1µL of 3.2µM SP6 promoter sequencing primer (primer sequence: GAT TTA GGT GAC ACT ATA G) added to each well.

3.5.2.5 Analysis of sequencing output

Each recombinant plasmid sequenced ideally should contain cloned 5C product comprising two 5C primers (one forward and one reverse primer). Sequencing reads were searched against a database of 5C primers (appendix table A5) and corresponding primers identified with the help of Dr. Krzysztof Poterlowicz (University of Bradford, UK). A number of sequences were also manually checked, including those identified by as not matching a 5C primer pair. In order to manually match sequence reads to primer 5C

primer pairs, *Eco*RI sites juxtaposing the pSTBlue-1 vector insertion site were used to isolate putative 5C product sequence, putative 5C sequence checked for the presence of a *Hin*dIII restriction site, and the sequence used to search a database of 5C primers (appendix table A5). Where a forward and reverse primer could not be found matching an isolated sequence exactly (due to base pair substitution resulting from erroneous sequencing), genome position corresponding to the sequence in question was identified using the online UCSC mouse BLAT search tool (UCSC, 2012). The genome position identified using BLAT was then used to identify corresponding 5C primers according to primer start/end position. For primer pair matches, primer pair and individual primer frequencies were calculated. Primer pair frequencies were used to group primer pairs according to separation distance.

The results of this analysis indicate that of the 95 5C clones successfully sequenced, 73% of sequences match a forward and reverse 5C primer pair. Of the remaining 27%, 18% match only one identified primer and 9% cannot be matched to any primer sequence (figure 14).

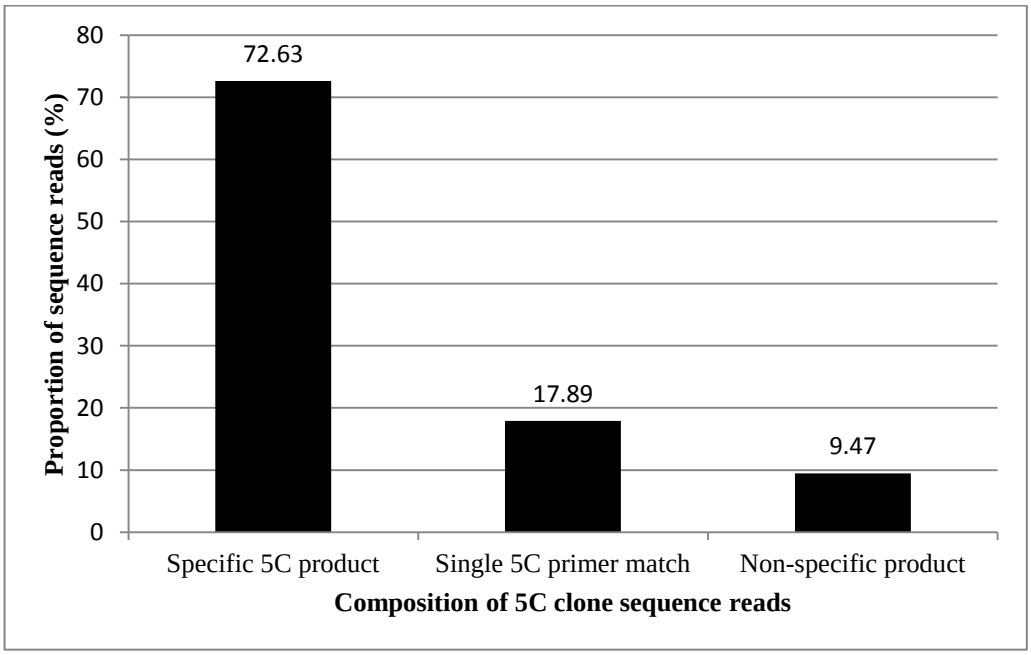

Figure 14. Sanger sequencing of cloned 5C preparation revealed the majority of sequenced clones comprise a specific 5C product (72.63% of clones sequenced). The *y*-axis indicates the composition of reads obtained by sequencing 95 5C clones, which

either comprise a specific 5C product consisting of one forward and reverse pair of 5C primers (appendix table A5) or non-specific or un-identifiable product. The *x*-axis represents the proportion of each product as a percentage of all reads obtained.

The relationship between the genomic separation distance and frequency of interaction between 5C primers was then assessed for the population of 95 5C clones sequenced (figure 15). Stochastic movement of the chromatin fibre within the three dimensional space of the nucleus results in random collisions between regions of chromatin. Broadly speaking, the probability of two regions of chromatin randomly colliding is reduced with increasing genomic separation distance. However, it is probable a locus may be preferentially folded such that a particular degree of separation is associated with an increased interaction frequency. In addition, in a 3C or a 5C library, the representation of interactions between two regions of chromatin is limited by the frequency with which a particular restriction site is distributed throughout the genome; below a certain separation distance (dependent upon the type of restriction site in question) there are fewer possible interactions that can be captured during the preparation of 3C libraries because the number restriction sites is reduced. Among 5C clones sequenced, the proportion of pairwise interactions occurring over a separation distance of less than 1Mb exceeds those occurring over distances greater than 1Mb, however within the kilo base scale of separation distances, interactions occurring between 0.1 and 1Mb are more frequent (figure 15).

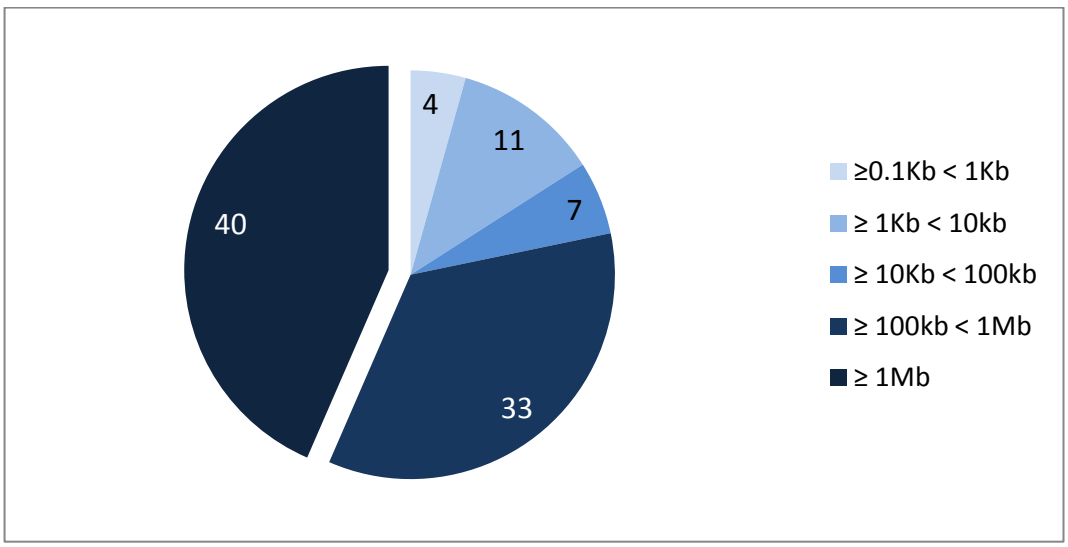

Figure 15 5C product (pairwise chromatin interactions detected using LMA) represented as number of 5C clones sequenced and grouped according to the 2D genomic separation distance between spatially interacting loci. Sanger sequencing of cloned 5C product was used as a control for 5C library quality prior to deep-sequencing 5C libraries.

The primary objective of cloning and sequencing a 5C library using the Sanger method was to analyse the ligation frequency of individual primers. Several 5C primers were detected that either produced a relatively large amount of product or were identified as being non-unique, both within and outside of the target region. These primers were subsequently removed from the 5C primer pool prior to the generation of libraries for deep-sequencing. The pool used to generate 5C clones sequenced using the Sanger method comprised 381 forward and 382 reverse primers (145, 542 total possible interactions). This number was subsequently reduced to 358 forward and 365 reverse (130, 670 total possible interactions).

3.6 5C sample preparation for paired-end deep-sequencing

Four 3C libraries were generated, two from primary mouse keratinocytes, two from primary mouse thymocytes. For each of these libraries, ~1.5-3µg of 5C product was generated using optimised preparation conditions of 200 kilo genome copies, 25 PCR cycles, and a primer pool concentration of 0.4fmol per 5C primer (appendix table A5). In order to generate ~1.5-3µg of 5C product, 15 5C reactions (primer annealing and ligation) were performed and subsequently split into 90 ligation-mediated amplification reactions, and amplification product pooled and purified.

5C product was prepared for multiplex paired-end (PE) illumina® sequencing using the HiSeq 2000 platform. PE adapters for multiplex sequencing and PE PCR primers were custom designed and each library was coupled to custom sequencing adapters modified with an in-line ‘barcode’ or ‘index’ sequence (figure 16) for multiplex sequencing. Adapter coupled libraries were gel purified (figure 17) and then enriched, in duplicate, using the illumina paired-end PCR amplification primers (table 4) to detect and amplify adapter-coupled libraries.

The amplified, adapter-coupled libraries were then gel purified once again. After purification, the final enriched adapter-coupled libraries run as a distinct, sharp band of 233bp when resolved on a 2% agarose/0.5X TBE gel (figure 17). Measured using the NanoDrop 1000 spectrophotometer, each library has a 260:280 ratio of ~1.8-2. 10µL of a 10nM solution of each prepared, 'indexed' library were sent to EMBL, Heidelberg, Germany for deep-sequencing using one lane of the illumina Hi-Seq 2000 platform. Sequencing was performed at the European Molecular Biology Laboratory (EMBL) sequencing core.

3.6.1 Custom oligonucleotide design and preparation

A 6 nucleotide index sequence was inserted before the final 3' end nucleotide of the upstream illumina PE adapter (figure 16) making it possible to pool multiple samples without the requirement of an additional index sequencing read. Index sequences were kindly provided by Dr Vladimir Benes (EMBL, Heidelberg). A complementary 6 nucleotide sequence was added to the 5' end of the downstream adapter to preserve accurate ligation of 5' and 3' adapters (figure 16). Downstream adapters were 5' phosphorylated and a phosphorothioate bond incorporated between the last two nucleotides of the upstream adapter (Quail et al., 2008). Standard illumina PE PCR primers (table 4) were used to amplify adapter-ligated product. A 3' phosphorothioate bond was inserted between the last two 3' end nucleotides of PE PCR primer 2.0 (Quail et al., 2008).

100µM stock dilutions of lyophilised, HPLC purified, adapter oligos, re-suspended in 10mM Tris:Cl, pH 7.5, (figure 16) were mixed pairwise in equimolar ratio and hybridised at 97°C for 3 minutes followed by 72 cycles temperature decrement of 1°C/minute in a 5X concentration of 50mM Tris:Cl, pH 7.5, and 50mM NaCl buffer.

A.	Adapter Sequence
Index	
GCCAAT	5' ACACTCTTTCCCTACACGACGCTCTTCCGATCGCCAAT*T 3

5' P- ATTGGCGATCGGAAGAGCGGTTCAGCAGGAATGCCGAG 3’

CTTGTA 5' ACACTCTTTCCCTACACGACGCTCTTCCGATCCTTGTA*T

5' P- TACAAGGATCGGAAGAGCGGTTCAGCAGGAATGCCGAG

B.

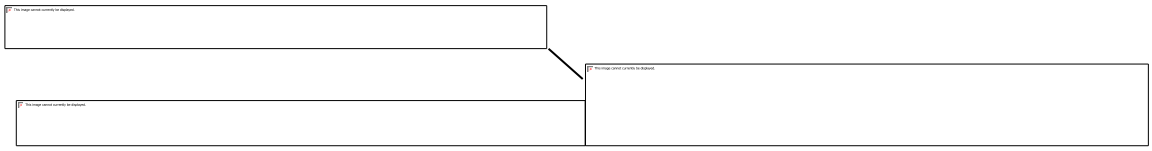

Figure 16 A. Example of custom designed PE adapters containing an in-line barcode sequence (red) of six nucleotides. * phosphorothioate bond between the last two 3’ nucleotides. B. 5’ and 3’ barcoded adapter pairs are hybridised, forming a y shaped structure, which is then ligated to the ‘A-tailed’ 5C product.

3.6.2 PE sample preparation

5C product was pooled and purified using the QIAquick PCR Purification kit. Loaded columns were incubated with PE wash buffer for 5 minutes prior to centrifugation. Elution was performed in two stages. Firstly, 40µL pre-heated (65ºC) buffer EB were added to columns and columns left at RT for 3 minutes before centrifugation. Secondly, a further 40µL of pre heated buffer EB was added and columns centrifuged. Purified and concentrated 5C product was run on a 2% agarose/0.5X TBE gel containing 0.5µg/mL ethidium bromide against DNA mass ladder of a known concentration and 5C product concentration quantified.

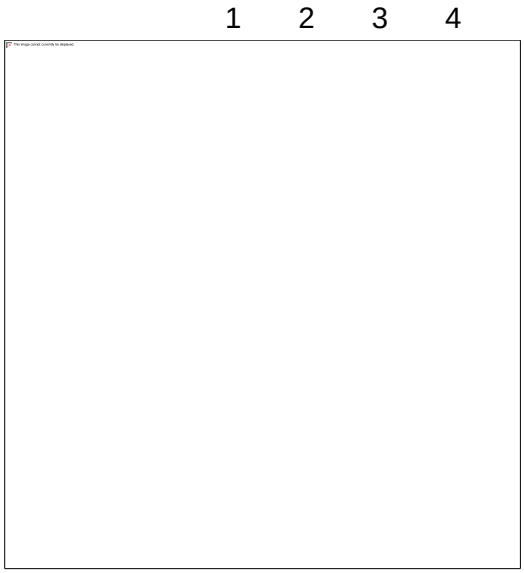

Figure 17 Representative gel image of purified 5C library. 0.5µL (lane 2) and 0.2µL (lane 3) of pooled, purified, keratinocyte 5C library resolved on a 2% agarose/0.5X TBE gel against a low DNA mass ladder of known concentration (lane 1).

'A-tailing' was performed using 1.5µg of purified 5C product in a 30µl reaction containing 1X *Taq* DNA Polymerase standard buffer (NEB), 0.17U/µL of *Taq* DNA polymerase (NEB), and 0.33mM dATP incubated at 72ºC for 45 minutes. The reaction mixture was gradually cooled and purified using the Qiagen MinElute PCR Purification Kit®. PE barcoded adapters were ligated to the A-tailed 5C product in a 50µL ligation reaction containing the 10µL A-tailing adapter-ligated 5C product, 1X Quick T4 DNA Ligase buffer (NEB), and 200U/µL Quick T4 DNA ligase (NEB). Adapter ligated 5C product was purified by running for 2 hours at 4ºC on a long 2% agarose/0.5X TBE gel containing 0.5µg/mL ethidium bromide and extracted using the QIAquick Gel Extraction Kit®. A 1X w/v amount of isopropanol was added prior to binding DNA to the extraction column. A 0.1X volume of the eluted adapter-ligated 5C product (180bp) was run on a 2% agarose/0.5X TBE gel containing 0.5µg/mL ethidium bromide against a low DNA mass molecular weight marker of known concentration in order to validate size selection and quantify product yield for subsequent enrichment (figure 18).

Figure 18 5C products adapter-ligated with illumina PE adapters containing an inline barcode sequence of six nucleotides resolved on a 2% agarose/0.5X TBE gel run alongside a low DNA mass ladder of known concentration (lanes 1, 2, 7 & 8). Lanes 3-6: left-right, 5C keratinocyte preparations 1 and 2 and thymocyte preparations.

Eluted adapter-ligated 5C library was amplified using the following reaction conditions: 10ng of adapter-ligated 5C product, 0.35µM of PAGE purified paired-end primer 1.0; 0.35µM of PAGE purified paired-end primer 2.0, 0.2mM of dNTP mixture, a 1X concentration of *Pfu*Ultra II Fusion DNA Polymerase buffer, and 1µL of *Pfu*Ultra II Fusion DNA Polymerase (Stratagene). Amplified adapter-ligated 5C product was isolated by running on a long 2% agarose/0.5X TBE gel containing 0.5µg/mL ethidium bromide and eluted using the QIAquick Gel Extraction Kit, as before. A 0.1X volume of the eluted amplified adapter ligated 5C product (233bp) was run on a 2% agarose/0.5X TBE gel containing 0.5µg/mL ethidium bromide alongside a molecular weight marker of know concentration in order to validate size selection (figure 19). The concentration and purity of the enriched, adapter-ligated library was measured using the NanoDrop 1000 spectrophotometer.

Figure 19 Amplified, adapter ligated 5C product after size selection, four libraries, two keratinocyte (lanes 3 & 4) and two thymocyte (lanes 5 & 6) derived from discrete cell preparations resolved on a 2% agarose/0.5X TBE gel alongside a low DNA mass ladder (lanes 1,2 7, & 8).

3.7 Analysis of deep-sequenced 5C libraries

Indexed 5C libraries were sequenced on the Illumina HiSeq2000 platform in Germany at the EMBL Genome Core, courtesy of Vladimir Benes. For replicate keratinocyte libraries between 18,055,207 and 24,872,262 valid paired end reads were obtained. Between 15,482,979 and 25,757,869 valid paired-end reads were obtained per library. De-multiplexing of indexed libraries was performed by Dr Krzystof Poterlowicz (University of Bradford) using Novobarcode. 5C data sets were processed, corrected for any bias generated during LMA, and peaks called for 5C interaction frequency matrices as per Phillips-Cremins *et al*., 2013 (Phillips-Cremins et al., 2013) by Dr Krzystof Poterlowicz. 5C data were correlated with ChIP-Seq data by Dr Krzystof Poterlowicz as per Phillips-Cremins *et al*., 2013, however default MACS parameters and *P* value cut-off of $P<10^{-5}$ used for calling peaks (Feng et al., 2012). Enrichment for ChIP-Seq factor occupancy at interrogated *Hin*dIII fragments was analysed as per Phillips-Cremins *et al*., 2013 with the help of Dr Krzystof Poterlowicz.

3.8 Microarray gene expression profiling

Gene expression profiling of cells used to generate 5C libraries was performed in order to correlate gene expression data with 5C data. Total RNA was isolated from one p100 plate separated from cells plated for 5C prior to fixation. 1mL of Ambion TRI Reagent solution (Invitrogen) was added to this plate and cells homogenized by pipetting. The TRI Reagent Solution protocol was followed in order to isolate RNA from DNA and proteins. Residual DNA was removed from isolated RNA using the Ambion TURBO DNA-free Kit (Invitrogen). To extract total RNA from thymocytes, $1x10^7$ thymocytes were removed prior to fixation and 1mL of TRI Reagent Solution added. Cells were homogenized by pipetting and RNA processed for microarray again using the TRI Reagent and TURBO DNA-free kits from Invitrogen. Total purified RNA was amplified using the Arcturus RiboAmp PLUS kit (Applied Biosystems). Labelling of cDNA was performed by MOGene (St Louis, MO, USA) and microarray analysis performed using a 41K Whole Mouse Genome 60-mer oligo microarray (Agilent Technologies) at MOGene (St Louis, MO, USA).

3.9 Microaray gene expression profiling of laser capture micro-dissected epidermis

8μm cryopreserved tissue sections were transferred to MMI membrane slides (Molecular Machines and Industries) and prepared for laser capture micro-dissection (LCM) using the Arcturus HistoGene LCM Frozen Section Staining Kit (Applied Biosystems). Sections were cut immediately prior to LCM and stored momentarily on dry-ice. Sections were stained sequentially immediately prior to LCM. LCM of each section was performed in under 2 hours in order to minimise RNA degradation and captured dissected tissue stored on dry-ice. Total RNA was subsequently isolated using the ReliaPrep RNA Cell Miniprep system (Promega) and amplified using the Arcturus RiboAmp PLUS kit (Applied Biosystems). Microarray gene expression profiling was performed using a 41K Whole Mouse Genome 60-mer oligo microarray (Agilent Technologies). LCM of K14BRG1$^{\Delta/\Delta}$ (Indra et al, 2005) and age matched WT epidermis was performed in duplicate and cDNA generated for each replicate pooled prior to microarray analysis.

Labelling of cDNA and microarray analyses were performed by MOGene (St Louis, MO, USA). LCM Microarray expression data for each cell type were normalised to corresponding reference RNA. RT-PCR of unamplified reference RNA and reference RNA obtained after two rounds of amplification using the Arcturus RiboAmp PLUS kit (Applied Biosystems) was used to control for extraneous sources of variation in gene expression caused by the amplification procedure.

3.10 RT-PCR Microarray validation

Selected differentially expected candidate genes were validated using qRT-PCR. Primers to amplify candidate gene coding regions (table 2) were designed using the Primer3 primer design web-tool (Koressaar and Remm, 2007; Untergasser et al., 2012). Total RNA was isolated using the Ambion TRI Reagent Solution protocol and residual DNA removed using the Ambion TURBO DNA-free Kit (Invitrogen). RNA concentration and purity were assayed using UV spectrophotometry and cDNA synthesised from total RNA using the Promega Reverse Transcription System Kit (Promega). For the validation of microarray gene expression profiling of LCM tissue, total RNA isolated using the ReliaPrep RNA Cell Miniprep system (Promega) and amplified using the Arcturus RiboAmp PLUS kit (Applied Biosystems) was used.

Candidate genes were amplified using the default two-step Step One Applied Biosystems instrument Fast cycling regime (1 cycle: 20 seconds at 95ºC; 40 cycles: 3 seconds at 95ºC, followed by 30 seconds at 60ºC) and the following reaction composition: 5µL Fast SYBR® Green Master Mix (Applied Biosystems), 1µL of a 5µM primer stock (an equimolar mix of forward and reverse primer stocks, (table 2), 0.5µL of cDNA (undiluted reaction product), and 3.5µL of water. Relative quantification of candidate gene expression was performed using the $2^{-\Delta\Delta CT}$ method (Livak and Schmittgen, 2001). A minimum of two biological replicates and three technical replicates were used to validate respective microarray data. The C_T standard deviation of replicate samples was >0.3. Between target and calibrator samples, the C_T standard deviation of the internal control gene (glyceraldehyde 3-phosphate dehydrogenase and/or peptidylprolyl isomerase A genes) used was <0.5.

3.11 Haematoxylin and Alkaline Phosphatase staining

Frozen 9μm histological sections were dried at room temperature for 15 minutes and then fixed in acetone for 10 minutes at -20°C. After fixation, sections were washed twice in 1X PBS (0.05M, pH 7.5), 5 minutes per wash. Developing solutions were prepared immediately before use. A 104mL solution containing 0.52g of Tris(hydroxymethyl)aminomethane base (Trizma Base), 0.158g Tris(hydroxymethyl)aminomethane hydrochloride (Trizma HCl, Sigma), and 0.92g NaCl was first prepared. To 0.03g of sodium nitrite 750μL of water were added drop-wise. To the resultant solution, 300μL of New Fuchsin added. Tris and Fuchsin solutions were mixed and, to this mixture, 0.075g Napthol AS-BI Phosphate diluted in 900μL Dimethylformamide added. Sections were incubated in this freshly prepared 105mL of development solution for 15 minutes at room temperature. After alkaline phosphatase staining, sections were washed twice in 1X PBS, stained with haematoxylin for 45 seconds, and then rinsed in running water before being mounted with hard-setting mounting medium (appendix table A2).

3.12 Immunofluorescence staining

Frozen 9μm histological sections were fixed in 4% PFA/1 X PBS for 10 minutes Sections were then washed three times in 1X PBS, 5 minutes per wash. Sections were blocked with a solution of 10% donkey serum, 0.25% fish skin gelatin (w/v), 0.2% BSA in 1X PBS (w/v). For nuclear staining, Triton X-100 was added to a final concentration of 0.1%. Anti-Loricrin, anti-K10, and anti-K14, antibodies (table 5) were diluted in 1% BSA/PBS as indicated in table 5. Anti-ki67 antibody (table 5) was diluted 200 fold in 2% Trtion X-100, 1% BSA, 4% saponin (w/v). After incubation with primary antibody overnight at 4°C, sections were washed 3 times in 1X PBS, 5 minutes per wash, before incubation with 1:200 dilution of donkey anti-rabbit Alexa Fluor 488 conjugated secondary antibody (Invitrogen) in 1% BSA at room temperature for 1 hour. Sections were washed a final 3 times in 1X PBS and incubated with a 0.5μg/mL solution of Dapi in 1X PBS for 10 minutes at room temperature. Dapi stained sections were then rinsed in distilled water and mounted using VectaShield (Vector Labs) mounting medium for immunofluorescence.

BRG1 was detected using rabbit anti-mouse BRG1 antibody (Santa Cruz) to stain tissue fixed and prepared for three dimensional fluorescent *in situ* hybridization (3D FISH). Antigen retrieval was performed prior to staining. Sections were equilibrated by incubating for 5 minutes in 10mM sodium citrate buffer, pH 6.0, and heat-induced epitope retrieval performed by heating sections to boiling point twice at 800W in a microwave and cooling for two minutes between. De-masked sections were washed in 1X PBS three times, 5 minutes per wash. BRG1 antibody was diluted 1:200 in a solution containing 4% BSA and 0.2% Tween in 1X PBS and antibody and tissue incubated together overnight at 4°C. Sections were washed three times in 1X PBS, 5 minutes per wash, and antibody detected by incubating with a 1:200 dilution of donkey anti-rabbit Alexa Fluor 488 conjugated secondary antibody for 1 hour at room temperature. After staining with secondary antibody detection, sections were washed three times in 1X PBS, 5 minutes per wash. Sections were incubated with a 0.5µg/mL dilution of Dapi in 1X PBS for 10 minutes at room temperature and rinsed in water before mounting.

3.13 Terminal deoxynucleotidyl transferase dUTP nick end labeling

Terminal deoxynucleotidyl transferase dUTP nick end labeling (TUNEL) was performed using Millipore TUNEL Apoptosis Detection Kit reagents as follows. Freshly sectioned quick frozen cryopreserved tissue were fixed in 4% PFA/1X PBS for 10 minutes at room temperature. Slides were washed in 1X PBS, three washes, 5 minutes each, before incubating in a 2:1 mix of ethanol/acetic acid for 5 minutes at -20°C. Slides were then washed in PBS and incubated with terminal deoxynucleotidyl transferase (TdT) buffer (Millipore) for 10 minutes. A 90:5:5 ration of 10X TdT buffer, 250µM Biotin-dUTP solution, and TdT enzyme (3U/µL) (Millipore) were incubated with tissue for 60 minutes at 37°C. labelling was stopped by incubating slides in a 1:9 ratio of Stop buffer (Millipore): 1X TB buffer (Millipore) for 5 minutes at room temperature. Slides were washed 4 times in PBS, two minutes per wash. Blocking was performed for 20 minutes at room temperature with Blocking buffer (Millipore). Tissue was incubated with a 1-part Avidin-FITC: 9-parts blocking solution (Millipore) mixture for 30 minutes. After two 15 minute washes in 1X PBS, slides were mounted using VectaShield Mounting Medium for

Flouresnce. As a positive control, tissue was treated with a 1μg/mL solution of DNase I and subsequently washed in PBS for 15 minutes prior to end-labelling.

3.14 Fluorescence Activated Cell Sorting

Neonate mouse epidermis was isolated as detailed above. Epidermis extracted following the treatment of whole skins with trypsin was deposited and triturated in 4% chelex-treated, Ca_{2+} depleted, FBS/Ca2+ free MEM Eagle-EBSS with NEAA (Lonza Cat. No. BE06-174G) to achieve a single cell suspension of epidermal keratinocytes. This suspension was filtered through first a 70μm nylon cell strainer and then a 40μm cell strainer. Keratinocytes were pelleted by centrifuging at 200 RCF for 5 minutes at 4°C. The resultant cell pellet was washed by re-suspending in 2% chelex-treated, Ca2+ depleted FBS/PBS and again centrifuging. After washing, pelleted keratinocytes were re-suspended to a concentration of $1x10^7$ cells/mL. Four 50μL aliquots of cell suspension were diluted in 250μL of 2% chelex-treated, Ca_{2+} depleted FBS/PBS, respectively. To two of these aliquots, 6μL of 1:50 dilution of Fluorescein Isothiocyanate (FITC)-conjugated Sca-1 (appendix table A4) and a 1:50 dilution of Allophycocyanin (APC)-conjugated α6 antibody (appendix table A4) were respectively added. The remaining volume of undiluted cell suspension was divided into 800μL aliquots and to each aliquot 16μL of a 1:50 dilution of Sca-1 and 16μL of a 1:50 dilution of α6 antibody added. Staining was performed for 1 hour at 4°C with continual rotation. DAPI was added at a final concentration of 1μg/mL to double-stained cells and to one aliquot of unstained cells immediately prior to cell sorting in order to assess cell viability. The remaining aliquot of unstained cells was used to correct for cell auto-fluoresce. FACS sorting of $\alpha6^{bri}$/ Sca-1+/ epidermal keratinocytes was performed by Dr Andrei Mardaryev (University of Bradford) using the Beckman Coulter MoFlo™ cell sorter. Gated and sorted Sca-1^{bri}/$\alpha6^{bri}$ epidermal keratinocytes were pelleted, snap frozen, and stored at -80°C.

3.15 Directional whole transcriptome sequencing

Three individually sorted lots of $3x10^6$ sorted Sca-$1^{bri}/\alpha6^{bri}$ epidermal keratinocytes were used to generate replicate indexed strand specific RNA-Seq libraries. 3-5µg of total RNA was isolated from each batch of cells using the Ambion TRI Reagent Solution protocol and residual DNA removed using the Ambion TURBO DNA-free Kit (Invitrogen). DNase treated RNA was ethanol precipitated and the purity of RNA assayed using the Implen NanoPhotometer and concentration determined using the Qubit 2.0 Fluorometer (Life Technologies). Ribosomal RNA was removed from total RNA samples using the Ribo-Zero™ Gold Kit (Epicentre) and ScriptSeq™ v2 RNA-Seq Library Preparation Kits. Analysis of the fragment size distribution of input total RNA (figure 20A), ribosomal RNA-depleted RNA (figure 20B), and indexed libraries (figure 20C) was performed at TUCF Genomics (Tufts University School of Medicine, Boston MA, U.S.A) using the Fragment Analyzer™ capillary electrophoresis (CE) instrument (Advanced Analytical Technologies). Libraries sequenced on one lane of the illumina® HiSeq 2500 platform (paired-end, 100bp read length) at TUCF Genomics (Tufts University School of Medicine, Boston MA, U.S.A). Paired end RNA-Seq read alignment was performed by Dr Krzystof Poterlowics using TopHat (Kim et al., 2013) and further analysis of RNA-Seq was performed by Dr Krzystof Poterlowics using the Cufflinks RNA-Seq analysis tools (Trapnell et al., 2012).

A.

B.

C.

Figure 20 (A) Representative gel and electropherogram showing the fragment size distribution of total RNA (replicate 1) used to generate RNA-Seq librraies. Peaks at 1923 and at 4849 nucleotides in length correspond to ribosomal RNS (rRNA) present in the sample (B) Representative gel and electropherogram showing the fragment size distribution of RNA sample following the depletion of rRNA (replicate 1) (C) Representative gel and electropherogram showing the fragment size distribution of complete indexed RNA-Seq libraries (replicate 1).

3.16 Chromatin immunoprecipitation followed by sequencing (ChIP-Seq) analysis using cross-linked chromatin

32% methanol-free EM grade paraformaldehyde (PFA) (Electron Microscopy Sciences) was added to filtered PMK in suspension at a final concentration of 1% to freshly isolated keratinocytes in suspension in supplemented primary keratinocyte medium (appendix table A2). Cells were fixed with PFA for 10 minutes at room temperature with intermittent gentle mixing, after which glycine was added to a final concentration of 125mM. Cells were split into aliquots of 5 x 10^6 cells after counting and pelleted by centrifuging for 5 minutes at 4°C, 200 RCF. Pelleted cells were washed by re-suspending in ice-cold PBS and pelleted once again by centrifuging for 5 minutes at 4°C and 2000 RCF. The washed, pelleted cells were then snap frozen and stored at -80°C.

Pelleted cells were re-suspended and incubated on ice for 15 minutes in 5mL of freshly prepared *cell lysis buffer* (appendix table A2). The resultant cell lysate was pelleted by centrifuging at 800 RCF for 5 minutes. The supernatant was discarded and the pellet re-suspended and incubated at room temperature for 15 minutes in 5mL of freshly prepared *buffer A* before being centrifuged again at 800 RCF for 5 minutes at 4°C. The supernatant was discarded and the resultant pellet re-suspended in 1mL of *sonication buffer*.

Chromatin was sheared via sonication at 40% amplitude for 25 minutes (Fisher Scientific™ Model 500, cup horn) to achieve a fragment size distribution between ~200 and 250 nucleotides in size. Sheared chromatin was centrifuged for 10 minutes at 18, 000 RCF, 4°C. 25µL of the resultant supernatant containing sheared chromatin were snap frozen and stored at -80°C for later use as an "input" DNA control. An additional 50µL of supernatant were transferred to a fresh 1.5mL tube and placed on ice.

To determine the efficiency of sonication and yield of chromatin obtained, to this 50µL of sheared chromatin, a 1X volume of 1X TE buffer, pH 8.0, 5.5µL of 10mg/mL Proteinase K, and 5.5µL of 10mg/mL of RNase A were added. Chromatin was incubated with RNase A and Proteinase K for 30 minutes at 37°C and then at 55°C for 1 hour. DNA purification was then performed using either phenol-chloroform extraction and ethanol precipitation or Qiagen MinElute columns. DNA yield was quantified using UV spectrophotometry (Implen NanoPhotometer®) and ~200-300ng of DNA ran on a 1.5% agarose/0.5X TBE gel containing 5µg/mL Ethidium Bromide alongside a 1Kb DNA ladder (figure 21A).

Re-suspended Protein A Dynabeads® (Life Technologies) were washed twice in *wash buffer*, blocked in 5% BSA/1% fish skin gelatine/1X PBS, washed in *dilution buffer*, and finally re-suspended using a 1X volume of *dilution buffer*. A 3X volume of *dilution buffer* was added to 250µL aliquots of supernatant containing sheared chromatin and samples incubated for 10 minutes at room temperature. 30uL of washed Dynabeads® (Life Technologies) in *dilution buffer* were added per aliquot and tubes incubated at 4°C with rotation for 1 hour. Dynabeads® (Life Technologies) were removed and 5µg of anti-BRG1 antibody (table 5) or of Normal Rabbit IgG control added to respective tubes. Immunoprecipitation was performed overnight with rotation at 4°C. 30µL of washed beads in 5% BSA/1X PBS were added to each tube following immunoprecipitation and tubes incubated for 3 hours at 4°C with rotation.

Tubes were placed on a chilled magnetic stand and the resultant supernatant, when clear, removed. Antibody bound Protein A Dynabeads® (Life Technologies) were then re-suspended in 1mL of freshly prepared pre-chilled *wash buffer 1* and incubated at 4°C with rotation. Tubes were placed on a chilled magnetic stand again and the supernatant removed when clear. Beads were then likewise washed for 5 minutes at 4°C once in 1mL of *wash buffer 2* and *wash buffer 3* and twice in 1mL of 1X TE buffer pH 8.0, respectively (5 minutes per wash). After washing twice for 5 minutes at 4°C in TE buffer, beads were re-suspended in 200µL of 1X TE buffer pH 8.0. 0.25µL of un-precipitated chromatin (input control) was thawed and made up to 200µL with TE buffer.

To diluted "input" control and immunoprecipitated chromatin, 11µL of 10mg/mL RNase A and 11µL of Proteinase K were added. Tubes were incubated first at 37°C for 30 minutes and then at 55°C for 1 hour on a thermal shaker (Eppendorf) set at 1200rpm. To tubes containing digested chromatin, a 5X volume of Qiagen PB buffer (Qiagen) was added, tubes vortexed for 30 seconds at high speed, and placed on a magnetic stand for upwards of a minute. DNA was isolated from the supernatant, when clear, using the Qiagen MinElute kit. Elution in a 10µL volume of buffer EB (Qiagen) was performed twice using buffer EB heated to 50°C. Membrane bound DNA was incubated with pre-heated buffer EB for 3 minutes prior to elution. Additional buffer EB was added to eluted samples to bring the final elution volume up to 20µL. The purity of DNA was analysed

via UV spectrophotometry (Implen NanoPhotometer®). DNA yield was quantified using the Qubit 2.0 Fluorometer (Life Technologies).

Prior to preparing ChIP–Seq libraries, ChIP qPCR analysis of BRG1 occupancy within the Cldn1 gene promoter (Lopardo et al., 2008) (positive control) and BRG1 intronic region (negative control) was performed using the default two-step Step One Applied Biosystems instrument Fast cycling regime (1 cycle: 20 seconds at 95ºC; 40 cycles: 3 seconds at 95ºC, followed by 30 seconds at 60ºC) and the following reaction composition: 5µL Fast SYBR® Green Master Mix (Applied Biosystems), 1µL of a 5µM primer stock (an equimolar mix of forward and reverse primer stocks, (table 3), 1µL of IP or input control sample, and 3µL of water. Real-time PCR was carried out in triplicate and the C_T standard deviation of replicate samples was >0.3. The specificity of PCR reactions was assessed using melt curve analysis profiles. The fold enrichment was calculated using the ΔΔCt method (Livak and Schmittgen, 2001):

$$\text{Fold Enrichment} = 2^{(-\Delta\Delta C_T[\text{ChIP/IgG}]}$$

$$\Delta C_{T\ [\text{normalised ChIP}]} = \left(C_T[_{\text{BRG1 Ab}}] - (C_T[_{\text{input}}] - \text{Log}_2(\text{input dilution factor}))\right)$$

$$\Delta C_{T\ [\text{normalised IgG}]} = \left(C_T[_{\text{Rb IgG}}] - (C_T[_{\text{input}}] - \text{Log}_2(\text{input dilution factor}))\right)$$

$$\Delta\Delta C_{T\ [\text{ChIP/IgG}]} = \Delta C_{T\ [\text{normalised ChIP}]} - \Delta C_{T\ [\text{normalised IgG}]}$$

A 1% fraction of diluted genomic DNA input control sample was used to normalise ChIP-qPCR data for sources of variability, therefore 6.644 cycles (i.e. log2 of a dilution factor of 100) were subtracted from input control C_T values ($C_{T\ [\text{input}]}$).

Indexed ChIP-Seq libraries were generated using the NEBNext® ChIP-Seq Library Prep Master Mix Set (New England BioLabs) for Illumina® and NEBNext® Multiplex Oligos for Illumina® (New England BioLabs). ChIP-Seq libraries were purified using the Qiagen MinElute PCR Purification kit (Qiagen) and quantified using the Qubit 2.0 Fluorometer (Life Technologies). The fragment size distribution of libraries generated was determined prior to sequencing by running ~200ng of each respective library on a 1.5% agarose/0.5X TBE gel containing 5µg/mL Ethidium Bromide alongside a 1kb DNA ladder (figure 21B). 10uL of a 20nM solution of each indexed library (genomic DNA input control and BRG1 ChIP-Seq libraries) were sent for sequencing on the illumina®

HiSeq 2500 platform (single-end, 50bp read length) at TUCF Genomics (Tufts University School of Medicine, Boston MA, U.S.A). 30-70 million single-end 50bp reads per library were generated. Sequencing reads were aligned to the mm9 mouse (*Mus musculus*) assembly by Dr. Krzystof Poterlowicz using Bowtie (Langmead et al., 2009). Regions of BRG1 occupancy were identified by Dr. Krzystof Poterlowicz (University of Bradford) using Sicer (default settings) (Zang et al., 2009).

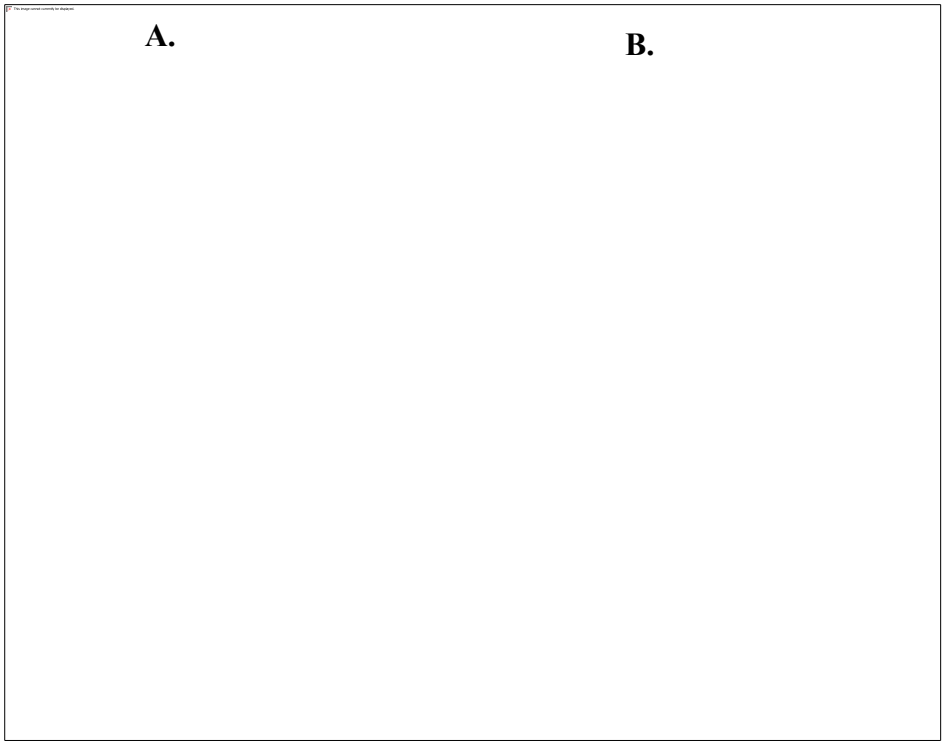

Figure 21 (A) Fragment size distribution following chromatin sheering using optimised sonication condiitons. Lanes 1 and 4: DNA ladder. Lane 2: 5μL of DNA puriifed after chromatin sheering. Lane 3: 2μL of DNA purified after chromatin sheering. (B) Representative electrophoregram. Size distribution of cross-linked chromatin immunoprecipitation sequencing (ChIP-Seq) libraries after size selelction. Lane 1: DNA ladder. Lane 2: ~200ng of sequencing library.

ChIP-Seq using cross-linked chromatin was also performed as detailed above using 2μg of antibody against H3K27ac per immunoprecipitation (appendix table A4). In addition, trichostatin A (TSA) was added to a final concentration of 100nM to all solutions (appendix table A3) immediately prior to use. Prior to the preparation of sequencing libraries, ChIP qPCR analysis of enrichment for acetylated H3K27 at the glyceraldehyde

3-phosphate dehydrogenase (GAPDH) gene promoter (table 3) and intergenic regions located on chromosomes 6 and 8 (table 3) was performed as described above. ChIP-Seq using chromatin cross-linked after isolation from FACS sorted $\alpha6^{bri/}$Sca1+ epidermal keratinocytes was performed using the ChIP-IT® High Sensativity kit (Active Motif) and antibodies against H3K27me3, CTCF, SATB1, Ringb1, RAD21, (appendix table A4) by Dr Anrei Mardaryev (University of Bradford, UK). Again, sequencing reads generated for each library were aligned to the mm9 mouse (*Mus musculus*) assembly by Dr. Krzystof Poterlowicz using Bowtie (Langmead et al., 2009). Regions of ChIP-Seq enrichment were identified by Dr. Krzystof Poterlowicz (University of Bradford) using MACS (default parameters) (Feng et al., 2012).

3.17 Native chromatin immunoprecipitation followed by sequencing (NChIP-Seq) analysis

Micrococcal nuclease (MNase) digestion and immunoprecipitation (IP) of chromatin isolated from Sca-$1^{bri}/\alpha6^{bri}$ FACS sorted epidermal keratinocytes and thymocytes freshly isolated as described above were performed using antibody against monomethylated H3K4 (table) as per Gilfillan *et al*, 2012 (Gilfillan et al., 2012). $1x10^6$ cells were used per MNase digestion and 1μg of antibody per IP comprising pre-cleared chromatin corresponding to $5x10^5$ cells. Prior to the preparation of sequencing libraries, ChIP qPCR analysis of enrichment for monomethylated H3K4 at the GAPDH gene promoter (table 3) and intergenic regions located on chromosomes 6 and 8 (table 3) as described above.

MNase digested genomic DNA input control and immunoprecipitated DNA indexed sequencing libraries were generated in duplicate for biological replicates using the NEBNext® ChIP-Seq Library Prep Master Mix Set (New England BioLabs) for Illumina® and NEBNext® Multiplex Oligos for Illumina® (New England BioLabs) and the fragment size distribution of libraries generated was determined as described above. 10uL of a 20nM solution of each indexed library (genomic DNA input control and BRG1 ChIP-Seq libraries) were sent for multiplex sequencing on one lane of the illumina® HiSeq 2500 platform (single-end, 50bp read length) at TUCF Genomics (Tufts University School of Medicine, Boston MA, U.S.A). Regions of monomethylated H3K4 enrichment

were identified by Dr. Krzystof Poterlowicz (University of Bradford) using MACS (default settings) (Feng et al., 2012). The results of ChIP-Seq analysis of the distribution of mono-methylated H3K4 in thymocytes, freshly isolated as described here, were found to be highly consistent with the results of ChIP-Seq analysis of the distribution of mono-methylated H3K4 in the thymus performed by Bing Ren lab, Ludwig Institute for Cancer Research, La Jolla, CA, US, and which have been made publicly available via ENCODE (GEO sample accession No.:GSM1000102) (Rosenbloom et al., 2013).

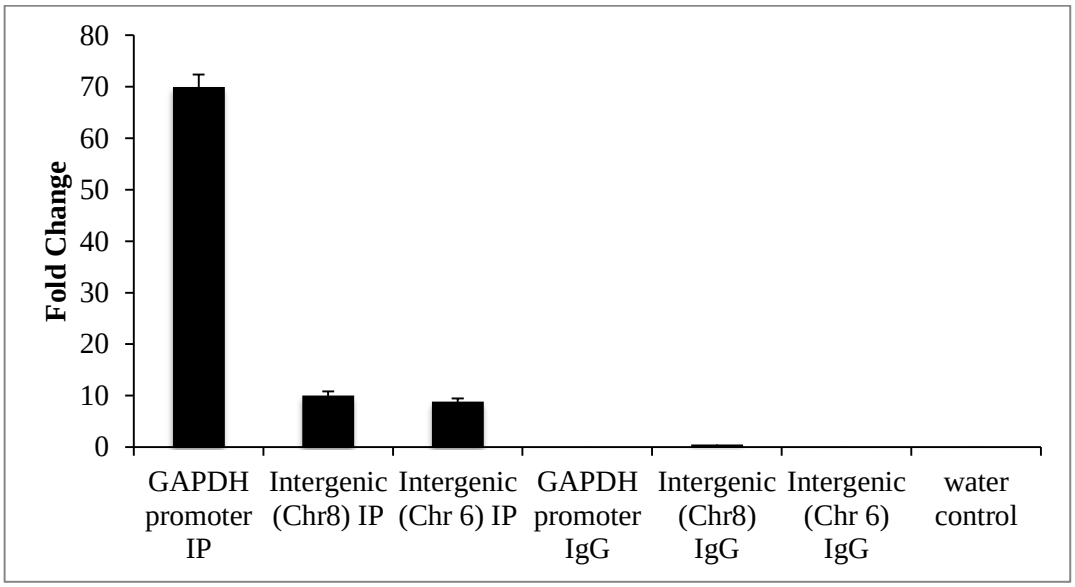

Figure 22 Relative fold enrichment at positive (GAPDH promoter) and negative (intergenic) control regions obtained following ChIP-qPCR analysis of H3K4me1 antibody immunoprecipittaion and corresponding IgG control ChIP samples. Representaive plot.

3.18 3D Fluorescent *In Situ* Hybridization

Labelled DNA probes were synthesised by nick-translation using fluorophore or biotin conjugated dUTP and individual, or pooled, BAC spanning target loci. Whole chromosome paints were labelled with Biotin conjugated dUTP by degenerate oligonucleotide-primed (DOP)-PCR. Labelled probes and chromosome paint were validated using 2D FISH on murine embryonic fibroblast metaphase spreads.

3.18.1 Preparation of mouse metaphase spreads

Neonatal mouse primary embryonic fibroblast nuclei isolated and prepared by Michal Gdula (University of Bradford, former Ph.D student) were stored at -20°C in fixative solution (a 1:3 ration of 100% methanol: 100% acetic acid) a concentration of $1x10^6$ nuclei/15mL. Spreads were prepared with reference to Deng *et al* (2003) (Deng et al., 2003). Nuclei were centrifuged at 200 RCF for 3 minutes at 4°C, the fixative decanted, and nuclei re-suspended in freshly prepared fixative solution.

Slides were placed in a dish in a water bath heated to 55°C covered and filled such that the ratio of the surface of water's surface (minus the surface area of the base of the dish in the water) to the volume of air between the flat lid and waters surface was 0.23. After allowing for the equilibration of temperature and humidity, one-two droplets of nuclei suspension were dropped onto slides. After evaporation of the fixative, slides were removed and slides carrying three or more metaphase spreads incubated in 70% ethanol overnight.

Slides were then transferred into 100% ethanol for 10 minutes and subsequently air dried for one week at room temperature in a closed box, after which they were incubated at 60°C in a hybridization oven for 2 hours. Slides were incubated in freshly prepared 0.05mg/mL pepsin/1X PBS solution for 10 minutes at 37°C and then incubated in 70% ethanol three times for 5 minutes at room temperature. Slides were dehydrated by passing though a series of increasing ethanol concentrations and once dry were stored at -20°C in a sealed plastic box.

3.18.2 Preparation of histological sections for the preservation of 3D nuclear architecture

The dorsal skin of euthanized neonate mice was removed and fixed overnight in 4% paraformaldehyde/1X PBS on a tube rotator at 4°C. Embryos >E11.5 were fixed likewise. After fixation, skins or whole embryos >E11.5 were washed for 5 minutes in 50mM NH_4Cl and then washed twice for 10 minutes in 0.1M phosphate buffer. Skins were

incubated in a 5% sucrose/0.1M phosphate buffer, pH 7.0, solution for 1 hour at 4°C and then in a 1:1 mix of 5% sucrose/0.1M phosphate, pH 7.0, buffer: 20% sucrose/0.1M phosphate buffer for 1 hour at 4°C before then incubated in a 20% sucrose/0.1M phosphate buffer solution overnight at 4°C. Skins and whole embryos were embedded in OCT using a 95% ethanol/dry ice slurry and stored at -80°C.

16μm frozen sections of FISH fixed tissue were dried at room temperature for 30 minutes. Sections were equilibrated in 10mM citrate buffer, pH 6.0, for 5 minutes at room temperature and sections subsequently heated up to 70-90°C in 10mM citrate buffer by bringing citrate buffer up to the boiling point in a microwave at 800W before cooling for two minutes. Four cycles of heating and cooling were performed before transferring sections to room temperature 2X SSC buffer. Sections were washed in 2X SSC at room temperature for 5 minutes and then transferred to 50% formamide/2X SSC buffer and incubated over night at 4°C in 50% formamide/2X SSC.

3.18.3 Preparation of cells for the preservation of 3D nuclear architecture

Thymocytes

Thymocytes were extracted from thyme as described above. Thymocytes were prepared for FISH as per Cremer *et al*, 2008 (Cremer et al., 2008) with the exception that slides, as opposed to coverslips, were coated with 1mg/mL Poly-L-lysine hydrobromide. A PAP pen was used to define a 22mm^2 area for coating with Poly-L-lysine, onto which ~200μL of thymocyte cell suspension in T cell medium (appendix table A2) (~1x10^7 cells/mL) were then added.

Keratinocytes

Freshly isolated keratinocytes isolated were seeded overnight at 32ºC with 8% $C0_2$ and 90% relative humidity onto the culture surface of a collagen coated 6 well plate containing one 22mm coverslip per well. Adherent keratinocytes were then prepared for FISH as per Cremer *et al*, 2008 (Cremer et al., 2008).

3.18.4 Generation of modified dUTPs for the generation of labelled DNA probes

Labeling of amine-modified DNA using Aminoallyl-dUTP (5-[3-aminoallyl]-2'-deoxyuridine-5'-triphosphate) and fluorescein isothiocyanate (FITC), biotin, and cyanine 3 mono NHS (Cy3) succinimidyl esters was conducted using the following conditions listed below. Aminoallyl-dUTP (5-(-3-Aminoallyl)-2'-deoxyuridine 5'-triphosphate, Sigma) was re-suspended in 0.2M bicarbonate buffer immediately prior to use.

For Digoxigenin labeling, 10µL 40mM Digoxigenin (3-amino-3-deoxydigoxigenin hemisuccinamide, succinnimidyl ester, Molecular Probes) dissolved in DMSO were combined with 10µl 20mM aminoallyl-dUTP, 15µl of water 10µl 0.2M bicarbonate buffer, and 10µl DMSO. For labelling with Cy3 10µL of a 20mM dilution of Cy3 (Amersham) in DMSO were combined with 10µL of 20mM aminoallyl dUTP, 10µL of water, and 0.2M bicarbonate buffer. For labelling with FITC, 10µL of a 40mM dilution of FITC (Molecular Probes) in DMSO were combined with 10µl of 20mM aminoallyl-dUTP, 10µl water, and 10µl 0.2M bicarbonate buffer. Finally, labelling with Biotin combined 10µL of 40mM Biotin (Bio-XX, Molecular Probes) in DMSO with 10µL of a 20mM dilution of aminoallyl-dUTP, 15µL water, and 10µL 0.2M bicarbonate buffer.

Labelling reactions were carried out for 3-4 hours at room temperature after which 2µl of 2M glycine (pH 8.0) were added to stop each reaction. To each reaction, a 4µl volume of 1 M Tris-HCl (pH 7.75) was added to stabilise the labelled nucleotides and water added to give a final concentration of mod-dUTP concentration of 1mM. That dUTP labelling reactions had resulted in the incorporation of fluorophore or biotin was confirmed by dotting a series of 0.1, 0.5, 1, and 2uL volumes of labelled probe onto a nylon membrane and heating membrane and sample at 80°C until dry (approximately 30 minutes). Blotted membrane was visualised using the XR Gel Doc™ system and Image Lab software (Bio-Rad).

3.18.5 Generation of labelled DNA probes for 3D FISH

10ng of BAC (appendix table A1) DNA were amplified using the GenomiPhi DNA amplification kit (illustra GenomiPhi V2, GE Healthcare), which utilises Phi29 DNA polymerase and random hexamer primers to non-specifically amplify whole genomic DNA via isothermal strand displacement amplification. 2µL of BAC DNA after amplification were run on a 0.8% agarose/TAE gel containing 0.5µg/mL ethidium bromide against a 1kb DNA ladder (figure 23).

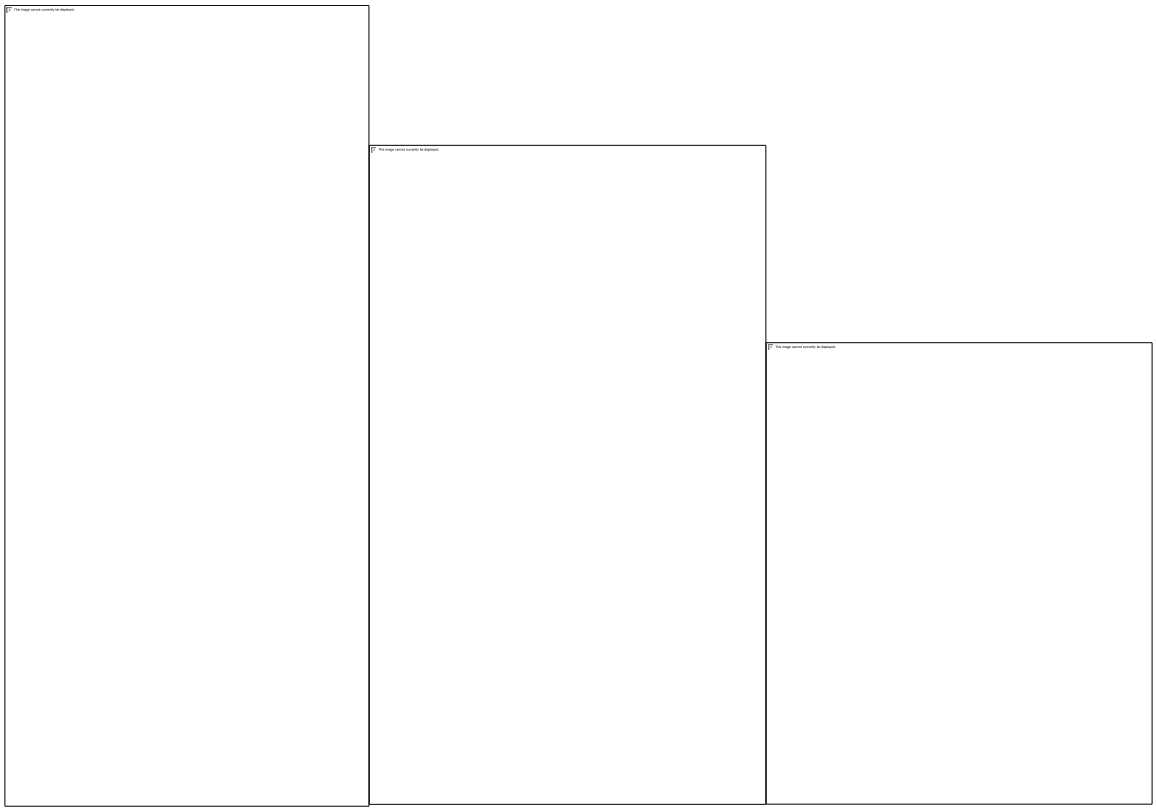

Figure 23 (A) 2µL of BAC DNA after amplification were run on a 0.8% agarose/TAE gel containing 0.5µg/mL ethidium bromide against a 1kb DNA ladder. (B) 5µL (replicate reactions lanes 1 & 2) of nick translation labelled DNA probe were run on a 1% agarose/TAE gel containing 0.5µg/mL ethidium bromide against a 1kb DNA ladder. (C) 5µL (lane 1) and 2µL (lane 2) of labelled re-amplified chromosome territory paint was run on a 1% agarose/1X TAE gel containing 0.5µg/mL of ethidium bromide alongside a 1Kb DNA ladder.

Amplified BAC DNA was then labelled via nick translation with either fluorophore modified aminoallyl-dUTP or Biotin conjugated aminoallyl-dUTP using the following reaction composition per 100µL reaction: 10µL of 10X nick translation buffer (0.5M Tris-

HCl, pH 7.5, 50mM $MgCl_2$, 0.05% BSA); 10µL of 0.1M mercaptoethanol; a 10µL volume of nick translation dNTP mix (0.5mM dATP, 0.5mM dGTP, 0.5mM dCTP, 0.1mM dTTP); 4µL of 1mM mod-dUTP (prepared as detailed above); 5µL of GenomiPhi amplified BAC DNA (undiluted, approximately 2µg of DNA); 0.1µg/mL DNaseI; 200U/mL DNA Pol I. Reactions were carried out at 30°C for 90 minutes after which time a 1X volume of stop mixture (20mM EDTA, 0.5% Dextran Blue, 20mM Tris HCl, 0.1M NaCl) was added. Labelled probe was stored at -20°C. 5µL of nick translation labelled DNA probe were run on a 1% agarose/TAE gel containing 0.5µg/mL ethidium bromide against a 1Kb DNA ladder (figure 23).

GenomiPhi amplified BAC RP23-66A15, RP24-75K3, RP23-425P7, RP23-480F10, RP23-66A15, and RP24-248L10 (appendix table A1) were pooled in equimolar amounts and collectively labelled with Cy3. 5µL of nick translation reaction were run on a 1% agarose/0.5X TBE gel containing 0.5µg/mL ethidium bromide against a 1Kb DNA ladder (figure 23B). As shown, the majority of product should run below 500bp.

3.18.6 Labelling and amplification of chromosome painting probe

Degenerate oligonucleotide PCR (DOP-PCR) was used to label and amplify chromosome territory 3 (MMU3) painting probe. Twice amplified flow sorted mouse chromosome 3 was provided by Prof. T. Cremer, Munich University, Germany. Secondary amplified paint was amplified further to generate tertiary amplified MMU3 paint and then labelled with Biotin by further DOP-PCR.

Per amplification reaction, the following were mixed: 10µL of 10X PCR buffer (Invitrogen); 4µL of 50mM $MgCl_2$; 2µL of 100µM 6MW primer (Sequence: 5' CCGACTCGAGNNNNNNATGTGG 3'; Eurofins MWG GmbH, Ebersberg, Germany) (Telenius et al., 1992); 8µL of 2.5mM dUTPs; 70µL of water; 1µL of secondary amplified MMU3 DNA (corresponding to 30-200ng of DNA); 1µL of 5U/µL *Taq* DNA Polymerase (Go*Taq*® DNA Polymerase, Promega). Secondary amplified MMU3 DNA was then re-amplified using the following thermal cycling regime: 94°C for 3 minutes, 35 cycles 94°C for 1 minute, 56°C for 1 minute, 72°C for 2 minutes, final extension 72°C 5

minutes. 2μL and 5μL of amplified chromosome territory paint was run on a 1% agarose/1X TAE gel containing 0.5μg/mL of ethidium bromide alongside a 1Kb DNA ladder. Amplified chromosome paint was stored at -20°C.

To label tertiary amplified MMU3 paint the following reaction conditions were used. Each reaction comprised: 10μL of 10X PCR buffer (Invitrogen magnesium chloride free 10X PCR reaction buffer Cat. No.Y02028); 4μL of 50mM (2mM) magnesium chloride; 2μL of 100μM (2μM) 6MW primer (Telenius et al., 1992) (Sequence: 5' CCGACTCGAGNNNNNNATGTGG 3'; Eurofins MWG GmbH, Ebersberg, Germany); 5μL of 2mM (0.1mM) dAGC mix; 8μL of 1mM (0.08mM) dTTP; 6μL of 1mM (60μM) Bio-dUTP (prepared as detailed above), 2μL of tertiary amplified MMU3 paint, and 1μL (5U/μL) of *Taq* polymerase were added. The following thermal cycling regime was then used to label re-amplified chromosome paint: 3 minutes at 94°C; 35 rounds of 30 seconds at 94°C, 1 minute at 56°C, and 30 seconds at 72°C; and a final extension step of 5 minutes at 72°C. 2 and 5μL of labelled amplified MMU3 paint were run alongside a 1Kb plus ladder on a 1% agarose/1X TAE gel containing 0.5μg/mL ethidium bromide (figure 23).

3.18.7 2D Fluorescent *In Situ* Hybridization

2D FISH was performed on mouse embryonic fibroblast metaphase spreads to check probe labelling and specificity as follows: 25μL of one FITC and one Cy3 or digoxygenin labelled probe were mixed with 25μL of chromosome 3 territory paint (Biotin-MMU3), 15μL of Cot1 or Hybloc DNA, and a 2.5X volume of ice cold glacial ethanol added. This mixture was then incubated at -80°C for 15-20 minutes and subsequently centrifuged at 18, 000 RCF for 15 minutes at 4°C. The resultant DNA pellet was briefly air dried at room temperature and a 1.5μL volume of deionised formamide added. Pelleted DNA was heated at ≤50°C in formamide and vortexed every 10 minutes until re-suspended. Once re-suspended, 1.5μL of hybridisation master mix (2XSSC/dextran sulphate) was added and the probe mixture mounted using a 0.17x15x15mm coverslip. The coverslip was sealed using Fixogum Rubber Cement (Marabu, Germany).

After drying rubber cement for 15-20 minutes, denaturation of DNA was performed at 75°C for 2 minutes using a hot block or thermo cycler and slide holder and probes hybridised overnight at 37°C in a humid dark chamber. After hybridisation, spreads were washes three times in 2X SSC at 37°C for 10 minutes and then once in 0.1X SCC for 10 minutes at 60°C. Biotin labelled chromatin painting probe was detected using a 1:100 dilution of Alexa Fluor 647 streptavidin conjugate (Invitrogen, Cat. No. A21370; stock aliquot: 1 mg: 500µl H_2O + 500µl glycerol) in 4%BSA/2X SSC solution. When present, digoxygenin hapten labelled BAC probe was detected using a 1:100 dilution of Indocarbocyanine, Cy3, conjugated mouse anti-digoxygenin (Jackson ImmunoResearch, Cat. No. 200-162-156; stock aliquot: 0.5 mg: 250µl H_2O + 250µl glycerol). After staining for indirect detection of biotin and hapten labelled probes for 1 hour at room temperature, spreads were washed three times for 5 minutes in 4X SSC buffer at 37°C, slides rinsed in distilled water and mounted with Vectashield mounting medium containing Dapi (Vector Labs).

3.18.8 3D Fluorescent *In Situ* Hybridization

3D FISH on p1.5 structurally preserved skin and E16.5 embryonic histological sections was performed as follows. 125µL of each of respectively labelled BAC DNA probes (appendix table 1) were mixed with 80µL of Cot1 or Hybloc™ competitor DNA (Applied Genetics Laboratories, Inc.) and a 2.5X volume of ice-cold glacial ethanol. DNA was precipitated by incubating the probe mixture for 20 minutes at -80°C and subsequently centrifuging the mixture at 18, 000 RCF for 15-20 minutes at 4°C. The resultant DNA pellet was briefly air dried at room temperature and a 15µL volume of deionised formamide added. DNA pellet and formamide were incubated at ≤50°C and vortexed at 10 minute intervals until the pellet was re-suspended. A 15µL volume of hybridisation master mix was then added and the mixture vortexted. The probe mixture was mounted using pre-prepared glass chambers created using 15mm coverslips and chambers sealed using Fixogum Rubber Cement (Marabu, Germany). After drying rubber cement for 15-20 minutes, probes were pre-hybridised over night at 37°C in a humid dark chamber after which DNA was denatured at 85°C for 5 minutes.

Hybridization was carried out for 40-48 hours at 37°C, after which tissue sections were washed three times in 2X SSC buffer at 37°C. Biotin labelled BAC probe was detected using a 1:100 dilution Alexa Fluor 647 streptavidin conjugate (Invitrogen, Cat. No. A21370; stock aliquot: 1 mg: 500µl H_2O + 500µl glycerol) in 4%BSA/2X SSC solution. Samples were incubated with diluted Fluor 647 streptavidin conjugate for 1 hour at room temperature and subsequently washed three times in 4X SSC for 10 minutes at 37°C and then once in 0.1X SSC at 60°C for 10 minutes. Sections were stained with 0.2µg/mL Dapi in 2XSSC for 10 minutes at room temperature and mounted using Vectashield mounting medium (Vector Labs) using a 0.17mmx15x15mm coverslip.

3D FISH on seeded 3D preserved keratinocytes and thymocytes was performed as follows. 62.5µL of each of respectively labelled BAC DNA probes (appendix table 1) were mixed with 40µL of Cot1 or Hybloc DNA and DNA and a 2.5X volume of ice-cold glacial ethanol. DNA was precipitated by incubating the probe mixture for 15-20 minutes at -80°C and subsequently centrifuging the mixture at 18, 000 RCF for 15-20 minutes at 4°C. The resultant DNA pellet was briefly air dried at room temperature and a 7.5µL volume of deionised formamide added. DNA pellet and formamide were incubated at ≤50°C and vortexed at 10 minute intervals until the pellet was re-suspended. A 7.5µL volume of hybridisation master mix was then added and the mixture vortexed. The probe mixture was mounted using round 22mm coverslips and Fixogum Rubber Cement (Marabu, Germany) used to place a seal around coverslip and slide. After drying rubber cement for 15-20 minutes, DNA was denatured at 85°C for 3 minutes.

Hybridization was carried out for 40-48 hours after which tissue sections were washed three times in 2X SSC buffer at 37°C. Biotin labelled BAC probe was detected using a 1:100 dilution of Alexa Fluor 647 streptavidin conjugate (Invitrogen, Cat. No. A21370; stock aliquot: 1 mg: 500µl H_2O + 500µl glycerol) in 4%BSA/2X SSC solution. Samples were incubated with diluted Fluor 647 streptavidin conjugate for 1 hour at room temperature and subsequently washed three times in 4X SSC for 5 minutes at 37°C. Sections were stained with 0.2µg/mL Dapi in 2XSSC for 10 minutes at room temperature and mounted using Vectashield mounting medium (Vector Labs) using a 0.17mmx22mm round coverslip. All 3D FISH experiments were performed in duplicate. 3D FISH on

seeded structurally preserved keratinocytes and thymocytes was performed at least twice using different cell preparations.

3.19 Immuno-FISH

3D FISH on histological sections was performed using BAC spanning the EDC region collectively labelled with Cy3. 125µL of labelled BAC-pool, 60µL MMU3 paint, 30µL of Cot1 or Hybloc DNA and a 2.5X volume of ice-cold glacial ethanol were combined. DNA was precipitated by incubating for 20 minutes at -80°C and subsequently centrifuging the probe-blocking DNA mixture at 18, 000 RCF for 20 minutes at 4°C. The resultant DNA pellet was briefly air dried at room temperature and re-suspended in hybridisation mixture (15µL formamide: 15µL of 20% dextran sulphate in 4X SSC). Probe pre-hybridisation was performed overnight and, after denaturing DNA for 5 minutes at 85°C, hybridisation was performed for 40-48 hours. After hybridization, 3 10 minutes washes in 2X SSC were performed at 37°C.

Sections were transferred to 1X PBS and then incubated with a 4% BSA/1X PBS/0.1% Triton X-100/0.1% Saponin blocking solution for 15 minutes at room temperature. Sections were incubated with a 1:20 dilution of mouse anti-splicing factor sc35 monoclonal antibody (Sigma) (diluted 1:1 in 50% glycerol) and a 1:100 dilution of Alexa Fluor 647 streptavidin conjugate (Invitrogen, Cat. No. A21370; stock aliquot: 1 mg: 500µl H2O + 500µl glycerol) in blocking solution were incubated overnight at 4°C. Sections were then washed three times in 1X PBS/0.05% Triton X-100, 5 minutes per wash. Mouse anti-splicing factor SC-35 antibody was detected by incubating with a 1:100 dilution of 2mg/mL Alexa Fluor 488 conjugated goat anti-mouse secondary antibody (Invitrogen) for 3 hours at 37°C. Sections were then washed in 1X PBS and counterstained with 0.5µg/mL DAPI in 1X PBS before mounting using VectaShield mounting medium.

3.20 3D FISH image acquisition and analysis

2D and 3D images were acquired using the confocal laser scanning microscope Zeiss LSM510 Meta (UV laser: Enterprise (351nm, 364 nm wave lengths); VIS lasers: Argon (458 nm, 477 nm, 488 nm, 514 nm), HeNe1 (543 nm) and HeNe2 (633nm)). Stacks of confocal images were acquired using the 63x/1.4 plan-apochromat oil objective lens and a voxel size of 100nm x 100 nm x 200 nm (z-axial distance: 200nm). All statistics were performed using R (R Development Core Team, 2010) and Microsoft Xcel. Image analysis was performed using ImageJ (Schneider et al., 2012) or Fiji (Schindelin et al., 2012) and the Zeiss LSM Image Browser (Carl Zeiss International).

To demonstrate co-localization of fluorescence emission at several wavelengths, scanning of 0.5µm TetraSpec™ beads (Life Technologies) was performed in order to correct for longitudinal, or axial, chromatic aberration. Images of 0.5µM TetraSpec beads were recorded in separate channels responding to the fluorophores used for labelling DNA probes. Image stacks were acquired using the 63x/1.4 plan-apochromat lens and a voxel size of 100nm x 100 nm x 200 nm as detailed above. For 30 beads, the centroids of each bead, in each channel, were calculated using the Sync Measure 3D ImageJ plugin. Mean axial shift values obtained for each axis were applied to locus coordinate measurements in Xcel in order to correct for chromatic aberration.

To measure the intergenic distances between fluorophore labelled DNA probes, the Fiji 3D Objects Counter plugin (Bolte and Cordelieres, 2006) was used to obtain the coordinates of respective FISH signal centroids after implementing spatial mean filtering on image stacks (Ollion et al., 2013). 66 centroid coordinates for 33 basal epidermal keratinocyte nuclei were acquired per sample. The average nuclear radius was determined for each nucleus, relative to the nuclear geometric centre (Ronneberger et al., 2008). Coordinates of several hundred points at the nuclear periphery were acquired per nuclei. Coordinates demarcating the nuclear periphery were averaged to estimate the coordinates of the nuclear geometric centre and the average nuclear radius of each nucleus calculated as a mean of the distance of the nuclear geometric centre to each point at the periphery selected. After correction for chromatin aberration, the radial position of FISH signal centroids was then calculated as the distance between centroid and nuclear centre. Centroid-nuclear centre distances were then normalised to the average nuclear radius of the corresponding nucleus.

The generation of histograms and quantile-quantile plots was used to visually assess the distribution of each data set. In addition the Anderson-Darling and Shapiro-Wilks tests was used to quantify a confidence level in the hypothesis that a particular data set fit a normal distribution. Statistical comparison between the radial position of the *Lor* and *Rps27* gene loci in BRG1 $ep^{-/-}$ and wild type nuclei was made using the Welch's two-sample *t*-test. For each data set the mean and standard error of the mean (SEM) were calculated. Comparison between *LOR* and *RPS27* inter-locus distances (both raw and normalised) in BRG1 $ep^{-/-}$ and wild type nuclei was made using the Welch's *t*-test. For each data set the mean and SEM were calculated. The median values for the nuclear radius of basal epidermal keratinocytes in BRG1 $ep^{-/-}$ and wild type skin were compared using the two-sample Kolmogorov–Smirnov test and the Median Absolute Deviation (MAD) calculated for each data set. Comparison of inter-locus distances marked by FISH of labelled DNA probes corresponding to the three loci, A (Chr3:91,894,818-92,021,235), B (Chr3:92,583,402-92,766,349), and C (Chr3:93,215,624-93,411,886), at the EDC that was performed on structurally preserved thymocytes, freshly isolated normal keratinocytes and on C57BL/6 p1.5 skin sections as described above in section) was made using the Wilcoxon-rank-sum test.

For basal keratinocyte E16.5 BRG1 $ep^{-/-}$ and basal wild type control nuclei, the position of the EDC, *LOR* and *RPS27* loci relative to MMU3 and the nuclear periphery was semi-quantitatively measured. Each probe signal centroid corresponding to a locus was categorized as occupying one of three positions within chromosome territory 3: internal, peripheral or central, as defined according to the proximity of each region to the nuclear centre. The total number of loci identified as occupying a central potion within territory 3 was divided equally between 'peripheral' and 'internal' categories. Pairwise comparison of the localisation of loci relative to MMU3 in BRG1 $ep^{-/-}$ and WT basal keratinocyte nuclei was made using the Chi Square goodness of fit test. Pairwise comparison of inter-loci distances was made using the Student's *t*-test after testing for normality using the Kolmogorov-Smirnov test.

3.21 BACs, oligo sequences, and antigens

3.21.1 Primer/NGS adapter sequences

Genomic region (mouse)	Distance from *Hin*dIII restriction site (bp)	Primer sequence
GAPDH-1	155	ATGGAGACCTGCCGCCGGCTCATCACAC
GAPDH-2	128	CGTGCTGTGACTTCGCACTTTTCTGATC

Table 1

Gene (mouse)	Accession number	Forward/reverse primer sequence
SMARCA/BRG1	NM_009351	F:CGTAAGCGTAAGCGAGAC R:CATCTTCTTGGTGAGGTTAGG
FLG2	NM_001013804	F:GGAACAGAAGGACAGGAG R:TATGTATATAGCGGAGTATTGC
GABPB2	NM_026493	F:TTCCACTTAGTTTCTGACATCTTG R:GTACATAAAGCTGCCAGACAAC
IVL	NM_008412	F:GCAGGAGAAGTAGATAGAG R:TTAAGGAAGTGTGGATGG
LCE1A1	NM_025984	F:TTCACCAGCAGAGATGTC R:CCAGACTACAGCAGGAAG
LCE1A2	NM_028625	F:TTCACCAGCAGAGATGTC R:TACAGCAGGAAGACACAG
LCE3	NM_033175	F:CCAGTTCCTGCCGAGATG R:ACTTTGGAGAGGGACACTTG
LOR	NM_175656	F:TTCCAAACCCTTCACATTTTAAG R:GGGAGGTAGTCATTCAGAAAC
RPS27	NM_033596	F:CTGCTCCACTGTCCTCTG R:GGTTCCCACTCATCTTCAATC
S100A9	NM_002965	F:CCTGACACCCTGAGCAAGAAG R:CAGCATCATACACTCCTCAAAGC
S100A6	NM_014624	F:AAGCTGCAGGATGCTGAAAT R: CCCTTGAGGGCTTCATTGTA

Table 2

Genomic Region (mouse)	Forward/reverse primer sequence
BRG1 893/1050	F: GCCCTTCCCAGTTTTTAAGATAG R:ACTCAAAGGCTGTCTGTCAGTTC
BRG1 1181/1440	F: GCAAATCGTTCCTACATCATCA R:AAGGAGAAACGTCCCCATATTT
CLD1 promoter	F: TGGAAGCATCCCTTGTTTTC R:TTGCTGTCCTCTCTGGGTCT
GAPDH promoter	F: ATCCTGTAGGCCAGGTGATG R: AGGCTCAAGGGCTTTTAAGG
Chromosome 8 intergenic (chr8:76183628-76183767)	F: AAGGGGCCTCTGCTTAAAAA R: AGAGCTCCATGGCAGGTAGA
Chromosome 6 intergenic (chr6:72428129-72428243)	F: CCCCTTTCTGAAGCACTCTG R: TAAGGCGTCATTTCCCAAAG

Table 3 (Mm9/GRC37)

Indexed PE NGS adapter/PCR primer name	Indexed PE NGS adapter/primer sequence
Mp19 adapter 1	[Phos]CGGAATAGATCGGAAGAGCGGTTCAGCAGGAATGCCGAG
Mp19 adapter 2	ACACTCTTTCCCTACACGACGCTCTTCCGATCTATTCCG*T
Mp46 adapter 1	[Phos]TTAGGCAGATCGGAAGAGCGGTTCAGCAGGAATGCCGAG
Mp46 adapter 2	ACACTCTTTCCCTACACGACGCTCTTCCGATCTGCCTAA*T
Mp31 adapter 1	[Phos]GCTCCAAGATCGGAAGAGCGGTTCAGCAGGAATGCCGAG
Mp31 adapter 2	ACACTCTTTCCCTACACGACGCTCTTCCGATCTTGGAGC*T
Mp8 adapter 1	[Phos]AACTTGAGATCGGAAGAGCGGTTCAGCAGGAATGCCGAG
Mp8 adapter 2	ACACTCTTTCCCTACACGACGCTCTTCCGATCTCAAGTT*T
PE PCR Primer 1	CAAGCAGAAGACGGCATACGAGATCGGTCTCGGCATTCCTGCTGAACCGCTCTTCCGATC*T
PE PCR Primer 2	AATGATACGGCGACCACCGAGATCTACACTCTTTCCCTACACGACGCTCTTCCGATC*T

Table 4 * Phosphorothioate bond

3.21.2 Antigen and antigen dilutions used in immunostaining reactions

Antigen	Host	Dilution	Manufacturer
P63a	Rabbit	1:200	Santa Cruz Biotechnology, Santa Cruz, CA, USA
SATB1	Rabbit	1:100	Cell Signaling, Denvers, MA, USA
Loricrin	Rabbit	1:1000	Covance, Emeryville, CA
Ki-67	Rabbit	1:200	Abcam, Cambridge, UK
SC-35	Mouse	1:20	Sigma, St Louis, MO
Smarca4/BRG1	Rabbit	1:200	Santa Cruz Biotechnology, Santa Cruz, CA, USA

Table 5

4 Results

4.1 The chromatin remodeler BRG1 modulates nuclear positioning of the EDC and programmes of EDC gene expression during epidermal ontogenesis

The inactive murine EDC locus occupies a position proximal to the nuclear periphery in dermal fibroblasts (Mardaryev et al., 2014), thymocytes (unpublished data) and is located within LADs in several mouse and human cell types (Guelen et al., 2008; Peric-Hupkes et al., 2010). During normal epidermal stratification *in utero*, keratinocyte-specific centripetal relocation of the EDC locus away from the nuclear periphery coincides with the increased association of the EDC with nuclear speckles and with the up-regulation of genes at the EDC locus at E16.5. In the absence of p63 however, it has been shown the locus remains situated in proximity with the nuclear periphery during epidermal stratification (Mardaryev et al., 2014).

A number of genes encoding chromatin-remodelling factors show altered expression levels in the epidermis of $p63^{-/-}$ mice, including BRG1. Shown to be a direct target of p63 (Mardaryev et al., 2014), BRG1 (also known as SMARCA4) is a catalytic component of the SWI-SNF chromatin-remodelling complex, which influences the regulation of transcription by actively disrupting histone–DNA contacts. BRG1 is expressed in basal keratinocytes from embryonic day 10.5 (E10.5) onwards and loss of BRG1 during epidermal morphogenesis leads to epidermal barrier defects associated with aberrant terminal keratinocyte differentiation (Indra et al., 2005). Moreover, tissue-specific activation dependent higher–order chromatin remodelling at the human major histocompatibility (MHC) locus at 6p21 and protrusion of the locus from chromosome territory 6 involves recruitment of BRG1 (Christova et al., 2007). To understand the potential contribution of BRG1 to the regulation of keratinocyte-specific programmes of gene expression and chromatin remodelling during epidermal ontogenesis, comparison was made between the epidermis of E16.5 BRG1 $ep^{-/-}$ (Indra et al., 2005) and wild type mice.

Tamoxifen was administered to K14CreER/BRG1$^{L2/L2}$ mice from day E10.5 onwards as described previously (Indra et al., 2005). In comparison with wild-type expression levels, microarray expression profiling and qRT-PCR analysis of laser-capture micro-dissected epidermal tissue showed a marked reduction in BRG1 transcript levels in the epidermis of K14BRG1$^{\Delta/\Delta}$ mice at E16.5 (figure 24C). Immunostaining against BRG1 in E16.5 K14BRG1$^{\Delta/\Delta}$ and wild-type skin sections showed BRG1 protein is largely absent throughout the epidermal compartment of K14BRG1$^{\Delta/\Delta}$ skin at E16.5 in comparison with the epidermis of E16.5 wild-type controls (figure 24A).

4.1.1 The expression of differentiation specific genes encoded at the EDC locus is altered in the epidermis of E16.5 K14BRG1$^{\Delta/\Delta}$ mice

Microarray analysis of RNA isolated from micro-dissected E16.5 K14BRG1$^{\Delta/\Delta}$ and wild type control epidermal tissue indicates the expression profile of several EDC genes encoding key components of the epidermal barrier is substantially altered by the K14-Cre driven genetic ablation of BRG1 at E10.5. During stratification of the embryonic epidermis in wild-type mice, the transcriptional activity of genes within the EDC in epidermal keratinocytes is substantially up-regulated. While EDC genes, including *LOR*, *FLG*, and members of the *SPRR, LCE, and S100* gene families, are expressed at low or moderate levels at E11.5, from E14.5 and E16.5 the expression of these genes is dramatically increased during the remainder of epidermal ontogenesis (Mardaryev et al., 2014). Microarray and immunoflourescence analyses of K14BRG1$^{\Delta/\Delta}$ epidermis show that following the ablation of BRG1, the expression of a number of these EDC genes, including *LOR*, and members of the *SPRR* and *LCE* families, is considerably reduced, although BRG1 deletion appears to differentially affect the expression of individual gene transcripts within the *SPRR* and *LCE* gene families (figure 24B-D).

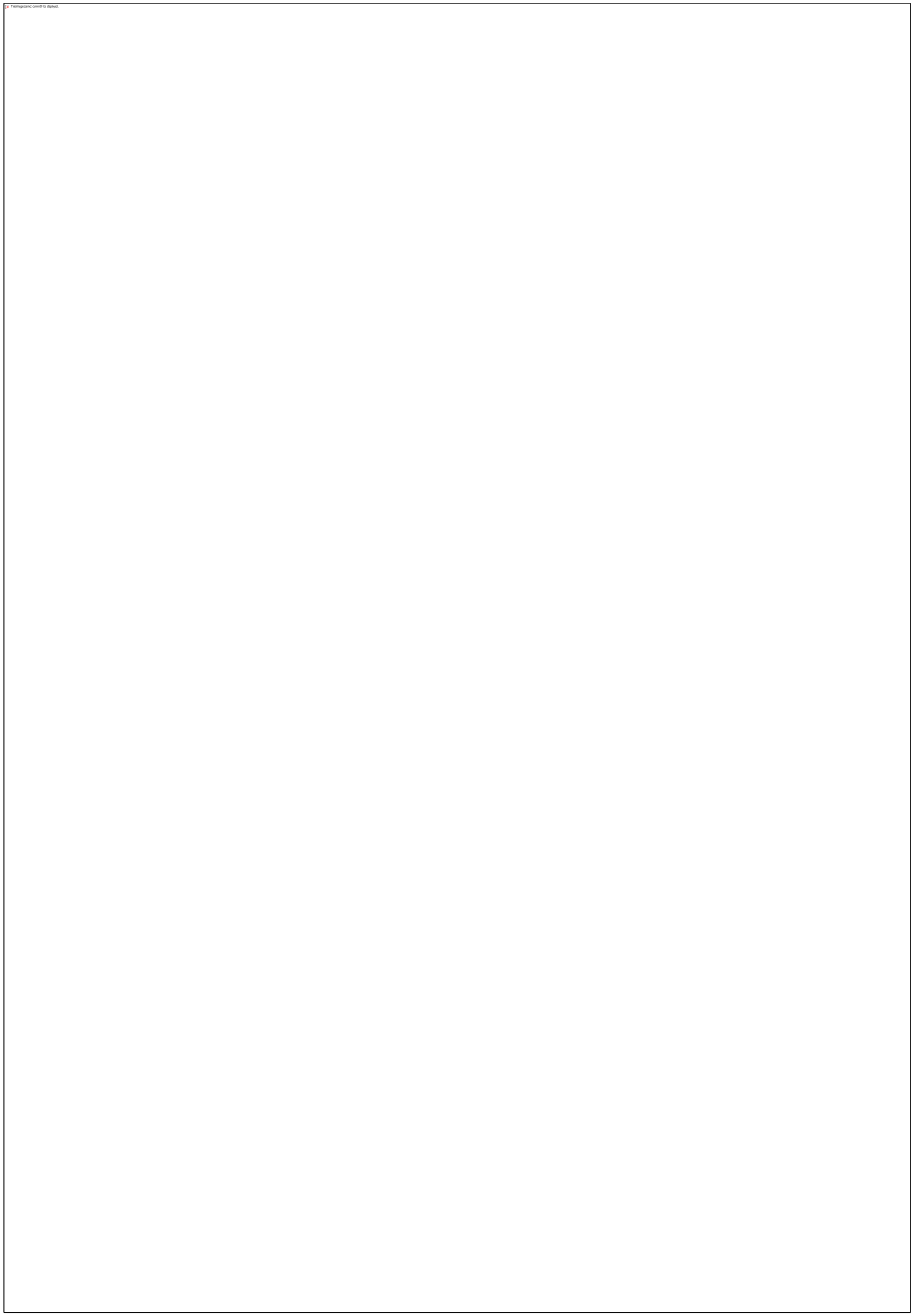

Figure 24 BRG1 deficiency during epidermal ontogenesis impacts upon the expression of differentiation specific genes within the epidermis. (A) Immunoflourescence staining of BRG1 in sections of murine wild-type (WT) and

K14BRG1$^{\Delta/\Delta}$ skin at embryonic day E16.5. (**B**) Comparison of DNA microarray data from laser-capture micro dissected (LCM) K14BRG1$^{\Delta/\Delta}$ and E16.5 control wild-type (WT) epidermis. Asterisk indicates where fold change (FC) in gene expression has been confirmed by quantitative real time PCR (qRT-PCR) analysis. (**C**) Confirmation of FC in EDC and BRG1 gene expression levels by qRT-PCR analysis of EDC and BRG1 gene expression in the epidermis of K14BRG1$^{\Delta/\Delta}$ mice. Gene expression values for K14BRG1$^{\Delta/\Delta}$ epidermis normalised to corresponding expression values in WT epidermis. Error bars show SEM (**D**) Immunoflourescence staining of loricrin in sections of WT and K14BRG1$^{\Delta/\Delta}$ skin at embryonic day E16.5.

4.1.2 BRG1 deficiency during epidermal ontogenesis results in a significant reduction in epidermal thickness at E16.5

The epidermis of K14BRG1$^{\Delta/\Delta}$ mice at E16.5 appears to be significantly (two-tailed *t*-test: t=4.212, df=57.702, P=8.987x10^{-5}) thinner than that of corresponding wild-type embryos (figure 25), although the use of terminal deoxynucleotidyl transferase dUTP nick end labelling (TUNEL) to mark apoptotic keratinocytes indicates epidermal BRG1 deficiency does not result in elevated levels of apoptosis in the epidermis at E16.5 (appendix figure A1). Staining against Ki67 in the epidermis of K14BRG1$^{\Delta/\Delta}$ mice at E16.5 indicates epidermal keratinocyte proliferation is not significantly (two-sample *t*-test: t=1.128, df=41.636, P=0.266) affected by the ablation of BRG1 (appendix figure 1A). However, loricrin transcript and protein levels are substantially reduced in the epidermis of E16.5 K14BRG1$^{\Delta/\Delta}$ mice (figure 24 B-D).

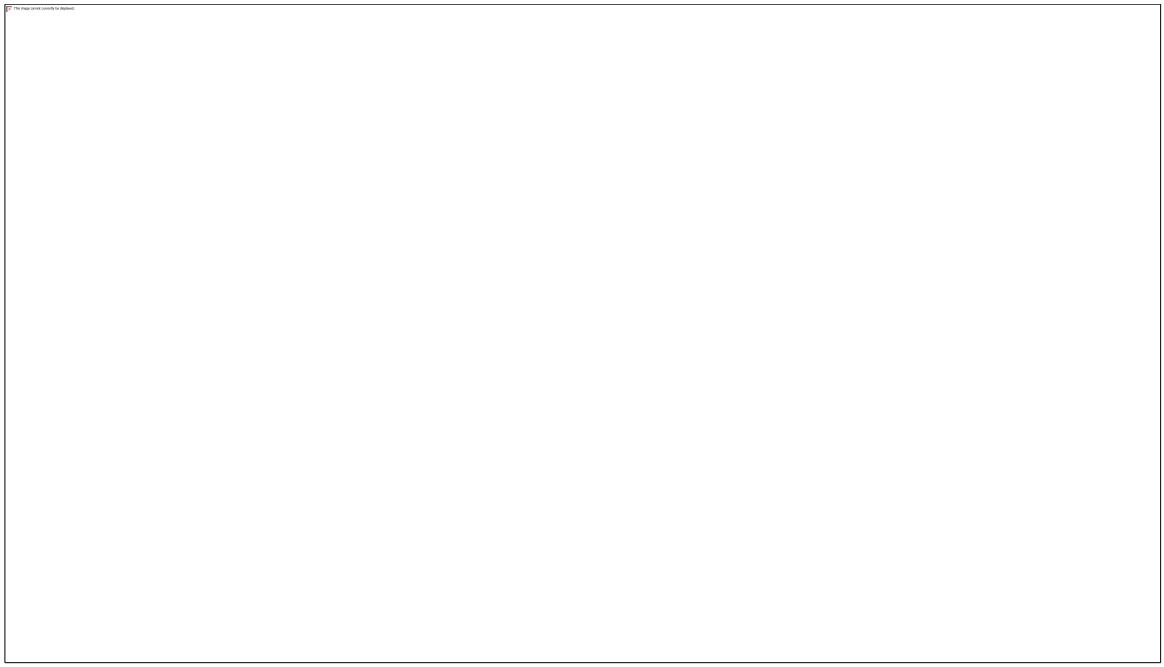

Figure 25. **Administering tamoxifen to E10.5 K14CreER/BRG1$^{fl/fl}$ mice results in a reduction in epidermal thickness at E16.5**. Epidermal thickness in: (**A**) haematoxylin stained sections of murine wild-type (WT) and K14BRG1$^{\Delta/\Delta}$ skin at embryonic day E16.5, bar = 20μM (**B**) The thickness of the epidermal layer in stained sections was measured as the distance between the top of the basement membrane and the bottom of the stratum corneum at four randomly selected points per section. Average epidermal thickness (μM) of K14BRG1$^{\Delta/\Delta}$ mice and wild-type control mice at E16.5. Mean and S.E.M; n=50 (No. biological replicates = 2), * P=8.987x10^{-5} (two-sample Student's *t*-test). Scale bars: 20μM.

4.1.3 BRG1 binds multiple sites at the EDC in epidermal keratinocytes

Chromatin-immunoprecipitation sequencing (ChIP-Seq) analysis of BRG1 bound chromatin and regions of enhancer-associated enrichment for H3K4 monomethylation and H3K27 acetylation was performed. ChIP-Seq analysis of BRG1 binding at the EDC and flanking regions shows BRG1 binds multiple distinct sites spanning the EDC, however limited BRG1 binding at candidate gene regulatory elements marked by enrichment for H3K4 monomethylation and H3K27 acetylation was observed (figure 26).

A.

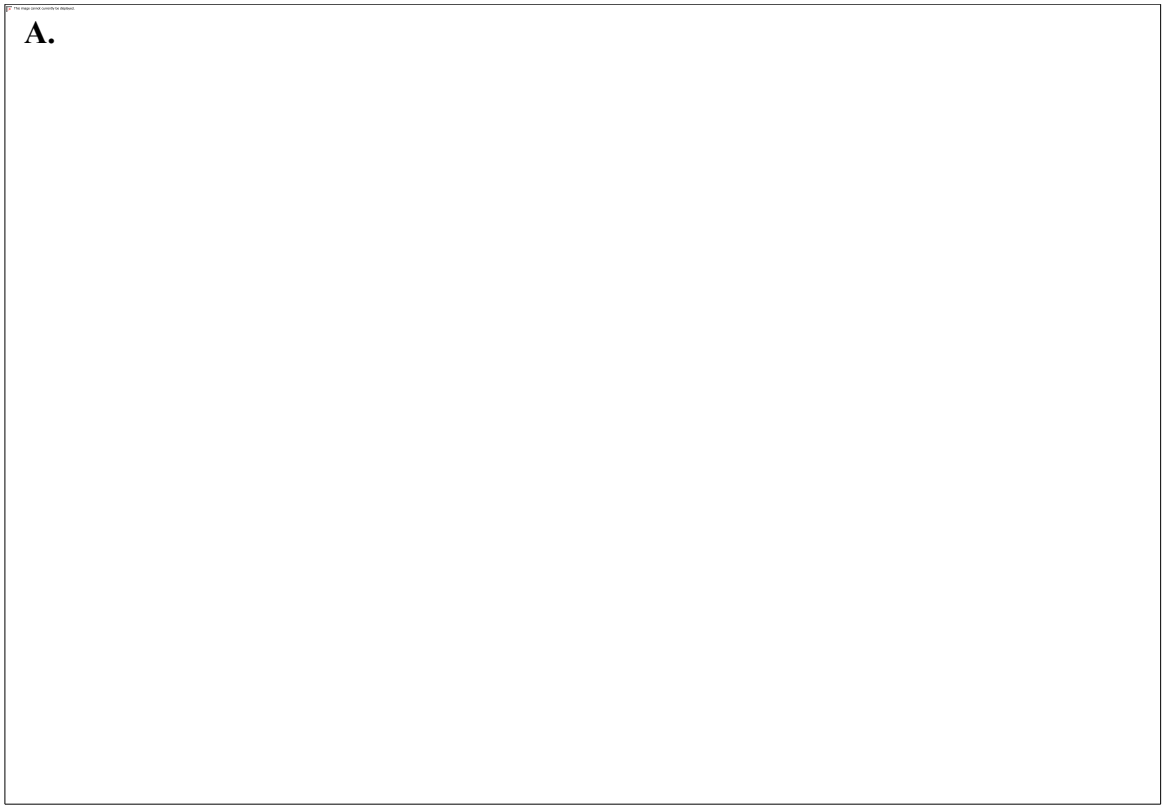

B.

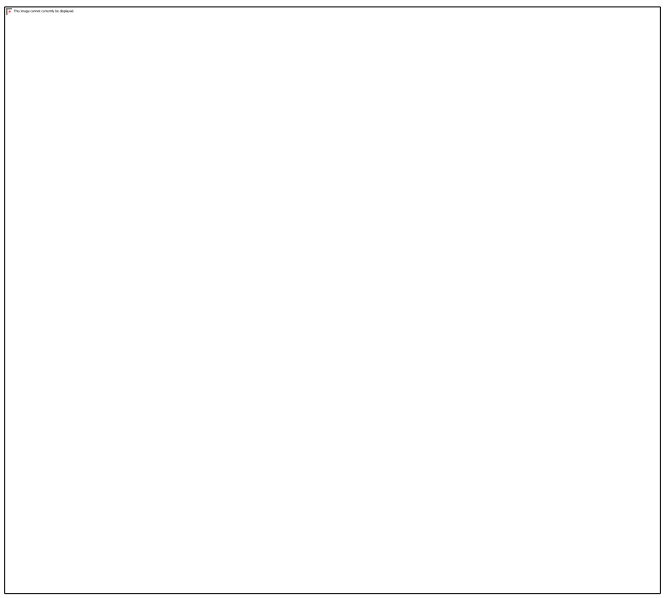

Figure 26 (**A**) Analysis of BRG1 Chromatin immunoprecipitation sequencing (ChIP-Seq) signal density at the Epidermal Differentiation Complex (EDC) in mouse epidermal keratinocytes. Normalised counts: reads per million (RPM) (**B**) Venn diagram showing unique and overlapping sites enriched for BRG1, monomethylated H3K4 (H3K4me1), and acetylated H3K27 (H3K27ac) occupancy.

4.1.4 The nuclear position of the EDC locus within basal keratinocyte nuclei is altered in the absence of BRG1

Multi-colour 3D fluorescence *in situ* hybridisation (FISH) was performed to determine the position of the murine EDC and *LOR* loci and the neighbouring, ubiquitously expressed, *RPS27* locus (figure 27) within the nuclei of basal keratinocytes in the embryonic epidermis of K14BRG1$^{\Delta/\Delta}$ and wild-type control mice at E16.5. To determine the position of the EDC, *LOR* and *RPS27* loci relative to CT3, chromosome paint was used to demarcate chromosome territory 3 (CT3) and regions within CT3 defined as either peripheral or internal as defined by their proximity to the nuclear periphery. As CT3 tends to be situated at the nuclear periphery (see figure 5), this also means loci located within the peripheral region of CT3 are located in proximity with the nuclear periphery.

In wild type basal epidermal keratinocytes the position of the loricrin gene locus, *LOR*, moves in relation to CT3 with the onset of epidermal stratification and the up-regulation of gene expression at the EDC locus during epidermal morphogenesis. While *LOR* is located predominantly within the region of CT3 located closest to the nuclear periphery in wild-type basal epidermal keratinocytes at E11.5, following the onset of epidermal stratification at E16.5, *LOR* is situated predominantly within the interior most area of CT3 (Mardaryev et al., 2014). In the epidermis of K14BRG1$^{\Delta/\Delta}$ mice, however, this sub-chromosomal relocation of the loricrin locus is not observed; in K14BRG1$^{\Delta/\Delta}$ basal epidermal keratinocytes at E16.5, the majority of *LOR* loci are located within the peripheral region of CT3 (figure 27 A-B). Comparison of the proportion of *LOR* loci positioned within the peripheral region of CT3 in basal keratinocyte nuclei in K14BRG1$^{\Delta/\Delta}$ and in wild type mice at E16.5 reveals a significant (Chi-square test: P=5.97x10^{-6}) difference in the sub-chromosomal localisation of the *LOR* locus as a result of the K14-Cre driven deletion of BRG1 at E10.5 (figure 27C).

3D FISH was performed using collectively labelled DNA probes spanning the EDC locus from 90,284,072bp to 93,411,886bp (*Mus musculus* assembly mm9/GRC build 37) in order to determine the localisation of the EDC locus in its entirety relative to CT3 in the basal epidermal layer of the K14BRG1$^{\Delta/\Delta}$ and wild-type control mice. In the epidermal

compartment of wild type mice at E11.5, the EDC locus is also located in within the external most region of CT3 in basal keratinocytes. Like that of *LOR*, the sub-chromosomal position of the EDC as a whole is also changed during epidermal stratification (Mardaryev et al., 2014) and at E16.5 the EDC is situated within the innermost region of CT3 in wild type basal keratinocyte nuclei. At E16.5 after K14-Cre driven deletion of BRG1 in basal keratinocyte nuclei, however, the position of the EDC is significantly (Chi-square test: $P=1.34x10^{-8}$) altered in comparison with age-matched control (wild type) keratinocyte nuclei. Rather than being located primarily within the internal part of CT3, the EDC in K14BRG1$^{\Delta/\Delta}$ epidermis is predominantly situated within the peripheral region of CT3 within basal keratinocyte nuclei at E16.5 (figure 27 B).

The relative position of the ubiquitously expressed *RPS27* locus within CT3, in contrast, appears unchanged (Chi-square test: $P=0.09$) by the K14-Cre driven ablation of BRG1; at E16.5 *Rps27* and is situated within the innermost region of CT3 both at E11.5 and at E16.5 in wild type and in K14BRG1$^{\Delta/\Delta}$ epidermal basal keratinocytes. *RPS27*, which is located 5' of the EDC on murine chromosome 3 at 90,016,647-90,017,537bp (assembly mm9/GRC build 37), neighbours the EDC locus but remains highly expressed prior to and during epidermal stratification (figure 27 B). Similarly, during normal development of the epidermal layer it has been observed that while the position of the EDC is changed, the positions of the RPS27 and GA-Binding Protein Subunit Beta-2 (*GABPB2*) locus, which is located at the 3' region flanking the EDC, remain constant (Mardaryev et al., 2014).

During normal epidermal stratification, the nuclear distance between the *RPS27* and *LOR* loci is reduced as the centripetal movement of the EDC locus brings *LOR* into greater proximity with the *RPS27* locus (Mardaryev et al., 2014). Analysis of the position of *LOR* relative to the geometric centre of wild type basal keratinocyte nuclei has shown that the sub-chromosomal re-positioning of *LOR* observed between E11.5 and E16.5 coincides with the centripetal translocation of the *LOR* locus away from the nuclear periphery and, concomitantly, with a decrease in the spatial separation between the *LOR* and *RPS27* loci (Mardaryev et al., 2014).

Comparison between the position of *LOR* relative to the geometric centre of K14BRG1$^{\Delta/\Delta}$ and age matched wild type basal epidermal keratinocyte nuclei reveals that the mean radial position of *LOR* at E16.5 is significantly (P<0.05) more peripheral (figure 27 D). At E16.5, the spatial separation distance between the *LOR* and *RPS27* loci in K14BRG1$^{\Delta/\Delta}$ basal epidermal keratinocyte nuclei is also significantly (two-tailed t-test: P<0.01) increased in comparison with that observed at E16.5 in the basal keratinocyte nuclei of wild type epidermis (figure 27 D-E). The mean inter-locus distance between *LOR* and *RPS27* was calculated for locus pairs both in nanometers and as a percentage of the average nuclear radius corresponding each respective pair of loci analysed in each tissue type. This helps correct for the effect any variation in nuclear size between K14BRG1$^{\Delta/\Delta}$ and wild type samples may have upon inter-locus distances between *LOR* and *RPS27*. A significant (two-tailed *t*-test: P<0.01) increase in the distance between the *LOR* and *RPS27* loci in BRG1 ep$^{-/-}$ E16.5 basal keratinocytes is apparent both when raw and normalised inter-locus distances are compared with wild type controls (figure 27 E-F). Although the sample (n=40) median BRG1 ep$^{-/-}$ keratinocyte nuclear radius (median=3974.918nm ± MAD 446.0841) was somewhat smaller than that of wild type nuclei (median=4198.513nm ± MAD 395.8274) No significant difference was found between the average nuclear radius of K14BRG1$^{\Delta/\Delta}$ and wild type control nuclei (two-sample Kolmogorov-Smirnov Test: D=0.277, P=0.120).

A.

B.

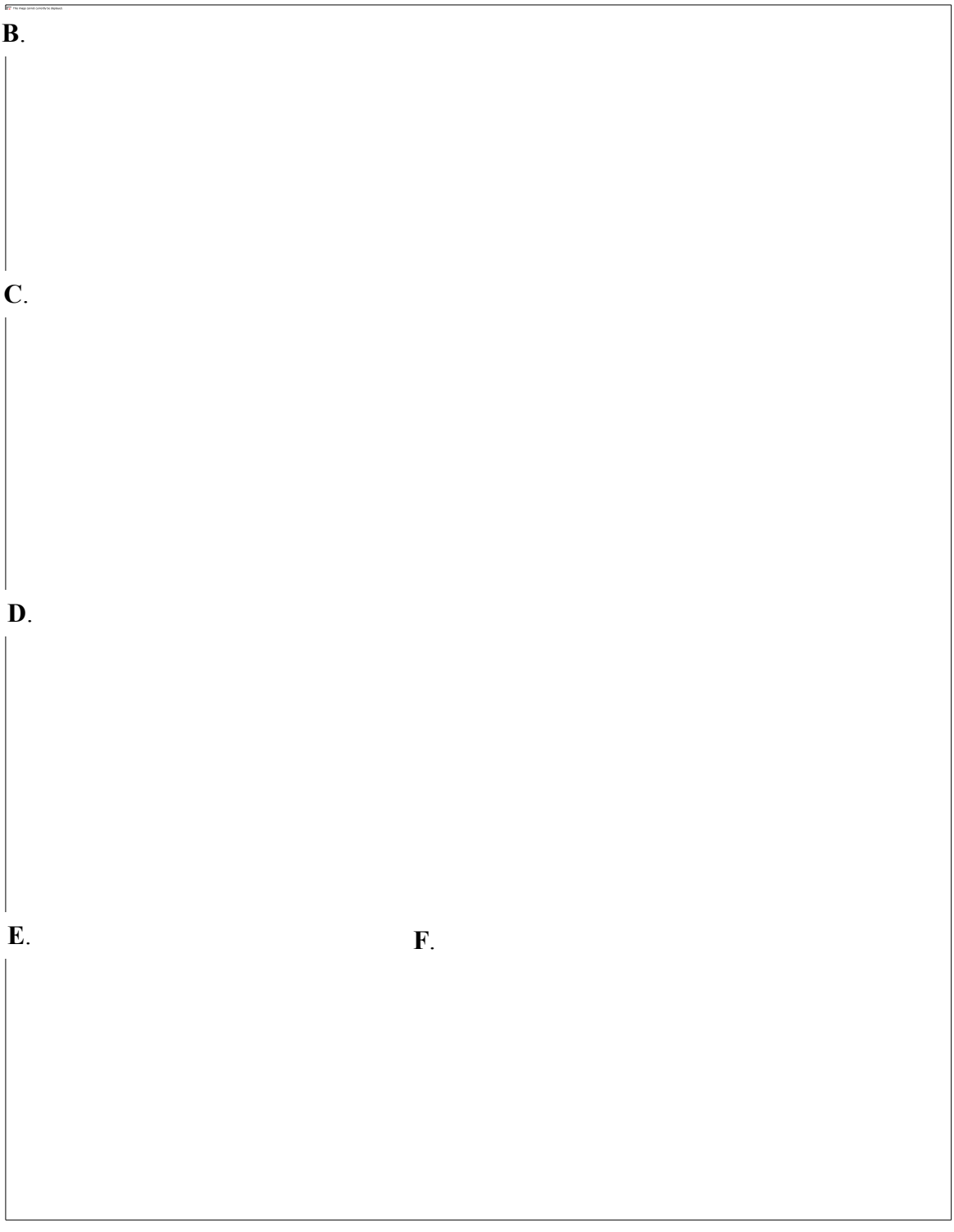

C.

D.

E.

F.

Figure 27. **BRG1 is involved in regulating the nuclear localisation of the EDC locus**. (**A**) Schematic showing the EDC and contiguous 5' and 3' genomic regions on chromosome 3. Positions of 3D FISH probes used to mark the EDC region, including the loricrin gene locus (*LOR*), are shown in green. The 3D FISH probe corresponding to the *RPS27* gene locus is shown in yellow. Scale bar represents 2μm (Mardaryev et al., 2014) (**B**) Multicolour 3D fluorescence *in situ* hybridisation (FISH) of DNA probes performed on skin sections showing labelling of the *LOR* and *RPS27* gene loci and chromosome painting of CT3 (MMU3). (**C**) Position of the *LOR*, *RPS27*, and EDC (90,016,647-90,017,537bp (assembly mm9/GRC build 37)) loci relative to CT3 in basal keratinocytes at E16.5 as revealed by FISH. Position presented as the frequency with which a locus was found to occupy either the internal or peripheral region of painted CT3; n = 50 nuclei (i.e. 100 loci). P-values for pairwise comparison (Chi-squared test) between wild type and K14BRG1$^{\Delta/\Delta}$ samples: *LOR*, P=5.97 x 10^{-6}; EDC, P=1.34 x 10^{-8}; *RPS27*, P=0.09. (**D**) Relative position of *LOR* to the geometric centre of the nucleus. Radial position presented as a percentage of the value of the corresponding average nuclear radius. Mean and SEM; * = two-sample *t*-test: *t*=2.290, df=117.628, *P*=0.024 (**E**) Spatial distance (nm) between the *LOR* and *RPS27* loci in basal keratinocytes at E16.5 as revealed by FISH. Mean and SEM; **P*= two-sample *t*-test: *t*=3.332, df=96.823, *P*=0.001 (**F**) Spatial distance between the *LOR* and *RPS27* loci in basal keratinocytes at E16.5 presented as a percentage of the corresponding average nuclear radius. Mean and SEM; * = two sample *t*-test: *t*=4.404, df=97.749, *P*=2.719x10^{-5} (two-tailed *t*-test).

4.1.5 The association of the EDC with nuclear speckles is reduced in the absence of BRG1

Multicolour 3D FISH of DNA probes spanning the EDC (from 90,284,072bp to 93,411,886bp; *Mus musculus* assembly mm9/GRC build 37) was performed on E16.5 K14BRG1$^{\Delta/\Delta}$ and wild type tissue sections in conjunction with immunofluorescence staining of SC-35 positive nuclear speckles. The total and local distribution of nuclear speckles in appropinquity with the EDC locus in basal keratinocytes was estimated in order to determine whether or not BRG1 deficiency affects the spatial association of the EDC locus with nuclear speckles, or vice versa. In wild type basal keratinocyte nuclei,

centripetal translocation of the EDC coincides with an increase in the number of nuclear speckles contiguous with the EDC. However, in K14BRG1$^{\Delta/\Delta}$ basal epidermal keratinocytes, positioning of the EDC towards the nuclear periphery at E16.5 correlates with a reduction in the number of SC-35 positive nuclear speckles located in close spatial proximity with the locus (figure 28). Although the number of nuclear speckles present in the vicinity of the EDC in K14BRG1$^{\Delta/\Delta}$ basal keratinocytes is significantly reduced (Wilcoxon rank-sum test: W=1467, *P*=0.012) (figure 28), the total number of SC-35 speckles per nucleus appears unaffected (P>0.05) (appendix figure A6).

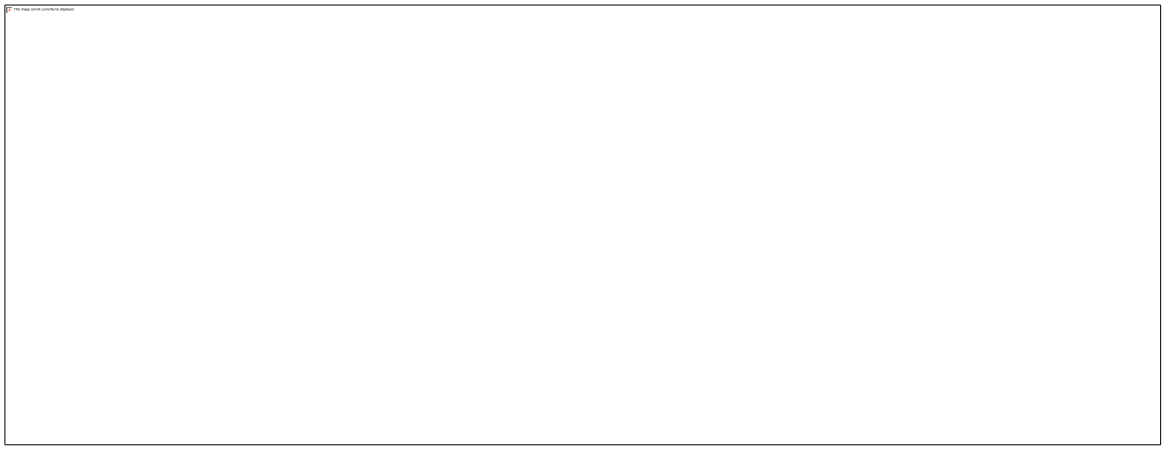

Figure 28 (**A**) **Epidermal knockdown of BRG1 results in the reduced spatial association of the EDC with SC-35 positive speckles.** Multi-colour 3D fluorescence *in situ* hybridisation (3D FISH) of labelled DNA probes spanning the epidermal differentiation complex (EDC) locus from 90,284,072bp to 93,411,886bp (*Mus musculus* assembly mm9/GRC build 37) (arrows) on wild type (WT) and K14BRG1$^{\Delta/\Delta}$ E16.5 basal epidermal keratinocytes combined with staining against SC-35. Scale bar represents 2μm (**B**) Quantification of the number of SC-35 nuclear speckles located in appropinquity with the EDC locus in control (wild type) and K14BRG1$^{\Delta/\Delta}$ E16.5 basal epidermal keratinocytes. Mean + S.E.M; n=80; **P*=0.012.

4.2 Higher-order chromatin folding and transcriptional regulation at the EDC locus

Microscopy based analyses of chromatin folding at the EDC in basal epidermal keratinocytes using a 3D FISH based approach has demonstrated that the global genome organizer SATB1 and ATP-dependent chromatin remodeler BRG1/Smarca4 are direct p63 targets involved in modulating the tissue-specific conformation and nuclear position of the EDC locus during epidermal ontogenesis (Fessing et al., 2011; Mardaryev et al., 2014). In addition, targeted analysis of chromatin folding at the EDC using 3C has recently revealed a long-range enhancer that forms contacts with multiple gene promoters at the EDC and exhibits specific long-range enhancer activity in keratinocytes cultured *ex vivo* under proliferative and differentiating conditions (Oh et al., 2014). Here, 3C-carbon copy (5C), ChIP-Seq, ChIP-chip data were parsed in order to map the linear and higher-order chromatin structural features associated with transcriptional regulation at a 5.3Mb region spanning the EDC on mouse chromosome 3.

4.2.1 The 3D higher-order structure of chromatin at the EDC region

In order to generate a comprehensive network of, potentially regulatory, chromatin interactions occurring at the EDC locus, 5C was used to interrogate chromatin spatial contacts at a 5.3Mb region (chr3: 89900000-95200000, assembly Mm9) located on chromosome 3 in freshly isolated normal collagen adherent epidermal keratinocytes (KC) from neonate C57BL/6 mice and in primary murine thymocytes (TC) isolated from 8 week old C57BL/6 mice. This region spans the murine EDC locus and also includes, between 89.9-90.3Mbp and 93.4-95.2, flanking regions that encode protein-coding genes expressed in a variety of tissues with no known specific function in the epidermis. Although regions neighbouring the EDC are either gene-poor or do not encode genes with a known specific function in the epidermis, it was hypothesised regulatory elements located outside of the EDC region may potentially be involved in functional long-range interactions with EDC gene regulatory elements.

Initially, microarray transcription profiling coupled with qRT-PCR analysis was used to compare patterns of protein-coding gene transcription at this region in KC and TC. The relative transcript profile corresponding to the target region shows that EDC gene transcription in KC, including the cluster of *S100a* genes located at ~90.3-90.5Mb on chromosome 3, is largely up-regulated in comparison with TC. The few protein coding genes within the EDC proper that are not shown to be up-regulated in KC include genes located at the EDC that have no known specific function in the epidermis and some members of the *S100A* family. While members of the S100 protein family have critical functions in the epidermis, some *S100* genes, including *S100A13,* are expressed in multiple tissues, including the thymus. A higher degree of similarity is observed in transcript levels corresponding to regions located from ~89.9-90.3Mbp and from ~93.4-95.2, at which a greater proportion of ubiquitously expressed genes with no epidermis-specific functions are located (figure 29).

In support of the microarray and qRT-PCR data generated here that suggest the EDC is largely silenced in TC, ENCODE ChIP-Seq data available covering the EDC and flanking regions in 8 week C57BL/6 mouse thyme show there is very little enrichment for bound RNAPII, or marks typically indicative of enhancers (H3K4me1 and H3K27ac) active promoters (H3K4me3), or actively transcribed gene bodies (H3K36me3) at the EDC (Rosenbloom et al., 2012; Shen et al., 2012). (ChIP-Seq data generated as described here that map the distribution of H3K4me1 in TC were found to correlate well with this published ENCODE ChIP-Seq data that map the distribution of H3K4me1 in thyme. In concordance with microarray profiling of transcription at the EDC and flanking regions in TC, ENCODE data show gene rich regions flanking the EDC are, on the contrary, enriched for RNAPII binding, mono- and tri-methylated H3K4, and acetylated H3K27. In KC, enrichment for acetylated H3K27 and monomethylated H3K4 was detected throughout the EDC locus as well as flanking regions via ChIP-Seq analyses performed as described here.

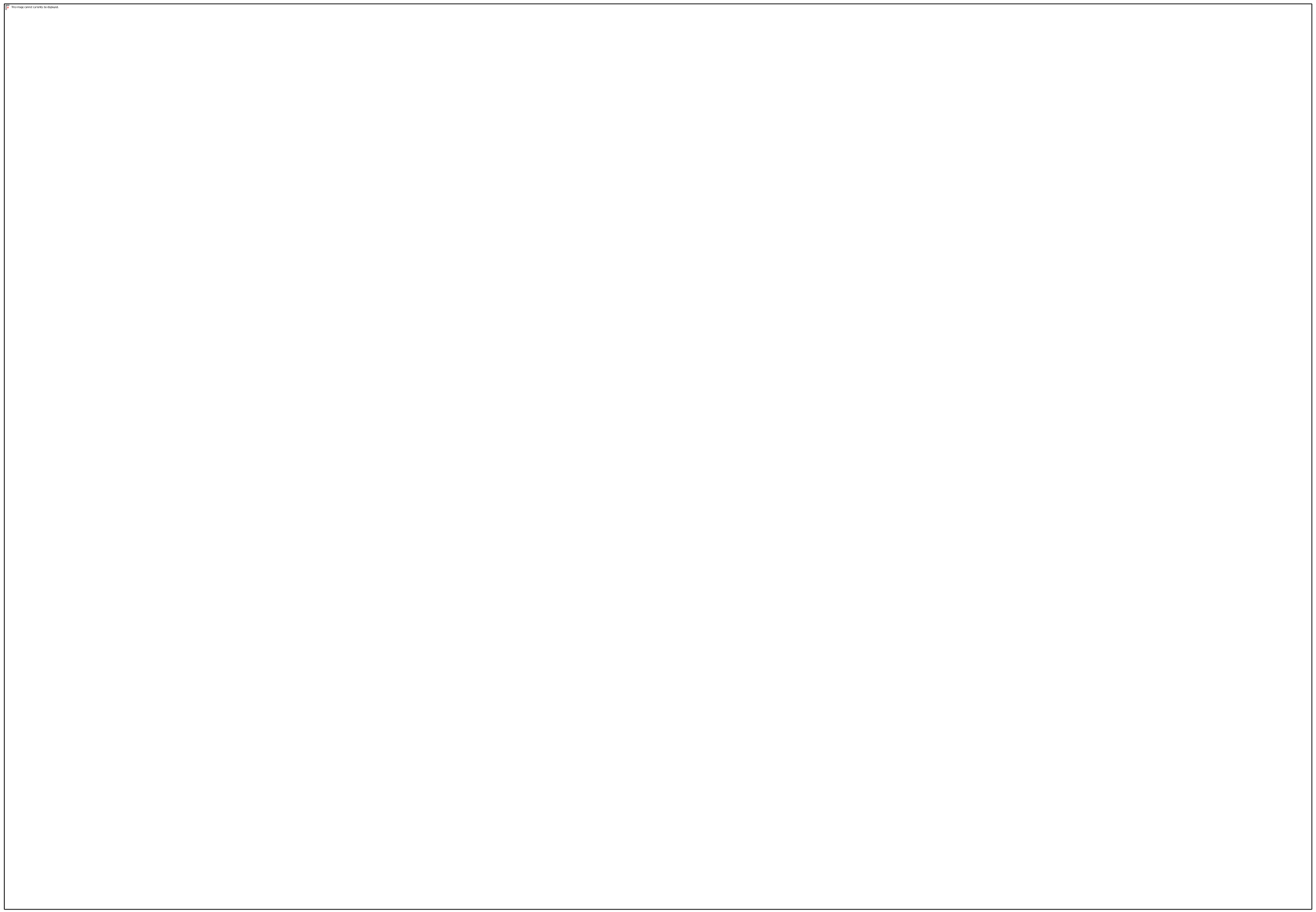

Figure 29. **(A)** mRNA transcript expression levels at a 5.3Mb region (89.9-95.2Mbp, Mmu9) spanning the epidermal differentiation complex (EDC) locus and neighbouring genomic regions in freshly isolated normal collagen adherent neonatal keratinocytes (KC) relative to thymocytes isolated from the thyme of 8 week old wild-type mice (TC) (log2 scale). **(B)** qPCR analysis of mRNA transcript expression levels at selected EDC loci in KC normalised to corresponding transcript expression levels in TC.

5C chromatin interaction frequency (IF) heatmaps were generated in duplicate for both KC and TC (appendix figure A3). A potential 124,593 *cis* pairwise chromatin interactions between chromatin fragments were interrogated within the 5.3Mb target region to generate 5C IF matrices using an alternating 5C primer design scheme (appendix figure A2). To assess the validity of 5C data generated, the reproducibility of duplicate 5C IF matrices was assessed and 5C IF data compared with existing circular chromosome conformation capture (4C) data (unpublished, see appendix figure A4). Comparison between the log of 5C counts for replicate KC matrices produces a Pearson correlation coefficient of 0.751. Less similarity was observed between KC and TC matrices and a Pearson correlation coefficient 0.577 is obtained when the log of KC and TC 5C counts are compared. Relative to KC, comparison between TC 5C matrices produces a lower Pearson correlation coefficient of 0.602 when the log of 5C counts are compared.

2D heatmaps generated that represent raw 5C IF counts reveal that within cell-type variability in the visible features of 5C heatmaps corresponding to replicate 5C data sets is markedly less than apparent between heatmaps representative of each different cell-type analysed (appendix figure A3). Furthermore, the KC 5C chromatin interaction profile obtained for the chromatin region encoding the loricrin gene locus was compared with that of existing circular chromosome conformation capture (4C) data for this locus (unpublished data) and substantial similarities between 5C and 4C loricrin interaction profiles observed (appendix figure A3). Importantly, in individual cells, 3D multicolour FISH was also used to analyse topological features mapped using 5C, which produces data representative of a large population of cells (in this instance, 6×10^7 cells per 5C library).

Visual comparison was made between 5C IF heatmaps representative of TC and KC 5C that were generated using a series of bin sizes ranging from 50-500Kb with no overlap between bin windows and also with sliding in 2X, 3X, and 4X step intervals. As previously described, directionality index (DI) tracks (Dixon et al., 2012) were generated to map the up- or downstream-interaction bias of chromatin fragments interrogated within the 5.3Mbp target region (Dixon et al., 2012) and the boundaries of topological chromatin domains that are characterised by regions divergent up- and down-stream interactions preferences are juxtaposed (Dixon et al., 2012; Nora et al., 2012; Phillips and Corces, 2009). DI tracks generated using a series of bin sizes ranging from 50Kb-500Kb were aligned to corresponding binned IF heatmaps representing 5C data generated for each cell type analysed.

This visual comparison of binned heatmaps paired with corresponding DI tracks was found to show that a large multi-mega base scale topological domain (with boundaries located at 90.38 and at 94.3Mbp when an window size of ~150Kb is used to bin 5C data, (see figure 30A) corresponds to the main body of the EDC locus, which comprises the *FLG*-like, *LCE*, and *SPRR* gene families and the majority of the *S100* family of genes, and contiguous gene poor regions in both KC and TC. Up- and down-stream of this domain, two separate topological domains, which extend beyond the margins of the region interrogated here using 5C,were found correspond to gene rich regions located outside of the main body of the EDC, although the 5' most of these topological domains also corresponds to the *S100A1, S100A13, S100A14, S100A16* genes (figure 30).

A series of mega- and kilo-base scale domains were found to be clearly visible at regions corresponding to the EDC in KC. A mega base-base scale topological domain was found to correspond to the EDC gene desert region located between around 90.5-91.8. A distinct mega base scale domain contiguous this region was also found to correspond to the *SPRR* and *LCE* gene clusters, the 3' boundary of which is located at ~92.9Mbp, between the *LCE* and *FLG*-like gene clusters. Mega- and kilo-base scale domains corresponding the target 5.3Mbp region were also apparent in TC, and found to occupy largely conserved positions in both cell types. However, topological domains corresponding to the target region in TC were found to appear weaker and less distinct in comparison, particularly with reductions in the window size used to bin 5C IF heatmaps.

As the genomic position of large-scale TAD identified in Hi-C data using a DI based HMM approach is largely conserved between cell types, the position of topological domain boundaries mapped here using 5C was also compared with published Hi-C data. However, it was found that published Hi-C data show the position of TADs located at the 5.3Mbp region interrogated here is not conserved between murine ES cell and cortex genomes (Dixon et al., 2012; Shen et al., 2012) (figure 30A & E).

To explore further the cell-type specific variation in chromatin structure at the EDC in KC and TC in individual cells, 3D multicolour FISH was employed to map the spatial separation between three loci located at the EDC region in structurally preserved TC, KC, and also in basal epidermal keratinocytes *in situ* in structurally preserved skin sections. It has previously been shown that the spatial separation of equidistant genomic loci within the 3D space of the nucleus is dependent upon whether or not loci are located in the same topological domain; in the 3D space of the nucleus, loci located an equal distance apart in the linear genome sequence but positioned within different topological domains have been shown to locate further apart than equidistant loci located within the same domain (Nora et al., 2012). To validate, at the single cell level, the finding that a boundary between topological domains is located at ~92.9 between the *LCE* and *FLG*-like gene families, FISH of labelled DNA probes (referred to as A, B, and C) corresponding to three regions, two (A and B) located within the domain located 5' of this boundary, and the third (C) within the second domain located 3' of this boundary (figure 30A) was performed on structurally preserved TC and KC. FISH was also performed on structurally preserved C57BL/6 neonate skin sections. Probes A and B correspond to a domain containing the *LCE* and *SPRR* gene family members. Probe C corresponds to a 3' region located outside of this domain that contains the *S100A10, S100A11,* and fused-type S100 protein *TCHHL1* (Trichohyalin-like 1) genes (figure 30A).

The linear genomic distance between loci probes A and B (716,849bp) correspond to is somewhat larger (77,970bp) than that which separates the loci B and C hybridise to (638,880bp). The distance in micrometres between these three loci in 3D in TC, KC, and *in situ* basal epidermal keratinocyte nuclei was measured and, in addition, inter-locus distances calculated as a percentage of the average radius of each nucleus analysed, in

order to correct for any effect of variation in the average diameter of KC, basal epidermal keratinocyte, and TC nuclei upon the degree of separation between loci.

It was found that in both structurally preserved KC and TC, the average distance (both before and after normalisation) between A and B in 3D is significantly ($P<0.05$) smaller that that between B and C, which correlates with 5C IF matrices that show the EDC is organised into at least two distinct mega base-scale topological domains. In basal keratinocytes, the average distance detected (both before and after normalisation) between A and B is also significantly ($P<0.05$) smaller than that between B and C (figure 30).

It was found the distance between A-B in KC tends to be somewhat smaller than that detected between A-B in basal keratinocytes. However, the difference in distance between A-B in KC and basal cells was not overall, that is before and after normalisation, found to be significant ($P>0.05$) (appendix table A6). The average nuclear volume measured for KC was also found to be somewhat larger, however over all these differences were not found to be significantly ($P>0.05$) different. These findings therefore suggest that the process of isolating and fixing KCs for 5C did not substantially affect chromatin folding at the EDC, which implies that using 5C to map chromatin folding at the EDC in KCs is an acceptable tool with which to study of chromatin organisation and transcriptional regulation at the EDC in basal epidermal keratinocytes.

An all-by-all comparison of inter-locus distances between TC and each keratinocyte cell population showed inter-locus distances in TC are significantly larger ($P<1x10^{-6}$) (figure 30 and appendix table A8). This finding indicates that chromatin at the EDC in TC is less condensed than chromatin at the EDC in KC and in basal epidermal keratinocytes. At the EDC in TC, ENCODE ChIP-Seq data reveal a distinct lack of H3K27 trimethylation, which is catalysed by the PRC2-EZH1/2 complex and is frequently associated with the recruitment of PRC1, and, in turn, the PRC1-RING1A/B driven mono-ubiquitination of histone H2A and chromatin compaction (Margueron and Reinberg, 2011). The PRC2-Ezh1 complex has also been found to mediate chromatin compaction to a certain extent, however these results indicate polycomb mediated chromatin compaction is not required for transcriptional repression at the EDC in TC.

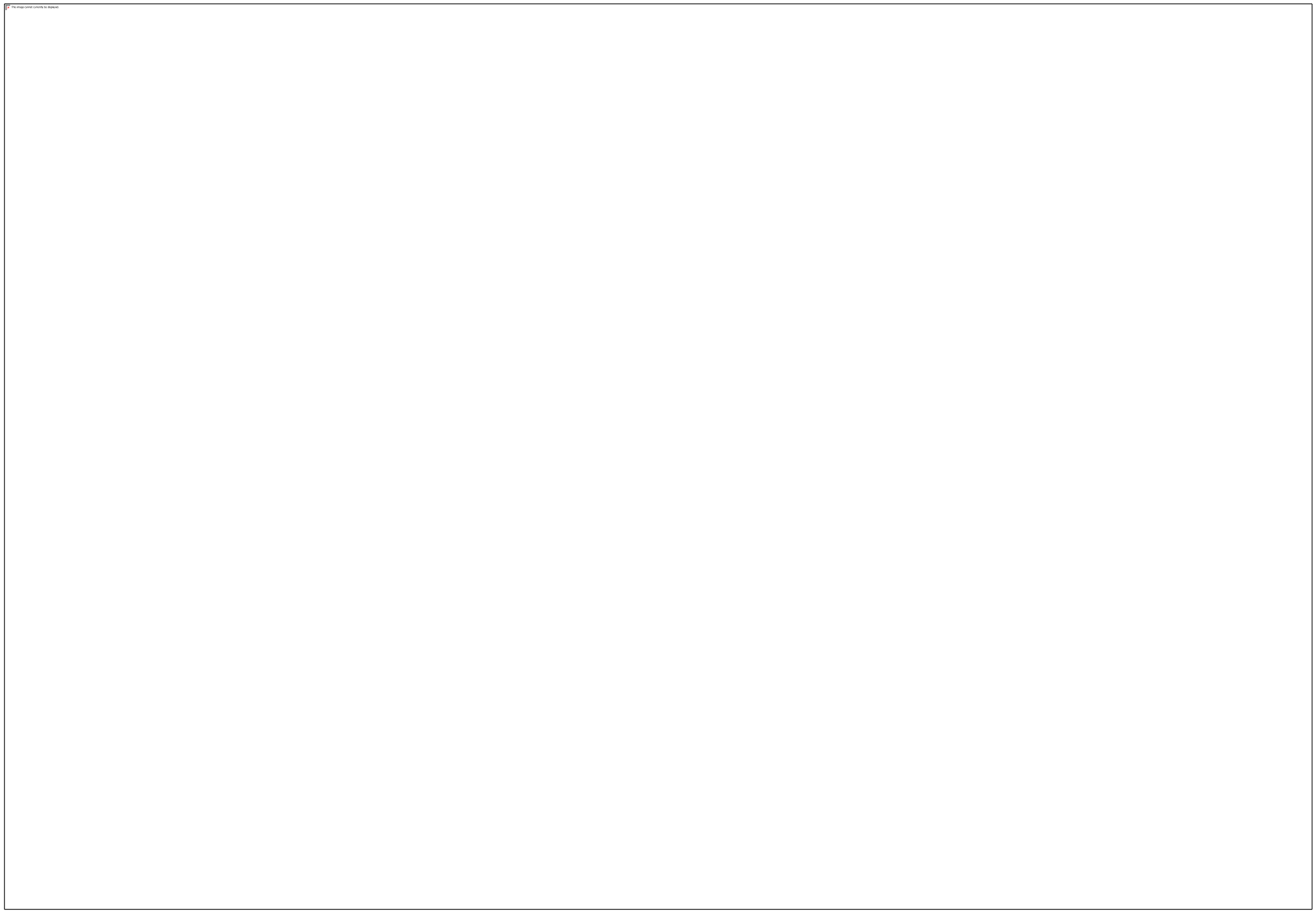

Figure 30 (A) Heatmap representation (150Kb bin, step 3X step size) of chromatin interactions at a 5.3Mb region spanning the EDC and neighbouring genomic loci in KC captured using 3C-carbon copy technology (5C). UCSC gene and corresponding directionality index (D.I.) tracks, and locus coordinates (Mmu9) are shown below. Hi-C domains: the position of domains mapped for cortex (top) and ES cells (bottom) using the Hi-C approach are also shown (Dixon et al., 2012). Labelled DNA 3D-FISH probes (boxes A-C) detecting corresponding domains at this region are shown in yellow, red, and green **(B)** Multicolour 3D FISH of labelled DNA probes (shown in A) on KC and basal epidermal keratinocytes, B **(C)** Median distances between probes A-B and B-C in KC before and after normalisation. Error bars show the median absolute deviation. *=P <0.01 (Wilcoxon rank sum test) **(D)** Distribution of inter-locus distances in KC (left) and basal epidermal keratinocytes (right). **E)** Heatmap representation (150Kb bin, step 3X step size) of chromatin interactions at a 5.3Mb region spanning the EDC and neighbouring genomic loci in TC captured using 5C. UCSC gene and corresponding directionality index (D.I.) tracks, and locus coordinates (Mmu9) are shown below. Hi-C domains: the position of domains mapped for cortex (top) and ES cells (bottom) using the Hi-C approach are also shown (Dixon et al., 2012). Labelled DNA 3D-FISH probes (boxes A-C) detecting corresponding domains at this region are shown in yellow, red, and green **(F)** Multicolour 3D FISH of labelled DNA probes (shown in A) on TC **(G)** Distribution of inter-locus distances in TC **(H)** Median distances between probes A-B and B-C in KC, basal epidermal keratinocytes, and TC. Error bars show the median absolute deviation. *=P <0.01 (Wilcoxon rank sum test)**.**

4.2.2 Identification of a network of potentially regulatory long-range interactions involving putative enhancer elements and gene core promoters at the EDC

As previously described, a probabilistic modelling approach was used to remove from consideration background IF counts that could be attributed to the correlation between the frequency of stochastic, non-functional, chromatin interactions between loci and genomic separation distance, as well as those IF counts that could be attributed to spurious primer activity and artefacts introduced during 5C ligation mediated amplification (Phillips and Corces, 2009). 5C counts were transformed into z scores by normalising IF counts to

distance and only scores below an FDR of 1% in replicate 5C datasets were further analysed. KC IF matrices were found to comprise 864 significant ($P<0.01$) interactions. TC IF matrices were found to comprise 6612 significant ($P<0.01$) interactions. Of the 864 interactions identified in KC, 474 interactions were found to be significant only in replicate KC 5C IF matrices and 389 to have a z score below an FDR of 1% in both TC and KC replicate matrices.

The findings that chromatin at the EDC locus in KC is more compacted in comparison with TC, that topological domains at the 5.3Mbp target region interrogated using 5C in KC appear more distinct in comparison with TC when visualised using 2D IF heatmaps, particularly as heatmap bin sizes are reduced, and that KC 5C IF matrices comprise a smaller number of interactions in comparison with TC matrices suggests a continuum of preferential interactions between multiple loci at the EDC and, potentially, also looping mediated compaction of the EDC in KCs. Conversely, these findings may suggest that interactions between loci at the EDC region in thymocytes are more random, although it cannot as yet be said that the increased number of chromatin interactions represented by TC 5C data does not, at least in part, reflect the representation of a higher incidence of non-specific ligation events in TC 5C data. Further analysis of TC 5C data is needed to fully understand to what extent biological or extraneous factors have contributed to the differences observed in TC and KC IF profiles.

For FACS sorted $\alpha6^{bri}$/Sca-1+ epidermal IFE keratinocytes, ChIP-Seq was used to map the distribution of putative enhancers and additional non-promoter regulatory elements marked by H3K4me1 and overlapping enrichment for H3K4me1 and H3K27ac, as well as the distribution of enrichment for the repressive H3K27me3 histone mark. IFE keratinocytes expressing the integrin α6 constitute the entire population of basal or proliferative keratinocytes and Sca-1 expression, which characterises several adult stem cell populations and is implicated in hematopoietic stem cell self-renewal (Ito et al., 2003) and lineage-commitment (Bradfute et al., 2005), and in the IFE is posited to mark committed progenitor keratinocytes that are characterised by reduced levels of plasticity relative to epidermal stem cells (Jensen et al., 2008; Triel et al., 2004).

Active transcription and enrichment for the active histone marks H3K4me1 and H3K27ac at interrogated fragments was found to be prevalent throughout targeted region (figure 31). To map the distribution of looping interactions involving potential proximal and distal regulatory elements in KC, the distribution of looping interactions at the EDC and targeted neighbouring regions found to involve interrogated restriction fragments located within or outside of 5Kb of a protein-coding gene transcription start site (TSS) was analysed. 60.5% of interactions interrogated in KC were found to involve fragments located within 5Kb of a TSS (hereafter referred to as proximal fragments), of which the majority comprise a pairwise interaction between a fragment located >5Kb from a TSS (hereafter referred to as a distal fragment) and a proximal fragment (figure 32).

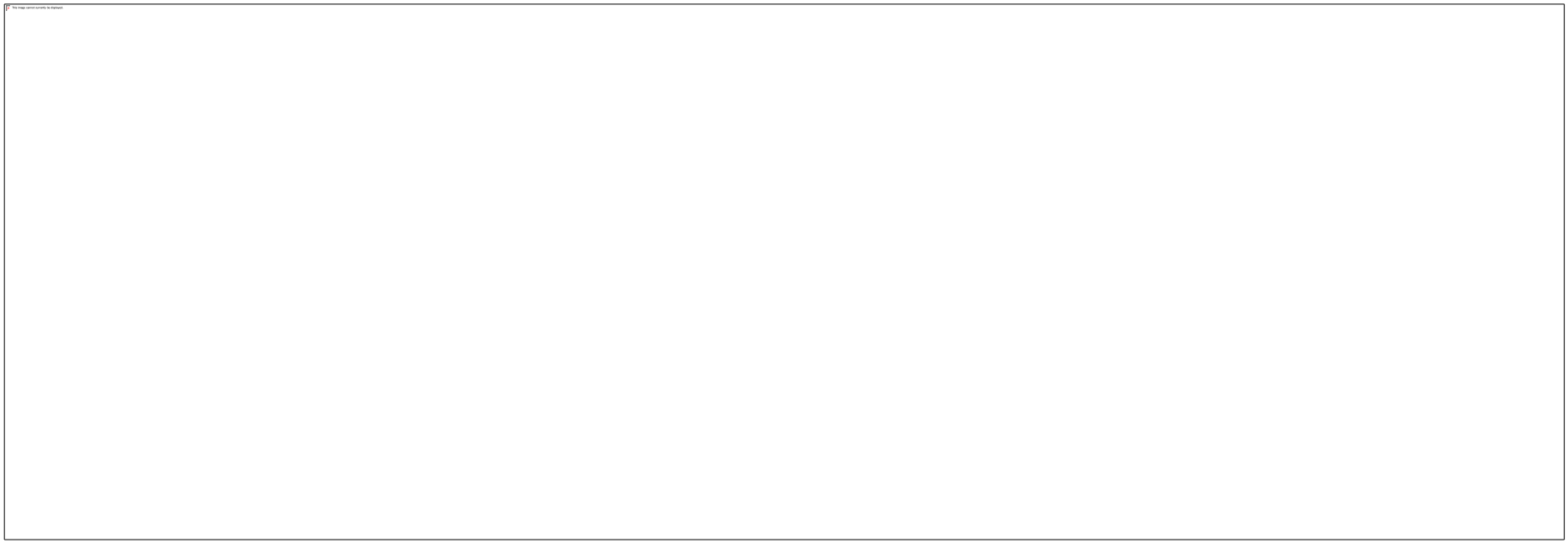

Figure 31 RNA-Seq assembly and ChIP-Seq peaks called for the 5.3Mbp region located on mouse chromosome 3 interrogated here using 3C-carbon copy (5C) technology.

Proximal (≤ 5kb from a gene TSS) chromatin fragments at the EDC and neighbouring genomic regions were found to form contacts with multiple proximal and distal fragments enriched for H3K4me1 and H3K27ac (figure 32A and D). Regions found to be enriched for H3K4me1 alone, and for both H3K4me1 and H3K27ac, mapped mainly to proximal fragments involved in looping interactions and are indicative of the involvement of enhancer elements in interactions (figure 32A and D). Enrichment for H3K27ac alone at proximal sites is indicative of the involvement of active promoter regions in looping interactions. In comparison, H3K27me3 enrichment was found to be more prevalent at distal interacting fragments (figure 32B and D) and, overall, was found to be less prevalent at interrogated fragments throughout the target region (figure 32C, E, F and G).

Fragments enriched for active marks alone, however, were not found to be preferentially involved in long-range looping interactions. Although less abundant, interrogated fragments enriched for H3K27me3, on the other hand, were found to be significantly more likely to be involved in looping interactions specific to KC than fragments not enriched for H3K27me3 (figure 32C, E, F-G). Overall in KC, a smaller, but significant (Fisher's exact test, $P<8.0E-4$), number of fragments enriched for overlapping regions of enrichment for H3K27me3 and H3K4me1 and H3K27ac were also found to be preferentially involved in looping interactions, although only fragments enriched for overlapping regions of H3K27ac and H3K27me3 enrichment were found to be preferentially involved in interactions found to be significant only in KC (figure 32C, E, F-G).

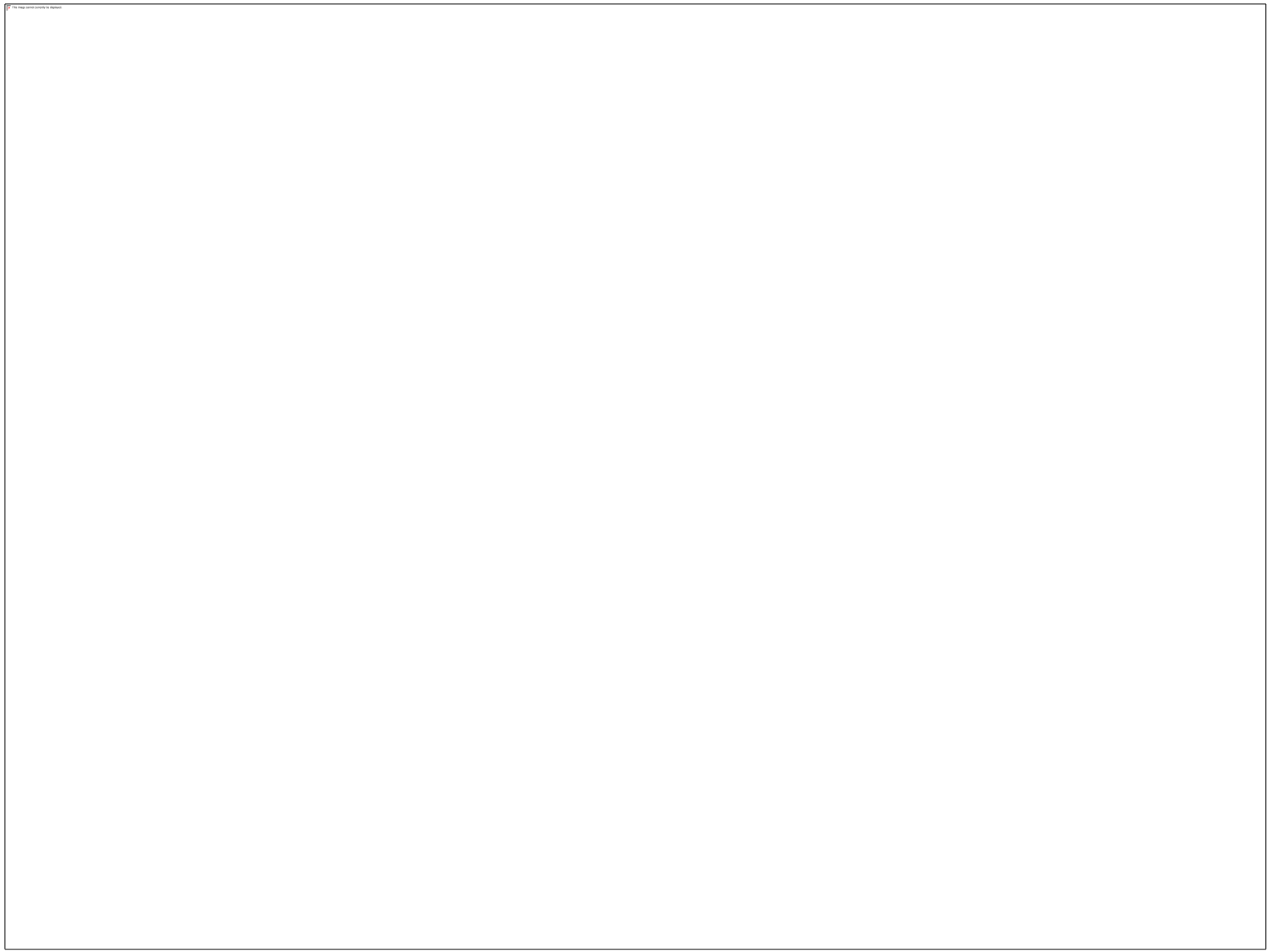
This image cannot currently be displayed.

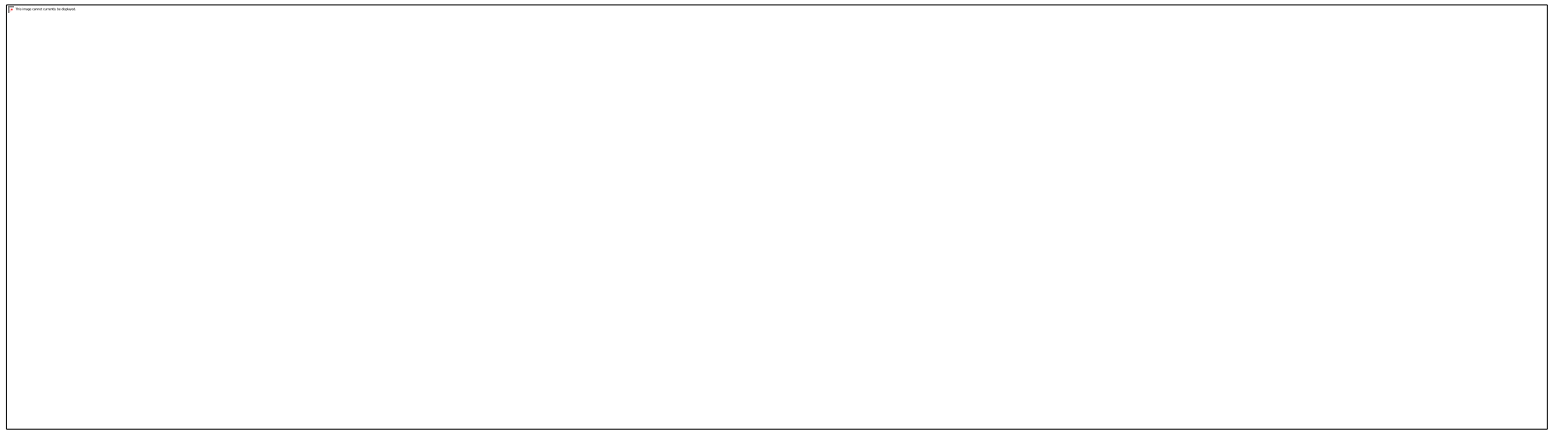

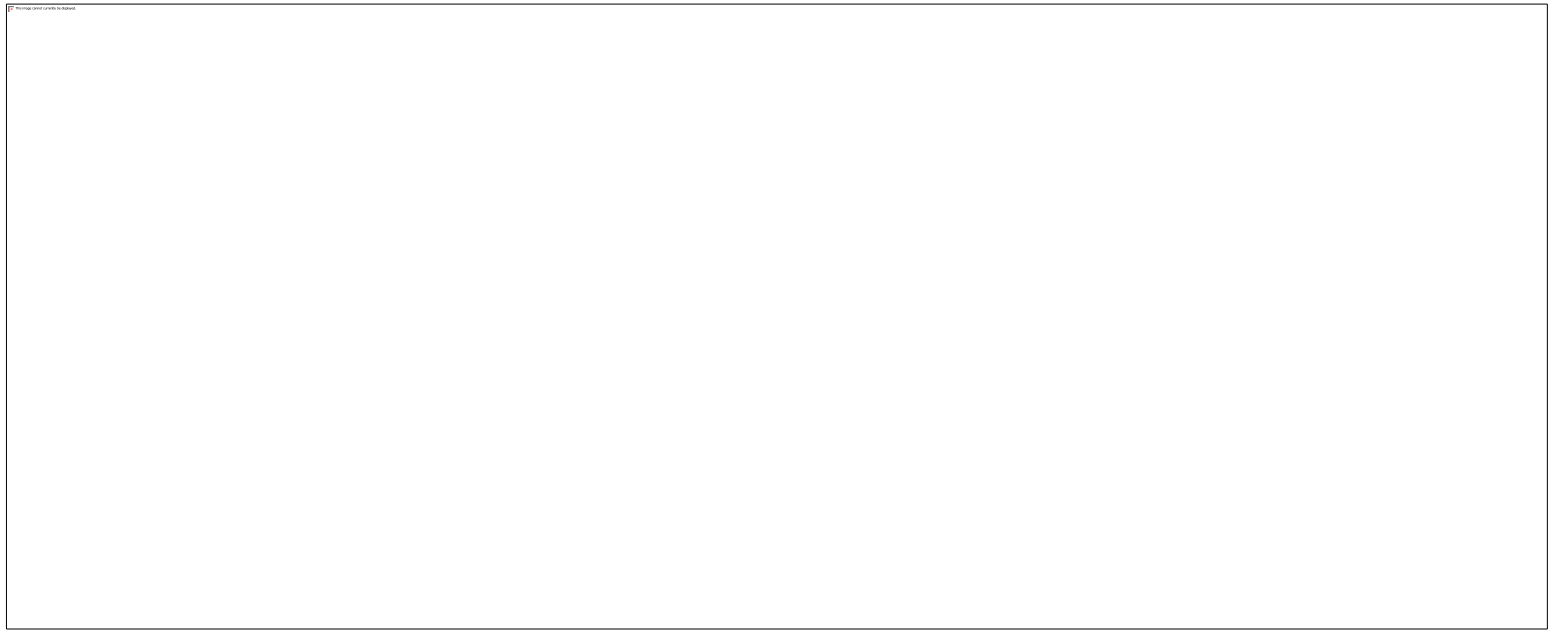

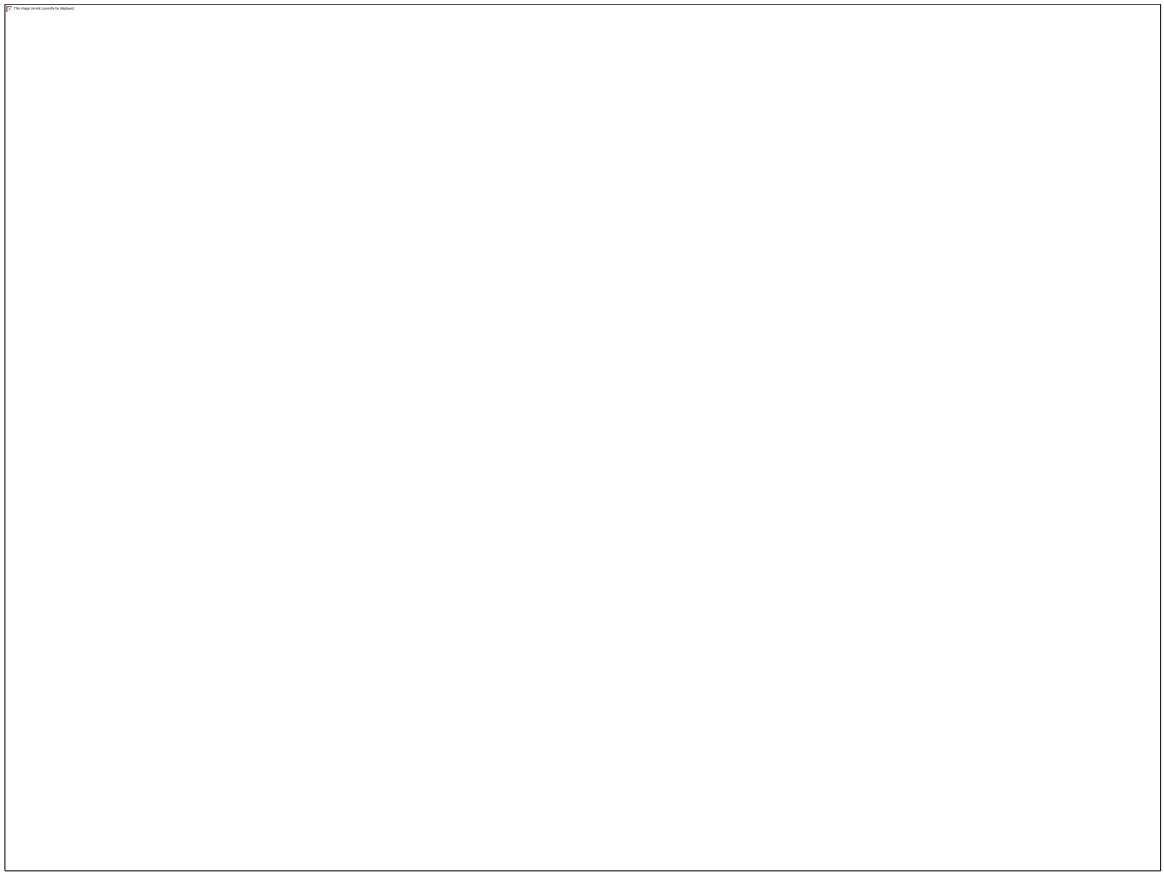

Figure 32 (A) Level and distribution of enrichment for interactions in KC involving proximal and distal candidate regulatory regions marked by enrichment for active histone modifications H3K27ac and H3K4me1. **(B)** Level and distribution of enrichment for interactions in KC involving proximal and distal regions enriched for the repressive histone mark H3K27me3. **(C)** Number of interactions identified in KC and the total number of potential looping interactions possible between interrogated chromatin fragments **(D)** Proportion of interactions in KC involving proximal and distal fragments **(E)** Proportion of interactions detected with a z score below an FDR of 1% in KC replicate 5C IF matrices and the proportion of interactions with a z score below an FDR of 1% in replicate TC and KC matrices **(F)** Level of enrichment for looping chromatin interactions involving chromatin regions enriched for histone tail modifications in KC in comparison with the level of enrichment for histone modifications expected at sites of background interaction (*=P<7E-4) and **(G)** also comparison between the level of enrichment for histone modifications present at sites of interaction in KC alone, in both TC and KC, and in background (*=P<1.5E-3).

It was recently reported that an evolutionarily conserved non-coding element CNE923 located 2.9Kb upstream of the involucrin gene TSS acts as an enhancer of EDC transcription in proliferating and differentiating conditions in keratinocytes cultured *ex vivo* ad forms spatial contacts with several long-range EDC gene promoters (de Guzman Strong et al., 2010; Oh et al., 2014). In epidermal progenitor cells characterised by α6 and Sca-1 surface marker expression, it was observed here that the murine CNE923 is not significantly ($P<10^{-5}$) enriched for either mono-methylated H3K4 or acetylated H3K27, although it was observed the corresponding interrogated *Hin*dIII fragment is enriched for bound BRG1 and SATB1 and is transcribed.

A ChIP-Seq peak called for H3K4me1 was found to correspond to a neighbouring transcribed region located upstream of CNE923 at Chr3: 92,377094-92, 378026. This region was found to be involved in multiple interactions with regions found by Oh *et al* (2014) to physically contact 923 (figure 33), including candidate regulatory regions marked by enrichment for H3K27ac and/or H3K27ac. Significant long-range interactions called for this region were found to involve fragments enriched for varying combinations of simultaneous SATB1, SATB2, BRG1, RAD21, transcription and co-factor factor binding mapped using ChIP-Seq data and published ChIP-on-chip tiling data for normal murine IFE keratinocytes (Nascimento et al., 2011).

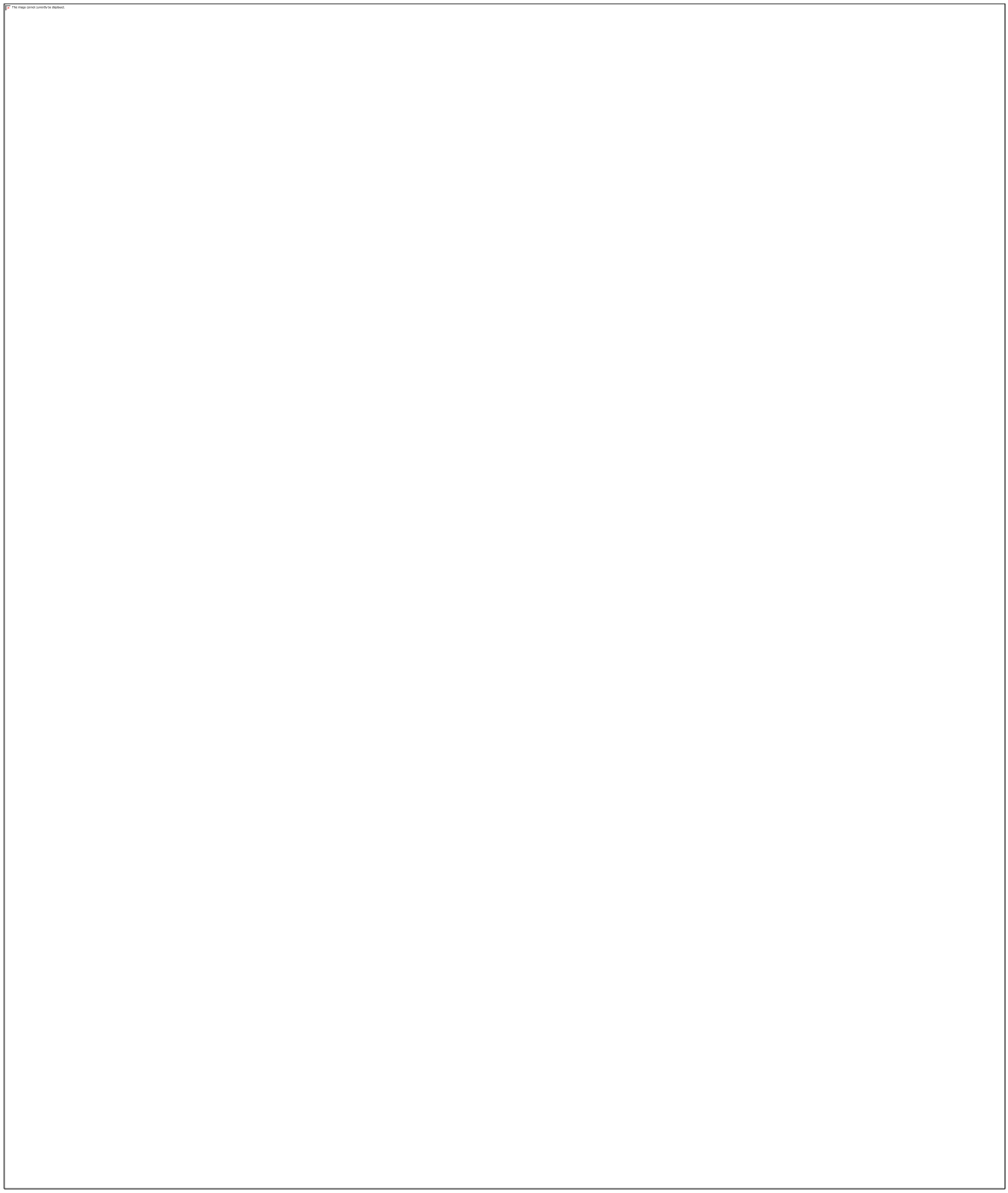

Figure 33 5C interactions called for a candidate enhancer element located immediately upstream of the *IVL* gene TSS. ChIP-Seq peaks called are shown for factors found to bind either the bait region or *Hin*dII fragments physically contacted by the bait region.

4.2.3 Regions bound by Special AT-rich binding proteins and cohesin are preferentially involved in looping interactions

To explore the mechanisms involved in regulating chromatin organisation at the EDC region, 5C data were correlated with ChIP-Seq data mapping the distribution of enrichment for SATB1, SATB2, the PRC1 protein RING1B, cohesin subunit RAD21, CTCF, and BRG1 binding events in FACS sorted $\alpha6^{bri}$/Sca-1+ epidermal IFE keratinocytes. The distribution of ChIP-Seq enrichment at interrogated fragments involved in looping interactions was then compared with the distribution of ChIP-Seq enrichment at all interrogated interactions.

Chromatin fragments enriched for RAD21, SATB1, and SATB2 binding alone were found to preferentially be involved in looping interactions in KC (Fisher's exact test, P<001) (figure 34B), and specifically in interactions specific to KC (Fisher's exact test, P<0.03) (figure 34A). Fragments enriched for RAD21 and SATB1 account for 45.9% and 34.5%, respectively, of all interactions identified at the target 5.3Mbp region interrogated in KC. A lesser but significant 15.3% of looping interactions identified in KC were found to involve fragments bound by SATB2. 27.2% of interactions were also found to involve chromatin fragments enriched for BRG1 binding in neonate $\alpha6^{bri}$/Sca-1+ epidermal IFE keratinocytes, however, fragments enriched for BRG1 binding were not found to be preferentially involved in looping interactions in KCs in comparison with the number of interrogated non-looping fragments enriched for BRG1 binding. Only 1.6% of interactions were found to involve chromatin fragments enriched for the PRC1 subunit RING1B and no overlap between enrichment for H3K27me3 and RING1B occupancy was detected (figure 34A).

Chromatin fragments enriched for co-localised SATB1+RAD21, SATB1+SATB2, and SATB2+RAD21 were also found to be preferentially involved in looping interactions (Fisher's exact test, P<0.01) (figure 34C). In KC specifically, chromatin fragments enriched for co-localised SATB1+SATB2 and SATB2+RAD21 were found to be preferentially involved in looping interactions (Fisher's exact test, P<4.5E-3) (figure 34D).

Interestingly, while 65.4% of sites of looping interaction found to be bound by SATB1 were also found to be enriched for bound RAD21, 91.7% of sites bound by SATB2 were

also found to be also enriched for RAD21 binding. In comparison, only 62.1% of SATB2 sites were found to overlap with SATB1 (figure 34C).

Co-localisation of the cohesin sub-unit Smc1 and CTCF has previously been shown correlate with the distribution of constitutive interactions comprising conserved topological domains in embryonic stem cells (ESC) and neural progenitor cells (NPC) (Phillips-Cremins et al., 2013). Here, chromatin fragments enriched for co-localised RAD21+CTCF were also found to be preferentially involved in looping interactions (Fisher's exact test, $P<0.05$) (figure 34E), however RAD21+CTCF bound fragments were only found to be preferentially involved in interactions found to be conserved in TC and KC ($P<0.03$) (figure 34F). 40.6% of interacting fragments enriched for bound RAD21 were found to be enriched for CTCF binding, which was predominately enriched at looping interactions between distal fragments (appendix figure A5). Sites bound by RAD21+CTCF account for 67.9% of CTCF enriched interacting fragments identified (figure 34). Sites enriched for RAD21 exclusive of enrichment for CTCF binding have been shown to regulate the formation of lineage specific interactions detected in ESC and NPC using 5C (Phillips-Cremins et al., 2013). Together these findings imply the majority of RAD21 bound fragments detected here are potentially involved in the formation of lineage-specific looping interactions in KC.

SATB1 bound H3K27me3 enriched regions and SATB1 bound H3K27ac regions were found to be preferentially involved in looping interactions found to be significant only in KC (figure 34G-H). In contrast, SATB2 bound H3K4me1 enriched regions were found to preferentially interact in KC and no preferential interaction between H3K27ac enriched regions simultaneously bound by SATB2 was detected (figure 34G). Simultaneous enrichment for SATB2 binding H3K4me1 occupancy was detected solely for interactions found to be significant only in KC (figure 34H).

Despite widespread enrichment for H3K4me1 and SATB1 occupancy at interrogated fragments, fewer interactions were found to involve H3K4me1 enriched regions bound by SATB1 and preferential interaction between these regions was not detected. Whereas 133 interactions were found to involve H3K27me3 enriched fragments bound by SATB1, only 112 were found to involve fragments enriched for SATB1 occupancy and

H3K4me1. 67 interactions involving sites enriched for both H3K27ac and SATB1 occupancy were detected (figure 34G). As found regarding SATB1, SATB2 bound H3K27me3 enriched regions were also discovered to be preferentially involved in looping interactions. Again a greater number of interactions involving regions enriched for H3K27me3 and SATB2 occupancy (80 interactions) than for H3K4me1 and SATB2 occupancy (39 interactions) were detected, despite the fact that overall more interrogated interacting fragments are enriched for H3K4me1 than are for H3K27me3. RAD21 was predominately found to occupy interacting regions enriched for H3K4me1 (216 interactions) although statistically significant preferential interaction between H3K27me3 enriched RAD21 (135 interactions) bound regions was detected for KC specific interactions. For interactions identified in KC that are conserved in TC, but not KC specific interactions, preferential interaction between H3K4me1 enriched RAD21 bound regions was detected (figure 34H).

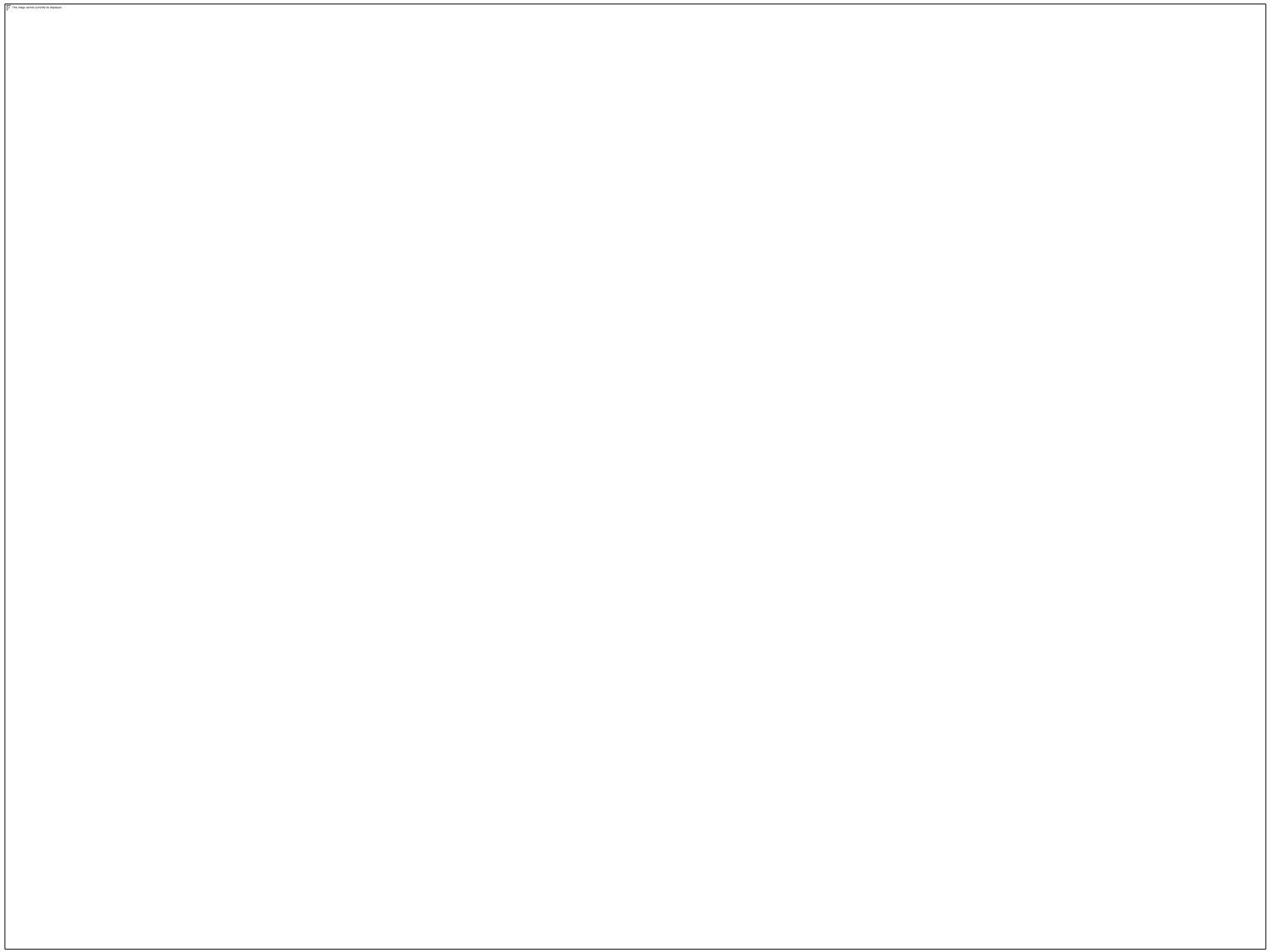
This image cannot currently be displayed.

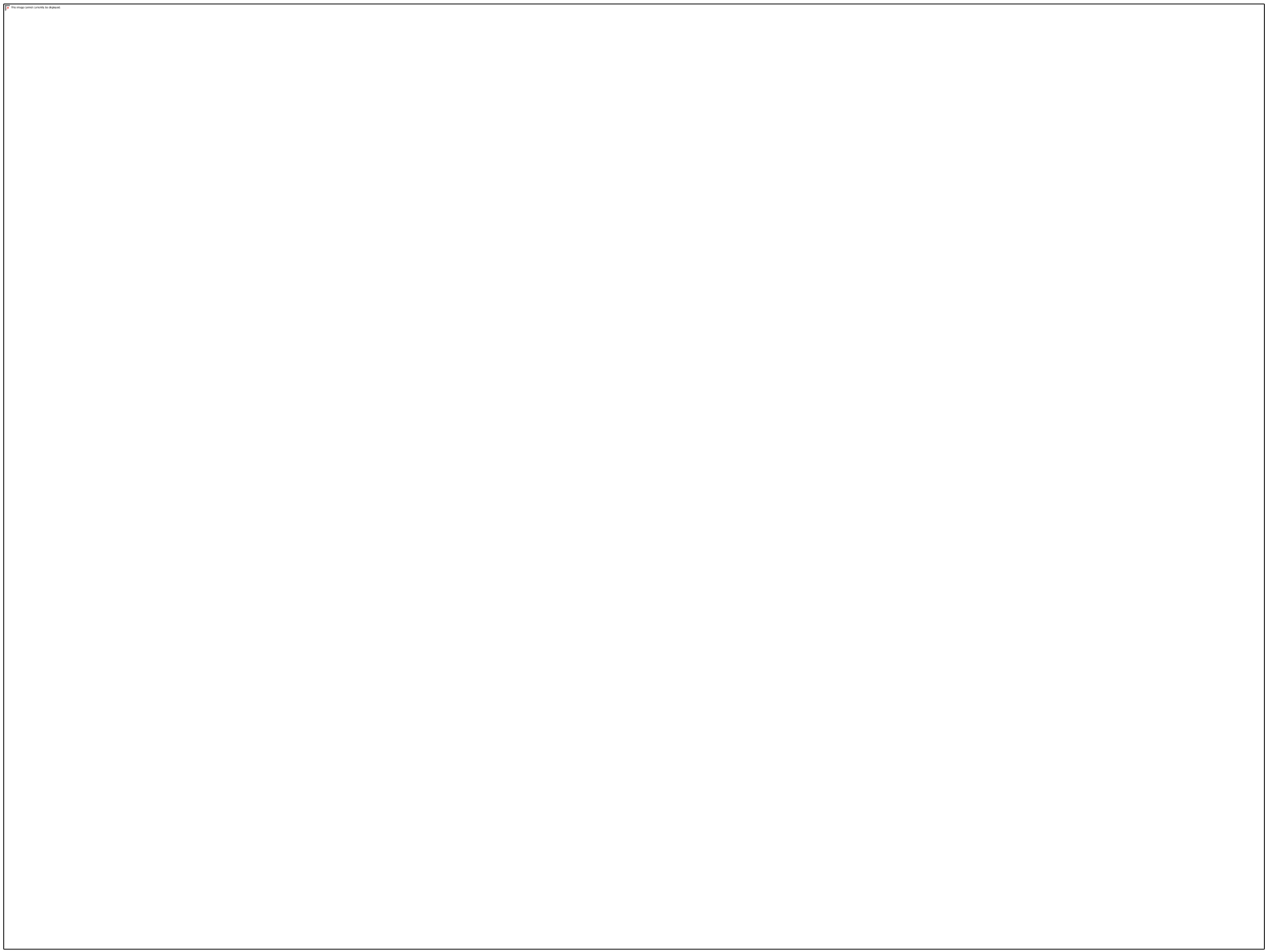

Figure 34 (A) Level of enrichment for looping chromatin interactions involving chromatin regions occupied by chromatin remodelling and architectural proteins in KC in comparison with the level of enrichment for histone modifications expected at sites of background interaction. (*=Fisher's exact test, *P*<2E-4) and **(B)** also comparison between the level of enrichment for occupancy present at sites of interaction in KC alone, in both TC and KC, and in background (*=Fisher's exact test, *P*<0.03) **(C & E)** Level of enrichment for simultaneous binding of chromatin remodelling and architectural proteins found to be associated with looping chromatin interactions in KC in comparison with background (C) *=Fisher's exact test *P*<2E-4 (E) *=Fisher's exact test *P*<0.02 **(D & F)** Level of enrichment for simultaneous binding of chromatin remodelling and architectural proteins found to be associated with looping chromatin interactions in KC only in comparison with interactions conserved in both TC and KC and those expected in background. (*=Fisher's exact test, *P*<0.03 **(G)** Enrichment for of bound SATB1, SATB2, and RAD21 at regions enriched for active and repressive histone modifications involved in looping interactions in comparison with background (*=Fisher's exact test *P*<2E-3; + = *P*<0.04) and **(H)** comparison between levels of occupancy at sites of interaction in KC alone, in both TC and KC, and those expected in background. *=Fisher's exact test *P*<0.05.

4.2.4 Special AT-rich binding proteins and cohesin co-localise with multiple additional transcriptional regulators at sites of looping chromatin interaction

The relationship between patterns of regional enrichment for bound chromatin remodellers shown to be enriched at looping interactions in KC and transcriptional regulators previously shown to be involved in controlling spatio-temporal patterns of EDC gene expression was then analysed using published ChIP-on-chip (tiling array) data mapping the distribution of enrichment for the de-acetylase complex sub-unit SIN3A (Nagy et al., 1997) and the RBP2 H3K4 specific de-methylase (Klose et al., 2007) at chromosome 3 in wild-type CBAxC57BL/6J IFE keratinocytes, as well as that of enrichment for the transcription factors C/EBPα and β, c-Myc, KLF4, MXI1, OVO1 and 2, AP-2γ (Nascimento et al., 2011).

Fragments enriched for RBP2, and overlapping regions of enrichment for both RBP2 and SIN3A were found to be preferentially involved in looping interactions, specifically in interactions significant only in KC (figure 35A&B). Interactions specific to KC found to involve candidate regulatory elements and regions marked by H3K27me3 were found also to be strongly enriched for RBP2 binding. SIN3A was found to occupy H3K27me3 enriched regions involved in interactions specific to KC as well as H3K27ac enriched regions, most likely promoter elements, involved in KC specific interactions (figure (figure 35D).

97% of SATB2 bound fragments involved in looping interactions (128 interactions) were found to be significantly enriched for RBP2 occupancy in addition to RAD21, which as discussed above, was found to occupy 91.7% of SATB2 enriched sites of looping interaction. A significant proportion of looping interactions identified in KC were also found to involve regions occupied by co-localised SATB2 and SIN3A (figure 35E). Enrichment for co-localisation between SATB2 and the co-repressors RBP2 and SIN3A was not detected at interactions found to be significantly represented in both TC and KC (figure 35F).

Preferential interaction between fragments enriched for co-localised SATB1+RBP2 and SATB1+SIN3A was also detected, although relative to RBP2, SIN3A was found to co-localise at a greater proportion (57.0%) of SATB1 bound sites of looping interaction. SATB1+RBP2 occupancy was found to comprise 41.9% of SATB1 bound sites of looping interaction. Conversely, it was found 48.4% of RBP2 enriched interaction sites in KC were found also to be enriched for SATB1 binding and 49.6% for SATB2. 73.9% of SIN3A enriched interaction sites were found also to be enriched for SATB1 binding and 32.2% for SATB2 binding (figure 35E).

Looping interactions specific to KC were found to preferentially involve fragment sites enriched for both RBP2 and RAD21 occupancy and also interacting fragments enriched for overlapping regions of SIN3A and RAD21 enrichment (figure 35F). Overall, 83.3% of RBP2 and 84.8% of SIN3A enriched interaction sites were found to be enriched for co-localised RAD21, which corresponds, respectively, to ~50% of RAD21 enriched sites of interaction in KC (figure 35E).

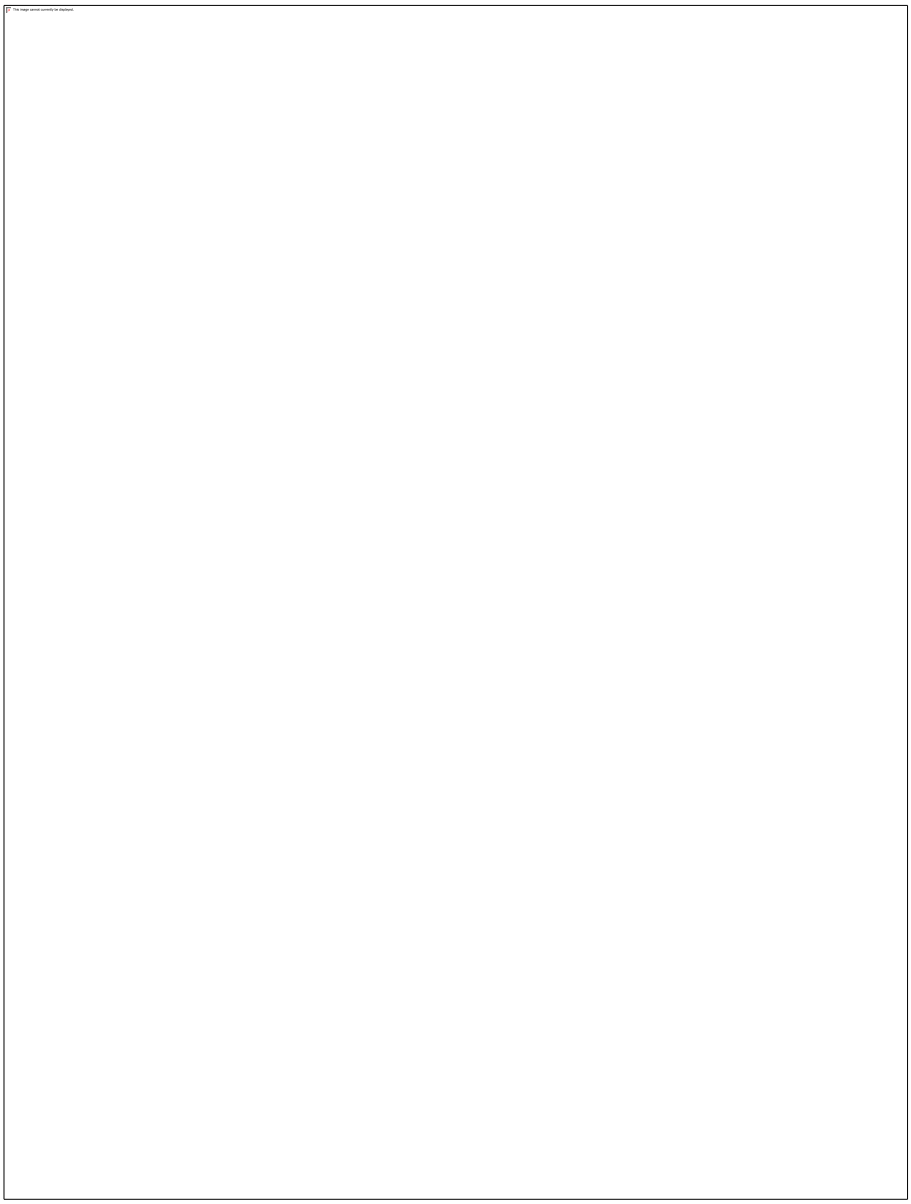

Figure 35 (A, C & E) Level of enrichment for looping chromatin interactions involving chromatin regions occupied by SIN3A, RBP2 and simultaneous enrichment for histone modifications or binding by combinations of SIN3A, RBP2, SATB1/2 and RAD21 in KC in comparison with background (A) *=Fisher's exact test, *P*<6E-6 (B) *=Fisher's exact test *P*<8E-5. + = P<0.02 (E) *=Fisher's exact test *P*<5E-4 **(B, D & F)** Comparison of levels of enrichment for combinations of bound RBP2, SIN3A, and chromatin remodellers, at regions enriched for active and repressive histone modifications involved in looping interactions significantly only in KC, in TC and KC, and in comparison with background (B) *=Fisher's exact test, *P*<0.02 (D) *=Fisher's exact test, *P*<5E-4 (F) *=Fisher's exact test, *P* <0.03

While no co-localisation of SATB1 with C/EBPβ at sites found to be preferentially involved in looping interactions was detected, a substantial number of fragments bound by co-localised SATB2+C/EBPβ and RAD21+ C/EBPβ were found to be preferentially involved in looping interactions in KC. Singly, C/EBPβ was also found to be enriched at fragments preferentially involved in looping interaction, however significant enrichment for C/EBPβ alone, and when co-localised with SATB2, was detected for interactions identified in KC that are also conserved in TC. (figure 36).

Enrichment for the co-localisation of OVO2 and C/EBPα with SATB1/2 and RAD21 was found only at fragments involved in interactions only found to be significant in KC. In addition, fragments enriched for bound SATB1+Klf4 were found to be preferentially involved in KC specific looping interactions. C/EBPα/β and OVO2 are expressed in the basal layer of the epidermis and, although little is known regarding the function Ovo2 has directly in regulating differentiation specific gene expression, C/EBP a and β have been shown to regulate the expression of EDC differentiation specific genes during the early stages of differentiation and, in conjunction, to regulate to regulate basal epidermal cell cycle arrest and commitment to terminal differentiation. (Eckert et al., 2004; Lopez et al., 2009; Maytin and Habener, 1998; Teng et al., 2007; Wells et al., 2009).

In addition, although not alone enriched at interactions, the c-Myc antagonist MXI1, of which SIN3A is an obligate partner (Alland et al., 1997; Rao et al., 1996), was found to co-localise with SATB1/2 and RAD21 at sites of looping interaction found to be significant only in KC (figure 36). The majority of transcription factor bound fragments shown to be preferentially involved in interactions in KCs were also found to be enriched for the enhancer mark H3K4me1 or repressive H3K27me3.

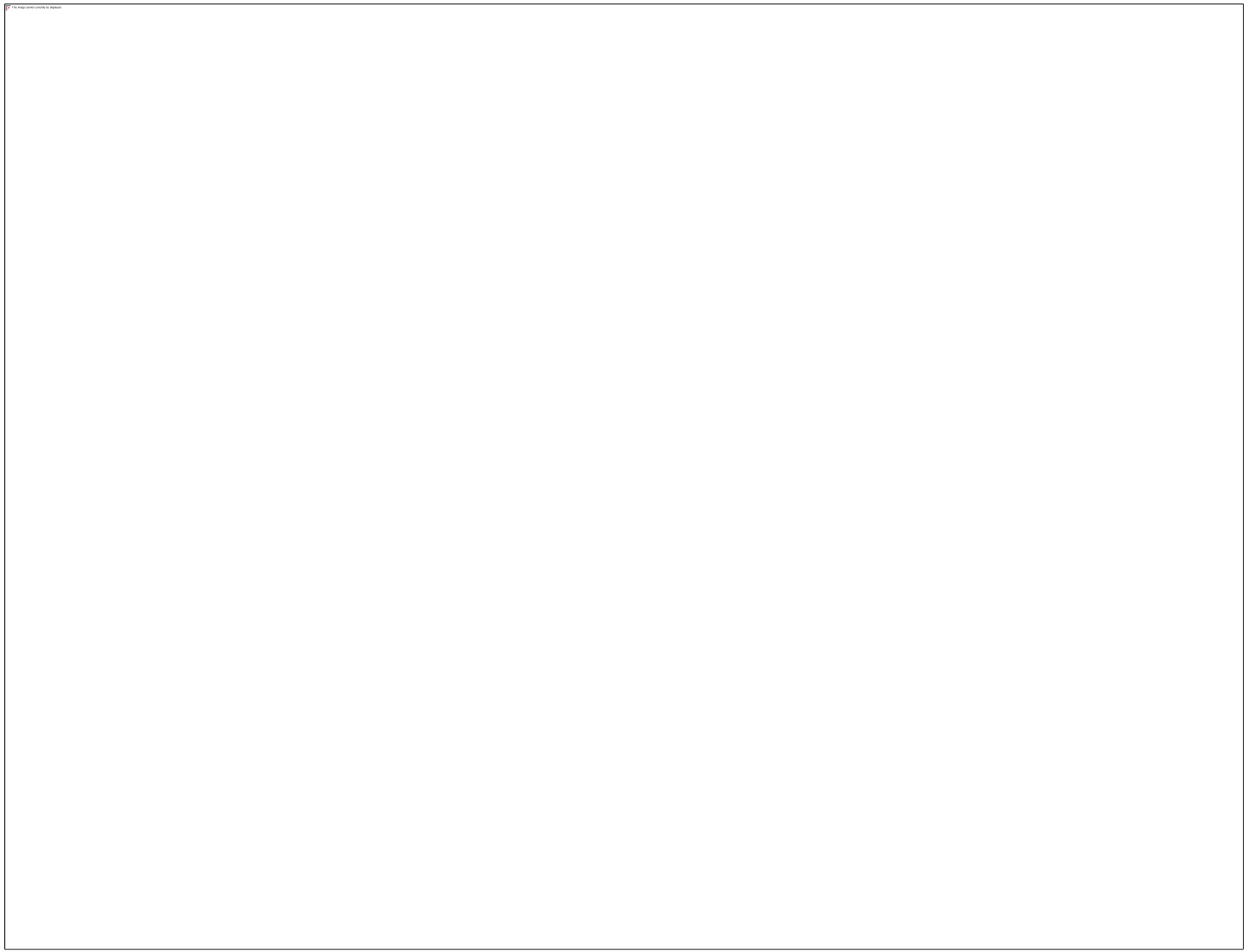

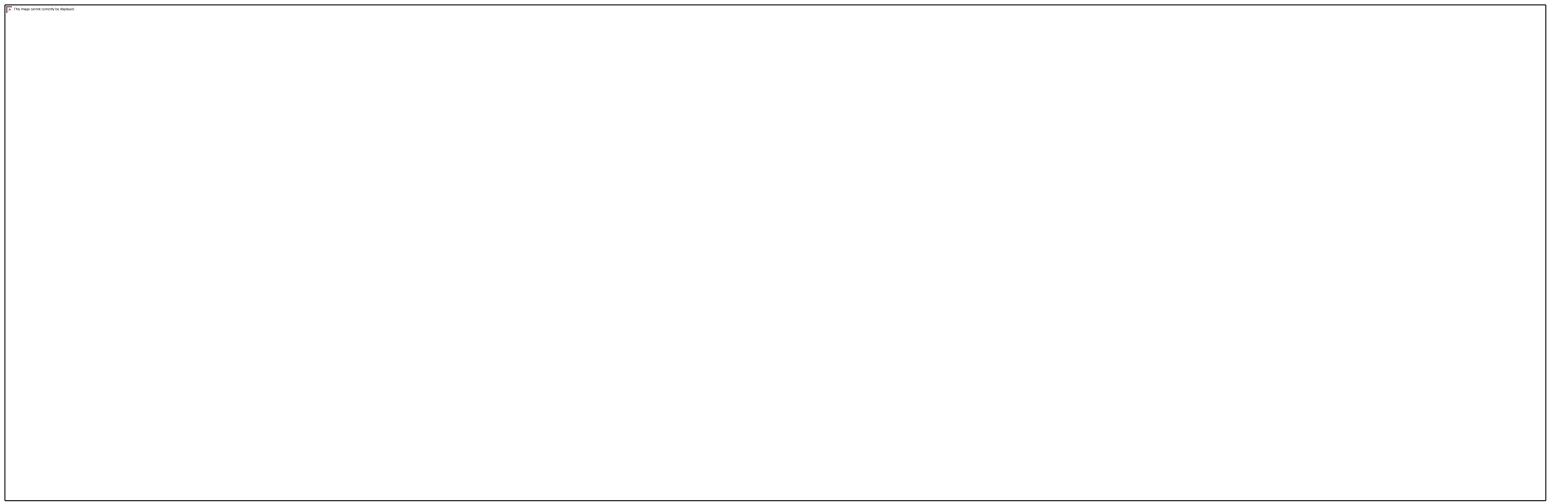

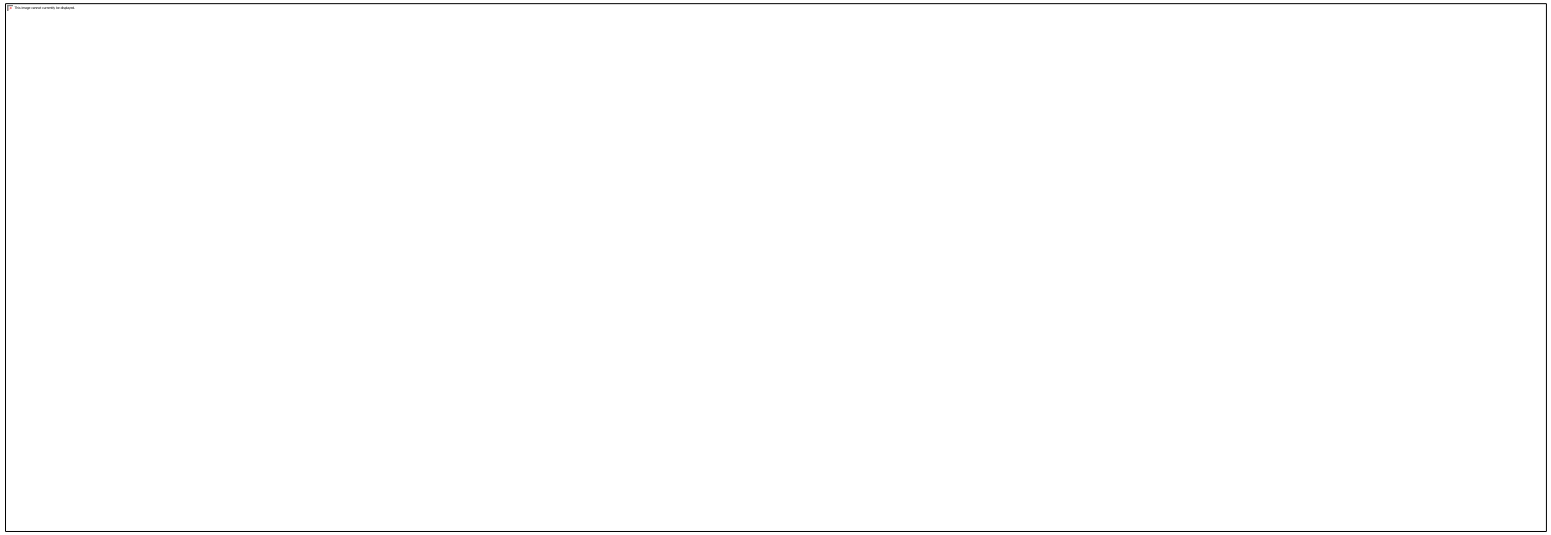

Figure 36 (A, C, E, & G) Level of enrichment for looping interactions involving chromatin regions occupied by transcription factors alone and co-localised with chromatin remodellers in KC in comparison with background. *=Fisher's exact test, $P<0.04$ **(B, D, F, & H)** Comparison of the level of enrichment for chromatin interactions involving regions occupied by transcription factors alone, or bound simultaneously by transcription factors and bound chromatin remodellers, in interactions significant only in KC, significant in TC and KC, and interactions expected in background. *=Fisher's exact test $P<0.05$.

5 Discussion

5.1 BRG1 regulates the transcriptional activity and spatial nuclear position of the EDC locus in basal epidermal keratinocytes

ATP-dependent chromatin-remodelling complexes play an important part in regulating temporal and spatial patterns of gene expression and thus are important regulators of a number of key developmental processes. SWI/SNF2 ATPase BRG1 is required during the early stages of embryonic development (Bultman et al., 2000) and has distinct developmental functions cell differentiation and organogenesis (Chi et al., 2003; Griffin et al., 2008; Indra et al., 2005). The results of this study reveal that BRG1 plays a critical role in regulating tissue-specific higher-order chromatin folding and transcription at the lineage-specific EDC locus during epidermal development.

A direct target of p63 (Mardaryev et al., 2014), BRG1 is normally expressed strongly in the basal layer of the epidermis, most spinous keratinocytes, and to a lesser extent granular keratinocytes (Indra et al., 2005). Results presented here show that the successful K14-CreER mediated ablation of BRG1 at E10.5 results in the aberrant expression of differentiation specific genes encoded at the EDC and morphological abnormalities in the epidermis at E16.5. A reduction in the expression of the corneal layer constituent protein loricrin is seen, EDC gene transcript levels are altered and the developing BRG1 deficient dorsal epidermal layer is significantly thinner at E16.5 and appears flattened.

Indra *et al* (2005) have previously reported that the conditional deletion of BRG1 results, at E18.5, in abnormal flattening of the dorsal epidermis, altered lipid processing, and increased permeability of the epidermal barrier. Data published by Indra *et al* and findings reported here together demonstrate that ablation of BRG1 during the early stages of epidermal development does not effect a change in levels of epidermal cell proliferation or apoptosis at either E18.5 or E16.5. However, these authors report that, although apparently flatter at E18.5, the thickness of the epidermal layer is not affected by ablation of BRG1, suggesting that between E16.5 and E18.5 there is an as yet unknown mechanism that operates to compensate for the effect BRG1 deficient has in the

epidermis at E16.5. In addition, while these authors report a change in the expression of transglutaminases required for assembly of the CE, the K14-Cre driven ablation of BRG1 was found not to impact upon the expression of loricrin (Indra et al., 2005). More work is needed to explain these differences and to fully define the impact developmental epidermal ablation of BRG1 has upon epidermal gene expression and the structure of the epidermal compartment.

It has previously been found that in the basal epidermal layer of $p63^{-/-}$ mice, BRG1 is among a number of chromatin-remodelling associated factors that exhibit reduced expression levels in the absence of p63. In the skin of $p63^{-/-}$ mice, arrested epidermal development correlates with marked changes in the higher-order folding of the chromatin fibre at the EDC. Preferentially located towards the nuclear periphery when inactive, with the up-regulation of transcription at the EDC during normal epidermal stratification the EDC moves inwards towards the nuclear interior. While located at the nuclear periphery prior to the onset of epidermal stratification, at E16.5, during epidermal stratification, the EDC is found to occupy a predominantly more internal position within a nuclear domain enriched for nuclear speckles. In contrast, in epidermal keratinocytes lacking p63 the nuclear location of the EDC locus remains peripheral. Notably, it has been shown that the above-described changes in the nuclear position of the EDC occur independently of neighbouring widely expressed gene loci, including *RPS27* (Mardaryev et al., 2014).

Here it is shown that the conditional ablation of BRG1 early during epidermal development results not only in changes in the transcript prolife of EDC genes but also in the nuclear position of the EDC within the basal layer of the epidermis, which at E16.5 in BRG1 deficient basal keratinocytes is located predominantly towards the nuclear periphery. The K14-CreER driven ablation of BRG1 prior to epidermal stratification does not affect the nuclear position of the neighbouring ubiquitously expressed *RPS27* gene locus, which appears to be constitutively located toward the nuclear interior during epidermal stratification and is not affected by an absence of p63.

It is well established that BRG1 acts to regulate gene transcription by catalysing changes in the arrangement and structure of nucleosomes at target gene proximal regulatory elements and co-associates with other transcriptional regulators at regulatory elements

(De et al., 2011; Euskirchen et al., 2011). Interestingly it has been shown that recombinant BRG1 protein is capable of nucleosomal remodelling (Phelan et al., 1999), however BRG1 naturally acts as part of the multi-subunit SWI/SNF complex and variable subunit composition potentially confers substantial functional diversity (Hargreaves and Crabtree, 2011; Narlikar et al., 2013). Transcription-associated changes in the higher-order chromatin folding and extra-territorial positioning of the interferon-γ (IFNγ) response genes *IRF1* and the MHC *TAP1*, *HLA-DRA*, and *CIITA* genes upon induction by IFNγ has been shown to require the STAT1 dependent recruitment of BRG1 to selected gene promoters (Christova et al., 2007). Additionally, it has been shown transcriptional regulation of the *CIITA* locus involves the recruitment of BRG1 to distal regulatory elements and BRG1 dependent long-range interaction of *CIITA* distal regulatory elements (Ni et al., 2008).

ChIP-Seq studies show BRG1 binding is enriched for at intergenic regions and evidence suggests BRG1 is involved widely in modulating chromatin structure and nuclear organisation, including the sub-structural organisation of nuclear lamina-associated compartments (De et al., 2011; Ho et al., 2009; Yu et al., 2013). Chromatin looping and long-range gene regulation at the α-globin locus requires BRG1 recruitment to distal α-globin gene regulatory elements (Kim et al., 2009a) and BRG1 is also required for chromatin looping and long-range gene regulation at the β-globin locus in erythroblast G1E cells cultured *ex vivo* (Kim et al., 2009b) and at the T-helper 2 (*TH2*) cytokine locus (Cai et al., 2006). In the erythroleukemic K562 cell line, integrated analysis of ENCODE Hi-C and ChIP-Seq data has revealed BRG1 occupancy is enriched for at a cluster of interactions between regions of chromatin characterised by DNase hypersensitivity, monomethylated H3K4, and binding by specific transcriptions factors (Lan et al., 2012).

Here ChIP-Seq was performed to map regions enriched for BRG1 binding events throughout the EDC. In combination with ChIP-Seq mapping of candidate enhancers marked by monomethylated H3K4 and acetylated H3K27, it was found a number of core promoter and enhancer regions throughout the EDC are enriched for bound BRG1. Among enhancers enriched for bound BRG1, candidate poised or active enhancers characterised by enrichment for monomethyated H3K4 were identified, as were several putative active enhancers marked by their enrichment for acetylated H3K27. The results

of this ChIP-Seq analysis together with microscopy based analysis of the spatial dynamics of the nuclear positioning of the EDC and neighbouring *RPS27* loci during epidermal development and following the ablation of p63 and BRG1 suggest BRG1 mediates p63 regulated tissue-specific chromatin folding at the EDC.

A substantial amount of data has been generated by separate studies of different model systems that pertains the extent to which the positioning of genes relative to the main body of CT is dependent upon transcriptional state (de Wit and de Laat, 2012; Dekker et al., 2013; Egecioglu and Brickner, 2011). High levels of active gene expression and a high gene density have been shown to correlate with the positioning of loci at the periphery of, or outside of, the main body of CT (Chambeyron and Bickmore, 2004; Chambeyron et al., 2005; Mahy et al., 2002a; Morey et al., 2007; Morey et al., 2009; Volpi et al., 2000; Williams et al., 2002). Despite the predominance of mRNA transcripts and small spliceosomal snRNPs peripheral to CT (Zirbel et al., 1993), however, the surface of CT do not *per se* provide a permissive environment for transcription: units of transcription are not restricted to the periphery of CT and data indicate macromolecular components of the transcription machinery can permeate compact chromatin domains. In addition there is considerable variability in the relationship between transcriptional activity and the position of different individual genes and gene clusters relative to the territory periphery (Mahy et al., 2002b; Markaki et al., 2010; Misteli, 2007; Verschure et al., 2003; Verschure et al., 1999).

It is posited instead that the co-association of active genes within domains enriched for RNAPII transcription factories and splicing speckles at the periphery of CT and within inter-territory lacunae, while not intrinsically necessary for transcription, may be involved in facilitating the efficient transcription of highly expressed genes and the formation of regulatory chromatin interactions in *cis* and in *trans*. Indeed, targeting the β-globin LCR to a number of unrelated genes has been shown to result in the increased association of several of these genes with RNAPII transcription factories at the edge of, or outside of CT, and with a degree of concomitant transitional up-regulation (Noordermeer et al., 2008).

In mouse basal epidermal keratinocytes it was observed here that, while the overall number of splicing speckles present in basal keratinocyte nuclei is not reduced as a consequence of the K14-CreER driven ablation of BRG1, the peripheral localisation of the EDC locus in the absence of BRG1 coincides with a significant reduction in the spatial proximity of the EDC locus with speckles. These results parallel earlier findings showing that the peripheral localisation of the EDC in the absence of p63 activity correlates with the reduced appropinquity of the EDC with nuclear speckles that can not be explained by an overall reduction in the number of nuclear speckles present in $p63^{-/-}$ keratinocyte nuclei (Mardaryev et al., 2014).

During normal epidermal ontogenesis, it is not clear whether the EDC moves into a domain already enriched for splicing factors or whether these factors aggregate around the activated EDC locus. More work is needed to understand the dynamics of the association of the active EDC with nuclear speckles the individual components of nuclear speckles (Spector and Lamond, 2011) and vice versa. Importantly, movement of the EDC during normal epidermal stratification precedes full activation of the EDC, which is reached in terminally differentiating keratinocytes of the mature adult epidermis. While it is clear transcription and co-transcriptional splicing is not restricted to speckles, the co-localisation of the active EDC with speckles located within a transcriptionally permissive nuclear domain may confer strategic benefits in maintaining high levels of transcription at the EDC, as required for keratinocyte differentiation and formation of the epidermal barrier. More works is also needed to elucidate the exact nature of this observed interaction between the EDC and speckles.

Additionally it should be noted that in human keratinocytes it has been shown, much as for the MHC region, that activation of the EDC is associated with looping of the EDC out from it's corresponding CT. While in human lymphoblasts the MHC is positioned outside of it's corresponding CT, the inactive EDC has been shown to occupy an internal position within it's CT. However, the active EDC occupies a predominantly extra-territorial position in differentiating human primary keratinocytes cultured *ex vivo* and to a lesser extent also in basal keratinocytes (Williams et al., 2002). Variation in the observed dynamics of the nuclear localisation of the mouse and human EDC loci may stem from differences in the structure of chromatin at and contiguous the EDC locus in humans and

mice. Although the EDC is highly evolutionarily conserved, the location of a gene desert region at the murine EDC substantially alters the local chromatin environment of the EDC region in mice in comparison with that of the EDC in humans and other primate species (figure 35).

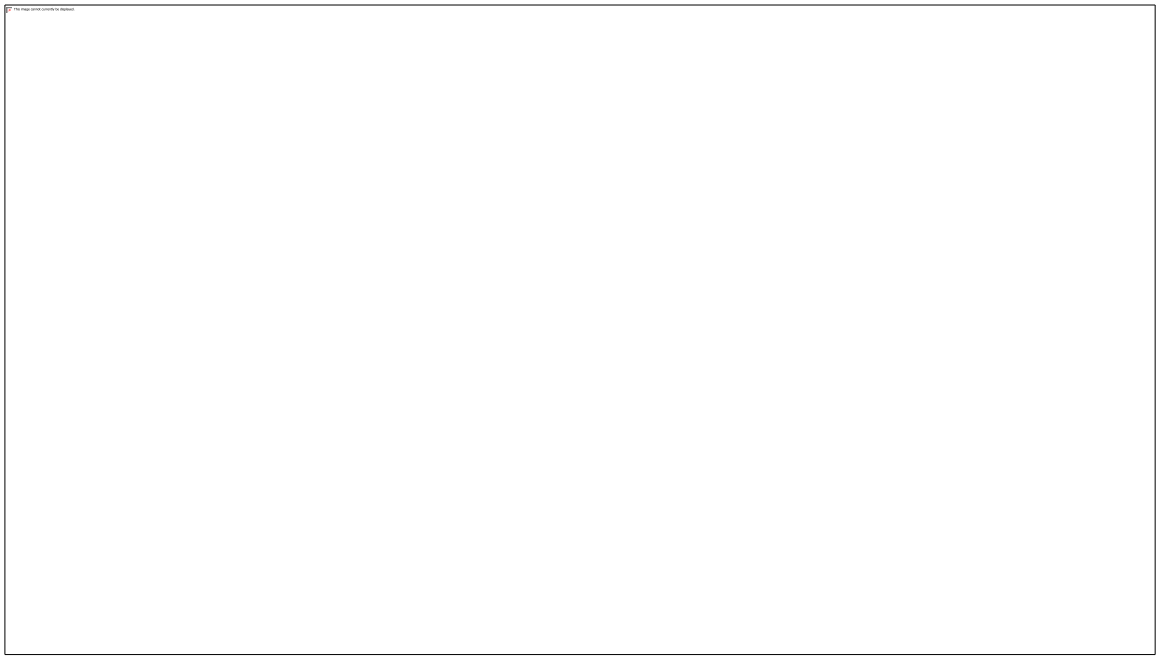

Figure 37 Structure of the human and mouse EDC regions. Based upon the UCSC genome browser *Homo sapiens* Hg18 and *Mus musculus* Mm9 genome assemblies. GC per cent and MULTIZ genome alignment tracks are shown. The location of human and mouse *S100* gene families is denoted in blue.

Chromatin remodelling by SATB1 and CHD4 is also implicated in the regulation of EDC gene expression. P63 has also been shown to regulate the Stab1, the ablation of which leads to a change in the overall volume of the EDC locus detected following FISH of probes spanning the EDC. The ablation of the NuRD complex ATPase component CHD4, which is posited to work in concert with lineage-specific transcription factors to mediate transcriptional activation during T cell development (Williams et al., 2004), results in the abnormal expression of epidermal markers of differentiation encoded at the EDC (Kashiwagi et al., 2007). Functional interactions between BRG1, as well as other chromatin remodellers, and transcription factors known to directly regulate EDC gene expression, such as members of the AP1, AP2, and OVO1, remain to be elucidated and further study is required to identify the molecular mechanisms by which BRG1 acts to modulate EDC gene expression.

5.2 Higher-order chromatin folding and potential mechanisms of long-range gene regulation at the EDC

Analyses of the higher-order folding of chromatin at the EDC and flanking regions presented here map a network of long-range interactions involving a large number of developmentally regulated EDC genes and candidate gene regulatory elements marked by combinations of enrichment for H3K4 mono-methylation, enrichment for both H3K4me1 and H3K27 acetylation, and also chromatin binding factor occupancy.

A hierarchy of multiple distinct topological domains, ranging in size from hundreds of kilo bases in size to multi mega-base scale domains, were detected at the murine EDC in keratinocytes. Using 3D-FISH it was found that chromatin at the murine EDC locus is more tightly folded when active in keratinocytes than when inactive in thymocytes. Correspondingly, domains comprising a large proportion of pairwise interactions occurring between loci located several mega-base pairs apart were detected using 5C technology. While conserved domain boundaries were detected at both the active and inactive EDC, in KC and TC respectively, organisation of chromatin at the EDC within domains appeared markedly more structured in keratinocytes, suggesting a continuum of preferential chromatin interactions shape the topology of chromatin at the active EDC. The majority of chromatin interactions in keratinocytes were found to involve regions corresponding to the position of core promoter and proximal regulatory regions, which suggest a large number of these interactions may have specific functions in the regulation of gene transcription.

While local enrichment for active the histone modifications H3K27ac and H3K4me1, in combination or alone, was not found to be significantly associated with the formation of chromatin loops, candidate non-promoter proximal regulatory regions enriched for binding by transcription factors and chromatin remodelling proteins, were found to be preferentially involved in looping interactions, including interactions involving candidate regulatory regions located at flanking regions outside of the EDC. Transcription factor binding and enrichment for bound SATB1/2 and RAD21 were found predominantly at potentially lineage-specific interactions found to be significantly represented only in keratinocytes.

Although less abundant than interrogated sites of interactions enriched for mono-methylated H3K4 or acetylated H3K27, sites enriched for tri-methylated H3K27 were found to be preferentially involved in looping interactions with multiple gene partners. Differences in the degree of distribution of H3K27me3 and active marks mapped at sites of interaction reflect differences in genome-wide patterns of enrichment for H3K27me3 and for the active marks H3K4 methylation an H3K27 acetylation, which tend to be enriched at focal points corresponding to promoter regions and putative distal regulatory elements. In contrast, H3K27 tri-methylation, which here was found to be distributed broadly across interactions involving distal interacting fragments as well as proximal regions, is found variously distributed at focal points corresponding to promoter regions, in broad blocks of enrichment at intergenic regions, and at gene bodies (Heintzman et al., 2007; Pauler et al., 2009).

Several studies support a role for PRC2 and enrichment for tri-methylation of H3K27 at focal regions corresponding to promoters and key developmentally regulated genes in regulating the expression of developmental genes and cell fate decisions in ES and lineage committed cells (Azuara et al., 2006; Barski et al., 2007; Bernstein et al., 2006; Bracken et al., 2006; Lee et al., 2006b; Mikkelsen et al., 2007; Zhao et al., 2007). In the basal epidermal layer, PRC2/EZH2 has previously been shown to inhibit AP1 binding at late-stage differentiation associated EDC gene promoters in basal keratinocytes during epidermal morphogenesis. The depletion of H3K27 tri-methylation accompanies embryonic keratinocyte stratification and terminal differentiation, enabling AP1 mediated transcriptional activation (Ezhkova et al., 2009), although the functions of PRC2 and H3K27me3 in adult keratinocytes are less well understood.

Co-enrichment for H3K27me3 at regions also enriched for active histone marks and transcription factor binding was detected specifically at the ~50% of sites of interaction identified in KC not also represented significantly in TC. Poised enhancer elements are marked by enrichment for H3K4me1, and potentially also H3K27me3, and in un-differentiated cells may be involved in readying lineage-specific genes for response to developmental cues (Creyghton et al., 2010). Similarly, promoters marked by a bivalent chromatin state – that is promoter elements enriched for both H3K4me3, a histone mark

associated with active promoters, and H3K27me3 – are implicated in regulating the expression of developmentally expressed genes (Bernstein et al., 2006; Cui et al., 2009; Harmston and Lenhard, 2013). The relationship between looping in *cis* between gene regulatory elements and histone modifications is still poorly understood and further study is required to establish if, and if so how, long-range gene regulation involving poised or bivalent enhancer and promoter elements is involved in regulating the expression of developmentally expressed genes in epidermal progenitor cells.

Binding by the JARID1 family H3K4 specific histone de-methylase RBP2, which has been shown to interact physically with PRC2 to regulate the transcription of developmental genes, was also found to be associated with the formation of looping interactions specific to keratinocytes. In murine ES cells, RBP2 activity has been reported to play a critical role in the suppression of an array of developmentally regulated PRC2 targets (Pasini et al., 2008). Here, the keratinocyte-specific preferential looping of regions simultaneously bound by RBP2 and enriched for H3K27me3 at the EDC region in proliferating keratinocytes was observed. Genome-wide mapping studies report RBP2 localises to H3K4me3 occupied promoter regions where it functions as a transcriptional repressor, although preferential looping interaction involving regions bound by RBP2 (Kdm5b) and enriched for H3K4me1 was also detected here. Only the JARID1 family members PLU1 and SMCX (RBP-2-like), however, have been previously shown to bind H3K4me1 enriched distal regions (Outchkourov et al., 2013).

A substantial proportion of sites, including regions enriched for active and repressive histone marks, bound by SATB1 were found to be preferentially involved in looping interactions, specifically those interactions specific to keratinocytes. SATB1 has been shown to regulate transcription at the MHC class I and T_H2 cytokine loci (Cai et al., 2006; Kumar et al., 2007) and in thymocytes to comprise a cage-like scaffold to which MAR regions are tethered (Cai et al., 2003; Cai et al., 2006). In basal epidermal keratinocytes, SATB1 is directly regulated by p63, which binds the core promoter region of the murine SATB1 gene (Fessing et al., 2011). Using FISH of probes spanning the murine EDC locus in basal keratinocytes, it has previously been shown that chromatin compaction at the EDC locus in basal epidermal keratinocytes is regulated SATB1. The volume occupied by chromatin at the EDC central domain has been shown to increase following

the ablation of SATB1 and to coincide with the perturbation of programmes of differentiation-specific EDC gene expression (Fessing et al., 2011).

Here, SATB2 was also found to be enriched at regions involved in the formation of keratinocyte-specific chromatin loops, including, H3K4me1 enriched and H3K27me3 enriched regions found to be preferentially involved in looping interactions. Closely related to SATB1, the SATB2 protein has been shown to exhibit cell- and tissue-specific patterns of association with AT-rich DNA sequences that demarcate putative MARs (Alcamo et al., 2008; Britanova et al., 2005; Dobreva et al., 2003; Szemes et al., 2006) and is involved in the regulation of cell- and tissue-specific developmental programmes of gene expression (Alcamo et al., 2008; Britanova et al., 2005; Britanova et al., 2008; Britanova et al., 2006; Dobreva et al., 2006; Dobreva et al., 2003; Szemes et al., 2006). SATB2 has also been shown to modulate local chromatin structural states and to interact with HDAC1 and metastasis associated protein MTA2, a component of the NuRD complex (Britanova et al., 2008; Gyorgy et al., 2008).

In ESC, SATB1 and SATB2 have also been reported to directly bind the Nanog locus and work in opposition to one another to regulate Nanog expression and ESC plasticity (Savarese et al., 2009). However, the independent activity of SATB1 and SATB2 is implicated in the regulation of additional genes encoding pluripotency factors and factor associated with ESC differentiation (Savarese et al., 2009) and in trophoblast stem cells, the knockdown of either SATB1 or SATB2 has been shown to promote stem cell differentiation at the expense of self-renewal (Asanoma et al., 2012).

Significant co-localisation of SATB1 and SATB2 at sites of keratinocyte-specific looping interaction was identified here, although only a partial overlap between SATB1 and SATB2 at interacting chromatin regions was observed. However, a striking degree of enrichment for co-localisation between SATB2 and the RBP2 histone HK4 de-methylase at sites of looping interaction was observed, with almost all SATB2 bound sites also found to be occupied by RBP2.

Concordant with earlier, published, findings SATB2 was also found frequently to co-localise with the HDAC complex partner protein SIN3A. An obligate MXI1 partner

involved in the suppression of c-Myc responsive genes, SIN3A acts to recruit HDACs to chromatin but has also been implicated in promoting transcriptional activation (Silverstein and Ekwall, 2005). Co-localisation of SATB2 and MXI1 was also found to be associated with the formation of keratinocyte-specific looping interactions, which likely, in part at least, reflects the interaction of MXI1 with SIN3A co-associated with SATB2. SIN3A has also been shown to negatively regulate gene expression in a HDAC-independent manner and to interact with BRG1 and BRM containing SWI/SNF complexes (Sif et al., 2001).

Co-localisation of SATB2 with C/EBPβ was found to be substantially associated with the formation of looping interactions and a large proportion of SATB2 bound sites of chromatin interaction were also found to be bound by C/EBPβ. SATB2 was also found to co-localise with Ovo2 and C/EBPα at sites found to be preferentially involved in keratinocyte-specific looping interactions. Further work is needed to establish if, and if so, how, SATB2 plays a functional role in regulating higher-order chromatin folding at the EDC. However findings presented here together with published data would appear to suggest that SATB2 acts as a MAR-bound docking site that mediates recruitment of transcriptional co-repressors, and potentially also co-activators, to multiple gene regulatory regions at the EDC region. In B cells, although not in non-lymphoid cell lines, SATB2 has been shown to positively regulate transcription in a manner shown to be modulated by the activity of the SUMO-E3 protein ligase PIAS1 (Dobreva et al., 2003).

Co-localisation of SATB1 with RBP2 and SIN3A found here to be associated with chromatin looping, although in comparison with SATB2, SATB1 was found to more frequently to bind independently of RBP2 and SIN3A. In T cells, SATB1 attachment to MARs has been shown to recruit the NuRD HDAC and ACF/CHRAC nucleosome remodelling complexes to chromatin (Yasui et al., 2002). However upon phosphorylation by PKC, SATB1 has also been shown to recruit the pCAF histone acetyltransferase in T cells (Pavan Kumar et al., 2006). While knockdown of SATB1 has been shown to perturb normal programmes of EDC gene expression and to lead to changes in the higher order chromatin structure of the EDC, the mechanisms involved in SATB1 mediated transcriptional regulation at the EDC in epidermal progenitor cells and differentiating keratinocytes are not yet understood.

Preferential interaction between a small proportion of SATB1 bound sites also occupied by C/EBPα and Ovo2 was also found, although in comparison with SATB2, SATB1 was found to also co-localise less frequently with transcription factors at sites of interaction. These findings suggest that SATB1, but not SATB2, may also be involved in functions at the EDC independent of the recruitment of transcriptional regulators to gene regulatory regions through control of global higher-order chromatin folding at the locus.

Substantial co-localisation of SATB1 and the cohesin sub-unit RAD21 at regions involved in the formation of keratinocyte-specific chromatin loops was also observed. An abundantly expressed multi-protein complex, cohesin comprises a SMC1/SMC3 heterodimer bound by RAD21 and STAG proteins. Together these proteins form a ring-like structure (Peters et al., 2008) that mediates chromatid cohesion during cell division (Diaz-Martinez et al., 2008) and also the formation of looping chromatin interactions involved in transcriptional regulation in interphase nuclei (Kagey et al., 2010; Merkenschlager and Odom, 2013; Parelho et al., 2008; Peters et al., 2008; Phillips and Corces, 2009; Schmidt et al., 2010).

In conjunction with the mediator complex, cohesin has been shown to regulate the formation cell-type specific chromatin loops between distal and proximal regulatory elements (Kagey et al., 2010; Phillips-Cremins et al., 2013). Phillips-Cremins *et al* (2013) have revealed that while networks of conserved interactions occur between regions of chromatin characterised by bound CTCF and cohesin, enrichment cohesin and the mediator complex is associated with the formation of cell-type specific chromatin domains within TADs that comprise cohesin dependent interactions between enhancer and proximal promoter elements involved in the long-range transcriptional regulation of lineage-specific genes (Phillips-Cremins et al., 2013).

Data presented here show that binding by the cohesin subunit RAD21 is strongly associated with chromatin looping at the EDC region in keratinocytes. Chromatin regions bound by cohesin/RAD21 and also co-localised RBP2 and SIN3A were also found to be preferentially involved in keratinocyte-specific looping interactions, as were regions

bound by co-localised cohesin/RAD21 and the transcription factors MXI1, C/EBPα, C/EBPβ, OVO2 and also KLF4.

Concordant with previously published findings, enrichment for bound cohesin/RAD21 and CTCF was detected at sites of interaction found to be present consistently in both TC and KC but not at sites found to be specific to KC. CTCF occupied invariant CTCF binding sites are prevalent through out the genome (Kim et al., 2007) and the co-localisation of CTCF and cohesin is implicated in the formation of looping chromatin-chromatin interactions and long-range gene regulation (Peters et al., 2008; Phillips and Corces, 2009; Wendt et al., 2008).

Phillips-Cremins *et al* (2013) have recently reported co-localised bound cohesin and CTCF appear to anchor chromatin interactions that are conserved between cell types and which comprise conserved TADs and sub-domains within TAD (Phillips-Cremins et al., 2013). In contrast, these authors report binding by RAD21 independently of CTCF is associated with the co-localisation of RAD21 with the mediator complex and regulation of lineage-specific long-range interactions between gene regulatory elements involved in controlling gene transcription (Phillips-Cremins et al., 2013). Further work is needed to more robustly analyse the cell-type specificity of patterns of chromatin factor binding reported here but these data suggest distinct patterns of chromatin binding factor occupancy characterise potentially regulatory keratinocyte-specific chromatin interactions spanning the EDC region.

Although these results show enrichment for BRG1 binding was detected at regions involved in chromatin interactions in keratinocytes, the level of enrichment for BRG1 at regions brought together by chromatin looping was not found to be significant in comparison with the overall distribution of BRG1 binding at the EDC and neighbouring regions. Therefore, although, as discussed in the above section, data presented here demonstrate that BRG1 modulates the nuclear re-positioning and transcriptional activity of the EDC locus and transcriptional regulation of the EDC during epidermal ontogenesis, 5C data do not show that BRG1 is involved in the formation or maintenance of chromatin loops potentially involved in long-range gene regulation at the EDC region in the postnatal epidermal cells.

6 Conclusions

1. BRG1 binds multiple loci at the murine EDC and, in epidermal progenitor cells, is involved in regulating the specific nuclear positioning of the EDC locus relative to visible nuclear sub-compartments within the 3D nuclear space during morphogenesis of the epidermal barrier. The activity of BRG1 in basal keratinocytes acts to modulate the expression of developmentally regulated differentiation-specific genes encoded at the EDC during epidermal stratification *in utero*.
2. In keratinocytes and in thymocytes, chromatin is folded into several topological domains at the 5.3Mb regions on mouse chromosome 3 that spans the EDC. In keratinocytes, chromatin at the central part of the EDC locus is more compacted than when inactive in thymocytes and forms a more restricted set of spatial interactions in comparison.
3. The majority of spatial chromatin interactions identified at the EDC region in keratinocytes involve gene promoters. A substantial number of these interactions also involve candidate enhancer elements marked by enrichment for H3K4me1 alone or enrichment for both H3K4me1 and H3K27ac.
4. Regions anchoring the spatial chromatin interactions identified at the EDC region are enriched for bound genome organisers SATB1 and SATB2, as well as for the cohesin complex subunit RAD21, which suggests these proteins may control higher-order chromatin folding at the EDC.
5. Previously shown to modulate chromatin compaction and transcription at the EDC in the stratified epidermis, results presented here suggest SATB1 acts to regulate transcription at the EDC by tethering chromatin loops at the EDC region and by facilitating the docking of chromatin remodelling enzymes involved in transcriptional regulation at sites of interaction.
6. These data suggest cohesin also is involved in organising global chromatin folding at the EDC region and in facilitating the recruitment of transcriptional regulatory to sites of looping interaction.
7. Findings presented here in addition indicate SATB2 acts to recruit or dock transcriptional regulators at sites of looping interaction involving loci located within, and outside of, the EDC, although evidence generate here suggest SATB2

is not independently involved in organising global chromatin folding at the EDC region.

8. Enrichment for the transcriptional co-repressors, including RBP2, and the PRC2-EZH1/2 associated mark H3K27me3 was found to be associated with the formation of looping interactions at the EDC. While the formation of looping interactions was not found to be associated with markers of transcriptional activation alone, candidate poised enhancers and promoters characterised by both active and repressive epigenomic marks were found to be preferentially involved in looping interactions.

In summary, these findings suggest that higher-order chromatin folding at the EDC brings together proximal and distal gene regulatory elements involved in the coordinated regulation of transcription at the locus in epidermal progenitor cells before full activation of differentiation-specific genes, as required for terminal keratinocyte differentiation. Results presented here suggest RPC2 and RBP2 complexes act to hold interacting gene regulatory elements at the EDC in a "poised" state in epidermal progenitor cells prior to differentiation.

7 Future directions

1. Data presented here correlate patterns of chromatin binding factor occupancy with the formation of chromatin loops at the EDC. Further analyses of data generated as described here are needed in order to robustly determine the cell-type specificity of looping interactions occurring at the EDC and between loci located at and outside of the EDC. Similarly, more work is needed to determine to what extent chromatin binding factors found here to be enriched at sites of looping interaction are involved in the formation of lineage-specific interactions between gene regulatory elements.
2. Further data are required to ascertain the functionality of lineage-specific looping interactions occurring at the EDC and between loci located at and outside of the EDC that involve candidate regulatory elements and enhancer-associated long non-coding RNAs.
3. Functional studies are required to establish if SATB2 is required for long-range gene regulation at the EDC and to what extent binding by SATB2 at the EDC and flanking regions is required for the orchestration of developmental programmes of EDC gene expression.
4. Knockdown of SATB1 has been shown to impact upon the transcription of EDC genes however a high resolution 3D FISH and 3C-technology based study of chromatin folding at the EDC in SATB1 knockout mice is needed to establish whether or not, and the extent to which, SATB1 shapes the formation of specific looping interactions between regulatory elements involved in the long-range regulation of gene transcription.
5. Questions regarding the epidermal phenotype of BRG1 ablation during epidermal development need to be addressed and further work is needed to understand the mechanisms by which BRG1 activity impacts upon gene expression at the EDC.
6. Further study is required to establish if, and if so the extent to which, chromatin folding and long-range gene regulation at the EDC region depends upon inter-dependent functions of SATB1/2 proteins, cohesin, and additional transcriptional regulators.
7. Future study could establish whether PRC2-EZH1/2 and RBP2 directly interact to co-ordinately regulate the suppression of premature differentiation-specific gene

expression at the EDC locus in epidermal progenitor cells and if PRC2-EZH1/2 and RBP2 are recruited to ‘bivalent domains’ at the EDC.

8 Appendix

Probe	BAC name	Featured Gene	BAC start*	BAC end*	gene start*	gene end*
Rps27	RP23-480F10	Rps27	89997746	90169775	90016591	90017569
EDC	RP24-318N12	S100a6	90284072	90451873	90416816	90418336
	RP24-61G19	Lor	91716002	91899804	91884193	91887064
	RP24-248L10	Ivl	92215201	92392463	91887064	92377637
	RP24-341I21	Lce3c	92634255	92806759	92748408	92749652
	RP23-425P7	S100a10	93215624	93411886	93359039	93368567
Gabpb2	RP24-363H12	Gabpb2	94926338	95086569	94985688	95021864
	RP23-301G22	-	91894818	92021235	-	-
	RP23-425P7	S100a11	93215624	93411886	93324418	93330210
	RP24-75K3	Lce3b	92583402	92766349	92736901	92738020

Table A1 Labelled DNA probe BACs (*Mm9/GRC37)

Buffer/medium	Composition
1X TE (Tris/EDTA) buffer, pH 8.0	100mM TRIS-HCl 10mM Ethylenediaminutesetetraacetic acid (EDTA)
1X TBE (Tris-Borate-EDTA) buffer	89mM Trizma® Base/Tris Base 89mM Boric Acid 2mM Ethylenediaminutesetetraacetic acid (EDTA)
Low calcium medium for primary mouse keratinocyte (PMK) culture	Lonza® no calcium EMEM containing: 4% chelex-treated foetal bovine serum (FBS); 0.05mM Calcium chloride, $CaCl_2$; 0.4µg/mL hydrocortisone; 5µg/mL insulin; 10mg/mL epidermal growth factor (EGF); 10^{-10} M cholera toxin; 2 x 10^{-9} M 3,3',5 triiodo-L-thyronine (T3); 2mM L-glutaminutese; 100U/mL penicillin; 100µg/mL streptomycin
Collagen coat for primary mouse keratinocyte (PMK) culture	0.97X Hanks Balanced Salt Solution (HBSS) 9.70µg/mL Bovine Serum Albuminutes (BSA) 19.40mM 4-(2-hydroxyethyl)-1-piperazineethanesulfonic acid (HEPES) 0.97X Vitrogen-100® Collagen
1X PBS (Phosphate buffered saline) pH7.4	137mM Sodium chloride, NaCl 2.7mM Potassium chloride, KCl 4.3mM Sodium phosphate dibasic, Na_2HPO_4 1.47mM Potassium phosphate monobasic, KH_2PO_4
T-cell medium	Gibco® RPMI medium 1640 (ATCC modification) 10% foetal bovine serum 0.1X 2-mercaptoethanol (ME)

Loading buffer	10% (w/v) Ficoll 400 (Sigma) Orange G Xylene cyanol

Table A2 Buffers and cell culture media

Buffer	Composition
Lysis buffer	2.5% Glycerol 50mM hydroxyethyl piperazineethanesulfonic acid (HEPES) 140mM Sodium chloride, NaCl 0.5% NP40 (Sigma) 0.25% Triton X-100 1mM Ethylenediaminutesetetraacetic acid (EDTA) 0.1X volume of Protease inhibitor cocktail solution (Sigma)
Buffer A	10mM Tris HCl pH8.0 200mM Sodium chloride, NaCl 1mM Ethylenediaminutesetetraacetic acid (EDTA) 0.1X volume of Protease inhibitor cocktail solution (Sigma)
Sonication buffer	10mM hydroxyethyl piperazineethanesulfonic acid (HEPES) 0.5% sodium dodecyl sulphate (SDS) 1mM Ethylenediaminutesetetraacetic acid (EDTA) 0.1X volume of Protease inhibitor cocktail solution (Sigma)
Dilution buffer	13.33mM Tris HCl, pH 8.0 200mM Sodium chloride, NaCl 1.33% Triton X-100 1.33mM Ethylenediaminutesetetraacetic acid (EDTA) 0.1X volume of Protease inhibitor cocktail solution (Sigma)
Wash buffer 1	150mM NaCl 20mM Tris HCl, pH 8.0 2mM Ethylenediaminutesetetraacetic acid (EDTA) 0.1% sodium dodecyl sulphate (SDS) 1% Triton X-100 0.1X volume of Protease inhibitor cocktail solution (Sigma)
Wash buffer 2	500mM NaCl 20mM Tris HCl, pH 8.0 2mM Ethylenediaminutesetetraacetic acid (EDTA) 0.1% sodium dodecyl sulphate (SDS) 1% Triton X-100 0.1X volume of Protease inhibitor cocktail solution (Sigma)
Wash buffer 3	250mM LiCl 10mM Tris HCl, pH 8.0 1mM Ethylenediaminutesetetraacetic acid (EDTA) 0.1% sodium dodecyl sulphate (SDS) 1% NP40
Elution buffer	100mM $NaHCO_3$ 1% SDS

Table A3 CHIP-Seq Solutions

Antigen	Host	Dilution	Manufacturer
ChIP			
H3K4me1	Rabbit	1μg/3-4μg of chromatin	Abcam, Cambridge, UK
H3K27ac	Rabbit	1μg/8-9μg of	Abcam, Cambridge, UK

		chromatin	
Smarca4/BRG1	Rabbit	1µg/2µg of chromatin	Santa Cruz Biotechnology, Santa Cruz, CA, USA
SATB1	Rabbit	1µg/6-7µg of chromatin	Abcam, Cambridge, UK
RAD21	Rabbit	1µg/6-7µg of chromatin	Abcam, Cambridge, UK
H3K27me3	Rabbit	1µg/6-7µg of chromatin	Active Motif, La Hulpe, Belgium
FACS			
FITC-Ly-6A/E (Sca-1)	Rat	1:2500	eBioscience Ltd., Hatfield, UK
APC-CD49f (α6)	Rat	1:2500	eBioscience Ltd., Hatfield, UK

Table A4 Antigen

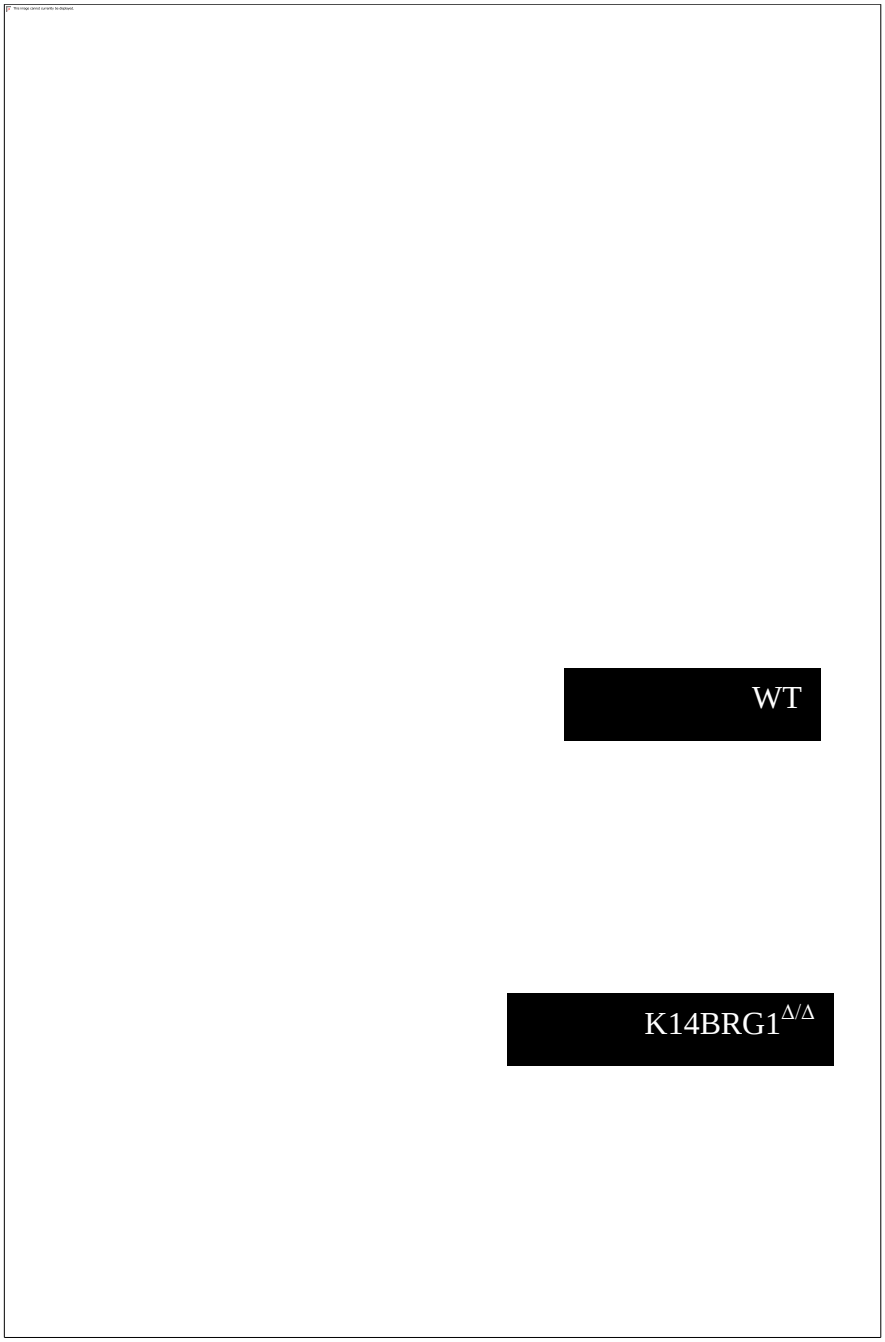

Figure A1 (A) Percentage of proliferating (Ki47 positive) of K14BRG1$^{\Delta/\Delta}$ and wild type (WT) epidermal keratinocytes. (B) Distribution of apoptotic epidermal keratinocytes as marked by terminal deoxynucleotidyl transferase dUTP nick end labeling (TUNEL) in wild type (WT) and K14BRG1$^{\Delta/\Delta}$ E16.5 histological sections.

A.

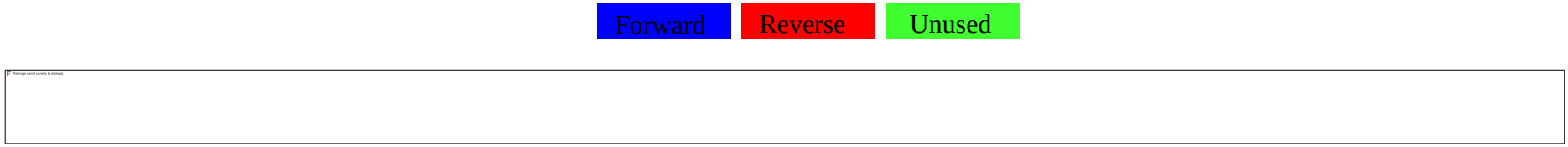

B.

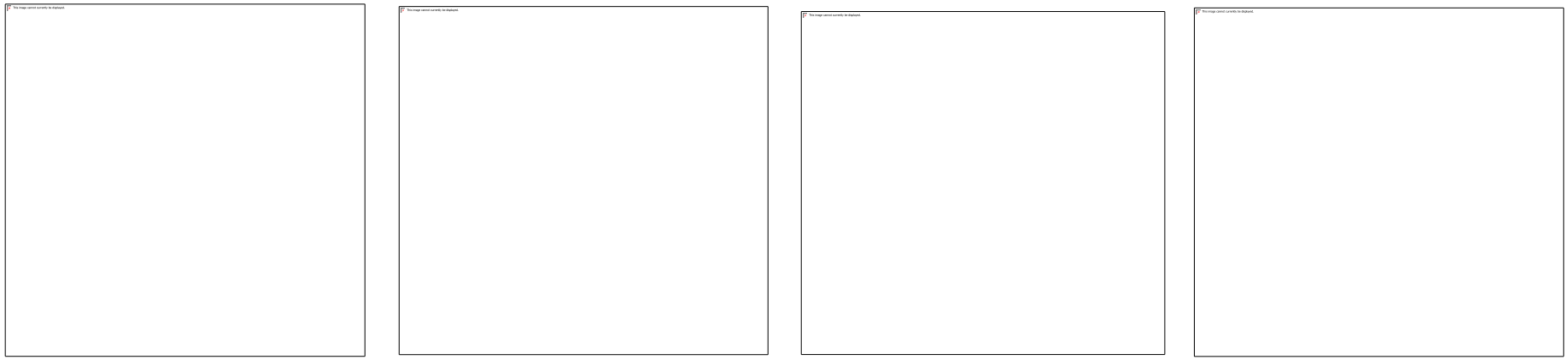

Figure A2 (A) Alternating 5C primer design spanning 89908091 to 95191527bp on murine chromosome 3 (*Mus musculus* assembly mm9/GRC build 37). Figure A2 (B) Raw count 5C pairwise interaction matrixes. KC and TC 5C library replicates. Left = KC replicates 1 and 2; right = TC replicates 1 and 2.

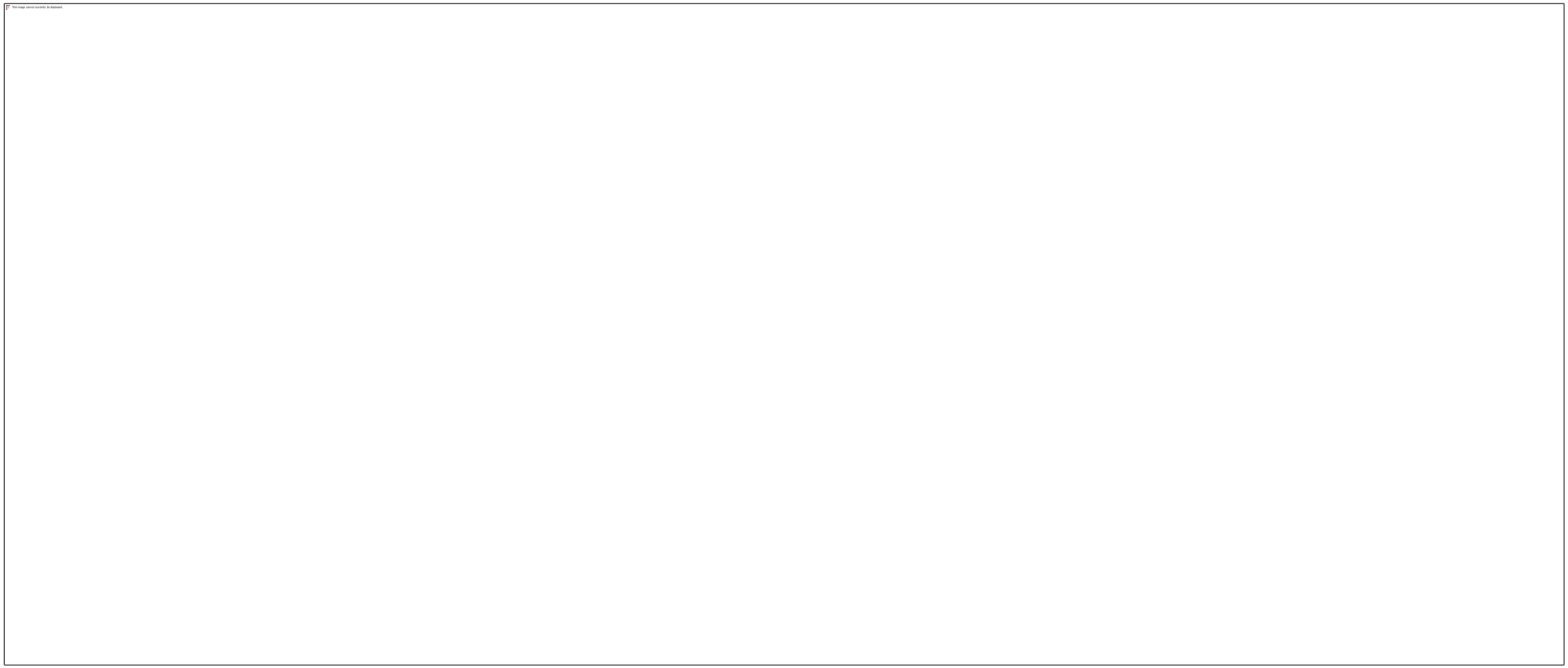

Figure A3 Comparison between 5C and 4C (Prof Vladimir A. Botchkarev and Dr Andrei Mardaryev, unpublished data) interaction counts involving restriction fragments spanning the loricrin gene locus. Green=4C interaction profile. Blue and red= 5C *Lor* anchored interaction profile generated for replicates 1 and 2.

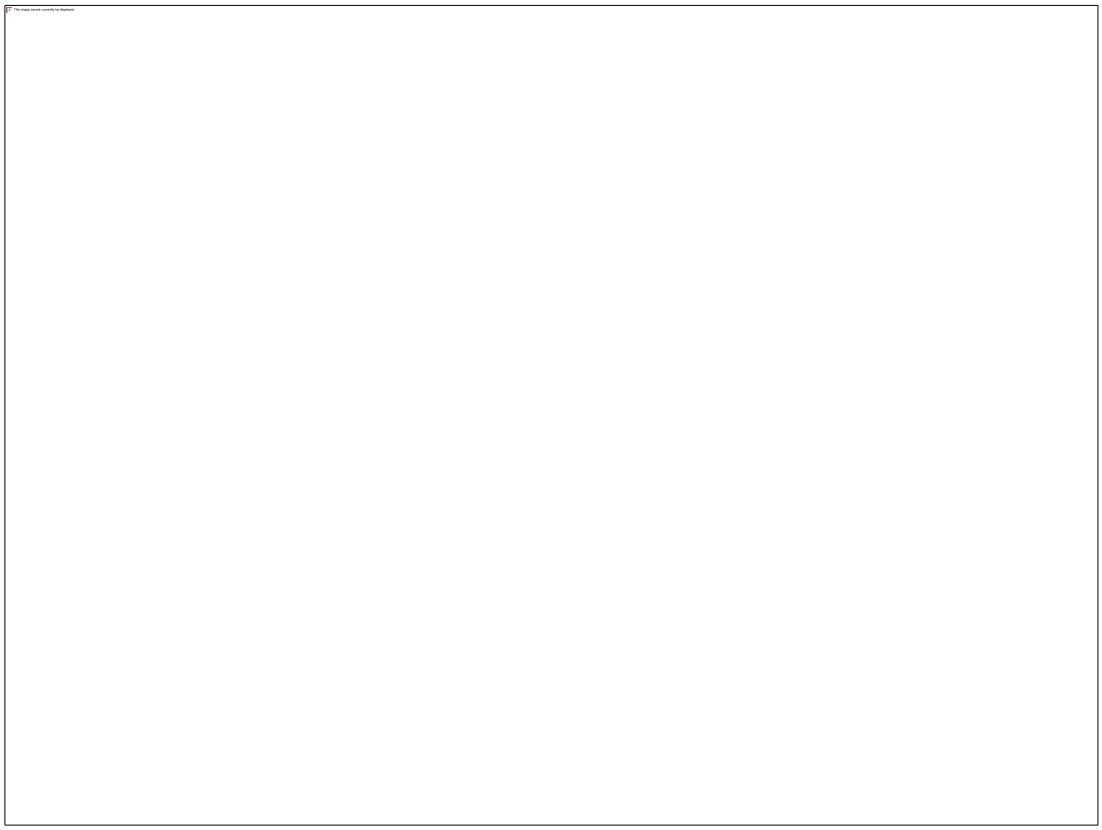

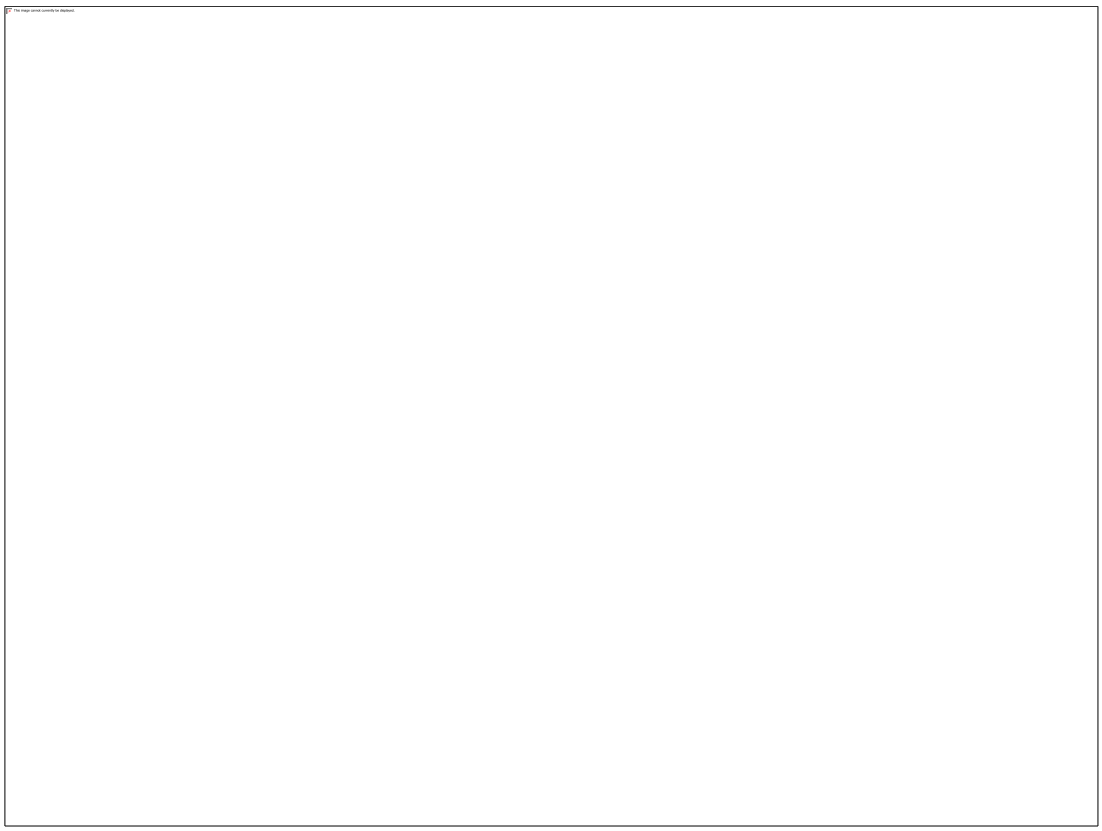

Figure A4 (**A**) Histograms of the relative radial position of *Lor* at E16.5 in K14CreER/BRG1$^{fl/fl}$ (BRG1 ep$^{-\backslash-}$) and control (wild type) basal epidermal keratinocyte

nuclei presented as a percentage of the corresponding average nuclear radius. (**B**) Histograms of the average nuclear radius at E16.5 in K14CreER/BRG1$^{fl/fl}$ (BRG1 ep$^{-\backslash-}$) and control (wild type) basal epidermal keratinocytes. (**C**) Histograms of the inter-locus distance (nm) between *Lor* and *Rps27* in K14CreER/BRG1$^{fl/fl}$ (BRG1 ep$^{-\backslash-}$) and control (wild type) basal epidermal keratinocyte nuclei. (**D**) Histograms of the inter-locus distance between *Lor* and *Rps27* in K14CreER/BRG1$^{fl/fl}$ (BRG1 ep$^{-\backslash-}$) and control (wild type) basal epidermal keratinocyte nuclei presented as a percentage of the corresponding average nuclear radius.

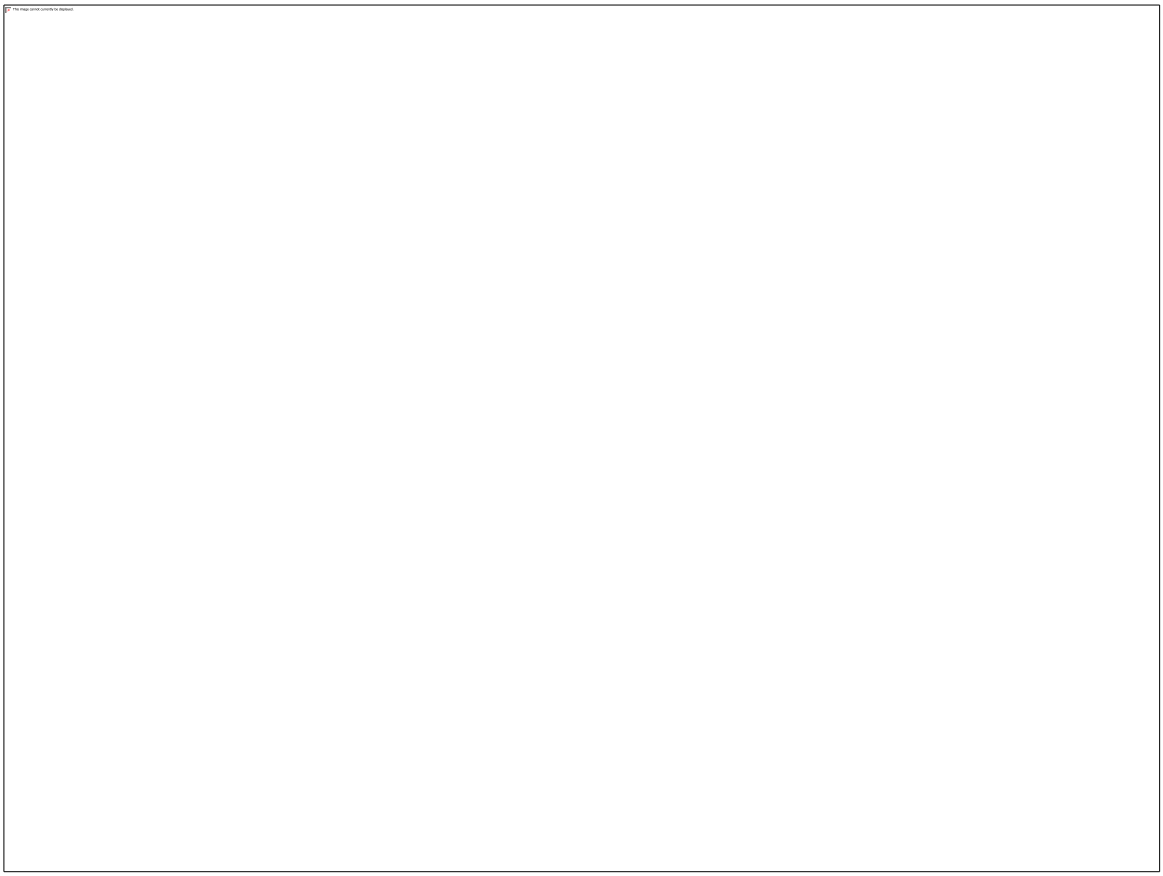

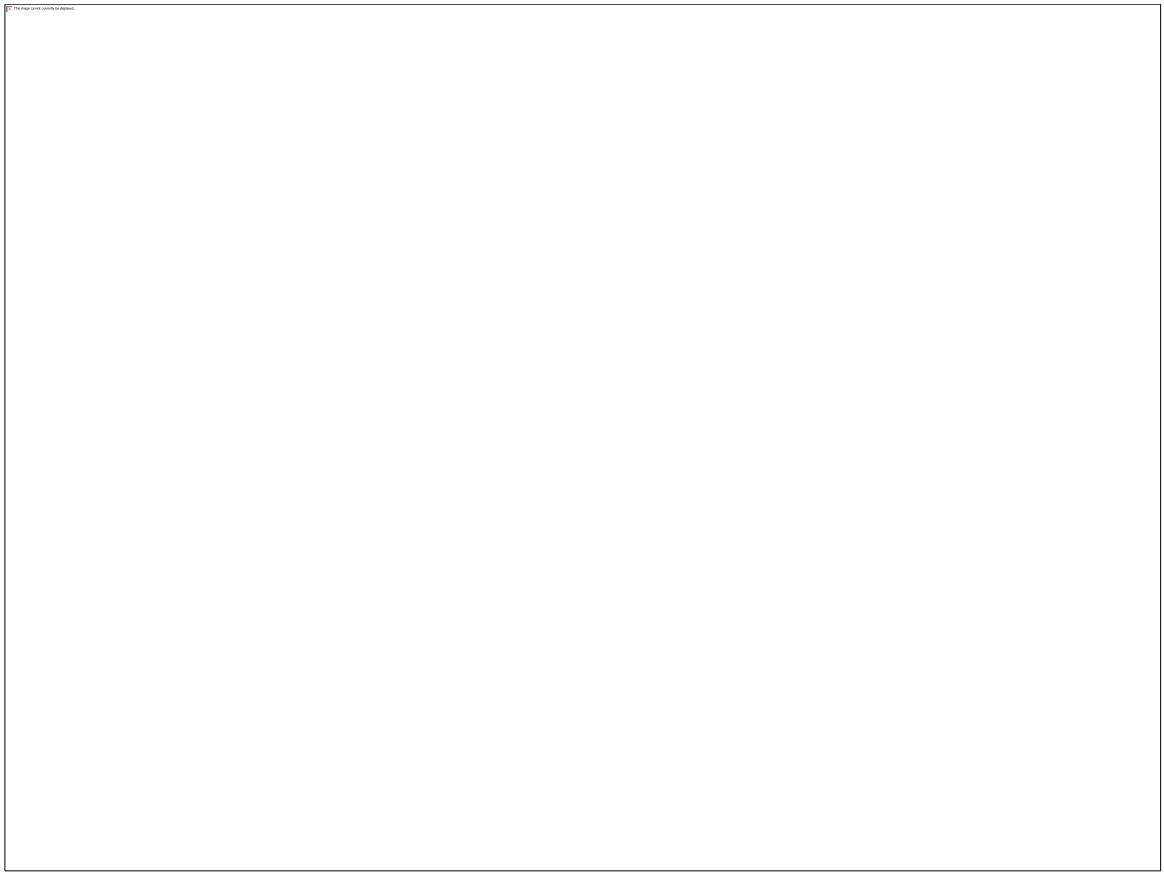

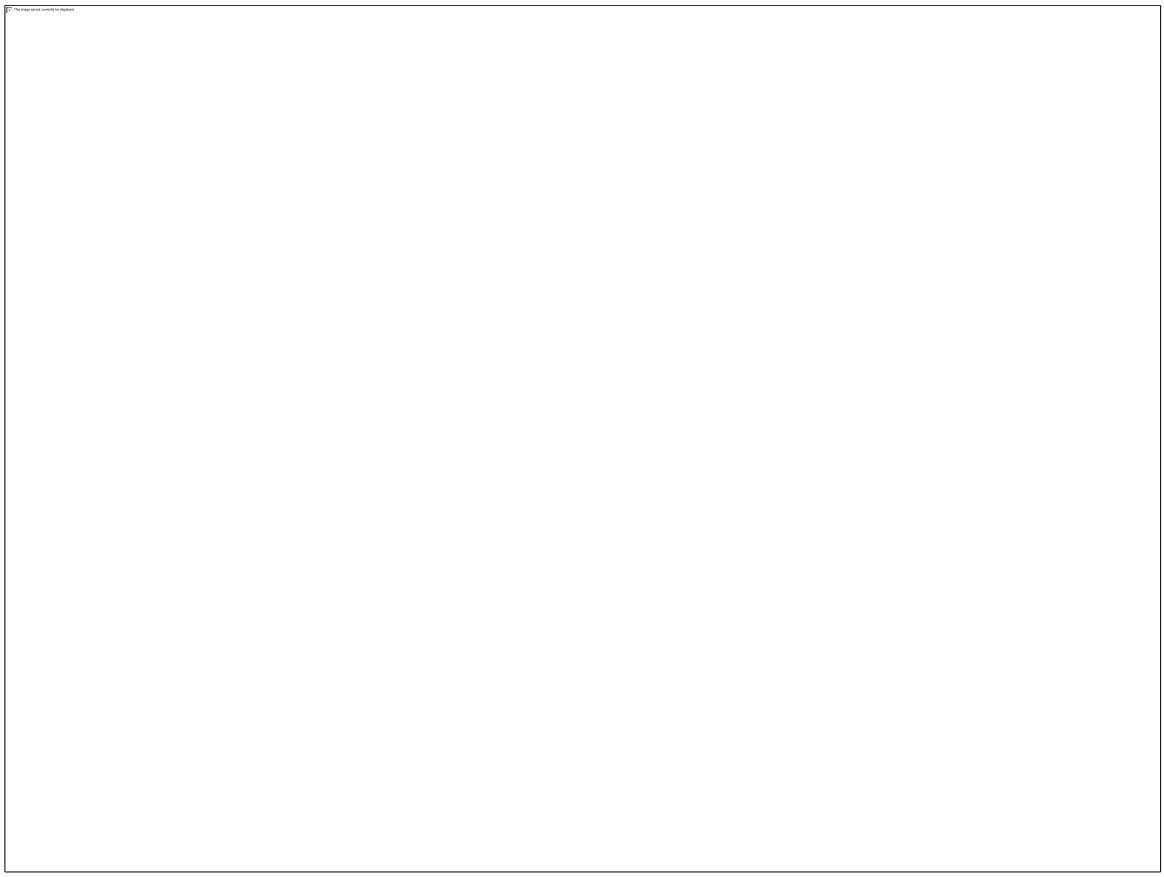

Figure A5 Histograms of the inter-locus distance between A-B (Chr3:91,958,027-92,674,876) and B-C (Crh3:92,674,876- 93,313,755) at the EDC in neonate C57BL/6 freshly isolated normal collagen adherent keratinocytes (KC), C57BL/6basal neonate basal epidermal keratinocytes, and in thymocytes freshly isolated from 8 week old C557BL/6 mice.

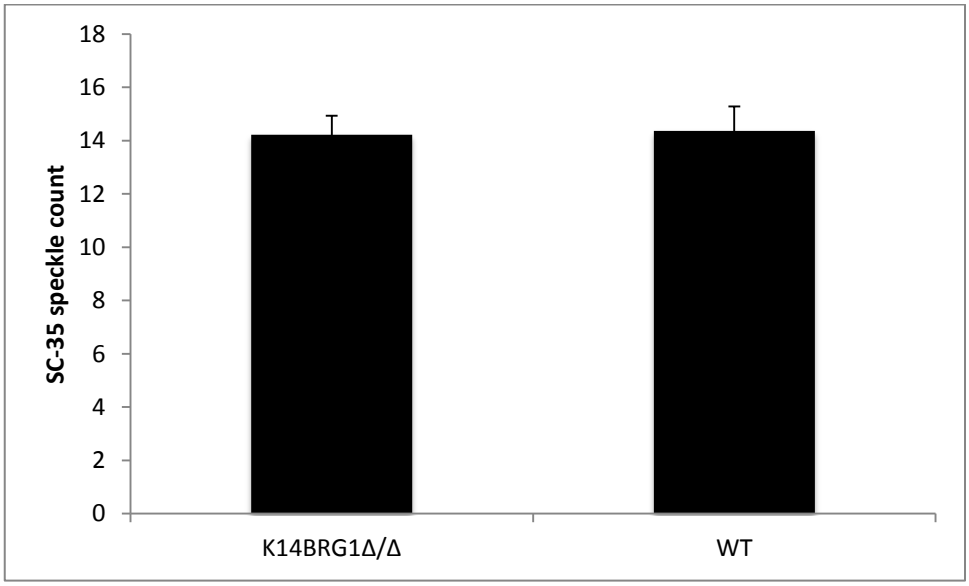

Figure A6 Average count of SC35 nuclear positive speckles detected at the midsection of E16.5 K14BRG$^{\Delta/\Delta}$ and wild type (WT) basal keratinocyte nuclei using immuno-FISH. Error bars show SEM.

References

Adams, J.C., and Watt, F.M. (1989). Fibronectin inhibits the terminal differentiation of human keratinocytes. Nature *340*, 307-309.

Alcamo, E.A., Chirivella, L., Dautzenberg, M., Dobreva, G., Farinas, I., Grosschedl, R., and McConnell, S.K. (2008). SATB2 regulates callosal projection neuron identity in the developing cerebral cortex. Neuron *57*, 364-377.

Alland, L., Muhle, R., Hou, H., Jr., Potes, J., Chin, L., Schreiber-Agus, N., and DePinho, R.A. (1997). Role for N-CoR and histone deacetylase in Sin3-mediated transcriptional repression. Nature *387*, 49-55.

Allis, C.D., Berger, S.L., Cote, J., Dent, S., Jenuwien, T., Kouzarides, T., Pillus, L., Reinberg, D., Shi, Y., Shiekhattar, R., *et al.* (2007). New nomenclature for chromatin-modifying enzymes. Cell *131*, 633-636.

Alvarez, J.D. (2000). The MAR-binding protein SATB1 orchestrates temporal and spatial expression of multiple genes during T-cell development. Genes Dev *14*, 521-535.

Andersen, B., Weinberg, W.C., Rennekampff, O., McEvilly, R.J., Bermingham, J.R., Jr., Hooshmand, F., Vasilyev, V., Hansbrough, J.F., Pittelkow, M.R., Yuspa, S.H., *et al.* (1997). Functions of the POU domain genes Skn-1a/i and Tst-1/Oct-6/SCIP in epidermal differentiation. Genes & development *11*, 1873-1884.

Apostolou, E., and Thanos, D. (2008). Virus Infection Induces NF-kappaB-dependent interchromosomal associations mediating monoallelic IFN-beta gene expression. Cell *134*, 85-96.

Arnold, I., and Watt, F.M. (2001). c-Myc activation in transgenic mouse epidermis results in mobilization of stem cells and differentiation of their progeny. Current biology : CB *11*, 558-568.

Asanoma, K., Kubota, K., Chakraborty, D., Renaud, S.J., Wake, N., Fukushima, K., Soares, M.J., and Rumi, M.A. (2012). SATB homeobox proteins regulate trophoblast stem cell renewal and differentiation. The Journal of biological chemistry *287*, 2257-2268.

Auden, A., Caddy, J., Wilanowski, T., Ting, S.B., Cunningham, J.M., and Jane, S.M. (2006). Spatial and temporal expression of the Grainyhead-like transcription factor family during murine development. Gene expression patterns : GEP *6*, 964-970.

Azuara, V., Perry, P., Sauer, S., Spivakov, M., Jorgensen, H.F., John, R.M., Gouti, M., Casanova, M., Warnes, G., Merkenschlager, M., *et al.* (2006). Chromatin signatures of pluripotent cell lines. Nature cell biology *8*, 532-538.

Baddeley, D., Chagin, V.O., Schermelleh, L., Martin, S., Pombo, A., Carlton, P.M., Gahl, A., Domaing, P., Birk, U., Leonhardt, H., *et al.* (2010). Measurement of replication structures at the nanometer scale using super-resolution light microscopy. Nucleic Acids Res *38*, e8.

Baker, M. (2011). Genomics: Genomes in three dimensions. Nature *470*, 289-294.

Bantignies, F., and Cavalli, G. (2011). Polycomb group proteins: repression in 3D. Trends in genetics : TIG *27*, 454-464.

Bantignies, F., Roure, V., Comet, I., Leblanc, B., Schuettengruber, B., Bonnet, J., Tixier, V., Mas, A., and Cavalli, G. (2011). Polycomb-dependent regulatory contacts between distant Hox loci in Drosophila. Cell *144*, 214-226.

Bao, X., Tang, J., Lopez-Pajares, V., Tao, S., Qu, K., Crabtree, G.R., and Khavari, P.A. (2013). ACTL6a enforces the epidermal progenitor state by suppressing SWI/SNF-dependent induction of KLF4. Cell stem cell *12*, 193-203.

Barski, A., Cuddapah, S., Cui, K., Roh, T.Y., Schones, D.E., Wang, Z., Wei, G., Chepelev, I., and Zhao, K. (2007). High-resolution profiling of histone methylations in the human genome. Cell *129*, 823-837.

Bau, D., Sanyal, A., Lajoie, B.R., Capriotti, E., Byron, M., Lawrence, J.B., Dekker, J., and Marti-Renom, M.A. (2011). The three-dimensional folding of the alpha-globin gene domain reveals formation of chromatin globules. Nature structural & molecular biology *18*, 107-114.

Beretta, C., Chiarelli, A., Testoni, B., Mantovani, R., and Guerrini, L. (2005). Regulation of the cyclin-dependent kinase inhibitor p57Kip2 expression by p63. Cell cycle *4*, 1625-1631.

Bergholz, J., and Xiao, Z.X. (2012). Role of p63 in Development, Tumorigenesis and Cancer Progression. Cancer microenvironment : official journal of the International Cancer Microenvironment Society *5*, 311-322.

Bernstein, B.E., Mikkelsen, T.S., Xie, X., Kamal, M., Huebert, D.J., Cuff, J., Fry, B., Meissner, A., Wernig, M., Plath, K., *et al.* (2006). A bivalent chromatin structure marks key developmental genes in embryonic stem cells. Cell *125*, 315-326.

Bickenbach, J.R., Greer, J.M., Bundman, D.S., Rothnagel, J.A., and Roop, D.R. (1995). Loricrin expression is coordinated with other epidermal proteins and the appearance of lipid lamellar granules in development. J Invest Dermatol *104*, 405-410.

Blanpain, C., Lowry, W.E., Pasolli, H.A., and Fuchs, E. (2006). Canonical notch signaling functions as a commitment switch in the epidermal lineage. Genes & development *20*, 3022-3035.

Blanpain, C., and Simons, B.D. (2013). Unravelling stem cell dynamics by lineage tracing. Nature reviews Molecular cell biology *14*, 489-502.

Bodega, B., Ramirez, G.D., Grasser, F., Cheli, S., Brunelli, S., Mora, M., Meneveri, R., Marozzi, A., Mueller, S., Battaglioli, E., *et al.* (2009). Remodeling of the chromatin structure of the facioscapulohumeral muscular dystrophy (FSHD) locus and upregulation of FSHD-related gene 1 (FRG1) expression during human myogenic differentiation. BMC Biol *7*, 41.

Bolte, S., and Cordelieres, F.P. (2006). A guided tour into subcellular colocalization analysis in light microscopy. Journal of microscopy *224*, 213-232.

Bolzer, A., Kreth, G., Solovei, I., Koehler, D., Saracoglu, K., Fauth, C., Muller, S., Eils, R., Cremer, C., Speicher, M.R., *et al.* (2005). Three-dimensional maps of all chromosomes in human male fibroblast nuclei and prometaphase rosettes. PLoS Biol *3*, e157.

Botchkarev, V.A., Gdula, M.R., Mardaryev, A.N., Sharov, A.A., and Fessing, M.Y. (2012). Epigenetic regulation of gene expression in keratinocytes. The Journal of investigative dermatology *132*, 2505-2521.

Bowcock, A.M., and Cookson, W.O. (2004). The genetics of psoriasis, psoriatic arthritis and atopic dermatitis. Hum Mol Genet *13 Spec No 1*, R43-55.

Boyle, S., Gilchrist, S., Bridger, J.M., Mahy, N.L., Ellis, J.A., and Bickmore, W.A. (2001). The spatial organization of human chromosomes within the nuclei of normal and emerin-mutant cells. Human molecular genetics *10*, 211-219.

Bracken, A.P., Dietrich, N., Pasini, D., Hansen, K.H., and Helin, K. (2006). Genome-wide mapping of Polycomb target genes unravels their roles in cell fate transitions. Genes & development *20*, 1123-1136.

Bradfute, S.B., Graubert, T.A., and Goodell, M.A. (2005). Roles of Sca-1 in hematopoietic stem/progenitor cell function. Experimental hematology *33*, 836-843.

Branco, M.R., and Pombo, A. (2006). Intermingling of chromosome territories in interphase suggests role in translocations and transcription-dependent associations. PLoS Biol *4*, e138.

Bridger, J.M., Boyle, S., Kill, I.R., and Bickmore, W.A. (2000). Re-modelling of nuclear architecture in quiescent and senescent human fibroblasts. Curr Biol *10*, 149-152.

Britanova, O., Akopov, S., Lukyanov, S., Gruss, P., and Tarabykin, V. (2005). Novel transcription factor SATB2 interacts with matrix attachment region DNA elements in a tissue-specific manner and demonstrates cell-type-dependent expression in the developing mouse CNS. The European journal of neuroscience *21*, 658-668.

Britanova, O., de Juan Romero, C., Cheung, A., Kwan, K.Y., Schwark, M., Gyorgy, A., Vogel, T., Akopov, S., Mitkovski, M., Agoston, D., *et al.* (2008). SATB2 is a postmitotic determinant for upper-layer neuron specification in the neocortex. Neuron *57*, 378-392.

Britanova, O., Depew, M.J., Schwark, M., Thomas, B.L., Miletich, I., Sharpe, P., and Tarabykin, V. (2006). SATB2 haploinsufficiency phenocopies 2q32-q33 deletions, whereas loss suggests a fundamental role in the coordination of jaw development. American journal of human genetics *79*, 668-678.

Brown, C.R., Kennedy, C.J., Delmar, V.A., Forbes, D.J., and Silver, P.A. (2008a). Global histone acetylation induces functional genomic reorganization at mammalian nuclear pore complexes. Genes & development *22*, 627-639.

Brown, J.M., Green, J., das Neves, R.P., Wallace, H.A., Smith, A.J., Hughes, J., Gray, N., Taylor, S., Wood, W.G., Higgs, D.R., *et al.* (2008b). Association between active genes occurs at nuclear speckles and is modulated by chromatin environment. The Journal of cell biology *182*, 1083-1097.

Brown, J.M., Leach, J., Reittie, J.E., Atzberger, A., Lee-Prudhoe, J., Wood, W.G., Higgs, D.R., Iborra, F.J., and Buckle, V.J. (2006). Coregulated human globin genes are frequently in spatial proximity when active. The Journal of cell biology *172*, 177-187.

Bultman, S., Gebuhr, T., Yee, D., La Mantia, C., Nicholson, J., Gilliam, A., Randazzo, F., Metzger, D., Chambon, P., Crabtree, G., *et al.* (2000). A BRG1 null mutation in the mouse reveals functional differences among mammalian SWI/SNF complexes. Molecular cell *6*, 1287-1295.

Byrne, C., Tainsky, M., and Fuchs, E. (1994). Programming gene expression in developing epidermis. Development *120*, 2369-2383.

Cai, S., Han, H.J., and Kohwi-Shigematsu, T. (2003). Tissue-specific nuclear architecture and gene expression regulated by SATB1. Nature genetics *34*, 42-51.

Cai, S., Lee, C.C., and Kohwi-Shigematsu, T. (2006). SATB1 packages densely looped, transcriptionally active chromatin for coordinated expression of cytokine genes. Nature genetics *38*, 1278-1288.

Candi, E., Terrinoni, A., Rufini, A., Chikh, A., Lena, A.M., Suzuki, Y., Sayan, B.S., Knight, R.A., and Melino, G. (2006). p63 is upstream of IKK alpha in epidermal development. Journal of cell science *119*, 4617-4622.

Cangkrama, M., Ting, S.B., and Darido, C. (2013). Stem Cells behind the Barrier. International journal of molecular sciences *14*, 13670-13686.

Capelson, M., Liang, Y., Schulte, R., Mair, W., Wagner, U., and Hetzer, M.W. (2010). Chromatin-bound nuclear pore components regulate gene expression in higher eukaryotes. Cell *140*, 372-383.

Casatorres, J., Navarro, J.M., Blessing, M., and Jorcano, J.L. (1994). Analysis of the control of expression and tissue specificity of the keratin 5 gene, characteristic of basal

keratinocytes. Fundamental role of an AP-1 element. The Journal of biological chemistry *269*, 20489-20496.

Chakalova, L., Debrand, E., Mitchell, J.A., Osborne, C.S., and Fraser, P. (2005). Replication and transcription: shaping the landscape of the genome. Nat Rev Genet *6*, 669-677.

Chakalova, L., and Fraser, P. (2010). Organization of transcription. Cold Spring Harb Perspect Biol *2*, a000729.

Chambeyron, S., and Bickmore, W.A. (2004). Chromatin decondensation and nuclear reorganization of the HoxB locus upon induction of transcription. Genes Dev *18*, 1119-1130.

Chambeyron, S., Da Silva, N.R., Lawson, K.A., and Bickmore, W.A. (2005). Nuclear re-organisation of the Hoxb complex during mouse embryonic development. Development *132*, 2215-2223.

Chattopadhyay, S., and Pavithra, L. (2007). MARs and MARBPs: key modulators of gene regulation and disease manifestation. Sub-cellular biochemistry *41*, 213-230.

Chavanas, S., Adoue, V., Mechin, M.C., Ying, S., Dong, S., Duplan, H., Charveron, M., Takahara, H., Serre, G., and Simon, M. (2008). Long-range enhancer associated with chromatin looping allows AP-1 regulation of the peptidylarginine deiminase 3 gene in differentiated keratinocyte. PLoS One *3*, e3408.

Chen, W., Xiao Liu, Z., Oh, J.E., Shin, K.H., Kim, R.H., Jiang, M., Park, N.H., and Kang, M.K. (2012). Grainyhead-like 2 (GRHL2) inhibits keratinocyte differentiation through epigenetic mechanism. Cell death & disease *3*, e450.

Chi, T.H., Wan, M., Lee, P.P., Akashi, K., Metzger, D., Chambon, P., Wilson, C.B., and Crabtree, G.R. (2003). Sequential roles of Brg, the ATPase subunit of BAF chromatin remodeling complexes, in thymocyte development. Immunity *19*, 169-182.

Chiang, M.F., Yang, S.Y., Lin, I.Y., Hong, J.B., Lin, S.J., Ying, H.Y., Chen, C.M., Wu, S.Y., Liu, F.T., and Lin, K.I. (2013). Inducible deletion of the Blimp-1 gene in adult epidermis causes granulocyte-dominated chronic skin inflammation in mice. Proceedings of the National Academy of Sciences of the United States of America *110*, 6476-6481.

Choi, D., Goo, H.G., Yoo, J., and Kang, S. (2011). Identification of RNF2-responding loci in long-range chromatin interactions using the novel 4C-ChIP-Cloning technology. Journal of biotechnology *151*, 312-318.

Christova, R., Jones, T., Wu, P.J., Bolzer, A., Costa-Pereira, A.P., Watling, D., Kerr, I.M., and Sheer, D. (2007). P-STAT1 mediates higher-order chromatin remodelling of the human MHC in response to IFNgamma. Journal of cell science *120*, 3262-3270.

Chuang, C.H., Carpenter, A.E., Fuchsova, B., Johnson, T., de Lanerolle, P., and Belmont, A.S. (2006). Long-range directional movement of an interphase chromosome site. Curr Biol *16*, 825-831.

Connelly, J.T., Gautrot, J.E., Trappmann, B., Tan, D.W., Donati, G., Huck, W.T., and Watt, F.M. (2010). Actin and serum response factor transduce physical cues from the microenvironment to regulate epidermal stem cell fate decisions. Nature cell biology *12*, 711-718.

Connelly, J.T., Mishra, A., Gautrot, J.E., and Watt, F.M. (2011). Shape-induced terminal differentiation of human epidermal stem cells requires p38 and is regulated by histone acetylation. PloS one *6*, e27259.

Contzler, R., Favre, B., Huber, M., and Hohl, D. (2005). Cornulin, a new member of the "fused gene" family, is expressed during epidermal differentiation. The Journal of investigative dermatology *124*, 990-997.

Cook, P.R. (2010). A model for all genomes: the role of transcription factories. J Mol Biol *395*, 1-10.

Cordisco, S., Maurelli, R., Bondanza, S., Stefanini, M., Zambruno, G., Guerra, L., and Dellambra, E. (2010). Bmi-1 reduction plays a key role in physiological and premature aging of primary human keratinocytes. The Journal of investigative dermatology *130*, 1048-1062.

Cork, M.J., Danby, S.G., Vasilopoulos, Y., Hadgraft, J., Lane, M.E., Moustafa, M., Guy, R.H., Macgowan, A.L., Tazi-Ahnini, R., and Ward, S.J. (2009). Epidermal barrier dysfunction in atopic dermatitis. J Invest Dermatol *129*, 1892-1908.

Court, F., Miro, J., Braem, C., Lelay-Taha, M.N., Brisebarre, A., Atger, F., Gostan, T., Weber, M., Cathala, G., and Forne, T. (2011). Modulated contact frequencies at gene-rich loci support a statistical helix model for mammalian chromatin organization. Genome Biol *12*, R42.

Cremer, M., Grasser, F., Lanctot, C., Muller, S., Neusser, M., Zinner, R., Solovei, I., and Cremer, T. (2008). Multicolor 3D fluorescence in situ hybridization for imaging interphase chromosomes. Methods in molecular biology *463*, 205-239.

Cremer, T., and Cremer, M. (2010). Chromosome territories. Cold Spring Harbor perspectives in biology *2*, a003889.

Creyghton, M.P., Cheng, A.W., Welstead, G.G., Kooistra, T., Carey, B.W., Steine, E.J., Hanna, J., Lodato, M.A., Frampton, G.M., Sharp, P.A., *et al.* (2010). Histone H3K27ac separates active from poised enhancers and predicts developmental state. Proceedings of the National Academy of Sciences of the United States of America *107*, 21931-21936.

Crisp, M., Liu, Q., Roux, K., Rattner, J.B., Shanahan, C., Burke, B., Stahl, P.D., and Hodzic, D. (2006). Coupling of the nucleus and cytoplasm: role of the LINC complex. The Journal of cell biology *172*, 41-53.

Croft, J.A., Bridger, J.M., Boyle, S., Perry, P., Teague, P., and Bickmore, W.A. (1999). Differences in the localization and morphology of chromosomes in the human nucleus. The Journal of cell biology *145*, 1119-1131.

Crutchley, J.L., Wang, X.Q., Ferraiuolo, M.A., and Dostie, J. (2010). Chromatin conformation signatures: ideal human disease biomarkers? Biomark Med *4*, 611-629.

Cseresnyes, Z., Schwarz, U., and Green, C.M. (2009). Analysis of replication factories in human cells by super-resolution light microscopy. BMC Cell Biol *10*, 88.

Cui, K., Zang, C., Roh, T.Y., Schones, D.E., Childs, R.W., Peng, W., and Zhao, K. (2009). Chromatin signatures in multipotent human hematopoietic stem cells indicate the fate of bivalent genes during differentiation. Cell stem cell *4*, 80-93.

Dai, X., and Segre, J.A. (2004). Transcriptional control of epidermal specification and differentiation. Current opinion in genetics & development *14*, 485-491.

de Guzman Strong, C., Conlan, S., Deming, C.B., Cheng, J., Sears, K.E., and Segre, J.A. (2010). A milieu of regulatory elements in the epidermal differentiation complex syntenic block: implications for atopic dermatitis and psoriasis. Human molecular genetics *19*, 1453-1460.

De, S., Wurster, A.L., Precht, P., Wood, W.H., 3rd, Becker, K.G., and Pazin, M.J. (2011). Dynamic BRG1 recruitment during T helper differentiation and activation reveals distal regulatory elements. Molecular and cellular biology *31*, 1512-1527.

de Wit, E., and de Laat, W. (2012). A decade of 3C technologies: insights into nuclear organization. Genes & development *26*, 11-24.

Dekker, J., Marti-Renom, M.A., and Mirny, L.A. (2013). Exploring the three-dimensional organization of genomes: interpreting chromatin interaction data. Nature reviews Genetics *14*, 390-403.

Dekker, J., Rippe, K., Dekker, M., and Kleckner, N. (2002). Capturing chromosome conformation. Science *295*, 1306-1311.

Deng, W., Lee, J., Wang, H., Miller, J., Reik, A., Gregory, P.D., Dean, A., and Blobel, G.A. (2012). Controlling long-range genomic interactions at a native locus by targeted tethering of a looping factor. Cell *149*, 1233-1244.

Deng, W., Tsao, S.W., Lucas, J.N., Leung, C.S., and Cheung, A.L. (2003). A new method for improving metaphase chromosome spreading. Cytometry Part A : the journal of the International Society for Analytical Cytology *51*, 46-51.

Deniaud, E., and Bickmore, W.A. (2009). Transcription and the nuclear periphery: edge of darkness? Current opinion in genetics & development *19*, 187-191.

Denning, M.F., Dlugosz, A.A., Cheng, C., Dempsey, P.J., Coffey, R.J., Jr., Threadgill, D.W., Magnuson, T., and Yuspa, S.H. (2000). Cross-talk between epidermal growth factor receptor and protein kinase C during calcium-induced differentiation of keratinocytes. Experimental dermatology *9*, 192-199.

Di Costanzo, A., Festa, L., Duverger, O., Vivo, M., Guerrini, L., La Mantia, G., Morasso, M.I., and Calabro, V. (2009). Homeodomain protein Dlx3 induces phosphorylation-dependent p63 degradation. Cell cycle *8*, 1185-1195.

Diaz-Martinez, L.A., Gimenez-Abian, J.F., and Clarke, D.J. (2008). Chromosome cohesion - rings, knots, orcs and fellowship. Journal of cell science *121*, 2107-2114.

Dingwall, C., and Laskey, R. (1992). The nuclear membrane. Science *258*, 942-947.

DiSepio, D., Jones, A., Longley, M.A., Bundman, D., Rothnagel, J.A., and Roop, D.R. (1995). The proximal promoter of the mouse loricrin gene contains a functional AP-1 element and directs keratinocyte-specific but not differentiation-specific expression. The Journal of biological chemistry *270*, 10792-10799.

Dixon, J.R., Selvaraj, S., Yue, F., Kim, A., Li, Y., Shen, Y., Hu, M., Liu, J.S., and Ren, B. (2012). Topological domains in mammalian genomes identified by analysis of chromatin interactions. Nature *485*, 376-380.

Dobreva, G., Chahrour, M., Dautzenberg, M., Chirivella, L., Kanzler, B., Farinas, I., Karsenty, G., and Grosschedl, R. (2006). SATB2 is a multifunctional determinant of craniofacial patterning and osteoblast differentiation. Cell *125*, 971-986.

Dobreva, G., Dambacher, J., and Grosschedl, R. (2003). SUMO modification of a novel MAR-binding protein, SATB2, modulates immunoglobulin mu gene expression. Genes & development *17*, 3048-3061.

Dorigo, B., Schalch, T., Kulangara, A., Duda, S., Schroeder, R.R., and Richmond, T.J. (2004). Nucleosome arrays reveal the two-start organization of the chromatin fiber. Science *306*, 1571-1573.

Dostie, J., and Dekker, J. (2007). Mapping networks of physical interactions between genomic elements using 5C technology. Nature protocols *2*, 988-1002.

Driskell, I., Oda, H., Blanco, S., Nascimento, E., Humphreys, P., and Frye, M. (2012). The histone methyltransferase Setd8 acts in concert with c-Myc and is required to maintain skin. The EMBO journal *31*, 616-629.

Drissen, R., Palstra, R.J., Gillemans, N., Splinter, E., Grosveld, F., Philipsen, S., and de Laat, W. (2004). The active spatial organization of the beta-globin locus requires the transcription factor EKLF. Genes Dev *18*, 2485-2490.

Eckert, R.L., Adhikary, G., Rorke, E.A., Chew, Y.C., and Balasubramanian, S. (2011). Polycomb group proteins are key regulators of keratinocyte function. J Invest Dermatol *131*, 295-301.

Eckert, R.L., Crish, J.F., Efimova, T., Dashti, S.R., Deucher, A., Bone, F., Adhikary, G., Huang, G., Gopalakrishnan, R., and Balasubramanian, S. (2004). Regulation of involucrin gene expression. The Journal of investigative dermatology *123*, 13-22.

Efimova, T., LaCelle, P., Welter, J.F., and Eckert, R.L. (1998). Regulation of human involucrin promoter activity by a protein kinase C, Ras, MEKK1, MEK3, p38/RK, AP1 signal transduction pathway. The Journal of biological chemistry *273*, 24387-24395.

Egecioglu, D., and Brickner, J.H. (2011). Gene positioning and expression. Current opinion in cell biology *23*, 338-345.

Elder, J.T., and Zhao, X. (2002). Evidence for local control of gene expression in the epidermal differentiation complex. Experimental dermatology *11*, 406-412.

Euskirchen, G.M., Auerbach, R.K., Davidov, E., Gianoulis, T.A., Zhong, G., Rozowsky, J., Bhardwaj, N., Gerstein, M.B., and Snyder, M. (2011). Diverse roles and interactions of the SWI/SNF chromatin remodeling complex revealed using global approaches. PLoS genetics *7*, e1002008.

Ezhkova, E., Lien, W.H., Stokes, N., Pasolli, H.A., Silva, J.M., and Fuchs, E. (2011). EZH1 and EZH2 cogovern histone H3K27 trimethylation and are essential for hair follicle homeostasis and wound repair. Genes & development *25*, 485-498.

Ezhkova, E., Pasolli, H.A., Parker, J.S., Stokes, N., Su, I.H., Hannon, G., Tarakhovsky, A., and Fuchs, E. (2009). EZH2 orchestrates gene expression for the stepwise differentiation of tissue-specific stem cells. Cell *136*, 1122-1135.

Faus, I., Hsu, H.J., and Fuchs, E. (1994). Oct-6: a regulator of keratinocyte gene expression in stratified squamous epithelia. Molecular and cellular biology *14*, 3263-3275.

Feng, J., Liu, T., Qin, B., Zhang, Y., and Liu, X.S. (2012). Identifying ChIP-seq enrichment using MACS. Nature protocols *7*, 1728-1740.

Ferone, G., Mollo, M.R., Thomason, H.A., Antonini, D., Zhou, H., Ambrosio, R., De Rosa, L., Salvatore, D., Getsios, S., van Bokhoven, H., *et al.* (2013). p63 control of desmosome gene expression and adhesion is compromised in AEC syndrome. Human molecular genetics *22*, 531-543.

Ferrai, C., de Castro, I.J., Lavitas, L., Chotalia, M., and Pombo, A. (2010). Gene positioning. Cold Spring Harbor perspectives in biology *2*, a000588.

Fessing, M.Y., Mardaryev, A.N., Gdula, M.R., Sharov, A.A., Sharova, T.Y., Rapisarda, V., Gordon, K.B., Smorodchenko, A.D., Poterlowicz, K., Ferone, G., *et al.* (2011). p63 regulates SATB1 to control tissue-specific chromatin remodeling during development of the epidermis. The Journal of cell biology *194*, 825-839.

Fischle, W., Wang, Y., and Allis, C.D. (2003). Histone and chromatin cross-talk. Curr Opin Cell Biol *15*, 172-183.

Frank, S.R., Schroeder, M., Fernandez, P., Taubert, S., and Amati, B. (2001). Binding of c-Myc to chromatin mediates mitogen-induced acetylation of histone H4 and gene activation. Genes & development *15*, 2069-2082.

Fraser, P., and Bickmore, W. (2007). Nuclear organization of the genome and the potential for gene regulation. Nature *447*, 413-417.

Frye, M., Fisher, A.G., and Watt, F.M. (2007). Epidermal stem cells are defined by global histone modifications that are altered by Myc-induced differentiation. PloS one *2*, e763.

Frye, M., Gardner, C., Li, E.R., Arnold, I., and Watt, F.M. (2003). Evidence that Myc activation depletes the epidermal stem cell compartment by modulating adhesive interactions with the local microenvironment. Development *130*, 2793-2808.

Frye, M., and Watt, F.M. (2006). The RNA methyltransferase Misu (NSun2) mediates Myc-induced proliferation and is upregulated in tumors. Current biology : CB *16*, 971-981.

Fuchs, E. (2007). Scratching the surface of skin development. Nature *445*, 834-842.

Fuchs, E., and Raghavan, S. (2002). Getting under the skin of epidermal morphogenesis. Nature reviews Genetics *3*, 199-209.

Fullwood, M.J., Liu, M.H., Pan, Y.F., Liu, J., Xu, H., Mohamed, Y.B., Orlov, Y.L., Velkov, S., Ho, A., Mei, P.H., *et al.* (2009). An oestrogen-receptor-alpha-bound human chromatin interactome. Nature *462*, 58-64.

Galande, S., Purbey, P.K., Notani, D., and Kumar, P.P. (2007). The third dimension of gene regulation: organization of dynamic chromatin loopscape by SATB1. Curr Opin Genet Dev *17*, 408-414.

Gdula, M.R., Poterlowicz, K., Mardaryev, A.N., Sharov, A.A., Peng, Y., Fessing, M.Y., and Botchkarev, V.A. (2013). Remodeling of three-dimensional organization of the nucleus during terminal keratinocyte differentiation in the epidermis. The Journal of investigative dermatology *133*, 2191-2201.

Geng, S., Mezentsev, A., Kalachikov, S., Raith, K., Roop, D.R., and Panteleyev, A.A. (2006). Targeted ablation of Arnt in mouse epidermis results in profound defects in desquamation and epidermal barrier function. Journal of cell science *119*, 4901-4912.

Ghamari, A., van de Corput, M.P., Thongjuea, S., van Cappellen, W.A., van Ijcken, W., van Haren, J., Soler, E., Eick, D., Lenhard, B., and Grosveld, F.G. (2013). In vivo live imaging of RNA polymerase II transcription factories in primary cells. Genes & development *27*, 767-777.

Gibcus, J.H., and Dekker, J. (2013). The hierarchy of the 3D genome. Molecular cell *49*, 773-782.

Gilfillan, G.D., Hughes, T., Sheng, Y., Hjorthaug, H.S., Straub, T., Gervin, K., Harris, J.R., Undlien, D.E., and Lyle, R. (2012). Limitations and possibilities of low cell number ChIP-seq. BMC genomics *13*, 645.

Goldman, R.D., Gruenbaum, Y., Moir, R.D., Shumaker, D.K., and Spann, T.P. (2002). Nuclear lamins: building blocks of nuclear architecture. Genes & development *16*, 533-547.

Gondor, A. (2013). Dynamic chromatin loops bridge health and disease in the nuclear landscape. Seminars in cancer biology *23*, 90-98.

Greer, E.L., and Shi, Y. (2012). Histone methylation: a dynamic mark in health, disease and inheritance. Nat Rev Genet.

Griffin, C.T., Brennan, J., and Magnuson, T. (2008). The chromatin-remodeling enzyme BRG1 plays an essential role in primitive erythropoiesis and vascular development. Development *135*, 493-500.

Grigoryev, S.A., Arya, G., Correll, S., Woodcock, C.L., and Schlick, T. (2009). Evidence for heteromorphic chromatin fibers from analysis of nucleosome interactions. Proc Natl Acad Sci U S A *106*, 13317-13322.

Guelen, L., Pagie, L., Brasset, E., Meuleman, W., Faza, M.B., Talhout, W., Eussen, B.H., de Klein, A., Wessels, L., de Laat, W., *et al.* (2008). Domain organization of human chromosomes revealed by mapping of nuclear lamina interactions. Nature *453*, 948-951.

Gyorgy, A.B., Szemes, M., de Juan Romero, C., Tarabykin, V., and Agoston, D.V. (2008). SATB2 interacts with chromatin-remodeling molecules in differentiating cortical neurons. The European journal of neuroscience *27*, 865-873.

Hall, L.L., Smith, K.P., Byron, M., and Lawrence, J.B. (2006). Molecular anatomy of a speckle. The anatomical record Part A, Discoveries in molecular, cellular, and evolutionary biology *288*, 664-675.

Han, H.J., Russo, J., Kohwi, Y., and Kohwi-Shigematsu, T. (2008). SATB1 reprogrammes gene expression to promote breast tumour growth and metastasis. Nature *452*, 187-193.

Hardman, M.J., Sisi, P., Banbury, D.N., and Byrne, C. (1998). Patterned acquisition of skin barrier function during development. Development *125*, 1541-1552.

Hargreaves, D.C., and Crabtree, G.R. (2011). ATP-dependent chromatin remodeling: genetics, genomics and mechanisms. Cell research *21*, 396-420.

Harmon, B., and Sedat, J. (2005). Cell-by-Cell Dissection of Gene Expression and Chromosomal Interactions Reveals Consequences of Nuclear Reorganization. PLoS Biol *3*, e67.

Harmston, N., and Lenhard, B. (2013). Chromatin and epigenetic features of long-range gene regulation. Nucleic acids research *41*, 7185-7199.

Heintzman, N.D., Stuart, R.K., Hon, G., Fu, Y., Ching, C.W., Hawkins, R.D., Barrera, L.O., Van Calcar, S., Qu, C., Ching, K.A., *et al.* (2007). Distinct and predictive chromatin signatures of transcriptional promoters and enhancers in the human genome. Nature genetics *39*, 311-318.

Heng, H.H., Goetze, S., Ye, C.J., Liu, G., Stevens, J.B., Bremer, S.W., Wykes, S.M., Bode, J., and Krawetz, S.A. (2004). Chromatin loops are selectively anchored using scaffold/matrix-attachment regions. Journal of cell science *117*, 999-1008.

Hewitt, S.L., High, F.A., Reiner, S.L., Fisher, A.G., and Merkenschlager, M. (2004). Nuclear repositioning marks the selective exclusion of lineage-inappropriate transcription factor loci during T helper cell differentiation. Eur J Immunol *34*, 3604-3613.

Ho, L., Ronan, J.L., Wu, J., Staahl, B.T., Chen, L., Kuo, A., Lessard, J., Nesvizhskii, A.I., Ranish, J., and Crabtree, G.R. (2009). An embryonic stem cell chromatin remodeling complex, esBAF, is essential for embryonic stem cell self-renewal and pluripotency. Proceedings of the National Academy of Sciences of the United States of America *106*, 5181-5186.

Hodgson, J.W., and Brock, H.W. (2011). Are polycomb group bodies gene silencing factories? Cell *144*, 170-171.

Hoffjan, S., and Stemmler, S. (2007). On the role of the epidermal differentiation complex in ichthyosis vulgaris, atopic dermatitis and psoriasis. Br J Dermatol *157*, 441-449.

Hopkin, A.S., Gordon, W., Klein, R.H., Espitia, F., Daily, K., Zeller, M., Baldi, P., and Andersen, B. (2012). GRHL3/GET1 and trithorax group members collaborate to activate the epidermal progenitor differentiation program. PLoS genetics *8*, e1002829.

Horike, S., Cai, S., Miyano, M., Cheng, J.F., and Kohwi-Shigematsu, T. (2005). Loss of silent-chromatin looping and impaired imprinting of DLX5 in Rett syndrome. Nat Genet *37*, 31-40.

Hu, Q., Kwon, Y.S., Nunez, E., Cardamone, M.D., Hutt, K.R., Ohgi, K.A., Garcia-Bassets, I., Rose, D.W., Glass, C.K., Rosenfeld, M.G., *et al.* (2008). Enhancing nuclear receptor-induced transcription requires nuclear motor and LSD1-dependent gene networking in interchromatin granules. Proceedings of the National Academy of Sciences of the United States of America *105*, 19199-19204.

Hu, Y., Baud, V., Delhase, M., Zhang, P., Deerinck, T., Ellisman, M., Johnson, R., and Karin, M. (1999). Abnormal morphogenesis but intact IKK activation in mice lacking the IKKalpha subunit of IkappaB kinase. Science *284*, 316-320.

Hu, Y., Baud, V., Oga, T., Kim, K.I., Yoshida, K., and Karin, M. (2001). IKKalpha controls formation of the epidermis independently of NF-kappaB. Nature *410*, 710-714.

Huber, M., Siegenthaler, G., Mirancea, N., Marenholz, I., Nizetic, D., Breitkreutz, D., Mischke, D., and Hohl, D. (2005). Isolation and characterization of human repetin, a member of the fused gene family of the epidermal differentiation complex. The Journal of investigative dermatology *124*, 998-1007.

Iborra, F.J., Pombo, A., Jackson, D.A., and Cook, P.R. (1996). Active RNA polymerases are localized within discrete transcription "factories' in human nuclei. J Cell Sci *109 (Pt 6)*, 1427-1436.

Ihrie, R.A., Bronson, R.T., and Attardi, L.D. (2006). Adult mice lacking the p53/p63 target gene Perp are not predisposed to spontaneous tumorigenesis but display features of ectodermal dysplasia syndromes. Cell death and differentiation *13*, 1614-1618.

Ihrie, R.A., Marques, M.R., Nguyen, B.T., Horner, J.S., Papazoglu, C., Bronson, R.T., Mills, A.A., and Attardi, L.D. (2005). Perp is a p63-regulated gene essential for epithelial integrity. Cell *120*, 843-856.

Imakaev, M., Fudenberg, G., McCord, R.P., Naumova, N., Goloborodko, A., Lajoie, B.R., Dekker, J., and Mirny, L.A. (2012). Iterative correction of Hi-C data reveals hallmarks of chromosome organization. Nature methods *9*, 999-1003.

Indra, A.K., Dupe, V., Bornert, J.M., Messaddeq, N., Yaniv, M., Mark, M., Chambon, P., and Metzger, D. (2005). Temporally controlled targeted somatic mutagenesis in embryonic surface ectoderm and fetal epidermal keratinocytes unveils two distinct developmental functions of BRG1 in limb morphogenesis and skin barrier formation. Development *132*, 4533-4544.

Ito, C.Y., Li, C.Y., Bernstein, A., Dick, J.E., and Stanford, W.L. (2003). Hematopoietic stem cell and progenitor defects in Sca-1/Ly-6A-null mice. Blood *101*, 517-523.

Jackson, B., Tilli, C.M., Hardman, M.J., Avilion, A.A., MacLeod, M.C., Ashcroft, G.S., and Byrne, C. (2005). Late cornified envelope family in differentiating epithelia--response to calcium and ultraviolet irradiation. J Invest Dermatol *124*, 1062-1070.

Jang, S.I., Karaman-Jurukovska, N., Morasso, M.I., Steinert, P.M., and Markova, N.G. (2000). Complex interactions between epidermal POU domain and activator protein 1

transcription factors regulate the expression of the profilaggrin gene in normal human epidermal keratinocytes. The Journal of biological chemistry *275*, 15295-15304.

Jang, S.I., Steinert, P.M., and Markova, N.G. (1996). Activator protein 1 activity is involved in the regulation of the cell type-specific expression from the proximal promoter of the human profilaggrin gene. The Journal of biological chemistry *271*, 24105-24114.

Jensen, U.B., Yan, X., Triel, C., Woo, S.H., Christensen, R., and Owens, D.M. (2008). A distinct population of clonogenic and multipotent murine follicular keratinocytes residing in the upper isthmus. Journal of cell science *121*, 609-617.

Jing, H., Vakoc, C.R., Ying, L., Mandat, S., Wang, H., Zheng, X., and Blobel, G.A. (2008). Exchange of GATA factors mediates transitions in looped chromatin organization at a developmentally regulated gene locus. Mol Cell *29*, 232-242.

Kagey, M.H., Newman, J.J., Bilodeau, S., Zhan, Y., Orlando, D.A., van Berkum, N.L., Ebmeier, C.C., Goossens, J., Rahl, P.B., Levine, S.S., *et al.* (2010). Mediator and cohesin connect gene expression and chromatin architecture. Nature *467*, 430-435.

Karasek, J., Smetana, K., Hrdlicka, A., Dubinin, I., Hornak, O., and Ohelert, W. (1972). Nuclear and nucleolar ultrastructure during the late stages of normal human keratinocyte maturation. The British journal of dermatology *86*, 601-607.

Kashiwagi, M., Morgan, B.A., and Georgopoulos, K. (2007). The chromatin remodeler Mi-2beta is required for establishment of the basal epidermis and normal differentiation of its progeny. Development *134*, 1571-1582.

Kelsell, D.P., and Byrne, C. (2011). SNPing at the Epidermal Barrier. J Invest Dermatol *131*, 1593-1595.

Kim, D., Pertea, G., Trapnell, C., Pimentel, H., Kelley, R., and Salzberg, S.L. (2013). TopHat2: accurate alignment of transcriptomes in the presence of insertions, deletions and gene fusions. Genome biology *14*, R36.

Kim, S.I., Bresnick, E.H., and Bultman, S.J. (2009a). BRG1 directly regulates nucleosome structure and chromatin looping of the alpha globin locus to activate transcription. Nucleic acids research *37*, 6019-6027.

Kim, S.I., Bultman, S.J., Kiefer, C.M., Dean, A., and Bresnick, E.H. (2009b). BRG1 requirement for long-range interaction of a locus control region with a downstream promoter. Proceedings of the National Academy of Sciences of the United States of America *106*, 2259-2264.

Kim, T.H., Abdullaev, Z.K., Smith, A.D., Ching, K.A., Loukinov, D.I., Green, R.D., Zhang, M.Q., Lobanenkov, V.V., and Ren, B. (2007). Analysis of the vertebrate insulator protein CTCF-binding sites in the human genome. Cell *128*, 1231-1245.

Kind, J., and van Steensel, B. (2010). Genome-nuclear lamina interactions and gene regulation. Curr Opin Cell Biol *22*, 320-325.

King, K.E., Ponnamperuma, R.M., Yamashita, T., Tokino, T., Lee, L.A., Young, M.F., and Weinberg, W.C. (2003). deltaNp63alpha functions as both a positive and a negative transcriptional regulator and blocks *in vitro* differentiation of murine keratinocytes. Oncogene *22*, 3635-3644.

Klose, R.J., Yan, Q., Tothova, Z., Yamane, K., Erdjument-Bromage, H., Tempst, P., Gilliland, D.G., Zhang, Y., and Kaelin, W.G., Jr. (2007). The retinoblastoma binding protein RBP2 is an H3K4 demethylase. Cell *128*, 889-900.

Koressaar, T., and Remm, M. (2007). Enhancements and modifications of primer design program Primer3. Bioinformatics *23*, 1289-1291.

Kornberg, R.D. (1977). Structure of chromatin. Annu Rev Biochem *46*, 931-954.

Kosak, S.T., Skok, J.A., Medina, K.L., Riblet, R., Le Beau, M.M., Fisher, A.G., and Singh, H. (2002). Subnuclear compartmentalization of immunoglobulin loci during lymphocyte development. Science *296*, 158-162.

Koster, M.I., Kim, S., Huang, J., Williams, T., and Roop, D.R. (2006). TAp63alpha induces AP-2gamma as an early event in epidermal morphogenesis. Developmental biology *289*, 253-261.

Koster, M.I., Kim, S., Mills, A.A., DeMayo, F.J., and Roop, D.R. (2004). p63 is the molecular switch for initiation of an epithelial stratification program. Genes & development *18*, 126-131.

Koster, M.I., and Roop, D.R. (2007). Mechanisms regulating epithelial stratification. Annual review of cell and developmental biology *23*, 93-113.

Kouwenhoven, E.N., van Heeringen, S.J., Tena, J.J., Oti, M., Dutilh, B.E., Alonso, M.E., de la Calle-Mustienes, E., Smeenk, L., Rinne, T., Parsaulian, L., *et al.* (2010). Genome-wide profiling of p63 DNA-binding sites identifies an element that regulates gene expression during limb development in the 7q21 SHFM1 locus. PLoS genetics *6*, e1001065.

Kumar, P.P., Bischof, O., Purbey, P.K., Notani, D., Urlaub, H., Dejean, A., and Galande, S. (2007). Functional interaction between PML and SATB1 regulates chromatin-loop architecture and transcription of the MHC class I locus. Nature cell biology *9*, 45-56.

Kumaran, R.I., Thakar, R., and Spector, D.L. (2008). Chromatin dynamics and gene positioning. Cell *132*, 929-934.

Kypriotou, M., Huber, M., and Hohl, D. (2012). The human epidermal differentiation complex: cornified envelope precursors, S100 proteins and the 'fused genes' family. Experimental dermatology *21*, 643-649.

Lajoie, B.R., van Berkum, N.L., Sanyal, A., and Dekker, J. (2009). My5C: web tools for chromosome conformation capture studies. Nat Methods *6*, 690-691.

Lallemand-Breitenbach, V., and de The, H. (2010). PML nuclear bodies. Cold Spring Harbor perspectives in biology *2*, a000661.

Lan, X., Witt, H., Katsumura, K., Ye, Z., Wang, Q., Bresnick, E.H., Farnham, P.J., and Jin, V.X. (2012). Integration of Hi-C and ChIP-seq data reveals distinct types of chromatin linkages. Nucleic acids research *40*, 7690-7704.

Langmead, B., Trapnell, C., Pop, M., and Salzberg, S.L. (2009). Ultrafast and memory-efficient alignment of short DNA sequences to the human genome. Genome biology *10*, R25.

LaPres, J.J., and Hudson, L.G. (1996). Identification of a functional determinant of differentiation-dependent expression in the involucrin gene. The Journal of biological chemistry *271*, 23154-23160.

Laurikkala, J., Mikkola, M.L., James, M., Tummers, M., Mills, A.A., and Thesleff, I. (2006). p63 regulates multiple signalling pathways required for ectodermal organogenesis and differentiation. Development *133*, 1553-1563.

Leask, A., Byrne, C., and Fuchs, E. (1991). Transcription factor AP2 and its role in epidermal-specific gene expression. Proceedings of the National Academy of Sciences of the United States of America *88*, 7948-7952.

LeBoeuf, M., Terrell, A., Trivedi, S., Sinha, S., Epstein, J.A., Olson, E.N., Morrisey, E.E., and Millar, S.E. (2010). Hdac1 and Hdac2 act redundantly to control p63 and p53 functions in epidermal progenitor cells. Developmental cell *19*, 807-818.

Lechler, T., and Fuchs, E. (2005). Asymmetric cell divisions promote stratification and differentiation of mammalian skin. Nature *437*, 275-280.

Lee, E., and Yuspa, S.H. (1991). Changes in inositol phosphate metabolism are associated with terminal differentiation and neoplasia in mouse keratinocytes. Carcinogenesis *12*, 1651-1658.

Lee, H., Quinn, J.C., Prasanth, K.V., Swiss, V.A., Economides, K.D., Camacho, M.M., Spector, D.L., and Abate-Shen, C. (2006a). PIAS1 confers DNA-binding specificity on the Msx1 homeoprotein. Genes Dev *20*, 784-794.

Lee, K., Adhikary, G., Balasubramanian, S., Gopalakrishnan, R., McCormick, T., Dimri, G.P., Eckert, R.L., and Rorke, E.A. (2008). Expression of Bmi-1 in epidermis enhances cell survival by altering cell cycle regulatory protein expression and inhibiting apoptosis. The Journal of investigative dermatology *128*, 9-17.

Lee, T.I., Jenner, R.G., Boyer, L.A., Guenther, M.G., Levine, S.S., Kumar, R.M., Chevalier, B., Johnstone, S.E., Cole, M.F., Isono, K., *et al.* (2006b). Control of developmental regulators by Polycomb in human embryonic stem cells. Cell *125*, 301-313.

Li, G., Ruan, X., Auerbach, R.K., Sandhu, K.S., Zheng, M., Wang, P., Poh, H.M., Goh, Y., Lim, J., Zhang, J., *et al.* (2012a). Extensive promoter-centered chromatin interactions provide a topological basis for transcription regulation. Cell *148*, 84-98.

Li, J., Zheng, H., Yu, F., Yu, T., Liu, C., Huang, S., Wang, T.C., and Ai, W. (2012b). Deficiency of the Kruppel-like factor KLF4 correlates with increased cell proliferation and enhanced skin tumorigenesis. Carcinogenesis *33*, 1239-1246.

Li, Q., Lu, Q., Hwang, J.Y., Buscher, D., Lee, K.F., Izpisua-Belmonte, J.C., and Verma, I.M. (1999). IKK1-deficient mice exhibit abnormal development of skin and skeleton. Genes & development *13*, 1322-1328.

Lichter, P., Cremer, T., Borden, J., Manuelidis, L., and Ward, D.C. (1988). Delineation of individual human chromosomes in metaphase and interphase cells by in situ suppression hybridization using recombinant DNA libraries. Human genetics *80*, 224-234.

Lichti, U., Anders, J., and Yuspa, S.H. (2008). Isolation and short-term culture of primary keratinocytes, hair follicle populations and dermal cells from newborn mice and

keratinocytes from adult mice for *in vitro* analysis and for grafting to immunodeficient mice. Nature protocols *3*, 799-810.

Lieberman-Aiden, E., van Berkum, N.L., Williams, L., Imakaev, M., Ragoczy, T., Telling, A., Amit, I., Lajoie, B.R., Sabo, P.J., Dorschner, M.O., *et al.* (2009). Comprehensive mapping of long-range interactions reveals folding principles of the human genome. Science *326*, 289-293.

Liu, X., Gao, Q., Li, P., Zhao, Q., Zhang, J., Li, J., Koseki, H., and Wong, J. (2013). UHRF1 targets DNMT1 for DNA methylation through cooperative binding of hemi-methylated DNA and methylated H3K9. Nature communications *4*, 1563.

Liu, Z., and Garrard, W.T. (2005). Long-range interactions between three transcriptional enhancers, active Vkappa gene promoters, and a 3' boundary sequence spanning 46 kilobases. Molecular and cellular biology *25*, 3220-3231.

Livak, K.J., and Schmittgen, T.D. (2001). Analysis of relative gene expression data using real-time quantitative PCR and the 2(-Delta Delta C(T)) Method. Methods *25*, 402-408.

Lodish, H., Berk, A., Kaiser, C. A. (2012). Molecular Cell Biology, Vol 7th Ed. (New York: W.H. Freeman & Company).

Lomvardas, S., Barnea, G., Pisapia, D.J., Mendelsohn, M., Kirkland, J., and Axel, R. (2006). Interchromosomal interactions and olfactory receptor choice. Cell *126*, 403-413.

Lopardo, T., Lo Iacono, N., Marinari, B., Giustizieri, M.L., Cyr, D.G., Merlo, G., Crosti, F., Costanzo, A., and Guerrini, L. (2008). Claudin-1 is a p63 target gene with a crucial role in epithelial development. PloS one *3*, e2715.

Lopez, R.G., Garcia-Silva, S., Moore, S.J., Bereshchenko, O., Martinez-Cruz, A.B., Ermakova, O., Kurz, E., Paramio, J.M., and Nerlov, C. (2009). C/EBPalpha and beta couple interfollicular keratinocyte proliferation arrest to commitment and terminal differentiation. Nature cell biology *11*, 1181-1190.

Lowell, S., Jones, P., Le Roux, I., Dunne, J., and Watt, F.M. (2000). Stimulation of human epidermal differentiation by delta-notch signalling at the boundaries of stem-cell clusters. Current biology : CB *10*, 491-500.

Luis, N.M., Morey, L., Mejetta, S., Pascual, G., Janich, P., Kuebler, B., Cozutto, L., Roma, G., Nascimento, E., Frye, M., *et al.* (2011). Regulation of human epidermal stem cell proliferation and senescence requires polycomb- dependent and -independent functions of CBX4. Cell stem cell *9*, 233-246.

Luxenburg, C., Pasolli, H.A., Williams, S.E., and Fuchs, E. (2011). Developmental roles for Srf, cortical cytoskeleton and cell shape in epidermal spindle orientation. Nature cell biology *13*, 203-214.

Machyna, M., Heyn, P., and Neugebauer, K.M. (2013). Cajal bodies: where form meets function. Wiley interdisciplinary reviews RNA *4*, 17-34.

Maestrini, E., Monaco, A.P., McGrath, J.A., Ishida-Yamamoto, A., Camisa, C., Hovnanian, A., Weeks, D.E., Lathrop, M., Uitto, J., and Christiano, A.M. (1996). A molecular defect in loricrin, the major component of the cornified cell envelope, underlies Vohwinkel's syndrome. Nat Genet *13*, 70-77.

Magnusdottir, E., Kalachikov, S., Mizukoshi, K., Savitsky, D., Ishida-Yamamoto, A., Panteleyev, A.A., and Calame, K. (2007). Epidermal terminal differentiation depends on B lymphocyte-induced maturation protein-1. Proceedings of the National Academy of Sciences of the United States of America *104*, 14988-14993.

Mahy, N.L., Perry, P.E., and Bickmore, W.A. (2002a). Gene density and transcription influence the localization of chromatin outside of chromosome territories detectable by FISH. J Cell Biol *159*, 753-763.

Mahy, N.L., Perry, P.E., Gilchrist, S., Baldock, R.A., and Bickmore, W.A. (2002b). Spatial organization of active and inactive genes and noncoding DNA within chromosome territories. The Journal of cell biology *157*, 579-589.

Mardaryev, A.N., Gdula, M.R., Yarker, J.L., Emelianov, V.N., Poterlowicz, K., Sharov, A.A., Sharova, T.Y., Scarpa, J.A., Chambon, P., Botchkarev, V.A., *et al.* (2014). p63 and BRG1 control developmentally regulated higher-order chromatin remodelling at the epidermal differentiation complex locus in epidermal progenitor cells. Development *141*, 101-111.

Marenholz, I., Heizmann, C.W., and Fritz, G. (2004). S100 proteins in mouse and man: from evolution to function and pathology (including an update of the nomenclature). Biochemical and biophysical research communications *322*, 1111-1122.

Marenholz, I., Rivera, V.A., Esparza-Gordillo, J., Bauerfeind, A., Lee-Kirsch, M.A., Ciechanowicz, A., Kurek, M., Piskackova, T., Macek, M., and Lee, Y.A. (2011). Association screening in the Epidermal Differentiation Complex (EDC) identifies an SPRR3 repeat number variant as a risk factor for eczema. J Invest Dermatol *131*, 1644-1649.

Marenholz, I., Zirra, M., Fischer, D.F., Backendorf, C., Ziegler, A., and Mischke, D. (2001). Identification of human epidermal differentiation complex (EDC)-encoded genes by subtractive hybridization of entire YACs to a gridded keratinocyte cDNA library. Genome research *11*, 341-355.

Margueron, R., and Reinberg, D. (2011). The Polycomb complex PRC2 and its mark in life. Nature *469*, 343-349.

Markaki, Y., Gunkel, M., Schermelleh, L., Beichmanis, S., Neumann, J., Heidemann, M., Leonhardt, H., Eick, D., Cremer, C., and Cremer, T. (2010). Functional nuclear organization of transcription and DNA replication: a topographical marriage between

chromatin domains and the interchromatin compartment. Cold Spring Harb Symp Quant Biol *75*, 475-492.

Markova, N.G., Karaman-Jurukovska, N., Pinkas-Sarafova, A., Marekov, L.N., and Simon, M. (2007). Inhibition of histone deacetylation promotes abnormal epidermal differentiation and specifically suppresses the expression of the late differentiation marker profilaggrin. The Journal of investigative dermatology *127*, 1126-1139.

Marshall, D., Hardman, M.J., Nield, K.M., and Byrne, C. (2001). Differentially expressed late constituents of the epidermal cornified envelope. Proceedings of the National Academy of Sciences of the United States of America *98*, 13031-13036.

Martens, J.A., and Winston, F. (2003). Recent advances in understanding chromatin remodeling by Swi/Snf complexes. Current opinion in genetics & development *13*, 136-142.

Martin, N., Patel, S., and Segre, J.A. (2004). Long-range comparison of human and mouse Sprr loci to identify conserved noncoding sequences involved in coordinate regulation. Genome research *14*, 2430-2438.

Mascre, G., Dekoninck, S., Drogat, B., Youssef, K.K., Brohee, S., Sotiropoulou, P.A., Simons, B.D., and Blanpain, C. (2012). Distinct contribution of stem and progenitor cells to epidermal maintenance. Nature *489*, 257-262.

Maytin, E.V., and Habener, J.F. (1998). Transcription factors C/EBP alpha, C/EBP beta, and CHOP (Gadd153) expressed during the differentiation program of keratinocytes *in vitro* and in vivo. The Journal of investigative dermatology *110*, 238-246.

McDade, S.S., Patel, D., and McCance, D.J. (2011). p63 maintains keratinocyte proliferative capacity through regulation of Skp2-p130 levels. Journal of cell science *124*, 1635-1643.

McGhee, J.D., and Felsenfeld, G. (1980). Nucleosome structure. Annu Rev Biochem *49*, 1115-1156.

Meaburn, K.J., Cabuy, E., Bonne, G., Levy, N., Morris, G.E., Novelli, G., Kill, I.R., and Bridger, J.M. (2007). Primary laminopathy fibroblasts display altered genome organization and apoptosis. Aging Cell *6*, 139-153.

Meaburn, K.J., Newbold, R.F., and Bridger, J.M. (2008). Positioning of human chromosomes in murine cell hybrids according to synteny. Chromosoma *117*, 579-591.

Medawar, A., Virolle, T., Rostagno, P., de la Forest-Divonne, S., Gambaro, K., Rouleau, M., and Aberdam, D. (2008). DeltaNp63 is essential for epidermal commitment of embryonic stem cells. PloS one *3*, e3441.

Mehta, I.S., Amira, M., Harvey, A.J., and Bridger, J.M. (2010). Rapid chromosome territory relocation by nuclear motor activity in response to serum removal in primary human fibroblasts. Genome Biol *11*, R5.

Meister, P., Towbin, B.D., Pike, B.L., Ponti, A., and Gasser, S.M. (2010). The spatial dynamics of tissue-specific promoters during C. elegans development. Genes Dev *24*, 766-782.

Mejetta, S., Morey, L., Pascual, G., Kuebler, B., Mysliwiec, M.R., Lee, Y., Shiekhattar, R., Di Croce, L., and Benitah, S.A. (2011). Jarid2 regulates mouse epidermal stem cell activation and differentiation. The EMBO journal *30*, 3635-3646.

Mellad, J.A., Warren, D.T., and Shanahan, C.M. (2011). Nesprins LINC the nucleus and cytoskeleton. Current opinion in cell biology *23*, 47-54.

Merkenschlager, M., and Odom, D.T. (2013). CTCF and cohesin: linking gene regulatory elements with their targets. Cell *152*, 1285-1297.

Mikkelsen, T.S., Ku, M., Jaffe, D.B., Issac, B., Lieberman, E., Giannoukos, G., Alvarez, P., Brockman, W., Kim, T.K., Koche, R.P., *et al.* (2007). Genome-wide maps of chromatin state in pluripotent and lineage-committed cells. Nature *448*, 553-560.

Mills, A.A., Zheng, B., Wang, X.J., Vogel, H., Roop, D.R., and Bradley, A. (1999). p63 is a p53 homologue required for limb and epidermal morphogenesis. Nature *398*, 708-713.

Milstone, L.M. (2004). Epidermal desquamation. Journal of dermatological science *36*, 131-140.

Mirny, L.A. (2011). The fractal globule as a model of chromatin architecture in the cell. Chromosome research : an international journal on the molecular, supramolecular and evolutionary aspects of chromosome biology *19*, 37-51.

Mischke, D., Korge, B.P., Marenholz, I., Volz, A., and Ziegler, A. (1996). Genes encoding structural proteins of epidermal cornification and S100 calcium-binding proteins form a gene complex ("epidermal differentiation complex") on human chromosome 1q21. The Journal of investigative dermatology *106*, 989-992.

Misteli, T. (2007). Beyond the sequence: cellular organization of genome function. Cell *128*, 787-800.

Mistry, D.S., Chen, Y., and Sen, G.L. (2012). Progenitor function in self-renewing human epidermis is maintained by the exosome. Cell stem cell *11*, 127-135.

Morar, N., Willis-Owen, S.A., Moffatt, M.F., and Cookson, W.O. (2006). The genetics of atopic dermatitis. J Allergy Clin Immunol *118*, 24-34; quiz 35-26.

Morasso, M.I., Markova, N.G., and Sargent, T.D. (1996). Regulation of epidermal differentiation by a Distal-less homeodomain gene. The Journal of cell biology *135*, 1879-1887.

Moretti, F., and Costanzo, A. (2009). A feedback regulatory loop between p63 and Dlx3: implications for epidermal differentiation. Cell cycle *8*, 1113.

Morey, C., Da Silva, N.R., Perry, P., and Bickmore, W.A. (2007). Nuclear reorganisation and chromatin decondensation are conserved, but distinct, mechanisms linked to Hox gene activation. Development *134*, 909-919.

Morey, C., Kress, C., and Bickmore, W.A. (2009). Lack of bystander activation shows that localization exterior to chromosome territories is not sufficient to up-regulate gene expression. Genome research *19*, 1184-1194.

Morey, L., and Helin, K. (2010). Polycomb group protein-mediated repression of transcription. Trends in biochemical sciences *35*, 323-332.

Mulder, K.W., Wang, X., Escriu, C., Ito, Y., Schwarz, R.F., Gillis, J., Sirokmany, G., Donati, G., Uribe-Lewis, S., Pavlidis, P., *et al.* (2012). Diverse epigenetic strategies interact to control epidermal differentiation. Nature cell biology *14*, 753-763.

Nagy, L., Kao, H.Y., Chakravarti, D., Lin, R.J., Hassig, C.A., Ayer, D.E., Schreiber, S.L., and Evans, R.M. (1997). Nuclear receptor repression mediated by a complex containing SMRT, mSIN3A, and histone deacetylase. Cell *89*, 373-380.

Narlikar, G.J., Sundaramoorthy, R., and Owen-Hughes, T. (2013). Mechanisms and functions of ATP-dependent chromatin-remodeling enzymes. Cell *154*, 490-503.

Nascimento, E.M., Cox, C.L., MacArthur, S., Hussain, S., Trotter, M., Blanco, S., Suraj, M., Nichols, J., Kubler, B., Benitah, S.A., *et al.* (2011). The opposing transcriptional functions of SIN3A and c-Myc are required to maintain tissue homeostasis. Nature cell biology *13*, 1395-1405.

Nemeth, A., Conesa, A., Santoyo-Lopez, J., Medina, I., Montaner, D., Peterfia, B., Solovei, I., Cremer, T., Dopazo, J., and Langst, G. (2010). Initial genomics of the human nucleolus. PLoS genetics *6*, e1000889.

Nestle, F.O., Di Meglio, P., Qin, J.Z., and Nickoloff, B.J. (2009). Skin immune sentinels in health and disease. Nature reviews Immunology *9*, 679-691.

Ng, K., Pullirsch, D., Leeb, M., and Wutz, A. (2007). Xist and the order of silencing. EMBO reports *8*, 34-39.

Nguyen, B.C., Lefort, K., Mandinova, A., Antonini, D., Devgan, V., Della Gatta, G., Koster, M.I., Zhang, Z., Wang, J., Tommasi di Vignano, A., *et al.* (2006). Cross-regulation between Notch and p63 in keratinocyte commitment to differentiation. Genes & development *20*, 1028-1042.

Ni, Z., Abou El Hassan, M., Xu, Z., Yu, T., and Bremner, R. (2008). The chromatin-remodeling enzyme BRG1 coordinates CIITA induction through many interdependent distal enhancers. Nature immunology *9*, 785-793.

Nickoloff, B.J., Qin, J.Z., Chaturvedi, V., Denning, M.F., Bonish, B., and Miele, L. (2002). Jagged-1 mediated activation of notch signaling induces complete maturation of human keratinocytes through NF-kappaB and PPARgamma. Cell death and differentiation *9*, 842-855.

Noordermeer, D., Branco, M.R., Splinter, E., Klous, P., van Ijcken, W., Swagemakers, S., Koutsourakis, M., van der Spek, P., Pombo, A., and de Laat, W. (2008). Transcription and chromatin organization of a housekeeping gene cluster containing an integrated beta-globin locus control region. PLoS genetics *4*, e1000016.

Noordermeer, D., de Wit, E., Klous, P., van de Werken, H., Simonis, M., Lopez-Jones, M., Eussen, B., de Klein, A., Singer, R.H., and de Laat, W. (2011). Variegated gene expression caused by cell-specific long-range DNA interactions. Nat Cell Biol *13*, 944-951.

Nora, E.P., Lajoie, B.R., Schulz, E.G., Giorgetti, L., Okamoto, I., Servant, N., Piolot, T., van Berkum, N.L., Meisig, J., Sedat, J., *et al.* (2012). Spatial partitioning of the regulatory landscape of the X-inactivation centre. Nature *485*, 381-385.

Oh, I.Y., Albea, D.M., Goodwin, Z.A., Quiggle, A.M., Baker, B.P., Guggisberg, A.M., Geahlen, J.H., Kroner, G.M., and de Guzman Strong, C. (2014). Regulation of the Dynamic Chromatin Architecture of the Epidermal Differentiation Complex is mediated by a c-Jun/AP-1-Modulated Enhancer. The Journal of investigative dermatology.

Okuyama, R., Ogawa, E., Nagoshi, H., Yabuki, M., Kurihara, A., Terui, T., Aiba, S., Obinata, M., Tagami, H., and Ikawa, S. (2007). p53 homologue, p51/p63, maintains the immaturity of keratinocyte stem cells by inhibiting Notch1 activity. Oncogene *26*, 4478-4488.

Ollion, J., Cochennec, J., Loll, F., Escude, C., and Boudier, T. (2013). TANGO: a generic tool for high-throughput 3D image analysis for studying nuclear organization. Bioinformatics *29*, 1840-1841.

Osborne, C.S., Chakalova, L., Brown, K.E., Carter, D., Horton, A., Debrand, E., Goyenechea, B., Mitchell, J.A., Lopes, S., Reik, W., *et al.* (2004). Active genes dynamically colocalize to shared sites of ongoing transcription. Nat Genet *36*, 1065-1071.

Osborne, C.S., Chakalova, L., Mitchell, J.A., Horton, A., Wood, A.L., Bolland, D.J., Corcoran, A.E., and Fraser, P. (2007). <italic>Myc</italic> Dynamically and Preferentially Relocates to a Transcription Factory Occupied by <italic>Igh</italic>. PLoS Biol *5*, e192.

Osoegawa, K., Tateno, M., Woon, P.Y., Frengen, E., Mammoser, A.G., Catanese, J.J., Hayashizaki, Y., and de Jong, P.J. (2000). Bacterial artificial chromosome libraries for mouse sequencing and functional analysis. Genome Res *10*, 116-128.

Outchkourov, N.S., Muino, J.M., Kaufmann, K., van Ijcken, W.F., Groot Koerkamp, M.J., van Leenen, D., de Graaf, P., Holstege, F.C., Grosveld, F.G., and Timmers, H.T. (2013). Balancing of histone H3K4 methylation states by the Kdm5c/SMCX histone demethylase modulates promoter and enhancer function. Cell reports *3*, 1071-1079.

Palmer, C.N., Irvine, A.D., Terron-Kwiatkowski, A., Zhao, Y., Liao, H., Lee, S.P., Goudie, D.R., Sandilands, A., Campbell, L.E., Smith, F.J., *et al.* (2006). Common loss-of-function variants of the epidermal barrier protein filaggrin are a major predisposing factor for atopic dermatitis. Nat Genet *38*, 441-446.

Palstra, R.J., de Laat, W., and Grosveld, F. (2008). Beta-globin regulation and long-range interactions. Adv Genet *61*, 107-142.

Papantonis, A., and Cook, P.R. (2011). Fixing the model for transcription: The DNA moves, not the polymerase. Transcription *2*, 41-44.

Parelho, V., Hadjur, S., Spivakov, M., Leleu, M., Sauer, S., Gregson, H.C., Jarmuz, A., Canzonetta, C., Webster, Z., Nesterova, T., *et al.* (2008). Cohesins functionally associate with CTCF on mammalian chromosome arms. Cell *132*, 422-433.

Parsa, R., Yang, A., McKeon, F., and Green, H. (1999). Association of p63 with proliferative potential in normal and neoplastic human keratinocytes. The Journal of investigative dermatology *113*, 1099-1105.

Pasini, D., Hansen, K.H., Christensen, J., Agger, K., Cloos, P.A., and Helin, K. (2008). Coordinated regulation of transcriptional repression by the RBP2 H3K4 demethylase and Polycomb-Repressive Complex 2. Genes & development *22*, 1345-1355.

Pauler, F.M., Sloane, M.A., Huang, R., Regha, K., Koerner, M.V., Tamir, I., Sommer, A., Aszodi, A., Jenuwein, T., and Barlow, D.P. (2009). H3K27me3 forms BLOCs over silent genes and intergenic regions and specifies a histone banding pattern on a mouse autosomal chromosome. Genome research *19*, 221-233.

Pavan Kumar, P., Purbey, P.K., Sinha, C.K., Notani, D., Limaye, A., Jayani, R.S., and Galande, S. (2006). Phosphorylation of SATB1, a global gene regulator, acts as a molecular switch regulating its transcriptional activity in vivo. Molecular cell *22*, 231-243.

Pederson, T. (2012). Is chromatin helical? Nat Rev Mol Cell Biol *13*, 6-6.

Pellegrini, G., Dellambra, E., Golisano, O., Martinelli, E., Fantozzi, I., Bondanza, S., Ponzin, D., McKeon, F., and De Luca, M. (2001). p63 identifies keratinocyte stem cells. Proceedings of the National Academy of Sciences of the United States of America *98*, 3156-3161.

Peric-Hupkes, D., Meuleman, W., Pagie, L., Bruggeman, S.W., Solovei, I., Brugman, W., Graf, S., Flicek, P., Kerkhoven, R.M., van Lohuizen, M., *et al.* (2010). Molecular maps of the reorganization of genome-nuclear lamina interactions during differentiation. Molecular cell *38*, 603-613.

Peters, J.M., Tedeschi, A., and Schmitz, J. (2008). The cohesin complex and its roles in chromosome biology. Genes & development *22*, 3089-3114.

Petrov, A., Pirozhkova, I., Carnac, G., Laoudj, D., Lipinski, M., and Vassetzky, Y.S. (2006). Chromatin loop domain organization within the 4q35 locus in facioscapulohumeral dystrophy patients versus normal human myoblasts. Proceedings of the National Academy of Sciences of the United States of America *103*, 6982-6987.

Phelan, M.L., Sif, S., Narlikar, G.J., and Kingston, R.E. (1999). Reconstitution of a core chromatin remodeling complex from SWI/SNF subunits. Molecular cell *3*, 247-253.

Phillips, J.E., and Corces, V.G. (2009). CTCF: master weaver of the genome. Cell *137*, 1194-1211.

Phillips-Cremins, J.E., Sauria, M.E., Sanyal, A., Gerasimova, T.I., Lajoie, B.R., Bell, J.S., Ong, C.T., Hookway, T.A., Guo, C., Sun, Y., *et al.* (2013). Architectural protein

subclasses shape 3D organization of genomes during lineage commitment. Cell *153*, 1281-1295.

Pinkel, D., Landegent, J., Collins, C., Fuscoe, J., Segraves, R., Lucas, J., and Gray, J. (1988). Fluorescence in situ hybridization with human chromosome-specific libraries: detection of trisomy 21 and translocations of chromosome 4. Proceedings of the National Academy of Sciences of the United States of America *85*, 9138-9142.

Pirozhkova, I., Petrov, A., Dmitriev, P., Laoudj, D., Lipinski, M., and Vassetzky, Y. (2008). A functional role for 4qA/B in the structural rearrangement of the 4q35 region and in the regulation of FRG1 and ANT1 in facioscapulohumeral dystrophy. PLoS One *3*, e3389.

Pirrotta, V., and Li, H.B. (2012). A view of nuclear Polycomb bodies. Curr Opin Genet Dev *22*, 101-109.

Quail, M.A., Kozarewa, I., Smith, F., Scally, A., Stephens, P.J., Durbin, R., Swerdlow, H., and Turner, D.J. (2008). A large genome center's improvements to the Illumina sequencing system. Nat Methods *5*, 1005-1010.

R Development Core Team (2010). R: A language and environment for statistical computing. (Vienna, Austria: : R Foundation for Statistical Computing).

Ragoczy, T., Bender, M.A., Telling, A., Byron, R., and Groudine, M. (2006). The locus control region is required for association of the murine beta-globin locus with engaged transcription factories during erythroid maturation. Genes Dev *20*, 1447-1457.

Rangarajan, A., Talora, C., Okuyama, R., Nicolas, M., Mammucari, C., Oh, H., Aster, J.C., Krishna, S., Metzger, D., Chambon, P., *et al.* (2001). Notch signaling is a direct determinant of keratinocyte growth arrest and entry into differentiation. The EMBO journal *20*, 3427-3436.

Rao, G., Alland, L., Guida, P., Schreiber-Agus, N., Chen, K., Chin, L., Rochelle, J.M., Seldin, M.F., Skoultchi, A.I., and DePinho, R.A. (1996). Mouse SIN3A interacts with and can functionally substitute for the amino-terminal repression of the Myc antagonist Mxi1. Oncogene *12*, 1165-1172.

Razin, S.V., Gavrilov, A.A., Pichugin, A., Lipinski, M., Iarovaia, O.V., and Vassetzky, Y.S. (2011). Transcription factories in the context of the nuclear and genome organization. Nucleic Acids Res *39*, 9085-9092.

Reddy, K.L., Zullo, J.M., Bertolino, E., and Singh, H. (2008). Transcriptional repression mediated by repositioning of genes to the nuclear lamina. Nature *452*, 243-247.

Rishi, V., Bhattacharya, P., Chatterjee, R., Rozenberg, J., Zhao, J., Glass, K., Fitzgerald, P., and Vinson, C. (2010). CpG methylation of half-CRE sequences creates C/EBPalpha binding sites that activate some tissue-specific genes. Proceedings of the National Academy of Sciences of the United States of America *107*, 20311-20316.

Roberson, E.D., Liu, Y., Ryan, C., Joyce, C.E., Duan, S., Cao, L., Martin, A., Liao, W., Menter, A., and Bowcock, A.M. (2012). A subset of methylated CpG sites differentiate psoriatic from normal skin. The Journal of investigative dermatology *132*, 583-592.

Ronneberger, O., Baddeley, D., Scheipl, F., Verveer, P.J., Burkhardt, H., Cremer, C., Fahrmeir, L., Cremer, T., and Joffe, B. (2008). Spatial quantitative analysis of fluorescently labeled nuclear structures: problems, methods, pitfalls. Chromosome research : an international journal on the molecular, supramolecular and evolutionary aspects of chromosome biology *16*, 523-562.

Rosenbloom, K.R., Dreszer, T.R., Long, J.C., Malladi, V.S., Sloan, C.A., Raney, B.J., Cline, M.S., Karolchik, D., Barber, G.P., Clawson, H., *et al.* (2012). ENCODE whole-genome data in the UCSC Genome Browser: update 2012. Nucleic acids research *40*, D912-917.

Rosenbloom, K.R., Sloan, C.A., Malladi, V.S., Dreszer, T.R., Learned, K., Kirkup, V.M., Wong, M.C., Maddren, M., Fang, R., Heitner, S.G., *et al.* (2013). ENCODE data in the UCSC Genome Browser: year 5 update. Nucleic acids research *41*, D56-63.

Rossi, M., Aqeilan, R.I., Neale, M., Candi, E., Salomoni, P., Knight, R.A., Croce, C.M., and Melino, G. (2006). The E3 ubiquitin ligase Itch controls the protein stability of p63. Proceedings of the National Academy of Sciences of the United States of America *103*, 12753-12758.

Sandilands, A., Sutherland, C., Irvine, A.D., and McLean, W.H. (2009). Filaggrin in the frontline: role in skin barrier function and disease. Journal of cell science *122*, 1285-1294.

Saunders, N., Dicker, A., Popa, C., Jones, S., and Dahler, A. (1999). Histone deacetylase inhibitors as potential anti-skin cancer agents. Cancer research *59*, 399-404.

Savarese, F., Davila, A., Nechanitzky, R., De La Rosa-Velazquez, I., Pereira, C.F., Engelke, R., Takahashi, K., Jenuwein, T., Kohwi-Shigematsu, T., Fisher, A.G., *et al.* (2009). SATB1 and SATB2 regulate embryonic stem cell differentiation and Nanog expression. Genes & development *23*, 2625-2638.

Scheffer, M.P., Eltsov, M., and Frangakis, A.S. (2011). Evidence for short-range helical order in the 30-nm chromatin fibers of erythrocyte nuclei. Proc Natl Acad Sci U S A *108*, 16992-16997.

Schermelleh, L., Carlton, P.M., Haase, S., Shao, L., Winoto, L., Kner, P., Burke, B., Cardoso, M.C., Agard, D.A., Gustafsson, M.G., *et al.* (2008). Subdiffraction multicolor imaging of the nuclear periphery with 3D structured illumination microscopy. Science *320*, 1332-1336.

Schindelin, J., Arganda-Carreras, I., Frise, E., Kaynig, V., Longair, M., Pietzsch, T., Preibisch, S., Rueden, C., Saalfeld, S., Schmid, B., *et al.* (2012). Fiji: an open-source platform for biological-image analysis. Nature methods *9*, 676-682.

Schlegelmilch, K., Mohseni, M., Kirak, O., Pruszak, J., Rodriguez, J.R., Zhou, D., Kreger, B.T., Vasioukhin, V., Avruch, J., Brummelkamp, T.R., *et al.* (2011). Yap1 acts downstream of alpha-catenin to control epidermal proliferation. Cell *144*, 782-795.

Schluter, H., Paquet-Fifield, S., Gangatirkar, P., Li, J., and Kaur, P. (2011). Functional characterization of quiescent keratinocyte stem cells and their progeny reveals a hierarchical organization in human skin epidermis. Stem cells *29*, 1256-1268.

Schmidt, D., Schwalie, P.C., Ross-Innes, C.S., Hurtado, A., Brown, G.D., Carroll, J.S., Flicek, P., and Odom, D.T. (2010). A CTCF-independent role for cohesin in tissue-specific transcription. Genome research *20*, 578-588.

Schneider, C.A., Rasband, W.S., and Eliceiri, K.W. (2012). NIH Image to ImageJ: 25 years of image analysis. Nature methods *9*, 671-675.

Schoenfelder, S., Sexton, T., Chakalova, L., Cope, N.F., Horton, A., Andrews, S., Kurukuti, S., Mitchell, J.A., Umlauf, D., Dimitrova, D.S., *et al.* (2010a). Preferential associations between co-regulated genes reveal a transcriptional interactome in erythroid cells. Nat Genet *42*, 53-61.

Schoenfelder, S., Sexton, T., Chakalova, L., Cope, N.F., Horton, A., Andrews, S., Kurukuti, S., Mitchell, J.A., Umlauf, D., Dimitrova, D.S., *et al.* (2010b). Preferential associations between co-regulated genes reveal a transcriptional interactome in erythroid cells. Nature genetics *42*, 53-61.

Schuettengruber, B., Martinez, A.M., Iovino, N., and Cavalli, G. (2011). Trithorax group proteins: switching genes on and keeping them active. Nature reviews Molecular cell biology *12*, 799-814.

Schwartz, Y.B., and Pirrotta, V. (2013). A new world of Polycombs: unexpected partnerships and emerging functions. Nature reviews Genetics *14*, 853-864.

Segre, J. (2003). Complex redundancy to build a simple epidermal permeability barrier. Curr Opin Cell Biol *15*, 776-782.

Segre, J.A., Bauer, C., and Fuchs, E. (1999). Klf4 is a transcription factor required for establishing the barrier function of the skin. Nature genetics *22*, 356-360.

Sellheyer, K., and Krahl, D. (2010). Blimp-1: a marker of terminal differentiation but not of sebocytic progenitor cells. Journal of cutaneous pathology *37*, 362-370.

Sen, G.L., Boxer, L.D., Webster, D.E., Bussat, R.T., Qu, K., Zarnegar, B.J., Johnston, D., Siprashvili, Z., and Khavari, P.A. (2012). ZNF750 is a p63 target gene that induces KLF4 to drive terminal epidermal differentiation. Developmental cell *22*, 669-677.

Sen, G.L., Reuter, J.A., Webster, D.E., Zhu, L., and Khavari, P.A. (2010). DNMT1 maintains progenitor function in self-renewing somatic tissue. Nature *463*, 563-567.

Sen, G.L., Webster, D.E., Barragan, D.I., Chang, H.Y., and Khavari, P.A. (2008). Control of differentiation in a self-renewing mammalian tissue by the histone demethylase JMJD3. Genes & development *22*, 1865-1870.

Sengupta, K., Camps, J., Mathews, P., Barenboim-Stapleton, L., Nguyen, Q.T., Difilippantonio, M.J., and Ried, T. (2008). Position of human chromosomes is conserved in mouse nuclei indicating a species-independent mechanism for maintaining genome organization. Chromosoma *117*, 499-509.

Sexton, T., Yaffe, E., Kenigsberg, E., Bantignies, F., Leblanc, B., Hoichman, M., Parrinello, H., Tanay, A., and Cavalli, G. (2012). Three-dimensional folding and functional organization principles of the Drosophila genome. Cell *148*, 458-472.

Shalom-Feuerstein, R., Lena, A.M., Zhou, H., De La Forest Divonne, S., Van Bokhoven, H., Candi, E., Melino, G., and Aberdam, D. (2011). DeltaNp63 is an ectodermal gatekeeper of epidermal morphogenesis. Cell death and differentiation *18*, 887-896.

Sharif, J., and Koseki, H. (2011). Recruitment of DNMT1 roles of the SRA protein Np95 (Uhrf1) and other factors. Progress in molecular biology and translational science *101*, 289-310.

Shen, Y., Yue, F., McCleary, D.F., Ye, Z., Edsall, L., Kuan, S., Wagner, U., Dixon, J., Lee, L., Lobanenkov, V.V., *et al.* (2012). A map of the cis-regulatory sequences in the mouse genome. Nature *488*, 116-120.

Shopland, L.S., Johnson, C.V., Byron, M., McNeil, J., and Lawrence, J.B. (2003). Clustering of multiple specific genes and gene-rich R-bands around SC-35 domains: evidence for local euchromatic neighborhoods. The Journal of cell biology *162*, 981-990.

Sif, S., Saurin, A.J., Imbalzano, A.N., and Kingston, R.E. (2001). Purification and characterization of mSIN3A-containing BRG1 and hBRM chromatin remodeling complexes. Genes & development *15*, 603-618.

Silverstein, R.A., and Ekwall, K. (2005). Sin3: a flexible regulator of global gene expression and genome stability. Current genetics *47*, 1-17.

Simon, J.A., and Kingston, R.E. (2009). Mechanisms of polycomb gene silencing: knowns and unknowns. Nat Rev Mol Cell Biol *10*, 697-708.

Simonis, M., Klous, P., Splinter, E., Moshkin, Y., Willemsen, R., de Wit, E., van Steensel, B., and de Laat, W. (2006). Nuclear organization of active and inactive chromatin domains uncovered by chromosome conformation capture-on-chip (4C). Nat Genet *38*, 1348-1354.

Simonis, M., Kooren, J., and de Laat, W. (2007). An evaluation of 3C-based methods to capture DNA interactions. Nat Methods *4*, 895-901.

Simpson, C.L., Patel, D.M., and Green, K.J. (2011). Deconstructing the skin: cytoarchitectural determinants of epidermal morphogenesis. Nature reviews Molecular cell biology *12*, 565-580.

Sinha, S., Degenstein, L., Copenhaver, C., and Fuchs, E. (2000). Defining the regulatory factors required for epidermal gene expression. Molecular and cellular biology *20*, 2543-2555.

Sinha, S., and Fuchs, E. (2001). Identification and dissection of an enhancer controlling epithelial gene expression in skin. Proceedings of the National Academy of Sciences of the United States of America *98*, 2455-2460.

Smart, I.H. (1970). Variation in the plane of cell cleavage during the process of stratification in the mouse epidermis. The British journal of dermatology *82*, 276-282.

Smith, F.J., Irvine, A.D., Terron-Kwiatkowski, A., Sandilands, A., Campbell, L.E., Zhao, Y., Liao, H., Evans, A.T., Goudie, D.R., Lewis-Jones, S., *et al.* (2006). Loss-of-function mutations in the gene encoding filaggrin cause ichthyosis vulgaris. Nat Genet *38*, 337-342.

Smith, Z.D., and Meissner, A. (2013). DNA methylation: roles in mammalian development. Nature reviews Genetics *14*, 204-220.

South, A.P., Cabral, A., Ives, J.H., James, C.H., Mirza, G., Marenholz, I., Mischke, D., Backendorf, C., Ragoussis, J., and Nizetic, D. (1999). Human Epidermal Differentiation Complex in a Single 2.5 Mbp Long Continuum of Overlapping DNA Cloned in Bacteria Integrating Physical and Transcript Maps. *112*, 910-918.

Spector, D.L., and Lamond, A.I. (2011). Nuclear speckles. Cold Spring Harbor perspectives in biology *3*.

Spilianakis, C.G., and Flavell, R.A. (2004). Long-range intrachromosomal interactions in the T helper type 2 cytokine locus. Nat Immunol *5*, 1017-1027.

Spilianakis, C.G., Lalioti, M.D., Town, T., Lee, G.R., and Flavell, R.A. (2005). Interchromosomal associations between alternatively expressed loci. Nature *435*, 637-645.

Starr, D.A., and Fridolfsson, H.N. (2010). Interactions between nuclei and the cytoskeleton are mediated by SUN-KASH nuclear-envelope bridges. Annual review of cell and developmental biology *26*, 421-444.

Stern, C.D. (2005). Neural induction: old problem, new findings, yet more questions. Development *132*, 2007-2021.

Sutherland, H., and Bickmore, W.A. (2009). Transcription factories: gene expression in unions? Nat Rev Genet *10*, 457-466.

Szczerbal, I., and Bridger, J.M. (2010). Association of adipogenic genes with SC-35 domains during porcine adipogenesis. Chromosome research : an international journal on the molecular, supramolecular and evolutionary aspects of chromosome biology *18*, 887-895.

Szemes, M., Gyorgy, A., Paweletz, C., Dobi, A., and Agoston, D.V. (2006). Isolation and characterization of SATB2, a novel AT-rich DNA binding protein expressed in development- and cell-specific manner in the rat brain. Neurochemical research *31*, 237-246.

Takizawa, T., Gudla, P.R., Guo, L., Lockett, S., and Misteli, T. (2008a). Allele-specific nuclear positioning of the monoallelically expressed astrocyte marker GFAP. Genes & development *22*, 489-498.

Takizawa, T., Meaburn, K.J., and Misteli, T. (2008b). The meaning of gene positioning. Cell *135*, 9-13.

Tanabe, H., Muller, S., Neusser, M., von Hase, J., Calcagno, E., Cremer, M., Solovei, I., Cremer, C., and Cremer, T. (2002). Evolutionary conservation of chromosome territory arrangements in cell nuclei from higher primates. Proceedings of the National Academy of Sciences of the United States of America *99*, 4424-4429.

Telenius, H., Carter, N.P., Bebb, C.E., Nordenskjold, M., Ponder, B.A., and Tunnacliffe, A. (1992). Degenerate oligonucleotide-primed PCR: general amplification of target DNA by a single degenerate primer. Genomics *13*, 718-725.

Teng, A., Nair, M., Wells, J., Segre, J.A., and Dai, X. (2007). Strain-dependent perinatal lethality of Ovol1-deficient mice and identification of Ovol2 as a downstream target of Ovol1 in skin epidermis. Biochimica et biophysica acta *1772*, 89-95.

Testoni, B., and Mantovani, R. (2006). Mechanisms of transcriptional repression of cell-cycle G2/M promoters by p63. Nucleic acids research *34*, 928-938.

Ting, S.B., Caddy, J., Hislop, N., Wilanowski, T., Auden, A., Zhao, L.L., Ellis, S., Kaur, P., Uchida, Y., Holleran, W.M., *et al.* (2005a). A homolog of Drosophila grainy head is essential for epidermal integrity in mice. Science *308*, 411-413.

Ting, S.B., Caddy, J., Wilanowski, T., Auden, A., Cunningham, J.M., Elias, P.M., Holleran, W.M., and Jane, S.M. (2005b). The epidermis of GRHL3-null mice displays altered lipid processing and cellular hyperproliferation. Organogenesis *2*, 33-35.

Tiwari, V.K., Cope, L., McGarvey, K.M., Ohm, J.E., and Baylin, S.B. (2008a). A novel 6C assay uncovers Polycomb-mediated higher order chromatin conformations. Genome research *18*, 1171-1179.

Tiwari, V.K., McGarvey, K.M., Licchesi, J.D., Ohm, J.E., Herman, J.G., Schubeler, D., and Baylin, S.B. (2008b). PcG proteins, DNA methylation, and gene repression by chromatin looping. PLoS Biol *6*, 2911-2927.

Trapnell, C., Roberts, A., Goff, L., Pertea, G., Kim, D., Kelley, D.R., Pimentel, H., Salzberg, S.L., Rinn, J.L., and Pachter, L. (2012). Differential gene and transcript expression analysis of RNA-seq experiments with TopHat and Cufflinks. Nature protocols *7*, 562-578.

Triel, C., Vestergaard, M.E., Bolund, L., Jensen, T.G., and Jensen, U.B. (2004). Side population cells in human and mouse epidermis lack stem cell characteristics. Experimental cell research *295*, 79-90.

Tseng, H., Biegel, J.A., and Brown, R.S. (1999). Basonuclin is associated with the ribosomal RNA genes on human keratinocyte mitotic chromosomes. Journal of cell science *112 Pt 18*, 3039-3047.

Tsuji, T., and Cox, A.J. (1977). Ultrastructural studies of nuclei and nucleoli in psoriatic epidermis, compared with those in normal epidermis. The Journal of investigative dermatology *69*, 205-210.

UCSC (2012). Mouse BLAT Search

Ullah, M., Pelletier, N., Xiao, L., Zhao, S.P., Wang, K., Degerny, C., Tahmasebi, S., Cayrou, C., Doyon, Y., Goh, S.L., *et al.* (2008). Molecular architecture of quartet MOZ/MORF histone acetyltransferase complexes. Molecular and cellular biology *28*, 6828-6843.

Umbarger, Mark A., Toro, E., Wright, Matthew A., Porreca, Gregory J., Baù, D., Hong, S.-H., Fero, Michael J., Zhu, Lihua J., Marti-Renom, Marc A., McAdams, Harley H., *et al.* (2011). The Three-Dimensional Architecture of a Bacterial Genome and Its Alteration by Genetic Perturbation. Molecular cell *44*, 252-264.

Untergasser, A., Cutcutache, I., Koressaar, T., Ye, J., Faircloth, B.C., Remm, M., and Rozen, S.G. (2012). Primer3--new capabilities and interfaces. Nucleic acids research *40*, e115.

Vakoc, C.R., Letting, D.L., Gheldof, N., Sawado, T., Bender, M.A., Groudine, M., Weiss, M.J., Dekker, J., and Blobel, G.A. (2005). Proximity among distant regulatory elements at the beta-globin locus requires GATA-1 and FOG-1. Mol Cell *17*, 453-462.

van Berkum, N.L., and Dekker, J. (2009). Determining spatial chromatin organization of large genomic regions using 5C technology. Methods in molecular biology *567*, 189-213.

Van Bortle, K., Ramos, E., Takenaka, N., Yang, J., Wahi, J.E., and Corces, V.G. (2012). Drosophila CTCF tandemly aligns with other insulator proteins at the borders of H3K27me3 domains. Genome research *22*, 2176-2187.

van Koningsbruggen, S., Gierlinski, M., Schofield, P., Martin, D., Barton, G.J., Ariyurek, Y., den Dunnen, J.T., and Lamond, A.I. (2010). High-resolution whole-genome sequencing reveals that specific chromatin domains from most human chromosomes associate with nucleoli. Molecular biology of the cell *21*, 3735-3748.

Verlaan, D.J., Berlivet, S., Hunninghake, G.M., Madore, A.M., Lariviere, M., Moussette, S., Grundberg, E., Kwan, T., Ouimet, M., Ge, B., *et al.* (2009). Allele-specific chromatin remodeling in the ZPBP2/GSDMB/ORMDL3 locus associated with the risk of asthma and autoimmune disease. Am J Hum Genet *85*, 377-393.

Versaevel, M., Grevesse, T., and Gabriele, S. (2012). Spatial coordination between cell and nuclear shape within micropatterned endothelial cells. Nature communications *3*, 671.

Verschure, P.J., van der Kraan, I., Manders, E.M., Hoogstraten, D., Houtsmuller, A.B., and van Driel, R. (2003). Condensed chromatin domains in the mammalian nucleus are accessible to large macromolecules. EMBO reports *4*, 861-866.

Verschure, P.J., van Der Kraan, I., Manders, E.M., and van Driel, R. (1999). Spatial relationship between transcription sites and chromosome territories. J Cell Biol *147*, 13-24.

Volpi, E.V., Chevret, E., Jones, T., Vatcheva, R., Williamson, J., Beck, S., Campbell, R.D., Goldsworthy, M., Powis, S.H., Ragoussis, J., *et al.* (2000). Large-scale chromatin organization of the major histocompatibility complex and other regions of human

chromosome 6 and its response to interferon in interphase nuclei. J Cell Sci *113 (Pt 9)*, 1565-1576.

Wang, Y., Fischle, W., Cheung, W., Jacobs, S., Khorasanizadeh, S., and Allis, C.D. (2004). Beyond the double helix: writing and reading the histone code. Novartis Found Symp *259*, 3-17; discussion 17-21, 163-169.

Wanzel, M., Herold, S., and Eilers, M. (2003). Transcriptional repression by Myc. Trends in cell biology *13*, 146-150.

Watt, F.M., Jordan, P.W., and O'Neill, C.H. (1988). Cell shape controls terminal differentiation of human epidermal keratinocytes. Proceedings of the National Academy of Sciences of the United States of America *85*, 5576-5580.

Wells, J., Lee, B., Cai, A.Q., Karapetyan, A., Lee, W.J., Rugg, E., Sinha, S., Nie, Q., and Dai, X. (2009). Ovol2 suppresses cell cycling and terminal differentiation of keratinocytes by directly repressing c-Myc and Notch1. The Journal of biological chemistry *284*, 29125-29135.

Wendt, K.S., Yoshida, K., Itoh, T., Bando, M., Koch, B., Schirghuber, E., Tsutsumi, S., Nagae, G., Ishihara, K., Mishiro, T., *et al.* (2008). Cohesin mediates transcriptional insulation by CCCTC-binding factor. Nature *451*, 796-801.

Westfall, M.D., Mays, D.J., Sniezek, J.C., and Pietenpol, J.A. (2003). The Delta Np63 alpha phosphoprotein binds the p21 and 14-3-3 sigma promoters in vivo and has transcriptional repressor activity that is reduced by Hay-Wells syndrome-derived mutations. Molecular and cellular biology *23*, 2264-2276.

Widom, J., and Klug, A. (1985). Structure of the 300A chromatin filament: X-ray diffraction from oriented samples. Cell *43*, 207-213.

Williams, C.J., Naito, T., Arco, P.G., Seavitt, J.R., Cashman, S.M., De Souza, B., Qi, X., Keables, P., Von Andrian, U.H., and Georgopoulos, K. (2004). The chromatin remodeler Mi-2beta is required for CD4 expression and T cell development. Immunity *20*, 719-733.

Williams, R.R., Azuara, V., Perry, P., Sauer, S., Dvorkina, M., Jorgensen, H., Roix, J., McQueen, P., Misteli, T., Merkenschlager, M., *et al.* (2006). Neural induction promotes large-scale chromatin reorganisation of the Mash1 locus. J Cell Sci *119*, 132-140.

Williams, R.R., Broad, S., Sheer, D., and Ragoussis, J. (2002). Subchromosomal positioning of the epidermal differentiation complex (EDC) in keratinocyte and lymphoblast interphase nuclei. Experimental cell research *272*, 163-175.

Williams, S.P., Athey, B.D., Muglia, L.J., Schappe, R.S., Gough, A.H., and Langmore, J.P. (1986). Chromatin fibers are left-handed double helices with diameter and mass per unit length that depend on linker length. Biophys J *49*, 233-248.

Winter, M., Moser, M.A., Meunier, D., Fischer, C., Machat, G., Mattes, K., Lichtenberger, B.M., Brunmeir, R., Weissmann, S., Murko, C., *et al.* (2013). Divergent roles of HDAC1 and HDAC2 in the regulation of epidermal development and tumorigenesis. The EMBO journal *32*, 3176-3191.

Woodcock, C.L., Frado, L.L., and Rattner, J.B. (1984). The higher-order structure of chromatin: evidence for a helical ribbon arrangement. J Cell Biol *99*, 42-52.

Woodcock, C.L., and Ghosh, R.P. (2010). Chromatin higher-order structure and dynamics. Cold Spring Harb Perspect Biol *2*, a000596.

Wu, C., Bassett, A., and Travers, A. (2007). A variable topology for the 30-nm chromatin fibre. EMBO Rep *8*, 1129-1134.

Wu, N., Rollin, J., Masse, I., Lamartine, J., and Gidrol, X. (2012). p63 regulates human keratinocyte proliferation via MYC-regulated gene network and differentiation

commitment through cell adhesion-related gene network. The Journal of biological chemistry *287*, 5627-5638.

Xu, M., and Cook, P.R. (2008). The role of specialized transcription factories in chromosome pairing. Biochim Biophys Acta *1783*, 2155-2160.

Yang, A., Schweitzer, R., Sun, D., Kaghad, M., Walker, N., Bronson, R.T., Tabin, C., Sharpe, A., Caput, D., Crum, C., *et al.* (1999). p63 is essential for regenerative proliferation in limb, craniofacial and epithelial development. Nature *398*, 714-718.

Yao, J., Fetter, R.D., Hu, P., Betzig, E., and Tjian, R. (2011). Subnuclear segregation of genes and core promoter factors in myogenesis. Genes Dev *25*, 569-580.

Yasui, D., Miyano, M., Cai, S., Varga-Weisz, P., and Kohwi-Shigematsu, T. (2002). SATB1 targets chromatin remodelling to regulate genes over long distances. Nature *419*, 641-645.

Yi, R., Poy, M.N., Stoffel, M., and Fuchs, E. (2008). A skin microRNA promotes differentiation by repressing 'stemness'. Nature *452*, 225-229.

Yu, Y., Chen, Y., Kim, B., Wang, H., Zhao, C., He, X., Liu, L., Liu, W., Wu, L.M., Mao, M., *et al.* (2013). Olig2 targets chromatin remodelers to enhancers to initiate oligodendrocyte differentiation. Cell *152*, 248-261.

Yu, Z., Lin, K.K., Bhandari, A., Spencer, J.A., Xu, X., Wang, N., Lu, Z., Gill, G.N., Roop, D.R., Wertz, P., *et al.* (2006). The Grainyhead-like epithelial transactivator Get-1/GRHL3 regulates epidermal terminal differentiation and interacts functionally with LMO4. Developmental biology *299*, 122-136.

Zang, C., Schones, D.E., Zeng, C., Cui, K., Zhao, K., and Peng, W. (2009). A clustering approach for identification of enriched domains from histone modification ChIP-Seq data. Bioinformatics *25*, 1952-1958.

Zhang, H., Pasolli, H.A., and Fuchs, E. (2011). Yes-associated protein (YAP) transcriptional coactivator functions in balancing growth and differentiation in skin. Proceedings of the National Academy of Sciences of the United States of America *108*, 2270-2275.

Zhang, Y., McCord, R.P., Ho, Y.J., Lajoie, B.R., Hildebrand, D.G., Simon, A.C., Becker, M.S., Alt, F.W., and Dekker, J. (2012). Spatial organization of the mouse genome and its role in recurrent chromosomal translocations. Cell *148*, 908-921.

Zhao, X.D., Han, X., Chew, J.L., Liu, J., Chiu, K.P., Choo, A., Orlov, Y.L., Sung, W.K., Shahab, A., Kuznetsov, V.A., *et al.* (2007). Whole-genome mapping of histone H3 Lys4 and 27 trimethylations reveals distinct genomic compartments in human embryonic stem cells. Cell stem cell *1*, 286-298.

Zhu, A.J., Haase, I., and Watt, F.M. (1999). Signaling via beta1 integrins and mitogen-activated protein kinase determines human epidermal stem cell fate *in vitro*. Proceedings of the National Academy of Sciences of the United States of America *96*, 6728-6733.

Zink, D., Amaral, M.D., Englmann, A., Lang, S., Clarke, L.A., Rudolph, C., Alt, F., Luther, K., Braz, C., Sadoni, N., *et al.* (2004). Transcription-dependent spatial arrangements of CFTR and adjacent genes in human cell nuclei. J Cell Biol *166*, 815-825.

Zirbel, R.M., Mathieu, U.R., Kurz, A., Cremer, T., and Lichter, P. (1993). Evidence for a nuclear compartment of transcription and splicing located at chromosome domain boundaries. Chromosome Res *1*, 93-106.